SPECTROSCOPIC STUDIES OF METAL(II) COMPLEXES AND APPLICATION OF THE Ni(II) COMPLEXES TO OLEFIN OLIGOMERISATION CATALYSIS

A thesis submitted to the

UNIVERSITY OF CAPE TOWN

in fulfilment of the requirements for the degree of

DOCTOR OF PHILOSOPHY

by

ALISON MARGARET ANNE BENNETT

BSc.(Hons) University of Cape Town

Department of Chemistry
University of Cape Town
Rondebosch, 7700
South Africa

March 1990

ACKNOWLEDGEMENTS

I would like to thank my supervisors, Prof D. A. Thornton and Dr G. A. Foulds, for guidance and encouragement and my friends in the Departments of Chemistry and Chemical Engineering for their ready advice and constant humour.

I am also indebted to the following people for their help:
Mr R. Forrester of the CSIR,
Dr M. Niven, Mr Z. Brown and Mr N. Hendricks of the Department of Chemistry, UCT,
the NEC, CSIR and FRD for financial support.

Finally, special thanks to my fiancé, Stephan, for his support and companionship throughout the course of my work.

ABSTRACT

Complexes of some divalent first row transition metal ions with various ligands have been prepared. These included *bis*-complexes of β-ketoenolate* ligands, nickel complexes of trialkylphosphine and nickel complexes containing phosphine and β-ketoenolate ligands, and finally, *tris*, *bis* and *mono*(ethylenediamine) complexes. Composition was ascertained by microanalysis and ^{1}H, ^{13}C NMR of the diamagnetic complexes. In addition, the crystal structure of one of the nickel β-ketoenolate triethylphosphine complexes was determined.

The infrared spectra of the above compounds have been examined over the range 4000-50 cm^{-1} with a view to determining band assignments based on metal ion substitution, ligand substitution (for phosphine and β-ketoenolate complexes), ligand and metal ion isotopic labelling [for *tris*(ethylenediamine) complexes] and anion substitution (for phosphine and ethylenediamine complexes). In each case, spectra-structure correlations have been established and are discussed.

Each of the nickel complexes prepared above was tested as a catalyst for the oligomerisation of 1-hexene. The experiments were carried out in batch at 40°C using toluene as solvent. Four different Lewis acid co-catalysts were tested and nickel : co-catalyst ratios of 1 : 1 and 1 : 10 were used. The effects of Lewis acid strength and concentration, nickel complex structure, a change in the donor chelating atom and the presence of phosphine ligands on the isomerisation, as well as the activity and selectivity of the oligomerisation reaction, are discussed.

Two polymer-supported catalyst complexes have been prepared; the first, by polymerisation of a nickel β-ketoenolate complex monomer and the second, by binding a nickel β-ketoenolate phosphine complex to a polystyrene support through the phosphine ligand. The resulting polymers were extensively characterised by microanalysis, infrared, ^{1}H and ^{13}C NMR, mass spectrometry, energy dispersive X-ray and thermal

* Throughout this abstract β-ketoenolates are considered to include mono- and dithio-β-ketoenolates.

techniques. In the presence of a ten-fold excess of the ethylaluminium dichloride co-catalyst, each supported complex formed an active 1-hexene oligomerisation and isomerisation system. The activity and selectivity of each system have been compared to that of their respective monomers. Finally, the polymerised β-ketoenolate monomer was tested at various temperatures as a propene oligomerisation catalyst and the effect of temperature on activity and selectivity is discussed.

LIST OF PUBLICATIONS

1. A. M. A. Bennett, G. A. Foulds and D. A. Thornton, The infrared spectra of the *tris*(ethylenediamine) complexes of first transition series metal(II) sulphates, *Spectrochim. Acta*, **45A** (1989) 219.

2. A. M. A. Bennett, G. A. Foulds and D. A. Thornton, The infrared spectra of ethylenediamine complexes - II. *Tris*-, *bis*- and *mono*(ethylenediamine) complexes of metal(II) halides, *Spectrochim. Acta*, **46A** (1990) 13.

3. A. M. A. Bennett, G. A. Foulds and D. A. Thornton, The IR and ^{1}H, ^{13}C NMR spectra of the nickel(II), copper(II) and zinc(II) complexes of 2,4-pentanedione, 4-imino-2-pentanone, 4-thioxo-2-pentanone and 2,4-pentanedithione: A comparative study, *Polyhedron*, **8** (1989) 2305.

4. A. M. A. Bennett, G. A. Foulds and D. A. Thornton, Synthesis of heterogeneous olefin oligomerisation catalysts using homogeneous nickel-chelate complexes as a basis, *Polyhedron*, (1989) in press.

5. A. M. A. Bennett, G. A. Foulds and D. A. Thornton, The IR and ^{1}H, ^{13}C NMR spectra of trialkyl- and triarylphosphine complexes of nickel(II) dihalides and their reaction products with nickel complexes of 4-thioxo-2-pentanone and 2,4-pentanedithione, *Polyhedron*, (1990) submitted for publication.

6. A. M. A. Bennett, G. A. Foulds, D. A. Thornton and K. J. Cavell, The catalytic olefin oligomerisation activity of a series of trialkyl- and triphenylphosphine derivatives of the nickel(II) complexes of 4-thioxo-2-pentanone and 2,4-pentanedithione, in preparation.

7. A. M. A. Bennett, G. A. Foulds, D. A. Thornton and A.F. Masters, The catalytic olefin oligomerisation and isomerisation activity of the nickel (II) complexes of 2,4-pentanedione, 4-imino-2-pentanone, 4-thioxo-2-pentanone and 2,4-pentanedithione: the affect of donor atom and co-catalyst on activity and selectivity, in preparation.

LIST OF CONFERENCE PROCEEDINGS

1. A. M. A. Bennett, G. A. Foulds and D. A. Thornton, *Inorganic '88*, Gordons Bay, South Africa, 1988.

2. A. M. A. Bennett, G. A. Foulds and D. A. Thornton, *Colloqium on Catalysis*, Vereeniging, South Africa, 1988.

3. A. M. A. Bennett, G. A. Foulds and D. A. Thornton, Abstract **T42**, *27 Int. Conf. Coord. Chem.*, Broadbeach, Australia, July 1989.

4. G. A. Foulds, A. M. A. Bennett and D. A. Thornton, Abstract **76**, *Conference on Applied Organometallic Chemistry*, Pokolbin, Australia, July 1989.

GLOSSARY

en	ethylenediamine (1,2-diaminoethane)
Ph	phenyl
Me	methyl
Et	ethyl
i-Pr	isopropyl
Bu	butyl
ν	stretching vibration
δ	bending vibration
ω	wagging vibration
τ	twisting vibration
ρ	rocking vibration
oop	out-of-plane, out-of-phase
ip	in-plane, in-phase
acac	2,4-pentanedionate ion
hfacac	hexafluoro-2,4-pentandionate ion
Nacac	4-imino-2-pentanonate ion
Sacac	4-thioxo-2-pentanonate ion
SacSac	2,4-dithiopentanonate
COD	1,5-cyclooctadiene
SHOP	Shell Higher Olefins Process
EDX	Energy Dispersive X-ray
TGA	Thermogravimetric Analysis
DTA	Differential Thermal Analysis
EXAFS	Extended X-ray Absorption Fine Structure

Although the dimensions of ν (frequency) and $\tilde{\nu}$ (wavenumber) differ, it is traditional to use them interchangeably. All spectral data in this thesis are given in terms of ν (cm^{-1}).

The use of Ångström units for bond lengths is still common practice in the literature. Conversion to SI units can simply be performed by:

$$1\text{Å} = 100\ \text{pm}$$

TABLE OF CONTENTS

CHAPTER 6 PHYSICAL METHODS

APPENDICES

CHAPTER 1

INTRODUCTION

INTRODUCTION

The first row transition elements, *i.e.* those containing outer electrons in the 3*d* electron shell, are reactive metals. The chemistry of these transition elements is largely concerned with the chemistry of coordination compounds or, as they are more usually called, complexes. The study of these complexes has contributed greatly to the understanding of the chemical bond and of inorganic chemistry as a whole. For many years complexes were regarded as of interest to the theoretical and inorganic chemist only, but now they play major roles in organic synthesis, biochemistry, analytical chemistry and polymerisation processes.

A coordination complex consists of a central metal atom or ion which is surrounded by a number of groups or donor molecules called ligands, which are attached to the metal by a coordinate bond. Our understanding of these compounds dates from the time of Alfred Werner. Werner presented his first paper on the subject in 1891 at the age of 25; in 1913 he received the Nobel Prize for chemistry.

The 1963 Nobel Prize was awarded jointly to two coordination chemists; Dr K. Ziegler of the Max Planck Institute in Germany and Professor G. Natta of the University of Milan in Italy. Their research was responsible for the development of the low-pressure polymerisation of ethene. In 1949 they made the initial discovery that long-chain aluminium alkyls could be produced by repeated insertion of ethene molecules into the Al-C bond. However, in 1952, after a long series of experiments, Ziegler observed a new and initially unwelcome effect. Termination occurred after only one insertion step and 1-butene was produced almost quantitatively. After further research this new phenomenon was attributed to traces of nickel salts present in the autoclave which was made of chrome-nickel steel. This phenomenom became known as the "nickel effect". A systematic study of the effect of other transition metals was undertaken and in 1953 Ziegler discovered the low-pressure polymerisation of ethene.

The discovery of the "nickel effect" revolutionised organonickel chemistry. The nickel salt / aluminium alkyl became a standard catalyst in organic synthesis. In addition, the observation that the presence of acetylene prolonged the catalyst lifetime indicated that ligand molecules would play an important role in perfecting these catalytic systems.

In the following study aspects of the preparation, characterisation and catalytic application of a variety of coordination complexes are investigated. In doing so certain ligands of interest have been selected. Firstly, the ethylenediamine (en) ligand, although of apparently simple composition (NH_2-CH_2-CH_2-NH_2) has been found to form a wide range of transition metal complexes with amazing structural diversity. As a result there has been some disagreement over the assignment of the bands in the infrared spectra of these complexes which are now re-examined. Furthermore, various nickel complexes are prepared and tested as homogeneous catalysts in an effort to ascertain the effect of structure on activity.

Secondly, complexes of the transition metals with β-ketoenolate ligand systems have also been the subject of numerous infrared spectroscopic studies. To date, there is still uncertainty associated with the assignment of their infrared metal-ligand vibrations. In addition, the *bis*(2,4-pentanedionato)nickel(II) and related complexes have been the subject of much attention as olefin oligomerisation catalysts. A series of similar compounds are prepared, characterised by an in-depth analysis of their infrared spectra and studied as prospective homogeneous oligomerisation catalysts. The effect of incorporating a phosphine into the catalytic system is also investigated.

Certain advantages are associated with heterogenising nickel complex catalysts to allow ease of catalyst separation from the reaction mixture. Accordingly, polymer supported analogues of two of the above systems are prepared, extensively characterised, and tested as olefin oligomerisation catalysts.

1.1 INFRARED SPECTROSCOPY

Infrared spectroscopy, since its inception, has proved to be an invaluable chemical tool. It has widespread application in compound identification, structure determination and quantitative analysis.

The middle- and far-infrared regions (4000-50 cm^{-1}) are most frequently studied as they provide extensive information on the structure and identification of the compound. The vibrational or rotational motion of molecules (with the exception of homonuclear species such as N_2 or Cl_2) causes a net change in dipole moment. A field is thus established which may interact with the electrical field associated with applied infrared radiation. If the frequency of the infrared radiation matches a natural vibrational frequency of the molecule, an energy transfer results causing a change in the amplitude of the molecular vibration. This is recorded as an absorption of radiation.

Molecular vibrations can be divided into two categories:

Stretching; which involves a continuous change in the interatomic distance along the bond axis
Bending; which involves a change in the angle between two bonds.

In addition, vibrational coupling can occur and this may change the characteristics of the vibration involved.

The precise assignment of bands in the infrared spectra of transition metal complexes to vibrations of specific atoms, is of value in determining direct information regarding many structural and bonding features. Interpretation of the spectra is complicated by intermolecular interactions, lowering of symmetry and extensive vibrational coupling. Assignment of the metal-ligand (M-L) modes is of particular interest with regard to the nature of the coordination within the metal complex. In addition to the relatively weak nature of the M-L bond, the high mass of the metal ion causes M-L vibrations to occur at low wavenumbers where further complications may arise due to the occurrence of lattice modes [1,2,3].

1.1.1 Group Theory

On approaching the assignment problem, the application of group theory to any one molecule of known symmetry elements allows for the prediction of the number of vibrational modes [4-7]. Each molecule is characterised by certain symmetry elements which determine the point group to which the molecule belongs. For each point group there is a character table on which the vibrational analysis is based, giving the number and symmetries of stretching and bending modes and their Raman and infrared activities. Group Theory is thus a quantitative discussion of symmetry.

Consider a molecule composed of N atoms. The movements of each atom may be resolved into components along the x-, y- and z-axes, resulting in a total of $3N$ possible movements in the molecule. Of these, six (for non-linear molecules) are translational and rotational while the remaining $3N$-6 are internal molecular vibrations. The symmetries of these vibrational modes are categorised by labelling each atom within the molecule with three Cartesian coordinates representing unit displacement vectors. On performing the symmetry operations of the molecular point group, $3N$ x $3N$ matrices arise, the character (χ) of each of which forms a reducible representation (Γ_{total}) of the point group.

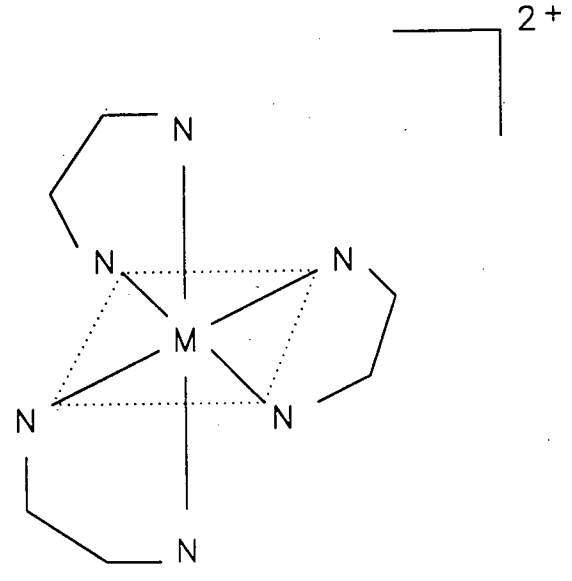

Figure 1.1 Octahedral $[Ni(en)_3]^{2+}$ with D_3 symmetry.

Consider more specifically the octahedral molecule $[Ni(en)_3]^{2+}$ (Fig. 1.1) which will be examined in Chapter 4.

D_3	E	$2C_3(z)$	$3C_2$
Γ_{total}	111	0	-3

To determine the symmetry species of all the possible molecular motions, the following reduction formula is used:

$$n_i = 1/h \; \Sigma \; \chi_R \; \chi_I \; N$$

where:

n_i = the number of times each irreducible representation appears in the reducible representation,

h = the point group order,

χ_R = the character of the reducible representation,

χ_I = the character of the irreducible representation,

N = the number of symmetry operations in each class.

Thus the 70 possible molecular motions for $[Ni(en)_3]^{2+}$ are:

$$\Gamma_{3N} = 18 \; A_1 + 19 \; A_2 + 37 \; E.$$

The irreducible representations relating to translation and rotation are listed in character tables. The representations responsible for vibrations are obtained by removing those responsible for translation and rotation.

For the molecule $[Ni(en)_3]^{2+}$;

Symmetries for all molecular motions:	$18 \; A_1 + 19 \; A_2 + 37 \; E$
Symmetries for translations:	$A_2 + E$
Symmetries for rotations:	$A_2 \quad E$
Symmetries for vibrations (Γ_{vib})	$18 \; A_1 + 17 \; A_2 + 35 \; E$

To determine the number of stretches and bends which constitute Γ_{vib}, internal displacement vectors are chosen as a new basis for point group representation. A reducible representation for the stretches is generated by vectors drawn along the bonds. Any vector unaffected by a symmetry operation contributes +1 to the matrix character, while any vector affected contributes zero. For $[Ni(en)_3]^{2+}$ this yields:

D_3	E	$2C_3(z)$	$3C_2$
$\Gamma_{stretch}$	39	0	1

which reduces to:

$$\Gamma_{stretch} = 7\ A_1 + 6\ A_2 + 13\ E.$$

Subtraction of $\Gamma_{stretch}$ from Γ_{vib} yields:

$$\Gamma_{bend} = 11\ A_1 + 11\ A_2 + 22\ E.$$

Infrared and Raman activities of vibrational modes are associated with accompanying changes concerning dipole moments and polarisability of the bonds, respectively. This can be read directly from the character table, any irreducible representation having the transformation properties of x, y or z being infrared active and one having transformation properties of x^2, y^2, z^2, xy, xz or yz being Raman active.

Thus for $[Ni(en)_3]^{2+}$, the 17 A_2 and 35 E bands will be infrared active giving a total of 52 predicted bands in the infrared spectrum. The 18 A_1 and 35 E bands will be Raman active. A total of 53 bands are thus predicted to be Raman active, 35 of which will be coincident with those observed in the infrared spectrum.

The conditions described above assume the molecule to be an isolated unit [4]. When a molecule occupies a site in a crystal it cannot be regarded as a separate entity, since the solid environment imposes its own symmetry restrictions. For a rigorous vibrational analysis the entire array of molecules should be considered, which is an impossible

task. However, two approximations, site group and factor group analysis may be used.

The site group approximation [8] ignores the intermolecular interactions but considers the symmetry of the surroundings of the molecule. The site symmetry, which is generally lower than the molecular symmetry, may be found if the space group, the point group of the isolated molecule, and the number of molecules per unit cell are known. Halford [8] derived tables listing possible site symmetries. On the grounds of a change in selection rules, vibrations forbidden by molecular symmetry may appear as weak bands if allowed by site symmetry.

Factor group analysis [9] is a more rigorous approximation as it considers the intermolecular interactions. In doing so it accounts for lattice modes and solid state splitting of non-degenerate vibrations of the free molecule. Factor group analysis is thus mainly applicable to neutral molecules with highly dipole-active oscillators in which the above splitting is significant [10].

The vibrational spectrum of a metal complex may be understood by considering the molecular symmetry, with possible activation of the forbidden vibrations through the lowering of molecular group symmetry. The data obtained from Group Theory thus provides us with a base from which to work when approaching the assignment problem.

1.1.2 Techniques Applied to the Assignment Problem

1.1.2.1 Comparison between Spectra of the Free Ligand and the Complex

Bands in the spectrum of the complex, that are absent from the spectrum of the free ligand, may be tentatively assigned as M-L modes. This method is limited by possible activation of some ligand vibrations, forbidden by the molecular symmetry of the ligand but allowed by the molecular symmetry of the complex. These may occur in the same region as M-L vibrations [10] and may result in incorrect assignments.

1.1.2.2 Comparison between Spectra of Isostructural Complexes

On the basis of symmetry considerations isostructural complexes should give rise to similar vibrational spectra, the changes in band position being determined by changes in the nature of bonding. Three variations may be applied.

Metal Ion Substitution

For isostructural complexes of identical ligands with differing metals, the M-L vibrations shift according to the properties of the metals. A theoretical study of the electrostatic repulsion between the electrons of the ligand orbitals and the metal orbitals in transition metal complexes has led to the development of Crystal Field Theory (CFT). This repulsion destroys the degeneracy of the five *d*-orbitals giving rise to orbitals of differing energies [11] [Fig. 1.2(a)]. The stability of transition metal complexes varies according to the electron population of the split orbitals. Only the *d*-orbitals are considered as the order of splitting in the *f*-orbitals is ten or twenty times less than in the *d*-orbitals and the *p*-orbitals are not split by the crystal field.

For example, in an octahedral environment, the crystal field splits into two sets with an energy difference given by $10Dq$ [Fig. 1.2(b)]. Three degenerate orbitals (t_{2g}), stabilised by $4Dq$, and two degenerate orbitals (e_g), destabilised by $6Dq$, result. As electrons preferentially occupy orbitals of low energy an overall stabilisation of the system occurs. Exceptions to this are the d^0, d^{10} and high spin d^5 systems in which the stabilisation effect of the t_{2g} electrons is offset by those in the e_g orbitals. The energy decrease resulting from this stabilisation is termed the crystal field stabilisation energy (CFSE).

In an octahedral environment the CFSE is given by [11]:

$$CFSE = -(0.4n_{t_{2g}} - 0.6n_{e_g})10Dq$$

where $n_{t_{2g}}$ and n_{e_g} are the numbers of t_{2g} and e_g electrons, respectively.

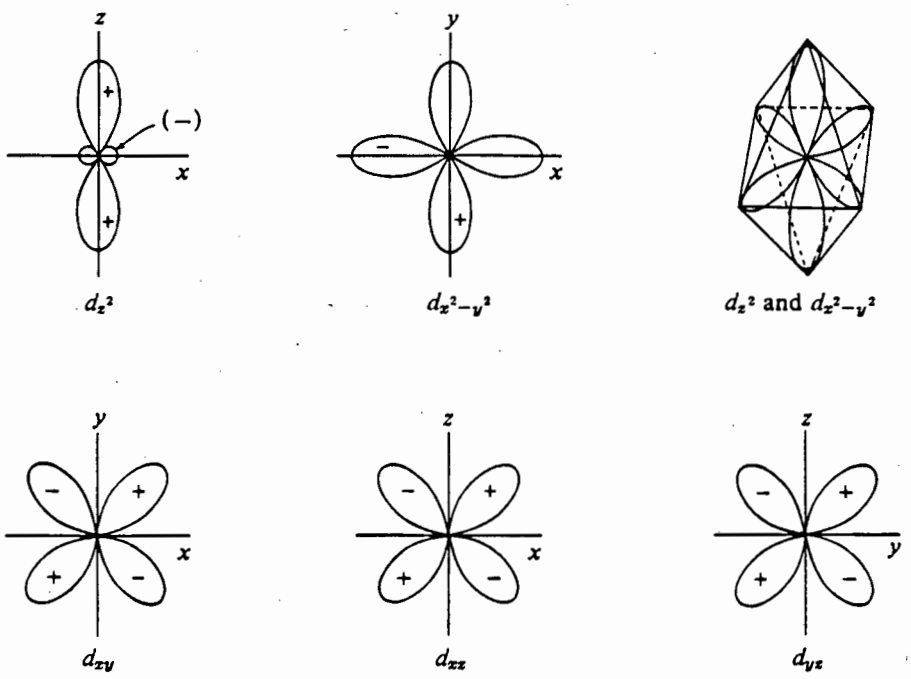

Figure 1.2(a) The *d*-orbitals.

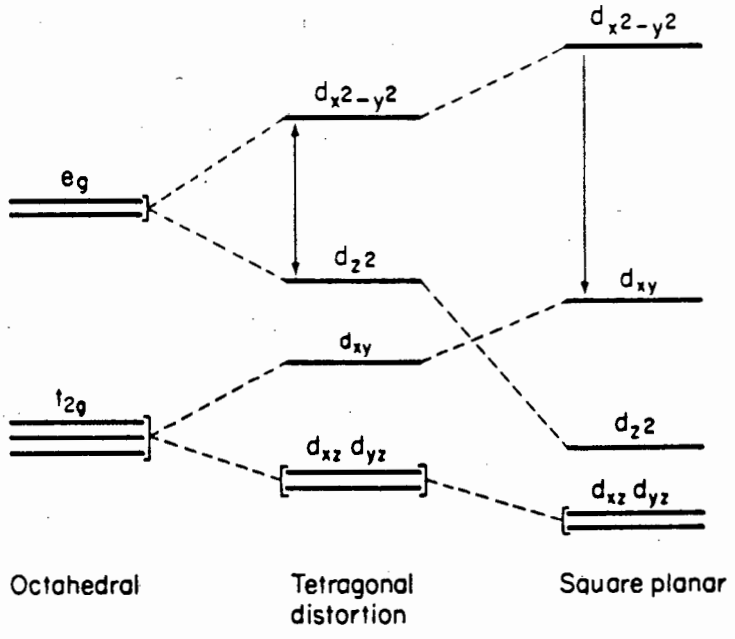

Figure 1.2(b) Splitting of *d*-orbitals in various types of complex.

The crystal field splitting parameter, $10Dq$, may be calculated from the relationship [13]

$$10Dq = fg$$

where f is a measure of the crystal field splitting power of the ligand relative to that of water ($f = 1$) and g is the spectroscopically determined magnitude of $10Dq$ for the octahedrally hydrated metal ion. The CFSE of tetrahedral complexes may be calculated in a similar manner.

Although CFSE is only a small contribution to the total bonding energy of the metal complex, other effects vary linearly through a series of complexes in which the transition metal ion is varied from d^0 to d^{10}. The CFSE is therefore superimposed on a reasonably constant or uniformly varying energy system. It is thus possible to distinguish crystal field effects from others which occur simultaneously.

Since CFSE influences M-L bond strength, the M-L force constants of an isostructural series of complexes with varying metals are expected to exhibit a variation with d-orbital population similar to that shown by thermodynamic properties [12,14]. In the absence of a significant mass effect, this same variation should hold for the M-L stretching frequencies (νM-L) in the infrared spectra of these complexes.

This has been shown to be the case by Thornton and co-workers [14-25] for several transition metal complex systems. Variations of νM-O have been found to correlate with the relative CFSE values of trivalent first transition metal acac complexes [14] (acac = 2,4-pentanedionate). Similar correlations have been obtained for νM-L in several series of divalent and trivalent metal tropolonate complexes [15], in divalent metal β-ketoenolates and their nitrogenous base adducts [16], divalent metal 2,2′-bipyridyl and 1,10-phenanthrolyl complexes [17], 2-thenoyltrifluoro-2,4-pentanedionates [18], anthranilates [19] and γ-substituted–acac complexes [20]. Studies have also extended to the second transition series for several complexes [21-25].

Ligand Substitution

For isostructural complexes of a particular metal with a range of similar ligands, vibrational frequencies are expected to appear in a similar pattern within a relatively narrow frequency range. This method is usually applied to a range of complexes with substituted ligands and has been used to assign νNi-O in substituted pyridine adducts of nickel complexes of acac [26] and νM-O in other metal β-ketoenolate complexes [27].

Halogen Substitution

For isostructural complexes containing coordinated halogens, the large change in the masses of the halogen ligand yields dramatic shifts in the metal-halogen vibrations. This allows for their easy identification [28,29].

1.1.2.3 Isotopic Labelling

Replacement of an atom by one of its isotopes results in a change in any vibration involving that atom. The expected shift of the band can be calculated by assuming the isotopically labelled atom (i) to be part of a simple harmonic diatomic molecule [30]. The vibrational frequency (ν) of such a molecule is represented by:

$$\nu = \frac{1}{2\pi c}\left[\frac{f}{\mu}\right]^{1/2}$$

while that for the isotopically labelled system is given by:

$$\nu^{i} = \frac{1}{2\pi c}\left[\frac{f}{\mu^{i}}\right]^{1/2}$$

where f = the harmonic force constant
μ = the reduced mass of the molecule
c = the velocity of light.

Assuming the force constants are unaltered by isotopic substitutions, the expected isotopic shifts may be calculated from:

$$\frac{\nu^i}{\nu} = \left[\frac{\mu}{\mu^i}\right]^{1/2}$$

where ν^i is always taken to be the heavier isotopomer [30].

Certain conditions affect the accuracy of the ν^i/ν ratio, namely, the number and nature of labelled atoms, the extent to which a labelled atom participates in a particular vibration and the extent of vibrational coupling.

Metal Isotopes

Isotopic labelling of the metal ion is a particularly powerful technique for assigning the metal-ligand vibrations [31]. Since the magnitude of the isotopic shift is dependent on the mass difference between the isotopes, isotopic pairs with the greatest mass difference are preferred. The metal isotopes $^{57}Fe/^{54}Fe$, $^{62}Ni/^{58}Ni$, $^{68}Zn/^{64}Zn$ and $^{53}Cr/^{50}Cr$ have been successfully employed to aid vibrational assignments [31-34]. Metal isotopic labelling has not been found to be as effective for the assignment of M-L bending vibrations [31]. This is probably due to the limitations of the simple harmonic diatomic molecule approximation [35]. Other limiting factors are the cost and limited availability of pure and stable metal isotopes.

Isotopically Labelled Ligands

Ligand isotopic labelling allows assignment of internal ligand vibrations as well as M-L modes. The greatest isotopic shifts can be expected for deuterated and tritiated molecules as these have the largest mass difference. The ligand donor isotopes ^{18}O and ^{15}N are frequently used and although the effect is not as large as on deuteration, shifts of up to 40 cm^{-1} in $^{18}O/^{16}O$-labelling have been

observed [30]. Multiple isotopic labelling [36-38] allows a complete understanding of the vibrational purity of the fundamental vibrations. A disadvantage of the ligand labelling technique is that low wavenumber bands originating from ligand vibrations and involving the donor atom may be erroneously assigned to M-L modes.

Lever *et al.* [39,40] have applied metal labelling to infrared studies of amino acid and diamine complexes while Hutchinson *et al.* [41] have carried out related studies on metal tropolonates. Labelling of the ligand donor atom has been used successfully in a wide variety of studies [19,25,42-45] such as assigning νM-L in salicylaldimine, tropolonate, 2,4-pentanedionate and anthranilate complexes. Isotopic labelling is thus an unambiguous and simple method of assigning bands in infrared spectra.

1.1.2.4 ν^D/ν^H Ratio

Ligand deuteration in a metal complex may yield further information about the ligand modes. Based on the simple harmonic diatomic oscillator, Thornton and co-workers [46,47] have examined the ν^D/ν^H ratio for several complexes of heterocyclic bases. The results of their studies may be summarised as follows:

(a) the ν^D/ν^H ratio lies within the range 0.68 to 0.85 for C-H modes,
(b) the ν^D/ν^H ratio lies within the range 0.85 to 1.00 for the ring modes.

This ratio serves as an effective distinction between C-H stretching (or bending) modes and ring stretching (or bending) modes. In addition, the ratio gives an indication of the degree of coupling between the vibrations. A lowering of the skeletal (ring) ratio from unity implies coupling to the C-H vibration [48]. Similarly, the C-H ratio is raised from 0.73 (the theoretical value) by coupling to a less sensitive skeletal vibration. Values of less than 0.73 may indicate a change in the nature of coupling as a result of labelling [48,49].

Although based on a simplistic model, the ν^D/ν^H ratio is helpful when used in conjunction with other more rigorous methods.

1.1.2.5 Normal Coordinate Analysis

A theoretical test of vibrational assignment is to model the molecule by normal coordinate analysis. Normal coordinate treatment by Wilson's *GF* matrix method [50,51] derives an equation as an expression of force constant:

$$|GF - E\lambda| = 0$$

where F = a matrix of force constants and normal coordinates,
G = a matrix involving molecular geometry and atomic mass,
E = the unit matrix,
λ = the frequency parameter ($4\pi^2c^2\omega^2$).

Difficulties arise as, when the matrix is expanded, there are many more terms involving the force constant than there are vibrational frequencies. Interactions between certain atoms giving rise to less important terms must thus be excluded [51].

The most commonly used analysis methods are various modifications of the Valence Force Field (VFF) and the Urey-Bradley Force Field (UBFF) analysis. The basic VFF assumption is that there is no interaction between the stretching and bending motions in the molecule (*i.e.* the off-diagonal elements in the *GF* matrix are zero) [50,51]. The UBFF combines the above assumption with the postulate that there are also important interactions between non-bonded atoms [50,51]. The methods lead to comparable results with very little difference between the Cartesian displacements produced by each [52].

The difficulty in evaluating the force constants used in the modelling of a molecule may be demonstrated by two normal coordinate analyses conducted by Nakamoto and co-workers. In their earlier work Nakamoto and Martell [53] used a simple UBFF calculation, while in their later work Nakamoto and Behnke [54] used a modified UBFF calculation. A

comparison of the data obtained (see Table 1.1) shows that the conclusions are contradictory.

Table 1.1 Normal coordinate analyses of complexes of acac.

1960 Calculations [53]		1967 Calculations [54]	
Frequency	**Assignment**	**Frequency**	**Assignment**
$1580cm^{-1}$	C=C asym. stretch (B_2)	$1563cm^{-1}$	C=O sym. stretch (A_1)
$1554cm^{-1}$	C=O sym. stretch (A_1)	$1538cm^{-1}$	C=C asym. stretch (B_2)
$1534cm^{-1}$	C=O asym. stretch (B_2)	$1429cm^{-1}$	C-CH_3 deg. def
$1415cm^{-1}$	C-CH_3 deg. def	$1380cm^{-1}$	C=O asym. stretch (B_2)
$1274cm^{-1}$	C=C sym. stretch (A_1)	$1288cm^{-1}$	C=C sym. stretch (A_1)

Differences:

1) Assignment of the C=O and C=C stretches above 1500 cm^{-1} are interchanged.
2) Assignment of the C-CH_3 degenerate deformation and the lower C=O stretch are interchanged.

The 1960 calculation was disproved by ^{18}O-labelling of [$Cu(acac)_2$] [44] which showed that the higher frequency component of the double absorption in the carbonyl region underwent a greater shift on ^{18}O-labelling than the lower frequency component. This suggests that the former is the νC=O mode and the latter νC=C. This led to a revision of the normal coordinate analysis in 1967 and highlights the advantage of applying several techniques to the band assignment problem thereby obtaining the most accurate results.

Of the techniques discussed, no single one is sufficient to allow completely unambiguous band assignment. Each is characterised by unavoidable pitfalls which limit the degree of certainty with which bands may be assigned. In the following study several of the above techniques are applied in an effort to overcome the limitations of each.

1.2 CATALYSIS

Olefins, particularly ethene, propene and butene, have been key building blocks in the petrochemical industry since its inception. In addition to their relatively low cost and ready availability, their reactivity allows for easy conversion to a wide range of useful products. More recently, the higher molecular weight linear alpha-olefins, generally in the range C_6 to C_{20}, have become desirable. For example, 1-decene serves as the basis for automatic synthetic lubricating oils which have extended change intervals to 12000 miles. 1-Dodecene and higher molecular weight alpha-olefins are useful in making a variety of biodegradable surfactants which have extensive household and industrial application.

In South Africa at present, the wide use of diesel in heavy transport and agriculture has created a large commercial demand for diesel fuels. It is thus of interest to use the significant amount of short chain olefins, in particular propene, produced as a by-product of the Fischer-Tropsch process in the manufacture of gasoline [55]. Oligomerisation of olefins is a general term applied to the chemical process of converting lower olefins to a higher molecular weight olefin product. Despite the fact that oligomerisation is indeed a feasible process, pure olefins are almost indefinitely stable at reasonable temperatures. A suitable catalyst is therefore necessary for what would otherwise be a very slow process. Olefin oligomerisation may be effected in a number of different ways depending on the catalyst used. The more widely studied systems are base catalysis, acid catalysis, organometallic synthesis and coordination complex catalysis.

Base Catalysis

Base catalysis, or anionic oligomerisation, has undergone considerable development as it allows for the preparation of 4-methyl-1-pentene, an intermediate in organic synthesis, from propene. The catalysts are usually alkali metals in the form of dispersions in hydrocarbon media

[56-59] or supported on carriers such as graphite or alumina [60]. Propene dimerisation is a three step process (Fig. 1.3).

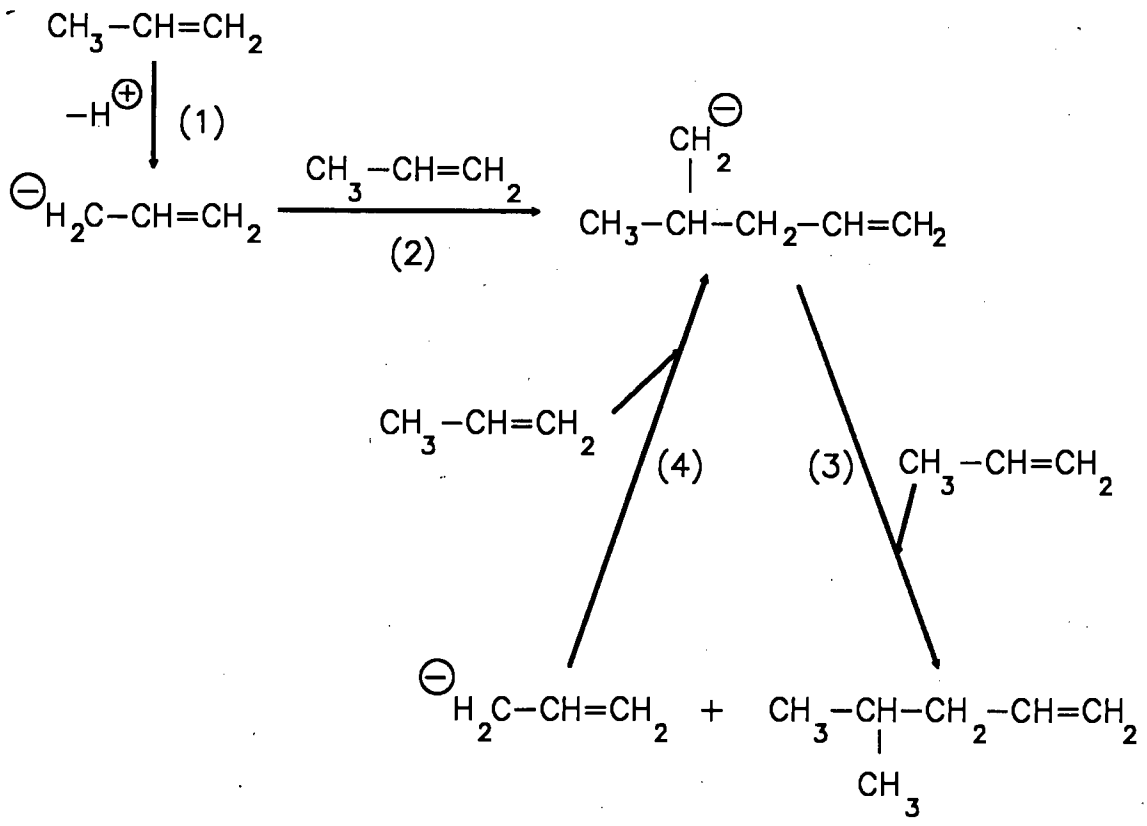

Figure 1.3 Mechanism of anionic propene dimerisation.

1. Initiation: a resonance stabilised allylic ion is preferentially formed.
2. Nucleophilic addition: occurs according to Markownikoff's rule.
3. Proton abstraction: yielding the dimer and new allylic ion.

The above reaction, at 200°C and 200 atm, exhibits 99% selectivity to 2-methyl-1-pentene, with very little polyaddition or isomerisation occurring [61].

Although the catalysts exhibit high product selectivity, only branched isomers are formed with none of the desirable linear alpha-olefins. In addition, the catalytic reaction is slow, thus necessitating the use of high temperatures (150-200°C) and pressures (50-200 atm) as well as long contact times.

Acid Catalysis

Acid catalysts, or cationic oligomerisation catalysts, are used extensively for the industrial production of olefin oligomers, *e.g.* isobutene dimers, propene trimers and tetramers and other products used as motor fuel constituents. Typical catalysts are mineral acids such as sulphuric and phosphoric acid. These may be used in the free form or chemically fixed to the surface of solid supports. In addition, Lewis acids such as BF_3, $AlCl_3$ and $ZnBr_2$ [62] catalyse oligomerisation. The true catalytic species in most of these Lewis acid systems is probably the super-acid formed in the presence of a proton source which is necessary for all acid catalysts. Dimerisation is again a three step process [63] (Fig. 1.4).

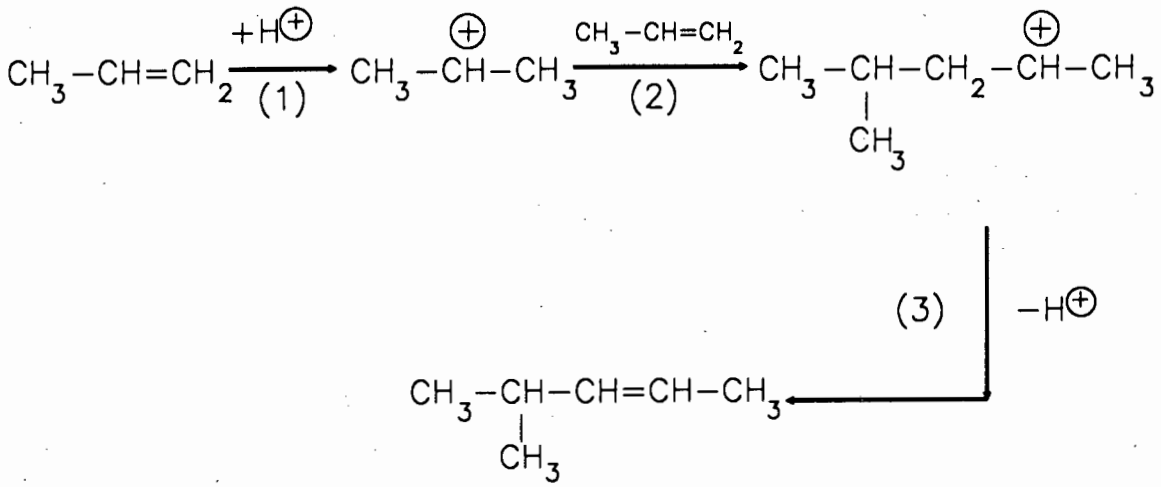

1. Initiation: Proton addition follows Markownikoff's rule.
2. Addition of the carbonium ion to the olefinic bond: This again follows Markownikoff's rule.
3. Proton elimination: This follows Saytseff's rule.

Figure 1.4 Mechanism of cationic propene dimerisation.

The carbonium ions formed are not stable and undergo extensive rearrangement to a number of possible ions [64]. As a result, in addition to producing only branched olefins, the reaction exhibits little selectivity. Internal olefins readily undergo oligomerisation

reactions *via* acid catalysis, whereas under similar conditions, ethene, for example, may remain unreacted.

Organometallic Synthesis

Organometallic synthesis has found extensive use in both olefin dimerisation [65] and production of higher oligomers. By reacting aluminium hydride and aluminium alkyl compounds with ethene, Ziegler *et al.* [66] synthesised organoaluminium compounds with growing alkyl groups attached to the metal. This "aufbau" reaction proceeds with high selectivity as long as the upper temperature limit is 200°C. When this method is applied to propene dimerisation at 180-200°C and 170-200 atm the selectivity for 2-methyl-1-pentene exceeds 99%.

Little is known about the true mechanism of organometallic synthesis but a basic three step process can be used to represent propene dimerisation (Fig. 1.5).

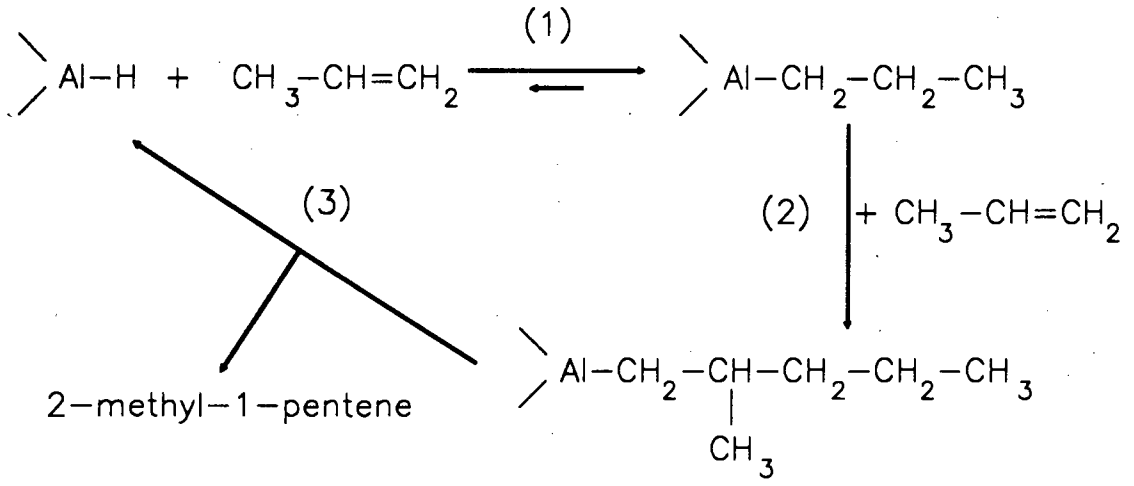

Figure 1.5 Proposed mechanism for propene dimerisation.

1. Initiation: A pre-established equilibrium lying essentially on the product side.
2. Carbon-carbon bond formation: This is seen as the rate limiting step.
3. β-Hydrogen elimination: This is fast, leading to very little polyaddition.

Under technical process conditions the hourly production is about 20g dimer per gram Al present.

Although control of this type of reaction appears possible and higher α-olefins can be dimerised, the product formed consists solely of β-carbon branched α-olefins [67].

Coordination Catalysis

In 1961 a method of ethene oligomerisation using soluble catalytic systems based on alkylaluminium halides and nickel compounds was proposed [68]. This marked the beginning of coordination catalysis and in subsequent years numerous reports and patents were filed on the subject [69-72]. These complex catalysts are extremely active towards dimerisation and oligomerisation of olefins under mild reaction conditions. In addition, changing the environment of the nickel atom, (the catalytic centre) enables remarkable control of selectivity and activity. These catalysts appear to have enormous potential in the synthesis of straight chain oligomers and, as a result, are the main thrust of this work.

1.2.1 Homogeneous Coordination Catalysis

1.2.1.1 Mechanistic Considerations

The mechanism of coordination catalysis is still not fully understood. The question is complicated by the fact that the same species catalyse numerous types of reaction, *e.g.* dimerisation, isomerisation, molecular rearrangements and even hydrogenation.

Olefin Oligomerisation

A common feature of all the active systems is the presence of a Ni-H or Ni-alkyl bond which is believed to be responsible for the initiation of the catalytic reaction [72(a),(b)]. (This is not necessarily the case when employing halide-free organoaluminium compounds or other low strength Lewis acids). Various oligomerisation mechanisms have been discussed [73] of which the β-hydrogen elimination mechanism (Fig. 1.6) is the most generally accepted [72].

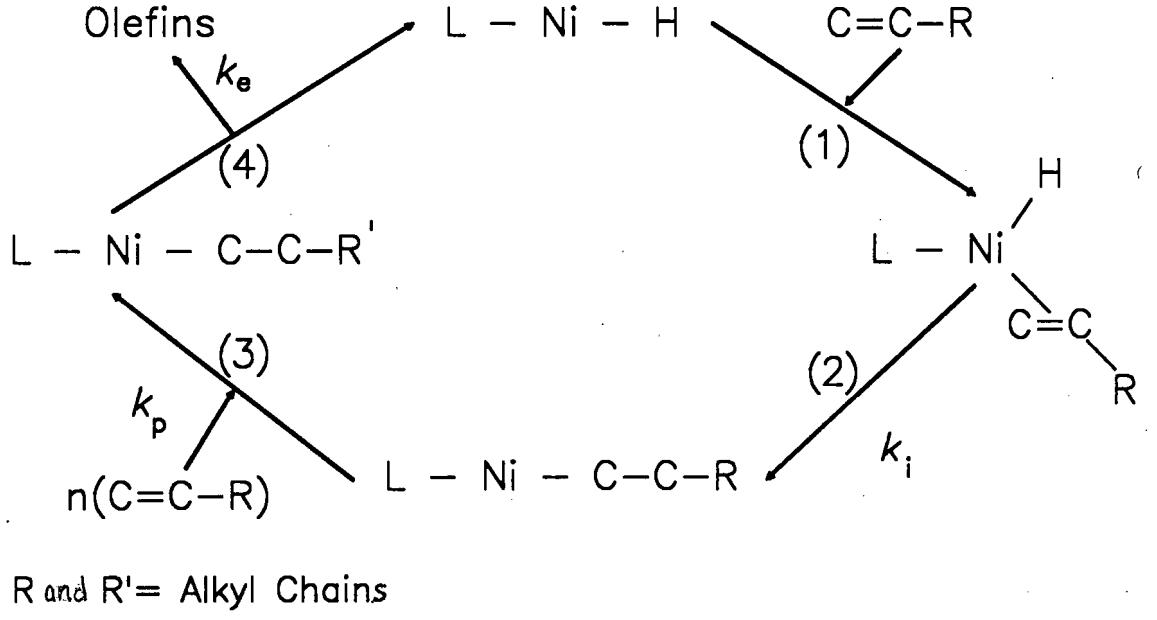

Figure 1.6 Mechanism of coordinative olefin oligomerisation.

1. Coordination of an olefin at a free coordination site.
2. Insertion of the olefin into the Ni-H bond.
3. Propagation of the reaction by insertion of further olefins into the Ni-alkyl bond.
4. Elimination of the oligomers by β-hydrogen elimination.

The relative values of k_p and k_e determine the molecular weight distribution of the products. If $k_p >> k_e$ a considerable number of insertion steps occur and higher olefins are formed. Alternatively if $k_p << k_e$, dimers and trimers predominate.

The reaction of unsymmetrical alkenes can result in a mixture of primary products depending on the direction of addition of the nickel hydride (Ni→H) to the alkene (Fig. 1.7). The initial hydride migration step can occur to give either a branched alkyl product ($H \rightarrow C_1$, $Ni \rightarrow C_2$) or a linear alkyl product ($H \rightarrow C_2$, $Ni \rightarrow C_1$). This step is reversible, and the ratio of the two species can be controlled thermodynamically and kinetically [74]. Similarly, alkene migration, implicit in the next step of the reaction, can also occur in two distinct directions giving four nickel alkyl intermediates. From these, after β-H elimination, 8 primary products are formed. In hexene dimerisation *cis-trans* as well as double bond isomerisation results in 72 possible C_{12} isomers.

Crystallographic determination of the complex formed on reaction of π-allylnickel chloride, PPh_3 (Ph = phenyl) and $AlMeCl_2$ (Me = CH_3) showed that the phosphine was bonded to the nickel and that interaction with the Lewis acid occurred *via* a chlorine bridge. The ligands adopt an essentially square planar arrangement around the nickel. On the basis of this and a large amount of experimental evidence [74] the most probable structure of the active complex for the phosphine-modified and phosphine-free catalysts are as represented in Fig. 1.8.

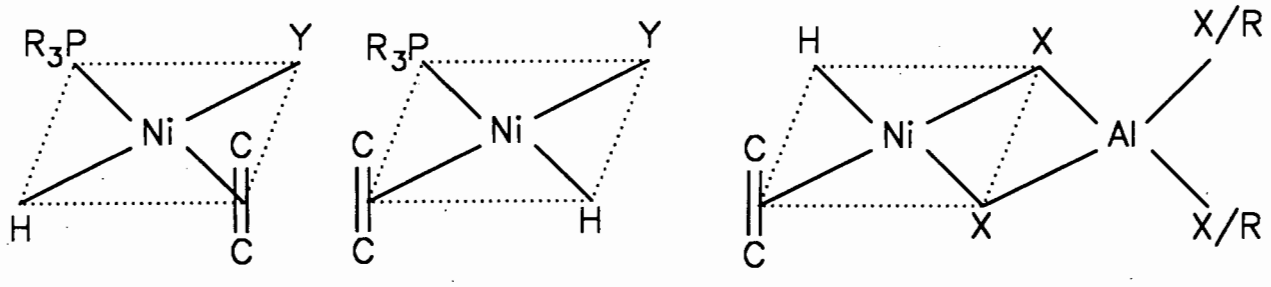

A **B** **C**

Y = Negatively charged component of active complex; usually an Al atom with its surrounding ligands,

X = anionic ligand; usually a halide.

Figure 1.8 Proposed active species in nickel complex catalysis.

A = Coordination of olefin *trans* to the phosphine ligand.

B = Coordination of olefin *cis* to the phosphine ligand.

C = Active complex in the phosphine-free system.

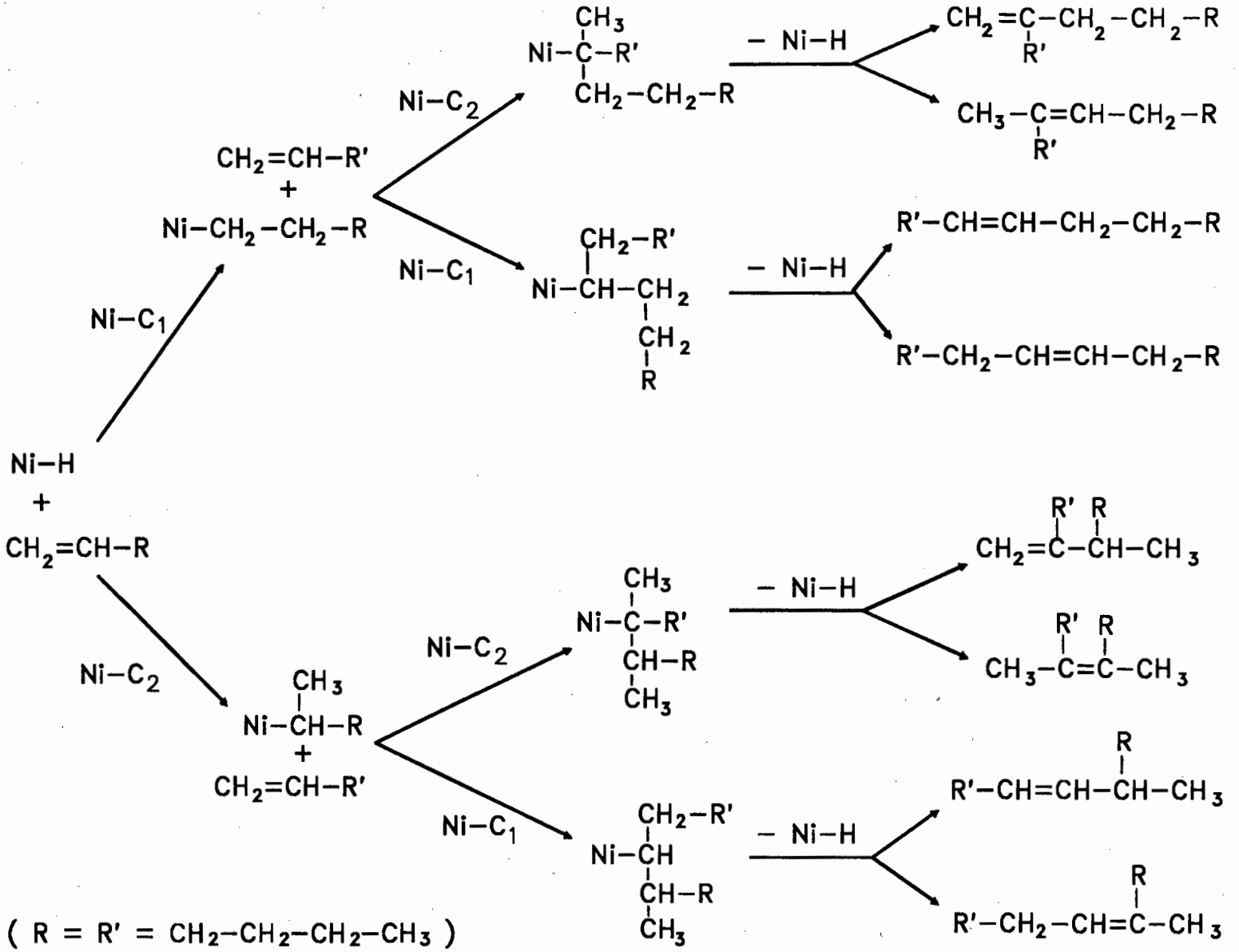

Figure 1.7 Scheme for the nickel catalysed dimerisation of 1-hexene.

It is possible that both A and B are catalytically active species and that differences observed in catalytic properties of systems having different ligands are due to variations in the population of A and B. By altering such ligands selectivity may be controlled. The functions and effects of the various ligands on the catalytic reaction will be discussed later.

Interesting deviations from the above proposed active species are those systems in which a halide-free aluminium compound of low Lewis acidity is used, *e.g.* $AlEt_3$ (Et = C_2H_5), $AlEt_2(OEt)$ [75] and $Al(i\text{-}Bu)_3$ (Bu = C_4H_9) [76]. Jones and Symes [75] studied the reaction of a $[Ni(acac)_2]$ / $AlEt_2(OEt)$ system. For ethene, propene, 1-butene and 1-hexene monomers, products of over 80% linearity were obtained. They proposed that the catalytic species is based on [Ni(acac)Et] which is stabilised by complex formation with the aluminium species and an olefin molecule. The complex in Fig. 1.9 may be envisaged as the active species.

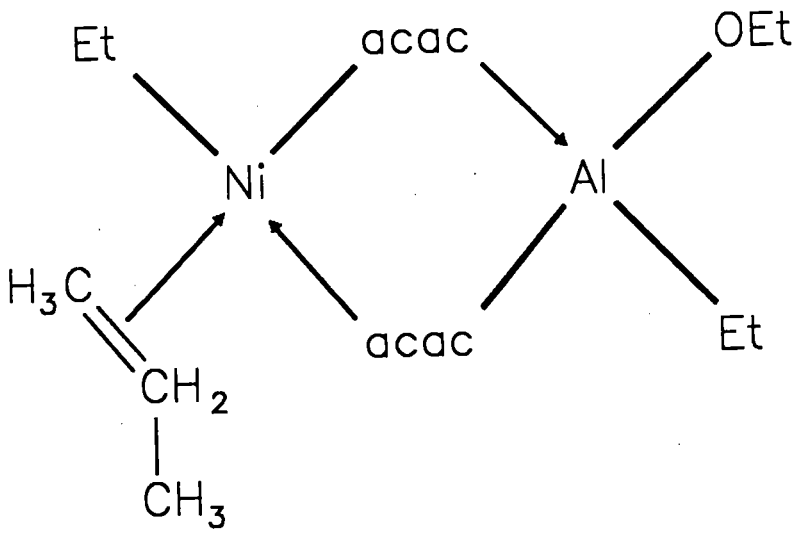

Figure 1.9 Proposed active species for halide-free systems.

There is no direct evidence for the bridging acac groups but the observed infrared frequencies of the metal-oxygen band, as well as the specific effects of β-ketoenolate groups, may well be related to the varying stabilities of the bridged complexes formed.

The mechanism involves an insertion into a Ni-H species formed from the Ni-Et bond. For dimerisation, the emergence of linear olefins as the primary product is contrary to the preferred spatial alignment for insertion. This may be explained by assuming that two olefin molecules are coordinated to nickel in a sterically preferred head to head arrangement [(A) in Fig. 1.10]. Once the rate determining step (1) has occurred, step (2) follows in such quick succession that there is no time for reorientation of the second olefin molecule.

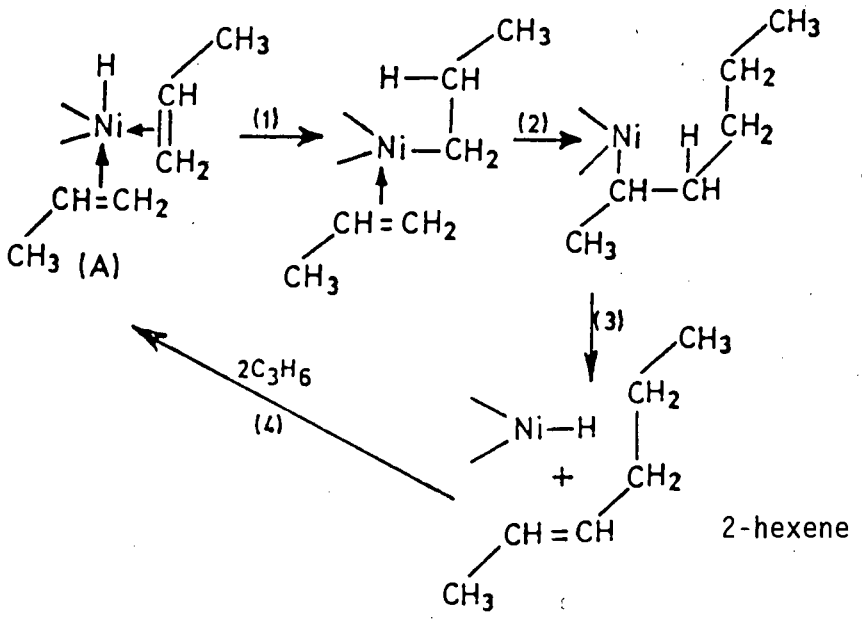

Figure 1.10 Mechanism of linear olefin dimerisation.

Contrary to this, Zhou *et al.* [76], investigated the [Ni(hfacac)$_2$] / Al(*i*-Bu$_3$) system (hfacac = hexafluoroacetylacetonate), and suggested that the mechanism of halide-free systems is similar to that of a halide-containing system, with the "steering" effect of the *β*-ketoenolate enforcing the unfavoured sequence of Ni→C$_1$ followed by Ni→C$_2$ addition (See Fig. 1.7). The mechanism proposed by Jones and Symes is supported when a nickelcyclopentane intermediate is invoked to explain the formation of cyclobutane [77]. It has also been shown stoichiometrically that nickelcyclopentane derivatives can be formed from *bis*(alkene)nickel complexes and, under suitable conditions, a hydride transfer causes decomposition to linear products [78].

Olefin Isomerisation

An inherent feature of coordination catalysts is their ability to isomerise olefins with respect to their *cis-trans* configuration as well as the position of the double bond [71]. In contrast to oligomerisation, isomerisation is an "easy" reaction which does not require the presence of a specific environment. A hydride addition-elimination sequence (Fig. 1.11) has been proposed as the mechanism for isomerisation.

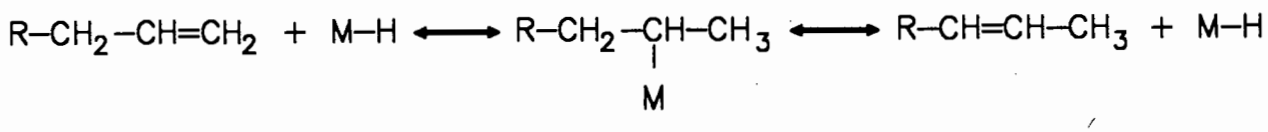

Figure 1.11 Addition-elimination mechanism for olefin isomerisation.

Isomerisation is observed in all cases of oligomerisation but has been specifically studied by some authors [79,80]. Generally speaking the straight chain olefins are readily brought to thermodynamic equilibrium without great differences in the rate of successive double bond migration steps along the chain. Butenes, for example, are isomerised up to their thermodynamic equilibrium before any dimerisation occurs. At 20°C this mixture will be 3.5% 1-butene, 23.5% *cis*-2-butene and 73% *trans*-2-butene. On the other hand, the presence of branching in the vicinity of the double bond decreases olefin reactivity and the passage of a double bond from or towards a tertiary carbon atom is comparatively slow. Hence, during isomerisation of 4-methyl-1-pentene, equilibrium is readily established between the carbons 1, 2 and 3 and is attained more slowly between all the isomers (Fig. 1.12).

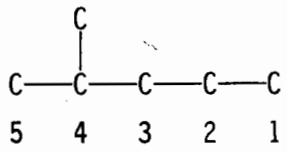

Figure 1.12 Carbon Skeleton of 4-methylpentene.

Cis-trans isomerisation is just as prevalent and generally occurs in a stepwise manner. The *cis*-isomer is formed initially and then isomerises, establishing an equilibrium in which the thermodynamically more stable *trans* form predominates.

Jones and Symes [75] found that using $[Ni(acac)_2]$ / $AlEt_2(OEt)$, 1-hexene isomerises to 2- and 3-hexene at twice the rate of dimerisation. When the β-ketoenolate ligand is altered, the relative rates of dimerisation and isomerisation of 1-hexene change. When the acac ligand is replaced by dibenzoylmethane, for example, the rate of isomerisation equals that of dimerisation [75].

1.2.1.2 Kinetics

Identifying the rate determining steps for the oligomerisation reaction is a precondition for influencing the rate and tailoring the catalyst. In addition, selectivity is a result of relative rates in the system.

Formation of metal-olefin complexes of the type in question is a rapid process. It is thus reasonable to analyse the general kinetics based on the assumption that the migratory insertion of olefins to M-C bonds represents the rate determining step and that all other steps are established in equilibrium. Assuming steady state kinetics in the reaction scheme shown in Fig. 1.13, the rate of dimerisation is given by equation (1).

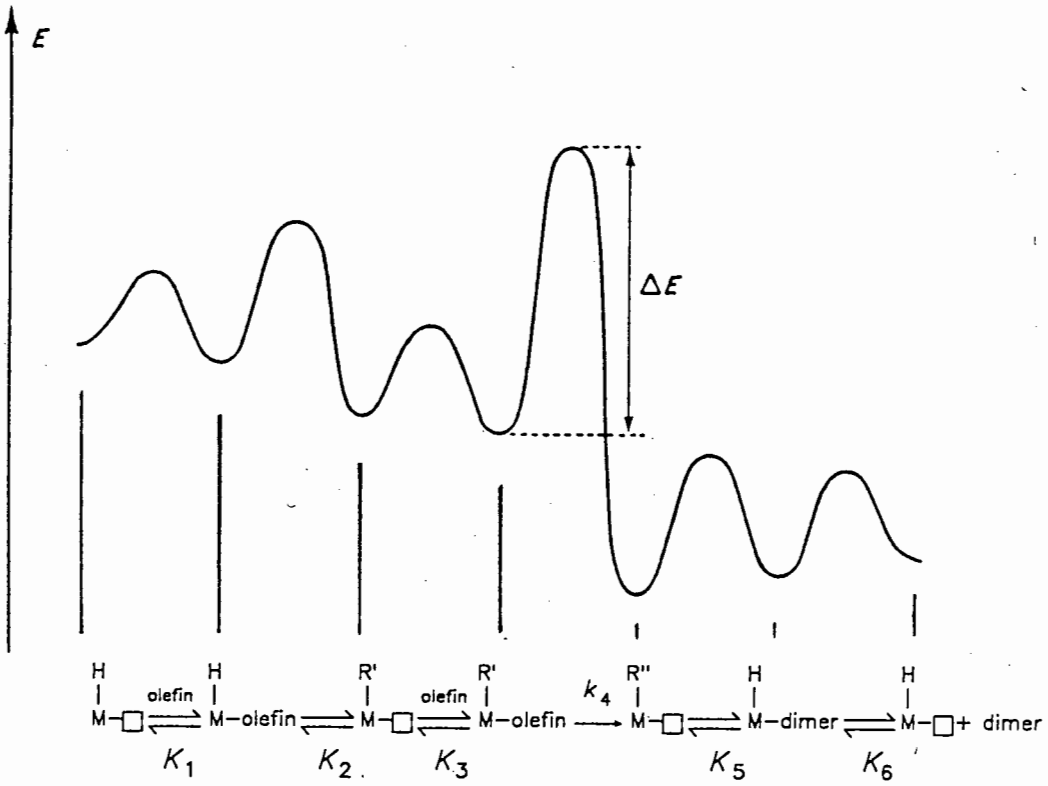

$$r_2 \sim k_4.K_1.K_2.K_3.[Ni]_{tot}.[M]^2 \qquad (1)$$

K = equilibrium constant

k_4 = rate constant for the rate limiting step

□ = free coordination site

M = monomer

Figure 1.13 Energy changes during dimerisation.

Consequently, if the concentration of active hydride having a free coordination site is proportional to the total concentration of the nickel present, the dimerisation rate should be first order in nickel and second order with respect to the concentration of monomer. This gives equation (2);

$$r_2 = f.k_4.K_1.K_2.K_3.[Ni]_{tot}.[M]^2 \qquad (2)$$

where $f = [Ni(□)H]/[Ni]_{tot}$.

Any factor that will decrease the concentration of the active hydride complex will retard the reaction. Consequently, the dimerisation

process is self-inhibiting in that olefinic dimers formed during the reaction will complex with [Ni(□)H] and therefore reduce its concentration.

Only a few reports concerning kinetic data have been published [72]. Observed kinetic orders with respect to monomer and nickel complex are in agreement with a "double insertion" mechanism in which migratory insertion represents the rate limiting step.

Again applying steady-state kinetics with the insertion step being rate limiting, the rate of trimerisation (r_3) is given by equation (3).

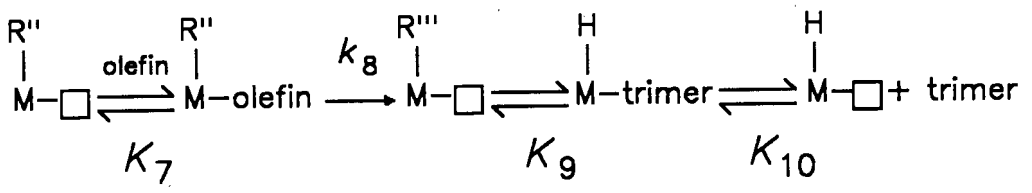

$$r_3 = k_8.K_5.K_6.K_7.[M(□)H].[M].[dimer] \qquad (3)$$

K = equilibrium constant
k_8 = rate constant for the rate limiting step
□ = free coordination site

Figure 1.14 Trimerisation rate.

Thus, as dimer concentration increases so does the rate of trimerisation. In addition, the observation that bulky ligands tend to favour dimerisation over trimerisation may be explained in the selective effect of bulky ligands to reduce the value of K_6.

No clear picture of the effect of Lewis acid concentration on reaction rate is available. It has been suggested that, since Lewis acids are usually present in a large excess relative to nickel, the rate of dimerisation in such systems is expected to be independent of Lewis acid concentration [62]. However, it has also been suggested that a complex

relationship exists between reaction rate and aluminium concentration [61].

1.2.1.3 Reactivity of Olefins

The generally accepted order of olefin reactivity follows the sequence;

ethene > propene > 1-pentene > 1-hexene > cycloalkene > isobutene [78].

Alkenes with internal double bonds are also dimerised, but more slowly, and they may undergo preliminary isomerisation to the corresponding α-alkenes. For example, 1-heptene and 3-heptene form the same dimers [81]. Another example is that of *n*-pentenes. In the catalytic system $[Ni(acac)_2]$ / $AlEt_2Cl$ at 0°C, carbon 1 of 1-pentene is fifty four times more reactive than carbon 3 of 2-pentene [61].

1.2.1.4 Nickel

Dimerisation, oligomerisation and related reactions have been reported to be catalysed by systems involving the majority of the Group VIII metals [61,82,83]. Particular interest has been shown in nickel-containing catalysts due to their exceptionally high activity (temperatures as low as -100°C have been used [74]). In addition to being less active than nickel, other platinum group metals have not found extensive practical application as oligomerisation catalysts for economic reasons.

A number of the most active oligomerisation catalyst systems contain d^8 complexes of divalent nickel [Ni(II)], in which square planar geometry is commonly encountered. In such complexes, the orbitals p_z, d_{xz} and d_{yz} have the correct symmetry for forming π-bonding perpendicular to the *xy*-plane. The d_{xy} and p_x, p_y orbitals are suitable for forming backbonds to empty orbitals of olefins perpendicular to the *xy*-plane [62]. The net result of such bonding is a stabilisation of the complex as indicated in Fig. 1.15 where the d_{xz} orbital is shown to be responsible for the bond.

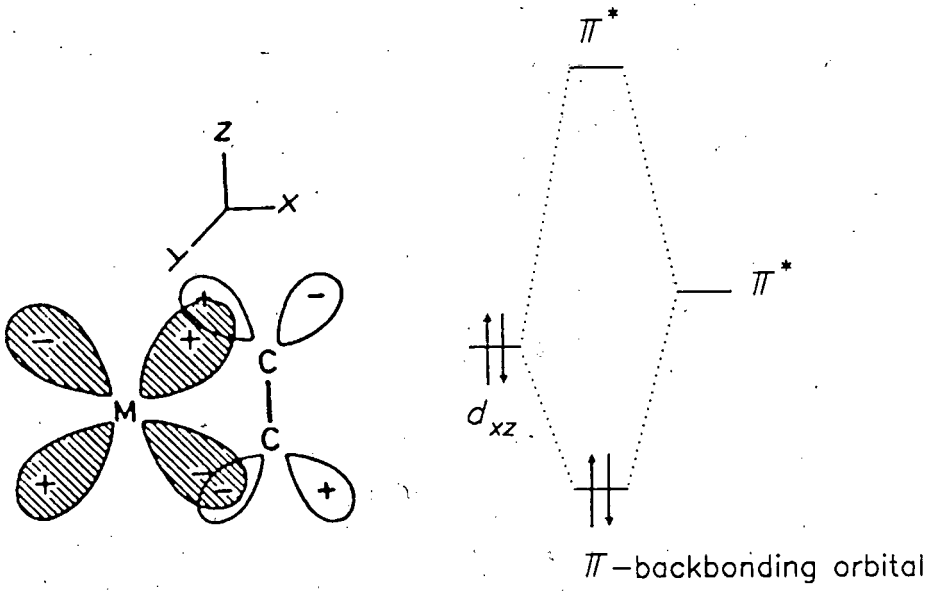

Figure 1.15 Orbital overlap for backbonding.

The diversity of possible catalytic reactions, as well as the attractive possibilities of directing the course and controlling the selectivity of the catalytic reaction by "tailoring the catalyst" are without equal among transition metal complex catalysts [84,74].

1.2.2 Heterogeneous Supported Catalysis

Although homogeneous catalysis is powerful, the problems encountered in separating products from the catalyst have led to heterogeneous systems being the favoured choice industrially. A relatively new field that has sparked extensive interest is that of supported metal catalysis, in which a homogeneous complex catalyst is heterogenised onto an insoluble support.

The motivation for supporting metal catalysts, in our case those used for the oligomerisation of olefins, can best be understood by comparing the advantages and disadvantages of homogeneous and heterogeneous catalysis. Under mild reaction conditions homogeneous catalysts are usually highly selective as only one type of active site is involved. In addition, activity and selectivity may be tailored by varying the

ligands attached to the metal. Furthermore, all the catalyst molecules are involved in the reaction unlike heterogeneous catalysts in which only surface molecules are available for participation in the catalytic process. Heterogeneous catalysts, although less active and specific are, in general, chemically and thermally more stable and have the overriding advantage of being easy to separate from the reactants and products. They may therefore be used in fixed bed reactors.

In an attempt to combine the advantages, and simultaneously eliminate the disadvantages, of each class of catalyst, homogeneous catalysts have been attached to supports in such a way as to preserve the ligand sphere and allow easy access of solvent and reactant to the catalytic site. These anchored catalysts should then function mechanistically as a homogeneous catalyst but would operate in a separate phase, facilitating catalyst separation.

Supported metal catalysis is a growing field and a large number of reviews give comprehensive coverage of the subject [85-90]. Several problems have been encountered when using supported catalysts. When the catalyst is merely impregnated onto the support or when the metal-support bond is weak, metal leaching (weeping) may occur. In such cases the advantage of easy catalyst-product separation is negated. A factor which may limit catalyst activity is substrate diffusion which is usually an order of magnitude slower than in liquids. The final limitation of the supported catalysts is preparative, in that it is difficult to obtain identical and uniform binding of the metal complex to the support.

1.2.2.1 Preparation of Supports

The types of support used may be divided into two groups: organic polymers and inorganic matrices.

Organic Polymers

Cross-linked polystyrene based materials are the most commonly used organic supports for transition metal catalysts. They allow systematic variation of physical form, cross-linking and the nature and distribution of the functional groups [91-94]. The styrene resins may be divided into two classes according to their degree of cross-linking. Highly cross-linked resin beads of large surface area (e.g. 20-60% divinylbenzene) are called macroporous or macroreticular resins. The attached catalyst lies mainly at the internal surface where it is accessible to solvents. The high cross-link prevents excessive diffusion into the core of the polymer particles. Lightly cross-linked microporous resins constitute the second class (e.g. 1-2% divinylbenzene). These resins swell in solvents and the entire internal volume is accessible to solvent and reagents. They must be used in swelling solvents to permit access to this internal volume.

Functionalisation of organic supports is often necessary to incorporate groups that can act as potential ligands. This is generally achieved using standard routes such as lithiation [95] and chloromethylation [96-99]. In addition, amination, phosphination, bromination and thiolation have also been used [100].

Certain polymers already contain donor groups and thus require no further chemical modification. These include polyvinylalcohol [101], polymeric Schiff bases [102], poly-L-methyleneimine [103], polyvinylpyridine [104] and polyvinylamine [105,106].

Inorganic Polymers

Inorganic supports have been more widely studied than their organic counterparts probably due to their superior thermal properties. Silica [107] and alumina [108] are the most popular matrices, although glasses, clays and zeolites have also been used.

The catalysts may be supported by impregnation [90] or by direct chemical bonding. Direct bonding can occur *via* surface hydroxyl groups

which react directly with the organometallic complexes, or *via* other functional groups [109]. Functionalisation is often similar to that used for organic polymers. A particularly relevant example is the introduction of a β-ketoenolate functionality using amino-functionalised silica gel [110] (Fig. 1.16).

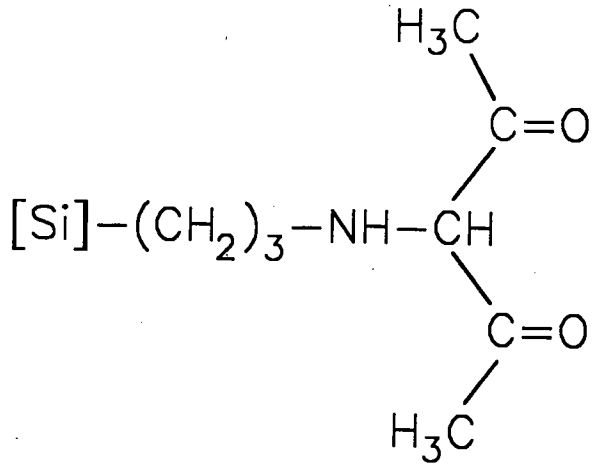

Figure 1.16 Amino-functionalised silica.

Essentially three techniques exist for binding metal complexes to functionalised matrices:

(1) direct reaction of the metal salt with the support [111,112],

(2) ligand displacement for monomeric neutral complexes [87,113-115],

(3) bridge splitting of dimeric complexes [116-118].

The most common of the above routes is displacement of a coordinated ligand by a ligand on the support.

Phosphine ligands are often used [90,111]. However, their lack of volatility causes them to compete with anchored phosphines during the reaction thus causing metal leaching. Supports with bidentate phosphine and nitrogen ligands have been prepared [85] in the hope that they may prevent metal leaching. The activity of each catalyst varies with each support with no single support being suitable for all types of catalyst [119,120].

The advantages associated with the use of inorganic matrices include high thermal and mechanical stability as well as good heat transfer properties. However, they lack chemical stability and flexibility which is essential, as the distance between the surface bound silica and the

functional group is critical [116]. Organic polymers, in addition to being chemically stable and flexible, have an upper limit of monofunctional groups five times in excess of inorganic supports.

Finally, an alternative to using functionalised supports is to polymerise functionalised monomers [121]. Although this gives control of the metal complex concentration and distribution throughout the support, undesirable side reactions may occur thus preventing their use as catalysts.

1.2.2.2 Effect of Supports on Catalytic Activity

There are several effects which are inherent to a catalyst confined to a support.

Diffusion

A major consequence of confining a catalyst to a solid is that reactants are not as free to access and leave the catalytic site. Where liquid diffusion rates are usually ~10^{-5} cm/s, diffusion through polymer matrices is often an order of magnitude slower (~10^{-6} cm/s) [87]. If the catalytic reaction is fast relative to diffusion, the catalyst is not used effectively. There are several ways in which diffusion limitations may be reduced: particle size may be reduced, pores may be enlarged and the overall surface area of the catalyst may be increased. Selective diffusion can be introduced by selecting the correct pore size. For example, shape selective olefin hydrogenation has been achieved using a heterogenised rhodium phosphine complex, by controlling the degree of swelling of the polymer [122].

Catalyst Concentration

Confinement of a transition metal complex to a solid enables the complex to be used in high concentrations as it does not suffer the solubility limitations which are sometimes encountered in homogeneous catalysts.

While homogeneous metal complex catalysts are usually used at a maximum of 10^{-3} M, catalysts supported on polymers and inorganic matrices may be used at effective concentrations of 2-5 M and 0.5-1 M, respectively.

Site Cooperation

One of the most interesting aspects of supported metal complex catalysis is the possibility of the simultaneous action of more than one type of catalytic (or binding and catalytic) site. Unusual catalytic activities have been recorded when such cooperation occurs [123]. Organic polymers are more effective than silica matrices due to their high density of active sites.

1.2.2.3 Catalyst Leaching

The loss, or leaching, of the metal from the catalyst is a critical problem in the use of supported catalysts. Similarly, decomposition of organometallic complexes to metals or metal oxides may occur. Leaching is most prevalent when ligands which bind the complex to the matrix are able to undergo reversible dissociation. The free metal in solution may be active and may therefore alter the selectivity of the reaction. Metal loss may be reduced by increasing the ligand concentration and the ligand : metal ratio within the support, avoiding the use of coordinating solvents and using chelating ligands. However, chelating ligands often cause changes in reactivity and selectivity, as they do when present in homogeneous systems [124].

The above effects emphasise the necessity of careful selection of metal complex, support and reaction conditions when designing a catalyst system. In this work, two polymer supported complexes have been prepared, characterised and tested as olefin oligomerisation catalysts.

REFERENCES

1. K. Nakamoto, Instrument News, **20** (1970) 1.

2. J.R. Ferraro, in "Low-Frequency Vibrations of Inorganic and Coordination Compounds", (1971), Plenum Press, New York.

3. D.M. Adams, J. Chem. Soc., (1964) 1771.

4. F.A. Cotton, in "Chemical Applications of Group Theory", 2nd Ed., (1971), Wiley, New York.

5. E.B. Wilson Jr., J.C. Decius and P.C. Cross, in "Molecular Vibrations", (1955), McGraw-Hill, New York.

6. D.C. Harris and M.D. Bertolucci, in "Symmetry and Spectroscopy", (1978), Oxford University Press, New York.

7. A. Vincent, in "Molecular Symmetry and Group Theory", (1977), Wiley, New York.

8. R.S. Halford, J. Chem. Phys., **14** (1946) 8.

9. D.M. Adams, Coord. Chem. Rev., **10** (1973) 183.

10. K. Nakamoto, in "Infrared and Raman Spectra of Inorganic and Coordination Compounds", 4th Ed., (1986), Wiley-Interscience, New York.

11. B.N. Figgis, in "Introduction to Ligand Fields", (1966), Wiley-Interscience, New York.

12. F. Basolo and R.G. Pearson, in "Mechanisms of Inorganic Reactions", 2nd Ed., (1967), Wiley, New York.

13. C.K. Jorgensen, in "Absorption Spectra and Chemical Bonding in Complexes", (1962), Pergamon Press, London.

14. R.D. Hancock and D.A. Thornton, J. Mol. Struct., **4** (1969) 361.

15. L.G. Hulett and D.A. Thornton, Spectrochim. Acta, **27A** (1971) 2019.

16. R.D. Hancock and D.A. Thornton, J. S. Afr. Chem. Inst., **23** (1970) 71.

17. G.C. Percy and D.A. Thornton, J. Mol. Struct., **10** (1971) 39.

18. G.S. Shephard and D.A. Thornton, Helv. Chim. Acta, **54** (1971) 2212.

19. G.S. Shephard and D.A. Thornton, J. Mol. Struct., **16** (1973) 321.

20. C.A. Fleming and D.A. Thornton, J. Mol. Struct., **17** (1973) 79.

21. R.D. Hancock and D.A. Thornton, J. Mol. Struct., **6** (1970) 441.

22. L.G. Hulett and D.A. Thornton, J. Mol. Struct., **13** (1972) 115.

23. L.G. Hulett and D.A. Thornton, Chimia, **26** (1972) 72.

24. G.C. Percy and D.A. Thornton, J. Inorg. Nucl. Chem., **34** (1972) 3369.

25. G.C. Percy and D.A. Thornton, J. Inorg. Nucl. Chem., **35** (1975) 2319.

26. J.M. Haigh, N.P. Slabbert and D.A. Thornton, J. Mol. Struct., **7** (1971) 199.

27. R.D. Hancock and D.A. Thornton, J. Mol. Struct., **4** (1969) 377.

28. G.A. Foulds and D.A. Thornton, Spectrochim. Acta, **37A** (1981) 917.

29. T.P.E. Auf der Heyde, G.A. Foulds, D.A. Thornton and G.M. Watkins, J. Mol. Struct., 77 (1981) 19.

30. S. Pinchas and I. Laulicht, in "Infrared Spectra of Labelled Compounds", (1971), Academic Press, London.

31. K. Nakamoto, Angew. Chem. Int. Edit., **11** (1972) 666.

32. Y. Saito, J. Takemoto, B. Hutchinson and K. Nakamoto, Inorg. Chem., **11** (1972) 2003.

33. B. Hutchinson, J. Takemoto and K. Nakamoto, J. Amer. Chem. Soc., **92** (1970) 3355.

34. M.L. Niven and D.A. Thornton, Spectrosc. Lett., **13** (1980) 419.

35. G.M. Watkins, PhD Thesis, University of Cape Town (1987).

36. G.A. Foulds, G.C. Percy and D.A. Thornton, Spectrochim. Acta, **34A** (1978) 1231.

37. M.L. Niven and D.A. Thornton, Inorg. Chim. Acta, **32** (1979) 205.

38. J.B. Hodgson, G.C. Percy and D.A. Thornton, Trans. Met. Chem., 4 (1979) 218.

39. G.N. Rayner Canham and A.B.P. Lever, Can. J. Chem., **50** (1972) 3866.

40. A.B.P. Lever and E. Mantovani, Can. J. Chem., **51** (1973) 514.

41. B. Hutchinson, D. Eversdyk and S. Olbricht, Spectrochim. Acta, **30A** (1974) 1605.

42. H. Musso and H. Junge, Tetrahedron Lett., (1966) 4003.

43. H. Junge and H. Musso, Spectrochim. Acta, **24A** (1968) 1219.

44. S. Pinchas, B.L. Silver and I. Laulicht, J. Chem. Phys., **46** (1967) 1506.

45. C.A. Fleming and D.A. Thornton, Spectrosc. Lett., **6** (1973) 245.

46. G.A. Foulds, J.B. Hodgson, A.T. Hutton, M.L. Niven, G.C. Percy, P.E. Rutherford and D.A. Thornton, Spectrosc. Lett., **12** (1979) 25.

47. J.B. Hodgson, G.C. Percy and D.A. Thornton, J. Mol. Struct., **66** (1980) 75.

48. J.R. Scherer, Spectrochim. Acta, **24A** (1968) 747.

49. Y. Kakiuti, H. Saito and T. Yokoyama, J. Mol. Spectrosc., **32** (1969) 247.

50. E.B. Wilson, J.C. Decius and P.C. Cross, in "Molecular Vibrations", (1955), McGraw-Hill, New York.

51. I.M. Mills, in "Calculation of Force Constants in Infrared Spectra and Molecular Structure", (1963), Elsevier, Amsterdam.

52. J.R. Scherer, Spectrochim. Acta, **20** (1964) 345.

53. K. Nakamoto and A.E. Martell, J. Chem. Phys., **32** (1960) 588.

54. G.T. Behnke and K. Nakamoto, Inorg. Chem., **3** (1967) 433.

55. M.E. Dry, in "Catalysis - Science and Technology", (1981), Springer-Verlag, Berlin, p. 159.

56. British Patent 824 917 (9 Dec 1959); Chem. Abstr., **54** (1960) 7557.

57. British Patent 868 945 (25 May 1961); Chem. Abstr., **56** (1962) 1342.

58. U.S. Patent 318 574 5 (25 May 1965); Chem. Abstr., **63** (1965) 4160.

59. U.S. Patent 325 527 2 (7 June 1966); Chem. Abstr., **65** (1966) 3743.

60. Belg. Patent 616 564 (15 May 1962); Chem. Abstr., **58** (1963) 2369.

61. G. Lefebvre and Y. Chauvin, in "Aspects of Homogeneous Catalysis" (1970), Carlo Manfredi, Milan, p. 107.

62. O.T. Onsager and J.E. Johansen, Chem. Met. Car. Bond, **3** (1985) 205.

63. V.S. Feldblyum and N.V. Obeschalova, Russ. Chem. Rev., **37** (1968) 789.

64. W.O. Haag and H. Pines, J. Amer. Chem. Soc., **82** (1960) 2488.

65. Chem. Week., **May 6** (1961) 73.

66. a) K. Ziegler, H-G. Gellert, H. Kuhlhom, H. Martin, K. Meyer, K. Nagel, H. Sauer and K. Zosel, Angew. Chem., **64** (1962) 323.
b) K. Ziegler, H-G. Gellert, K. Zosel, E. Holzkamp, J. Schneider, M. Soll and W-R. Kroll, Justus Liebigs Ann. Chem., **629** (1960) 121.

67. A.W. Shaw, C.W. Bittner, W.V. Bush and G. Holzman, J. Org. Chem., **30** (1965) 3286.

68. U.S. Patent 296 940 8 (1961); Chem. Abstr., **55** (1961) 16009.

69. J. Ewers, Angew. Chem. Int. Edit., **5** (1966) 584.

70. G. Wilke, B. Bogdanovic, P. Hardt, P. Heimbach, W. Keim, M. Kroner, W. Oberkirch, K. Tanaka, E. Steinrucke, D. Walter and H. Zimmerman, Angew. Chem., **78** (1966) 157.

71. Y. Chauvin, N.H. Phung, N. Guichard and G. Lefebvre, Bull. Soc. Chim. France, (1966) 3223.

72. O.T. Onsager, H. Wang and U. Blindheim,
a) Helv. Chim. Acta., **52** (1969) 187.
b) Helv. Chim. Acta., **52** (1969) 196.
c) Helv. Chim. Acta., **52** (1969) 215.
d) Helv. Chim. Acta., **52** (1969) 224.
e) Helv. Chim. Acta., **52** (1969) 230.

73. W. Keim, A. Behr and M. Roper, in "Comprehensive Organometallic Chemistry", (1982), Pergamon Press, New York, p. 371.

74. B. Bogdanovic, Adv. Organomet. Chem., **17** (1979) 105.

75. J.R. Jones and T.J. Symes, J. Chem. Soc. C, (1971) 1124.

76. K. Zhou, Z. Gao and W. Keim, Proc. VIIIth International Congress on Catalysis, Berlin, **V** (1984) 429.

77. R.H. Grubbs and A. Miyashita, J. Amer. Chem. Soc., **100** (1978) 7416.

78. P.W. Jolly, in "Comprehensive Organometallic Chemistry", (1982), Pergamon Press, New York, p. 615.

79. V.S. Feldblyum, Proc. IVth International Congress on Catalysis, Moscow, (1968).

80. G. Lefebvre and Y. Chauvin, Proc. VIIth World Petroleum Congress, Mexico, (1967).

81. British Patent 775 384 (22 May 1957); Chem. Abstr., **52** (1958) 12893.

82. J.T. van Gemert and P.R. Wilkinson, J. Phys. Chem., **68** (1964) 645.

83. N.H. Phung and G. Lefebvre, C. R. Acad. Sci., **C265** (1967) 519.

84. B. Bogdanovic and G. Wilke, Proc. VIIth World Petroleum Congress, Mexico, (1967).

85. C.U. Pittman, in "Comprehensive Organometallic Chemistry", (1982), Wiley, New York, p. 583.

86. C. Dumas and C.C. Hsu, Rev. Macromol. Chem. Phys. C, **24** (1984) 355.

87. D.D. Whitehurst, Chem. Tech., **Jan** (1980) 44.

88. V.A. Kabanov and V.I. Smetanyuk, Sov. Sci. Rev., **13** (1980) 83.

89. F.R. Hartley, in "Supported Metal Complexes", (1985), D. Reidel, Holland.

90. M. Peuckert and W. Keim, J. Mol. Catal., **22** (1984) 289.

91. S. Bhaduri, H. Khwaja and V. Khanwalker, J. Chem. Soc. Dalton, (1982) 445.

92. R.S. Drago, E.D. Nyberg and A.G. El Ámma, Inorg. Chem., **20** (1981) 2461.

93. B.M. Trost and E. Keinan, J. Amer. Chem. Soc., **100** (1978) 7779.

94. R.J. Card and D.G. Neckers, Inorg. Chem., **17** (1978) 2345.

95. M.J. Farrell and J.M. Frechet, J. Org. Chem., **41** (1976) 3877.

96. K.W. Pepper, H.M. Paisley and M.A. Young, J. Chem. Soc., (1953) 4097.

97. C. Leznoff, Chem. Soc. Rev., **3** (1974) 65.

98. Z.M. Michalska and D.E. Webster, Chem. Tech., (1975) 117.

99. S.L. Davydova and N.A. Plate, Coord. Chem. Rev., **16** (1975) 195.

100. J. Lieto, D. Milstein, R.L. Albright, J.V. Minkiewicz and B.C. Gates, Chem. Tech., **Jan** (1983) 46.

101. K. Kimura, Y. Inaki and K. Takemoto, Makromol. Chem., **175** (1974) 95.

102. J.J. Laverty and Z.G. Gardlund, J. Polym. Sci. A-1, **9** (1971) 243.

103. H. Hirai and T. Furata, J. Polym. Sci. Polym. Lett., **9** (1971) 459.

104. A.J. Moffat, a) J. Catal., **18** (1970) 193.
b) J. Catal., **19** (1970) 322.

105. Y. Inaki, K. Kimura and K. Takemoto, Makromol. Chem., **171** (1973) 19.

106. K. Kimura, Y. Inaki and K. Takemoto, Makromol. Chem., **175** (1974) 83.

107. L. Bonneviot, D. Olivier and M. Ché, J. Mol. Catal., **21** (1983) 415.

108. P.G. Bercik, K.J. Metzger and H.E. Swift, Ind. Eng. Chem. Prod. Res. Dev., **17** (1978) 214.

109. D.C. Locke, J. Chromatogr. Sci., **11** (1973) 120.

110. V.V. Skopenko, T.P. Lishko, T.A. Sukhan and A.K. Trofimchuk, Ukr. Khim. Zh., **46** (1980) 1028; Chem. Abstr., **94** (1981) 10560.

111. K.G. Allum, R.D. Hancock, I.V. Howell, R.C. Pitkethly and P.J. Robinson, J. Organomet. Chem., **87** (1975) 189.

112. M. Capka, P. Svoboda, M. Kraus and J. Hetflejs, Chem. Ind. London, (1972) 650.

113. R.B. King and E.M. Sweet, J. Org. Chem, **44** (1979) 385.

114. G. Strukul, M. Bonivento, M. Graziani, E. Cernia and N. Palladino, Inorg. Chim. Acta, **12** (1975) 15.

115. A.R. Sanger, L.R. Schallig and K.G. Tan, Inorg. Chim. Acta, **35** (1979) 325.

116. G. Sbrana, G. Braca, G. Valentini, G. Pazienza and A. Altomare, J. Mol. Catal., **3** (1978) 111.

117. L.D. Rollman, Inorg. Chim. Acta, **6** (1972) 137.

118. W.R. Cullen, D.J. Patmore, A.J. Chapman and A.D. Jenkins, J. Organomet. Chem., **102** (1975) C12.

119. D.G.H. Ballard, Spectrosc. Lett., **6** (1971) 219.

120. B. Rebenstorf, B. Jonson and R. Larson, Acta Chem. Scand., **A36** (1982) 695.

121. D.W. Macomber, M.D. Rausch, T.V. Jayaraman, R.D. Priester and C.U. Pittman, J. Organomet. Chem., **205** (1981) 353.

122. R.H. Grubbs and L.C. Kroll, J. Amer. Chem. Soc., **93** (1971) 3062.

123. C.U. Pittman and R.H. Hanes, J. Amer. Chem. Soc., **98** (1976) 5402.

124. W. Keim, B. Hoffman, R. Lodewick, M. Peuckert and G. Schmitt, J. Mol. Catal., **6** (1979) 79.

CHAPTER 2

β-KETOENOLATE COMPLEXES

2.1 INTRODUCTION

β-Ketoenolate ligands are characterised by the presence of β-carbonyl groups and may therefore undergo keto-enol tautomerism [1]. Under appropriate conditions, the enolic proton may be removed and replaced by a metal ion. The resulting complexes, the metal β-ketoenolates, have been studied for well over a hundred years and their physical and chemical properties have been the subject of a large number of publications as well as several reviews [2-4]. In addition to characterisation studies, nickel β-ketoenolate complexes have been extensively used as homogeneous catalysts.

2.1.1 Spectroscopic Studies

2.1.1.1 The 2,4-Pentanedionate Complexes

The most fundamental of the β-ketoenolate ligands studied is 2,4-pentanedione. Infrared vibrational assignments of the transition metal complexes of the 2,4-pentanedionate anion (acac) have been the subject of widespread controversy.

The 1960's saw several conflicting publications centred on the correct assignment of the C=C and C=O stretching vibrations (νC=C, νC=O). The quasi-aromatic structure of the metal β-ketoenolates implies the approaching equivalence of these two vibrations. Their infrared stretching frequencies are therefore expected to be similar, and in fact, two bands are observed in the 1600-1500 cm^{-1} region where these two vibrations are expected to occur. The earliest attempts at assignment were those of Lecomte [5] and Duval *et al.* [6]. By considering the vibrations of 2,4-pentanedione to arise from the in-phase (ip) and out-of-phase (oop) vibrations of acetone they empirically assigned the higher frequency component of the doublet in the 1600-1500 cm^{-1} region to the νC=O vibration and the lower frequency band to νC=C. The fact that no band was observed in the 1750-1700 cm^{-1} region suggests that the ligand is not present in the keto-form. Bellamy and

Branch [7] proposed that, since the C=O stretch in organic molecules is usually more intense than the C=C stretch, the stronger of the two bands in this region should be assigned to νC=O, regardless of its position. Nakamoto and Martell [8], on the basis of a normal coordinate treatment of [$Cu(acac)_2$], suggested that the νC=O and νC=C assignments of Duval *et al.* [6] should be reversed. However, their treatment was based on a simplified model which reduced the molecule to a single chelate ring, thereby neglecting interactions between chelate rings. They also assumed the methyl groups to be single units. Mikami *et al.* [9] undertook a more refined treatment in which the complete 29-body problem of [$Cu(acac)_2$] and 43-body problem of the iron(III) complex, [$Fe(acac)_3$], was considered. Their conclusions substantially supported the earlier work of Nakamoto and Martell [8] but were then reversed in a further theoretical treatment by Nakamoto and Behnke [10], in which the higher frequency band was assigned to νC=O and the lower frequency band to νC=C. A vibrational study of the ^{18}O-labelled chromium(III) complex [11] confirmed this assignment as labelling led to a shift of 13 cm^{-1} for the upper band towards lower frequency while no change was observed in the position of the band of lower frequency. Additional confirmation was provided by Junge and Musso [12] in the ^{18}O-, ^{13}C- and ^{2}H-labelling study of [$Cu(acac)_2$] and [$Al(acac)_3$]. In the copper complex ^{18}O-labelling led to a shift of -26cm^{-1} in the band of higher frequency, while a shift of only -5cm^{-1} was observed for the lower frequency band.

In more recent work, including ^{18}O- and metal isotope labelling studies of [$Zn(acac)_2$] [13] and an infrared and Raman isotopic labelling study of the copper(II) and palladium(II) complexes [14], νC=O has been consistently assigned to the higher frequency component of the band pair.

The assignment of metal-oxygen stretching vibrations (νM-O) in divalent metal-acac complexes has also been controversial. The normal coordinate treatments of Nakamoto and co-workers [8,15,16] on the copper(II) complex led to the assignment of a band near 600 cm^{-1} to νM-O coupled with a ring deformation mode. The second νM-O was assigned to a band near 450 cm^{-1}. This assignment was also given to a band calculated to occur at 320 cm^{-1} which was not observed because of the restricted range of determination.

Isotopic labelling of the metal ion [17] supported these assignments and led to the assignment of a third band between 350 and 300 cm^{-1} as the purest (vibrationally least coupled) νM-O. These results were further supported by Mikami *et al.* [9] who carried out more rigorous normal coordinate treatments on $[Cu(acac)_2]$, $[Pd(acac)_2]$ and $[Fe(acac)_3]$. Their calculations also showed that several other vibrations in the far infrared region comprise some M-O stretching character due to vibrational coupling. In their ^{18}O-labelling study of $[Cu(acac)_2]$, Junge and Musso [12] observed shifts of -16 and -7 cm^{-1} for the bands at 613 and 454 cm^{-1}, respectively. The third band near 300 cm^{-1} was beyond their range of measurement. These authors accordingly assigned the higher frequency band to νCu-O and the lower frequency band to a coupled νCu-O + $\delta C\text{-}CH_3$ vibration. To date, this controversy remains unresolved and even the most recent publications [13,14] show inconsistencies in band assignments.

A similar disagreement has arisen over the assignment of νCr-O in the trivalent complex $[Cr(acac)_3]$, for which both ^{18}O- and metal isotope labelling have been used to try to resolve the argument [11,17,18].

Substitution of oxygen by nitrogen or sulphur in the complexes of nominal formula $[M(acac)_2]$, yields spectroscopically interesting, four-coordinate complexes. Despite the interest which attaches to these novel β-ketoenolate analogues, their infrared spectra have received rather limited attention and coverage of this field has been piecemeal rather than systematically embracing several molecules under similar experimental conditions.

2.1.1.2 The 4-Imino-2-pentanonate Complexes, $[M(Nacac)_2]$

The substitution of an oxygen atom of 2,4-pentanedione by the imino group, NH, leads to the formation of the 4-imino-2-pentanone ligand (HNacac). The first recorded preparation of a metal chelate of this ligand was that of Combes and Combes [19] as early as 1892.

On account of the red colour and diamagnetism of the $[Ni(Nacac)_2]$ complex, Archer [20] proposed a square planar structure. In addition,

he observed that the ligand field spectrum is characteristic of compounds of the type *trans*-Ni(N_2O_2). A subsequent crystallographic study [21] confirmed *trans*-square planar structures for the Ni(II), Cu(II) and Pd(II) complexes.

Until recently, the most complete infrared study was of [Cu(Nacac)$_2$] by Holtzclaw *et al.* [22]. Few bands were assigned and, as the spectrum was recorded from Nujol mull, bands occurring in regions of strong Nujol absorbance were obscured. In 1978, McGee and Walter [23] published a detailed infrared investigation of the complexes [M(Nacac)$_2$] (M = Ni, Cu, Pd). In addition to observing temperature effects, assignments were proposed on the basis of normal coordinate analysis.

2.1.1.3 The 4-Thioxo-2-pentanonate Complexes, [M(Sacac)$_2$]

Initial attempts at preparing thio derivatives of β-ketoenols led to the formation of a chemically inert organic dimer [24]. The first successful preparation was of ethylthioacetoacetate [25] formed by the passage of H_2S through an alcoholic solution of ethylacetoacetate in the presence of HCl as catalyst. Subsequent modifications of this method led to the isolation of a large number of these chelate ligands.

A preliminary structural investigation of [Ni(Sacac)$_2$] indicated that the compound probably has *trans*-square planar configuration [26]. However, a three dimensional X-ray study of the analogous Pd(II) and Pt(II) complexes revealed *cis*-square planar structure [27]. In 1974, a single-crystal structure determination by Siiman *et al.* [28] also showed a *cis*-square planar structure for [Ni(Sacac)$_2$]. While the Cu(II) complex is expected to exhibit a similar structure, the Zn(II) complex is probably tetrahedral [28].

In contrast to the complexes of Nacac, the infrared spectra of these complexes have been extensively studied [29-35]. In the majority of earlier studies [33-35] band assignments were based on the first normal coordinate analysis of [Cu(acac)$_2$] by Nakamoto *et al.* [8]. This resulted in incorrect vibrational assignment of the band pair in the 1600-1470 cm^{-1} region, *i.e.* the upper component was assigned to νC=C and

the lower component to νC=O. A subsequent study by Ouchi *et al.* [29] revealed that, on substitution of the oxygen in the HSacac ligand with another sulphur atom, the band of higher frequency disappears. They accordingly assigned the band to νC=O.

2.1.1.4 The 2,4-Pentanedithionate Complexes, [M(SacSac)$_2$]

To date, attempts to synthesise the SacSac ligand have proved unsuccessful [32]. In each case the main product was a colourless, crystalline dimer bridged by the sulphur atoms [36]. It is therefore necessary to prepare metal chelate complexes of this ligand *in situ*. Interest expressed in these complexes stems from the ability of bidentate sulphur chelates to confer novel stereochemical, magnetic and spectral properties on transition metal ions. This is due, in part, to the ease with which sulphur can participate in π-bonding with the central metal ion. The dark colour and the diamagnetism of [Ni(SacSac)$_2$] suggests a monomeric, square planar structure. This has been confirmed by a single crystal structure determination [37].

The most detailed infrared analysis of the [Ni(SacSac)$_2$] complex is the normal coordinate treatment of Siiman and Fresco [38]. Assignments, however, extended to only 300 cm^{-1} and the spectrum has not been reported at lower frequencies.

In this Chapter the infrared and NMR spectra of the preparatively accessible Ni(II), Cu(II) and Zn(II) complexes of the four ligands, Hacac, HNacac, HSacac and HSacSac, are discussed. While the NMR spectra serve mainly to characterise the complexes, a comparative study of the effect of the altered ligand systems on the infrared spectra is made. In addition, the effect of substitution of the metal ion, considered in relation to the established structures of these molecules, assists in solving the assignment problem [39].

2.1.2 Catalytic Studies

In coordination oligomerisation, the majority of papers relate to monodentate ligand complexes. This is surprising as chelating ligands favour square planar structures which provide the appropriate orbitals to react with incoming olefins. In addition, the chelate should minimise the chance of coordinating olefins deactivating the catalyst.

The oligomerisation activity of β-ketoenolates has been extensively studied [40-45]. $[Ni(acac)_2]_3$ has been shown to exhibit high activity in the presence of various Lewis acid co-catalysts. Systematic studies by Keim *et al*. [44] showed that the acidity of the ligand has a dominant influence on the properties of the catalyst, an almost linear correlation between pK_a and activity being observed. The complex of the hexafluoro-2,4-pentanedione ligand (Hhfacac), the most acidic ligand examined, had the highest activity. Catalyst selectivity proved to be independent of the ligand, and dimers with 80% linearity and trimers with 50% linearity formed in all cases. The effect of the β-ketoenolate chelate was also investigated by Jones and Symes [42] who found that changing the substituents on the ligand alters the relative rates of isomerisation and dimerisation.

Closely related to the above complex catalysts are systems reported by Cavell and Masters [46,47], in which the β-ketoenolate ligand has been replaced by its dithio analogue. It is generally assumed that an electron donor, such as sulphur, may increase the activity of the catalyst [48] and this may explain why some of these complexes are among the most active oligomerisation catalysts in the literature.

Replacement of one bidentate ligand by a neutral ligand such as cyclooctadiene (COD) gives a Ni(I) complex, [Ni(acac)(COD)] [44,49]. These complexes exhibit high activity as COD is a good leaving group and therefore enhances Ni-H formation. In addition, the use of a Lewis acid to effect nickel reduction is obviated as the nickel is already in the favourable +1 oxidation state.

Complexes of bidentate chelates with a P-O combination are also square planar. Toluene solutions of the compounds shown in Fig. 2.1 [50-53] catalyse the linear oligomerisation of ethene giving isomers of 99%

linearity and >98% α-olefin content. All three complexes are active in the Shell Higher Olefins Process (SHOP), which is used industrially to manufacture α-olefins [54].

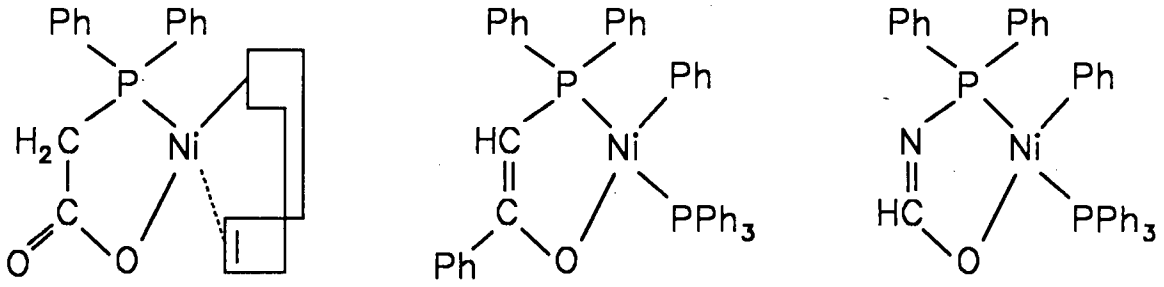

Figure 2.1 Nickel chelate catalysts for ethene oligomerisation.

As the literature is reviewed it becomes increasingly evident that each system requires an individual set of conditions to optimise activity. Aspects that need to be considered are described in the following discussion.

2.1.2.1 Lewis Acid Co-catalysts

While alkylaluminium compounds usually give rise to the most active catalysts, other Lewis acids such as BF_3, $TiCl_4$ or SbF_5 [55] can also be used in combination with nickel, as indeed can Bronsted acids such as H_2SO_4 or CF_3COOH [56]. The Lewis acid activates the catalyst and in doing so performs two functions:

(1) to form a free coordination site on the active species,
(2) to ensure that an active alkyl group is bound to the nickel.

When the Lewis acid reacts with the nickel(II) complex, either complex formation [Fig. 2.2(a)] or ligand exchange [Fig. 2.2(b)] may occur. In fact, it is likely that ligand exchange may proceed *via* the intermediate formation of a bimetallic complex.

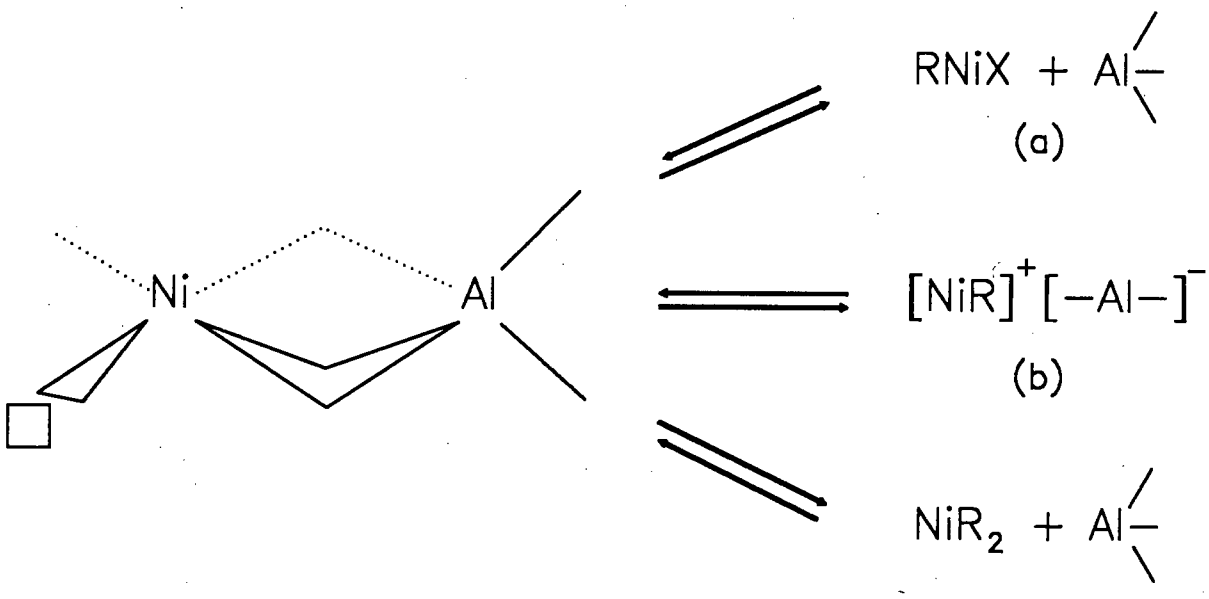

Figure 2.2 Formation of active nickel species *via* ligand exchange.

Of the three nickel species, cationic $[NiR]^+$ [Fig. 2.2(b)] is the most active [57,58]. Support for this is manifested by the fact that use of a strong Lewis acid, which would favour formation of ionic species, increases the reaction rate. For example, in a chlorobenzene medium dimerisation rate was observed to increase in the following order [55]:

$$AlEt_2Cl < AlEtCl_2 < Al_2Et_3Cl_3 \quad (Et = C_2H_5).$$

In addition, it is possible that the non-ionic, bimetallic complex [Fig. 2.2(a)] contributes to the total activity of the system [42]. High catalytic activity has been observed when using a mixture of mono- and di-alkylaluminium halides [40,59]. $AlEtCl_2$ promotes ionic complex formation, while $AlEt_2Cl$ ensures optimum alkylation of the nickel component.

It has been proposed that the Lewis acid affects the activity but not the selectivity of the catalyst [48]. While this may be true for $AlEt_2Cl$, $Al_2Et_3Cl_3$, $AlEtCl_2$ and $AlCl_3$ (all of which produce the same dimer distribution when used with the same nickel complex), when "weaker" Lewis acids are used, the concentration of linear dimers

increases. For example, when $AlEt_2F$ (a "weaker" acid than $AlEt_2Cl$) was used, the content of *n*-hexenes was about 50%, compared to 25% in the presence of $AlEt_2Cl$ [60]. In Lewis acid-free systems [42,47,49-52], or systems in which halide-free aluminium alkyls are used [49,61], up to 99% linearity has been observed.

Born *et al.* [62] observed that catalytic activity, isomerisation activity and product distribution are all influenced by the metal present in the Lewis acid.

A wide range of catalyst : co-catalyst ratios have been used in nickel catalysed oligomerisation systems. In halide-free systems, researchers have reported [42,49] that Lewis acid to nickel ratios ranging from one to four are optimum, with severe deactivation occurring at higher ratios. However, in the presence of alkylaluminium halides, ratios often in vast excess of the above have been successfully used [40,41,63-65]. At such high ratios there has been speculation that catalytic activity may be due to the aluminium species present [41]. However, Lefebvre and Chauvin [55] stated that when using a nickel catalyst, even in the presence of a large excess of Lewis acid, no "free acid" remains in the medium. Extended catalyst lifetime in the presence of excess Lewis acid may be attributed to the ability of the acid to act as a scavenger, thereby removing impurities present in the reaction mixture [66].

2.1.2.2 Temperature

Generally, reaction rate increases with increasing temperature. However, for each catalyst there is a critical temperature above which deactivation occurs [49]. The dimerisation reaction is usually conducted between -20°C and 40°C.

Temperature has been shown to have little effect on product composition [55]. However, when combined with a phosphine-modified catalyst, temperature control can be a powerful tool in controlling catalytic selectivity. This may be attributed to thermodynamic control of the first insertion reaction, which is reversible. Very low temperatures

allow careful control of isomerisation reactions and therefore allow the reactions to be targeted towards specific products.

2.1.2.3 Solvent

Owing to the presence of "hard" Lewis acidity, "hard" solvents have a detrimental effect on the reaction. If solvents are used, hydrocarbons and halohydrocarbons are best. Generally, reaction rate increases with increasing dielectric constant. Onsager *et al.* [67] observed that propene dimerisation is five times faster in chlorobenzene than benzene, while Cavell and Masters [46] recorded a similar activity increase when changing from toluene to chlorobenzene. The dimerisation of ethene is reported to be three times faster in *o*-dichlorobenzene than in chlorobenzene [59]. Consequently, it appears that the ionic or highly polarized catalytic species are the most active, as these are dissolved by the polar solvents. It has been proposed that, in chlorohydrocarbon solvent, aluminium trialkyls may undergo nickel catalysed halide substitution to form a stronger Lewis acid [59].

$$R\text{-}Cl + AlEt_3 \rightarrow R\text{-}Et + AlEt_2Cl$$

The ratio of isomerisation rate to oligomerisation rate also increases with dielectric constant. Accordingly, when unisomerised products are required, solvent free systems are preferred [55]. Finally, oligomerisation activity may also be solvent dependent. For example, in liquids which do not solubilise the catalyst, polymerisation may occur [51].

In this Chapter, nickel chelate complexes, based on those mentioned above, are studied as potential oligomerisation catalysts. Keim *et al.* [44] have studied systems in which the ligand donor atoms are oxygen and have altered substituents located at various positions on the β-ketoenolate ligand. Similar experiments by Cavell and Masters [46,47] looked at ligands with sulphur as the chelating atom. In the SHOP process P-O chelates have proved successful. However, no systematic study has been made of the effects of altering the ligand donor atoms. The present study addresses this problem by substituting sulphur and

nitrogen for oxygen as the donor atom and observing the effect on the catalytic properties of the complex.

Homogeneous reactions of the above have been carried out using a 1-hexene feed. Although interest is primarily in propene oligomerisation, many systems have been documented in which propene is dimerised to hexene [46,49,68]. It is the further oligomerisation of hexene which is of interest. In addition, the reactivity of 1-hexene is lower than propene [69], thus catalytic systems which are active for 1-hexene should prove even more so for propene. The lower activity also implies longer reaction times thus facilitating the study of the oligomerisation reaction relative to the competing isomerisation reaction. Working in "batch" (*i.e.* when all the monomer is introduced initially) also provides evidence for the isomerisation of monomer and products.

2.2 EXPERIMENTAL

2.2.1 Preparation of Complexes

Where possible, each of the following complexes was prepared:

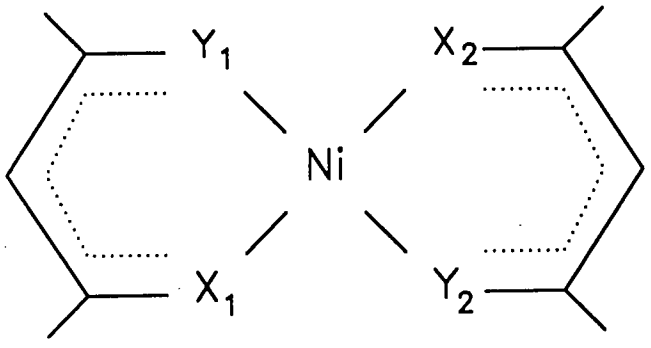

X = Y = O	$[M(acac)_2]$
X = Y = S	$[M(SacSac)_2]$
X_1= Y_2= O X_2= Y_1= S	$[M(Sacac)_2]$
X = O Y = NH	$[M(Nacac)_2]$

M = Ni, Cu, Zn

All complexes were prepared using analytical reagent grade solvents. Once isolated, each complex was dried over silica gel under reduced pressure.

2.2.1.1 $[Ni(acac)_2]_3$

This was prepared by the method of Charles and Pawlikowski [70]. To a solution of $NiCl_2.6H_2O$ (25 mmol) in water (25 ml), a solution of 2,4-pentanedione (50 mmol) in methanol (10 ml) was added. Finally, a solution of sodium acetate (50 mmol) in water (15 ml) was added. The resulting mixture was gently heated until pale blue crystals began to appear. Once the solution had cooled, the crystals were filtered and washed with water. The blue crystals analysed as the dihydrate, $[Ni(acac)_2(H_2O)_2]$. On heating under reduced pressure, dehydration occurred and dark green $[Ni(acac)_2]_3$ was formed [71].

2.2.1.2 $[Cu(acac)_2]$

The method of Charles and Pawlikowski [70], as outlined in 2.2.1.1 above, was followed except that $CuCl_2.2H_2O$ (25 mmol) was used in place of $NiCl_2.6H_2O$. Navy blue needle-like crystals formed immediately and after cooling, were filtered and washed with water. No further purification was necessary.

2.2.1.3 $[Zn(acac)_2(H_2O)]]$

The general method in 2.2.1.1 was followed substituting $ZnCl_2$ (25 mmol) for $NiCl_2.6H_2O$. A heavy white product was precipitated immediately. After filtration and washing with water, recrystallisation was effected by dissolving the product in hot 2,4-pentanedione and precipitating the crystals by addition of petroleum ether. Fine white needles resulted.

2.2.1.4 4-Thioxo-2-pentanone (HSacac)

Several methods were used in an attempt to synthesise this ligand. The base-catalysed reaction of Mayer *et al.* [72] proved the most successful method of preparation. Morpholine (50 mmol) was added to 2,4-pentanedione (500 mmol). Hydrogen sulphide gas (H_2S) was bubbled through the resulting yellow solution for 8 hours turning it bright orange. The solution was diluted with petroleum ether (100 ml), washed with dilute HCl and finally water. The petroleum ether was removed under reduced pressure and the remaining solution vacuum distilled. The pure HSacac ligand is yellow in colour and decomposes rapidly to an opaque red liquid.

The ligand is preferably stored in the form of a sodium salt [30]. Metallic sodium (18 mmol) was dissolved in absolute ethanol (16 ml) and the HSacac ligand (2.5 ml) was added with vigorous stirring. Addition of anhydrous ether (40 ml) resulted in the formation of yellow Na(Sacac) which was filtered, washed with ether and recrystallised by dissolving in ethanol and precipitating with ether.

2.2.1.5 [Ni(Sacac)$_2$]

This was successfully prepared *via* the general method of Chaston *et al.* [33]. Nickel acetate (1 mmol) was dissolved in hot ethanol (100 ml). Careful addition of HSacac (2 mmol) in ethanol (10 ml) resulted in a brown solution which, on cooling, yielded pure yellow-brown [Ni(Sacac)$_2$].

2.2.1.6 [Cu(Sacac)$_2$]

Copper acetate (1 mmol) was dissolved in hot 1:1 water-acetone solution (10 ml). On addition of HSacac (2 mmol), brown [Cu(Sacac)$_2$] crystals formed immediately. Purity was not improved after recrystallisation from 1:1 water-acetone.

2.2.1.7 [Zn(Sacac)$_2$]

The method of Siiman and Fresco [30] was followed. Addition of a solution of zinc nitrate (1 mmol) in water (10 ml) to a solution of Na(Sacac) (2 mmol) in water (5 ml) caused immediate precipitation of the product. The white crystals were filtered and washed with water. No further purification was necessary.

2.2.1.8 [Ni(Nacac)$_2$]

The 4-imino-2-pentanone ligand (HNacac) was prepared by reaction of excess 25% aqueous ammonia with 2,4-pentanedione. The water was removed under reduced pressure. The resulting ligand is a white solid which melts slowly at room temperature.

The nickel complex was prepared following the method of Hseu *et al.* [73]. Nickel acetate (10 mmol) was dissolved in water (30 ml) and 25% aqueous ammonia (50 drops). The HNacac ligand (21 mmol) in 95% ethanol (20 ml) was added resulting in a blue precipitate. On gentle heating on

a water bath the crystals turned dark red. Subsequent filtration and recrystallisation from 95% ethanol yielded the pure complex.

2.2.1.9 [Cu(Nacac)$_2$]

The method of Hseu *et al*. [73] was followed. $Cu(NO_3)_2.3H_2O$ (10 mmol) was dissolved in water (30 ml) and 25% aqueous ammonia (50 drops) was added. To this was added HNacac (21 mmol) in 95% ethanol (20 ml). Dark grey crystals formed immediately. The solution was allowed to stand overnight. Subsequent filtration and recrystallisation from 95% ethanol resulted in dark blue-grey needles.

2.2.1.10 [Ni(SacSac)$_2$]

This was prepared using the method of Barraclough *et al*. [36]. 10% w/w Ethanolic-HCl (EtOH-HCl) was prepared by bubbling HCl gas through absolute ethanol. The concentration of HCl was measured by titration against a standard solution of sodium hydroxide. Nickel carbonate (25 mmol) was dissolved in the EtOH-HCl and the solution cooled to 0°C. 2,4-Pentanedione (100 mmol) was added and H_2S bubbled through the solution for 2 hours. At the end of this time the solution had changed from blue to dark brown and dark brown crystals had separated. Barraclough *et al*. [36] suggested that separation of the crystals from the solution at this stage yields [Ni(Sacac)$_2$]. However, microanalysis of this product revealed the presence of a mixture of both [Ni(SacSac)$_2$] and [Ni(Sacac)$_2$], or that the compound [Ni(Sacac)(SacSac)] had formed. These crystals were therefore left suspended in solution, heated to 60°C and H_2S bubbled through the mixture for a further 2 hours. The resulting black-brown crystals were filtered and washed with methanol until the washings were colourless. No further purification was necessary.

2.2.1.11 Unsuccessful Preparations

There is no reported method for the preparation of $[Zn(Nacac)_2]$. Attempts at preparing this complex led to the precipitation of $Zn(OH)_2$. Lowering the pH of the solution caused hydrolysis of the ligand and subsequent formation of $[Zn(acac)_2]$.

Attempted preparations of both $[Zn(SacSac)_2]$ and $[Cu(SacSac)_2]$ were unsuccessful. Following an analogous method to that used for $[Ni(SacSac)_2]$ led to the isolation of the insoluble, disulphide bridged ligand dimer [32].

2.2.2 Catalytic Runs

2.2.2.1 1-Hexene Oligomerisation

Except where otherwise specified, the following reaction conditions were kept constant for all homogeneous catalytic runs:

Temperature	:	40°C
Pressure	:	1 atmosphere
Vessel	:	batch flask
Olefin feed	:	1-hexene 96% (15 ml)
Solvent	:	Toluene A.R. (60 ml)
Sample volume	:	1 ml
Co-catalyst concentration	:	25% wt in toluene (Aldrich)
Amount of Ni catalyst	:	1×10^{-3} mol Ni

Both the olefin feed (1-hexene) and the solvent (toluene) were dried over sodium wire and distilled under N_2 prior to use. To exclude any water associated with the catalyst molecules, each was placed in toluene and azeotroped for several hours under N_2. All transferals of the catalyst, solvent and feed to the reaction vessel were carried out in a dry, oxygen-free atmosphere. The final addition to the reaction vessel which activated the system was that of the co-catalyst.

The vessel was kept under a positive pressure of argon and samples were taken at regular intervals. These samples were immediately mixed with methanol to effect catalyst deactivation. The temperature of the reaction mixture was monitored constantly and controlled *via* a thermostatted oil bath.

2.2.2.2 Product Analysis

Each liquid sample was analysed using gas-liquid chromatography. A Varian 3400 GC was used with a 2.2 mm internal diameter (I.D.), 3 m long stainless steel column packed with 3% OV-101 on chromosorb WHP-SP. The following settings were used:

Detector	Flame ionisation
Flowrates: N_2	16 ml/min
H_2	30 ml/min
Air	300 ml/min
Injector temperature	250°C
Detector temperature	310°C
Column temperature programme	40°C (5 min); 10°C/min to 180°C; 20°C/min to 300°C; 300°C (3 min)
Sample volume	3 μl.

Isomer distribution was determined using a Varian 3600 GC with a 0.531 mm I.D., 30 m long fused silica megabore column coated with 1.5 μm of DB-1 (100% methylpolysiloxane). The settings were as follows:

Detector	Flame ionisation
Flowrates: N_2 (column)	4.5 ml/min
N_2 (detector)	25.5 ml/min
H_2	30 ml/min
Air	300 ml/min
Injector temperature	150°C
Detector temperature	250°C
Column temperature programme	40°C (5 min); 10°C/min to 230°C; 230°C (2 min)
Sample volume	0.05-0.3 μl.

The results from each analysis were reported as mass %. The definition of mass % as used in the discussion is:

$$\text{Mass \%} = \frac{(\text{Peak area olefin } x)\ R_f x}{\sum_{x=1}^{n} (\text{Peak area olefin } x)\ R_f x}$$

n = number of olefins present

$R_f x$ = response factor of olefin x.

The response factor of an olefin with a carbon number greater than five is one.

2.3 RESULTS

2.3.1 Analytical Data

Table 2.1 Analytical data for the complexes of acac, Nacac, Sacac and SacSac.

	Calculated			Found		
Compound	**%C**	**%H**	**%N**	**%C**	**%H**	**%N**
$[Ni(acac)_2(H_2O)_2]$	41.0	6.2	-	41.3	5.9	-
$[Cu(acac)_2]$	45.9	5.4	-	46.0	5.4	-
$[Zn(acac)_2(H_2O)]$	42.6	5.7	-	42.7	5.7	-
$[Ni(Nacac)_2]$	47.1	6.3	11.0	47.1	5.9	10.9
$[Cu(Nacac)_2]$	46.6	5.5	10.9	46.2	5.7	10.6
$[Ni(Sacac)_2]$	41.6	4.9	-	41.7	4.8	-
$[Cu(Sacac)_2]$	40.9	4.8	-	40.3	5.3	-
$[Zn(Sacac)_2]$	40.6	4.8	-	40.3	4.7	-
$[Ni(SacSac)_2]$	37.4	4.4	-	37.5	4.3	-

2.3.2 Infrared Data

Table 2.2 Frequencies (cm^{-1}) and assignments for the metal complexes of acac, Nacac, Sacac and SacSac.

acac complexes			Nacac complexes		Sacac complexes			SacSac complex	Assignment
Ni	Cu	Zn	Ni	Cu	Ni	Cu	Zn	Ni	
3409		3300							νO-H
			3283	3287					νN-H
3074	3075	3070	3038	3034	3010		3014	3030	νC-H (γCH)
2986	2992	2992	2985	2984	2978	2976	2973		
	2960	2957	2951	2952			2950		νC-H (CH_3)
2920	2920	2919	2915	2915	2911	2911	2911	2920	
1652		1615							δO-H
1605	1577	1598	1591	1587	1565	1573	1584		νC=O
	1550		1553	1531	1520	1520		1552	combination
1518	1527	1510	1525	1522	1474	1491	1489	1491	νC=C
			1475	1455					δN-H
1461	1455	1455	1434	1435	1440		1439	1430	δC-H deg def
1407	1415	1398			1420	1422	1413	1415	
			1382	1380					νC-N
1360	1352	1368	1351	1349	1371	1352	1363	1348	δC-H sym def
					1338	1337	1338		
1260	1272	1258	1244	1225	1234	1224	1225	1229	νC-C + νC-CH_3
			1229	1214	1227	1202			
1197	1187	1187	1188	1187	1117	1112	1112	1156	δC-H ip
			1180	1176					
1019	1018	1017	1020	1015	1016	1013	1020	1009	ρCH_3
			952	938					
					985	960	979	979	ρCH_3 + νC-S
928	935	929	933	928	935	928	925	925	νC-CH_3 + νC=O
			830	819					δN-H oop
			808						
765	779	772	789	786	813	811		826	δC-H oop
	769	755	756	809	806	805	801		
					720	711	703	747	νC-S
								703	

Table 2.2 contd...

acac complexes			Nacac complexes		Sacac complexes			SacSac complex	Assignment
Ni	Cu	Zn	Ni	Cu	Ni	Cu	Zn	Ni	
675	682	653	703	686					ring def + νM-L
			681	647				648	
658	651	(653)			672	675			ring def
			658	617	662	636	639		
589	611	570	623	582	642	614	615		ring def + νM-L
					620	570			
550	550	552	552	554	498	503	(499)	556	δC-CH_3 + ring def
		555							νZn-O
		433							νZn-OH_2
427	454	408	481	463	492	471	499		νM-O
		388							
(427)	430	421	456	436					ring def
			421	408					νM-L
			361	334					
			315	277					νM-N
275									νNi-OH_2
255	288	239			409	387	398		νM-O
					396	379	386	390	νM-S
(255)	265	262	292	296	373	361	364	374	ring def
					308	264	274	286	νM-S
		210[a]	(234)[b]	230[b]			247	240	
220	217	171	234	228	252	217	221	227	δL-M-L
195			195	185	196	184	197	216	
139	166								
107	102		100	103	149	147	152	149	ring oop
85	90	88	125	120	112	96	140	122	δL-M-L
					84	85	91	95	
	74	81	75	74		78	78	82	lattice + δCH_3 oop
60	60	66	60	67	53		62		

[a] This band has been assigned to a C-C-C bend since it is unaffected by ^{18}O- or $^{64,68}Zn$-labelling [13]
[b] Assigned to τC-CH_3 [23]

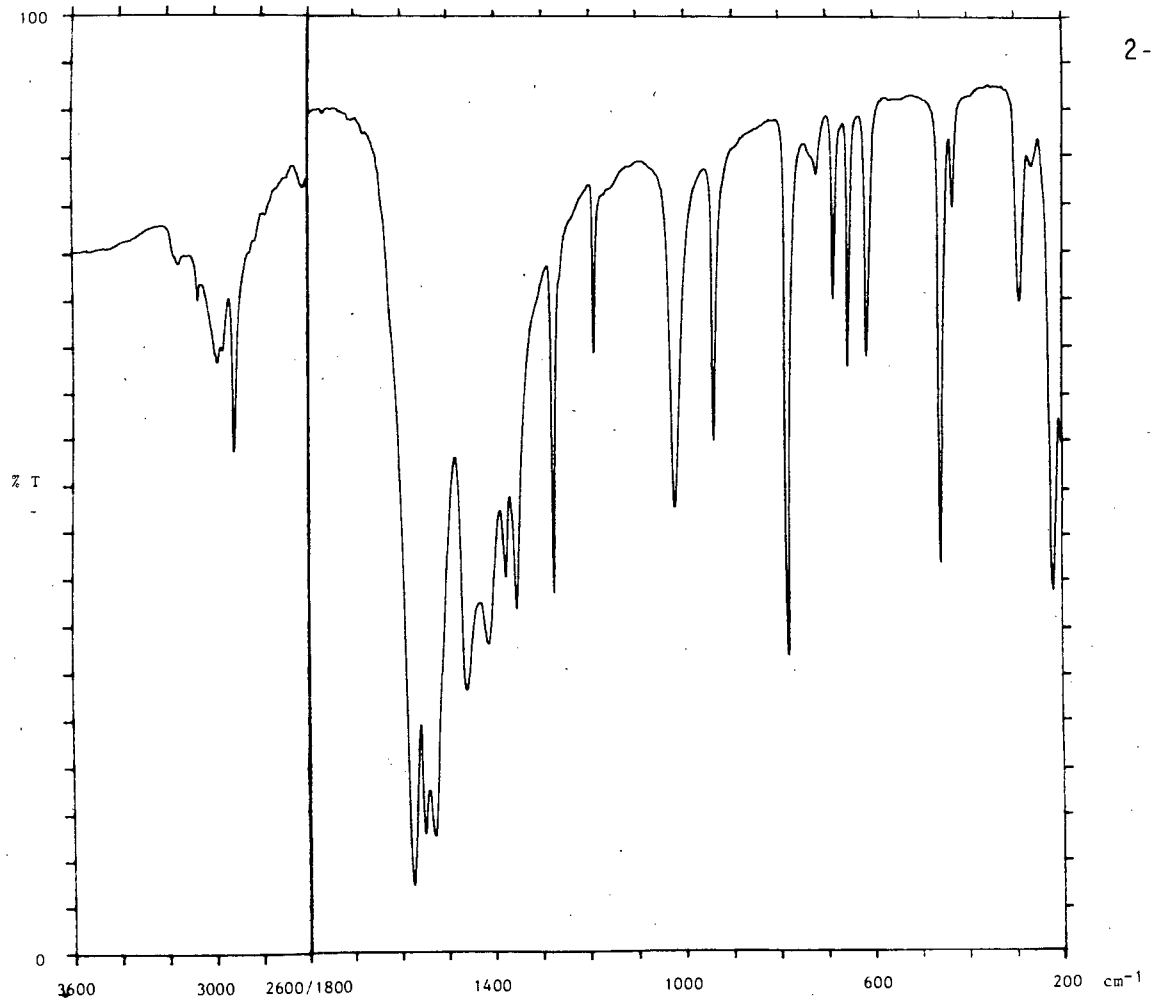

Figure 2.3(a) Mid-infrared spectrum of $[Cu(acac)_2]$.
HCBD: 3600-2600 cm^{-1}, Nujol: 1800-200 cm^{-1}

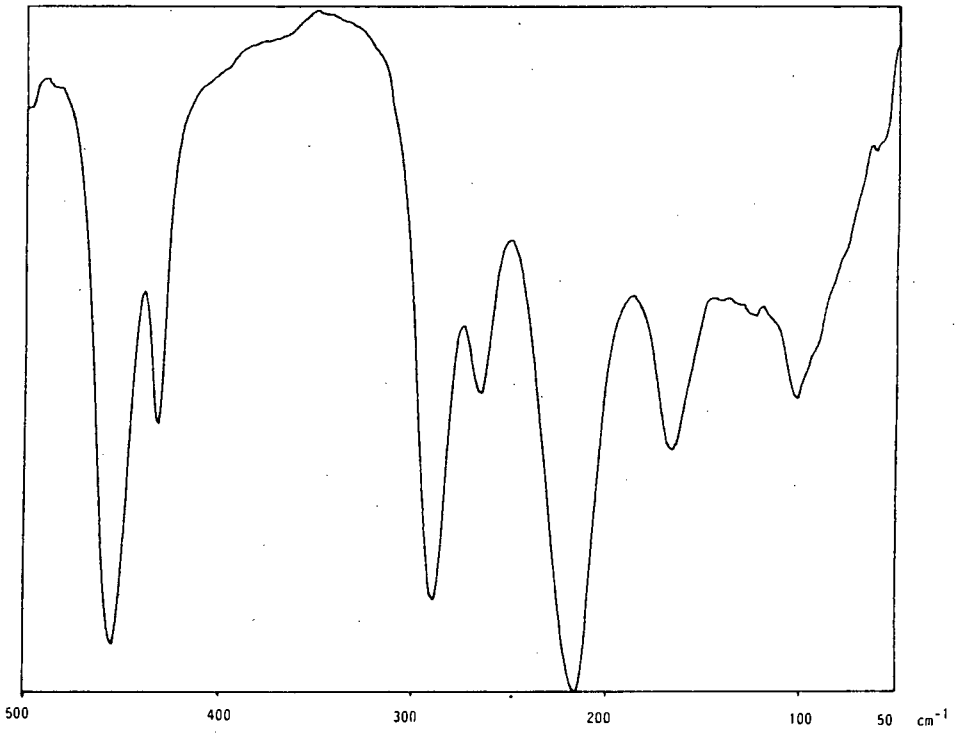

Figure 2.3(b) Far-infrared spectrum of $[Cu(acac)_2]$.

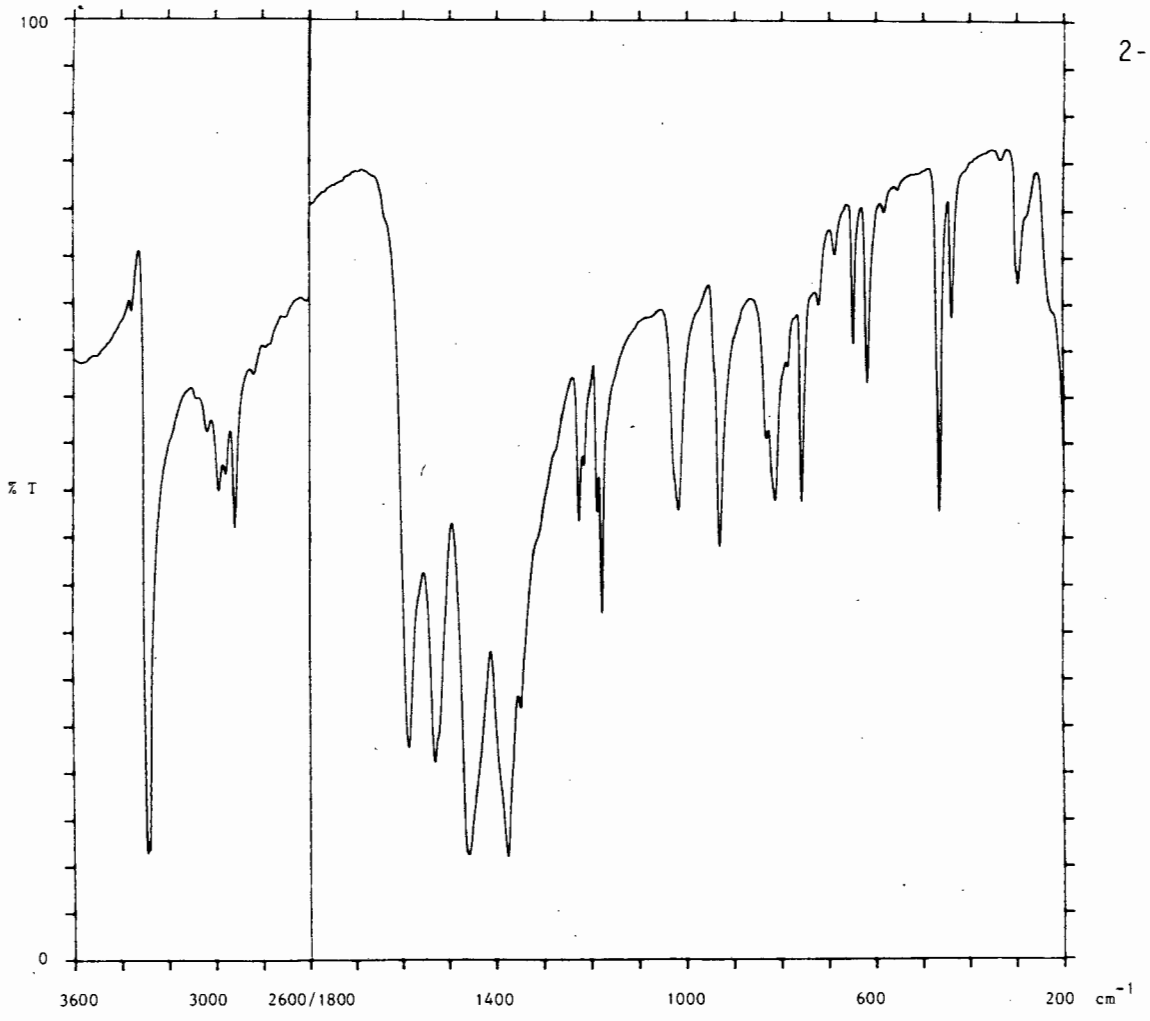

Figure 2.4(a) Mid-infrared spectrum of $[Cu(Nacac)_2]$.
HCBD: 3600-2600 cm^{-1}, Nujol: 1800-200 cm^{-1}

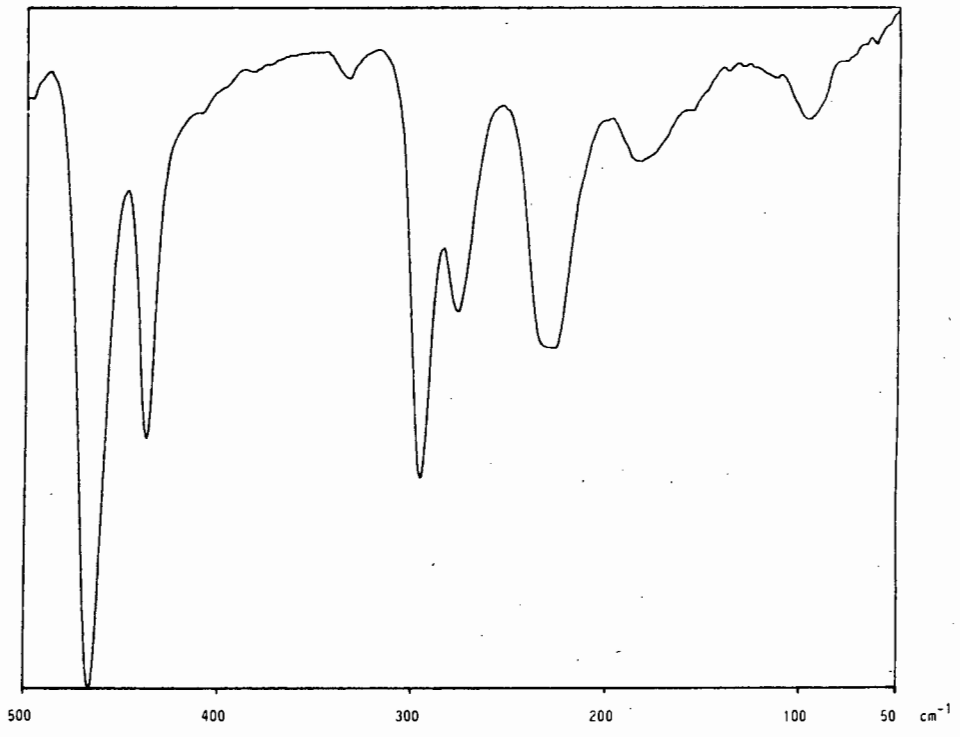

Figure 2.4(b) Far-infrared spectrum of $[Cu(Nacac)_2]$.

2.3.3 ^{1}H and ^{13}C NMR Results

Table 2.3 ^{1}H and ^{13}C NMR data (ppm)*.

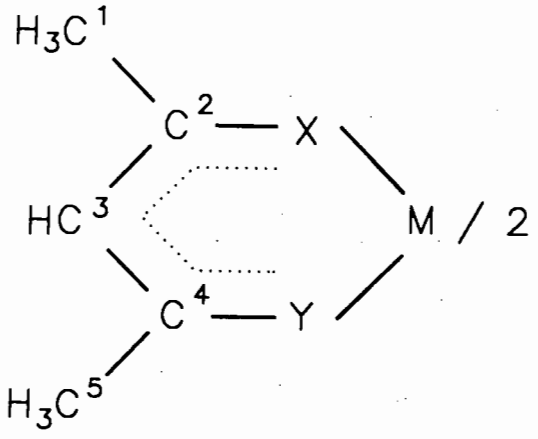

^{1}H NMR Chemical shift data (ppm)*

M	X	Y	$C^{1}H_3$	$C^{5}H_3$	$C^{3}H$	NH
Zn	O	O	1.9	1.9	5.4	-
Zn	O	S	2.4	2.2	6.5	-
Ni	O	NH	1.7	1.8	4.8	4.9
Ni	O	S	2.4	2.2	6.5	-
Ni	S	S	2.3	2.3	7.1	-

^{13}C NMR Chemical shift data (ppm)*

M	X	Y	C^{1}	C^{2}	C^{3}	C^{4}	C^{5}
Zn	O	O	37.79	204.38	110.46	204.38	37.79
Zn	O	S	35.57	199.39	118.79	184.83	30.98
Ni	O	NH	25.25	176.54	97.20	166.79	24.27
Ni	O	S	28.97	190.60	118.56	178.28	28.59
Ni	S	S	32.68	183.74	131.56	183.74	32.68

* All spectra were run in $CDCl_3$ with the exception of $[Zn(acac)_2]$ which was run in CD_3COCD_3

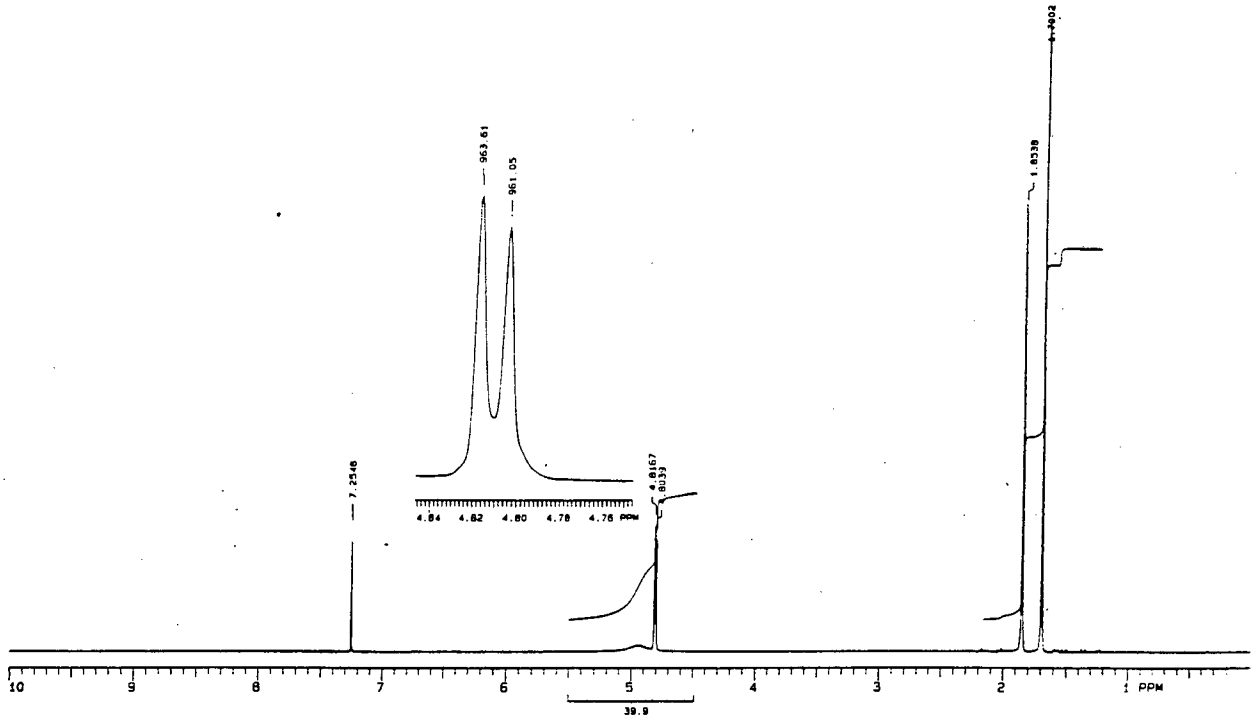

Figure 2.5(a) ^{1}H NMR spectrum of $[Ni(Nacac)_2]$, (0-10 ppm).

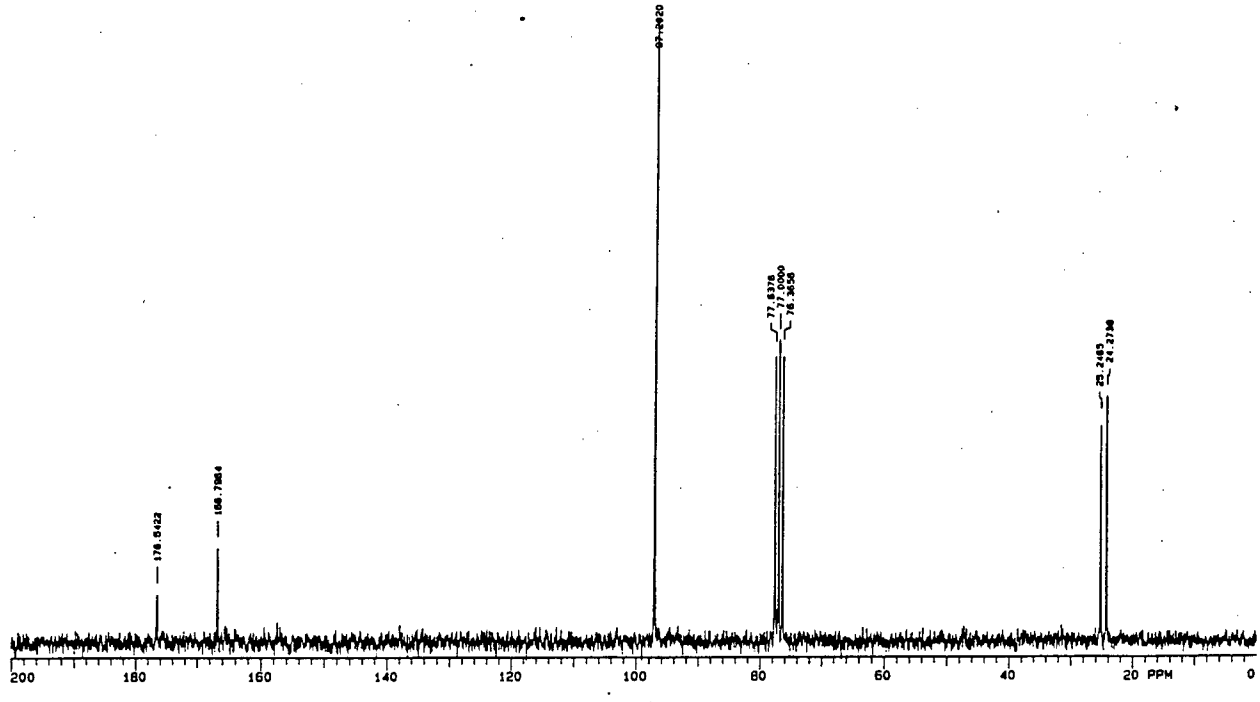

Figure 2.5(b) ^{13}C NMR spectrum of $[Ni(Nacac)_2]$, (0-200 ppm).

2.3.4 Catalytic Run Data

Each of the Tables below represents the data accumulated by gas-liquid chromatographic analysis of the liquid samples taken at various time intervals during the catalytic run. The catalyst, co-catalyst and relative molar amounts of each are given above each Table. Unless otherwise stated, the data values are expressed as a percentage of the total mass of olefins present in the sample.

Examples of original spectra are given in Appendix I.

Table 2.4 $[Ni(acac)_2]_3 : AlEt_3 = 1 : 1$

Time(min)	%1-hex	%3-hex	%*tr*-2-hex	%*cis*-2-hex	$\%C_{12}$	$\%C_{18}$
0	100.0	-	-	-	-	-
10	34.1	4.2	20.6	11.1	26.7	3.3
20	26.8	4.7	23.6	11.8	29.0	3.6
40	23.9	4.8	24.0	11.7	31.5	3.9
60	22.0	5.6	25.1	11.4	32.0	4.3
120	16.1	6.6	26.6	11.0	34.9	5.1
210	11.4	8.8	28.3	11.3	35.0	5.2
330	8.1	9.1	27.5	11.3	37.8	6.1

hex = hexene

tr = *trans*

Table 2.5 $[Ni(acac)_2]_3$: $AlEt_3$ = 1 : 1

Time(min)	%1-hex	%2- + 3-hex	$\%C_{12}$	$\%C_{18}$
0	100.0	-	-	-
15	30.3	41.3	25.0	3.4
30	24.5	42.7	29.2	3.6
45	20.9	43.0	31.9	4.2
90	16.3	45.5	33.2	5.0
180	11.4	48.4	35.2	5.2
181*	55.7	24.2	17.5	2.6
195	40.4	31.2	25.1	3.3
240	31.3	37.4	27.9	3.4
315	23.8	41.8	30.5	3.9

* After addition of further 1-hexene (15 ml)

Table 2.6 $[Ni(acac)_2]_3$: $AlEt_3$ = 1 : 4

Time(min)	%1-hex	%3-hex	%*tr*-2-hex	%*cis*-2-hex	$\%C_{12}$
0	100.0	-	-	-	-
10	5.8	15.5	62.0	16.6	-
50	5.3	16.3	61.8	16.6	-
190	1.5	18.3	62.6	17.4	-

Table 2.7 $[Ni(acac)_2]_3 : AlEt_3 = 1 : 10$

Time(min)	%1-hex	%3-hex	%*tr*-2-hex	%*cis*-2-hex	$\%C_{12}$
0	100.0	-	-	-	-
10	1.0	18.2	64.9	15.9	-
60	0.9	18.5	65.1	15.5	-
300	1.1	18.5	65.5	14.9	-

Table 2.8 $[Ni(acac)_2]_3 : AlEt_2Cl = 1 : 1$

Time(min)	%1-hex	%3-hex	%*tr*-2-hex	%*cis*-2-hex	$\%C_{12}$
0	100.0	-	-	-	-
10	1.1	17.9	64.2	14.0	2.9
20	1.0	17.8	64.2	13.1	3.9
40	1.0	17.6	63.3	13.3	4.8
60	0.9	17.6	64.0	13.3	4.0
120	0.8	17.5	63.9	13.3	4.2
210	0.8	17.5	63.6	13.3	4.6

Table 2.9 $[Ni(acac)_2]_3 : AlEt_2Cl = 1 : 10$

Time(min)	%1-hex	%3-hex	%*tr*-2-hex	%*cis*-2-hex	$\%C_{12}$
0	100.0	-	-	-	-
10	1.1	20.5	61.6	15.5	2.4
20	0.9	20.4	61.4	14.0	3.2
60	1.0	19.8	59.2	17.3	2.8
120	1.0	20.3	61.0	14.5	3.1
210	0.8	20.4	61.3	14.4	2.9
300	0.9	19.8	61.9	14.8	3.3

Table 2.10 $[Ni(acac)_2]_3 : Al_2Et_3Cl_3 = 1 : 1$

Time(min)	%1-hex	%3-hex	%*tr*-2-hex	%*cis*-2-hex	$\%C_{12}$
0	100.0	-	-	-	-
30	1.0	18.9	60.4	16.9	2.8
60	1.2	18.9	62.5	13.5	3.9
120	0.9	19.1	62.9	13.4	4.0

Table 2.11 $[Ni(acac)_2]_3 : Al_2Et_3Cl_3 = 1 : 10$

Time(min)	%1-hex	%3-hex	%*tr*-2-hex	%*cis*-2-hex	$\%C_{12}$
0	100.0	-	-	-	-
10	1.1	17.4	57.6	16.3	7.5
20	1.0	17.5	57.6	16.4	7.4
40	1.0	17.5	57.7	16.0	8.2
120	0.9	17.2	57.6	15.8	8.5
210	0.9	17.5	57.7	15.3	8.6

Table 2.12 $[Ni(acac)_2]_3 : AlEtCl_2 = 1 : 1$

Time(min)	%1-hex	%3-hex	%*tr*-2-hex	%*cis*-2-hex	$\%C_{12}$
0	100.0	-	-	-	-
10	1.0	19.0	60.9	17.2	1.8
20	0.9	19.0	61.0	17.1	1.9
40	1.0	19.2	61.6	16.0	2.2
60	1.0	19.3	62.0	15.4	2.3
120	1.1	19.3	62.8	13.1	3.8
210	0.9	19.2	63.1	12.5	4.1

Table 2.13 $[Ni(acac)_2]_3$: $AlEtCl_2$ = 1 : 10

Time(min)	%1-hex	%3-hex	%*tr*-2-hex	%*cis*-2-hex	$\%C_{12}$
0	100.0	-	-	-	-
10	0.7	10.8	32.4	8.7	47.2
20	0.6	9.8	29.2	7.6	52.2
40	0.6	8.1	27.7	7.0	56.1
60	0.5	8.0	26.8	6.8	57.3
120	0.5	7.6	26.6	6.8	58.1
210	0.5	7.4	26.3	7.0	58.6
300	0.5	7.7	26.6	7.1	57.8

Table 2.14 $[Ni(acac)_2]_3$: $AlEtCl_2$ = 1 : 10

Time(min)	%1-hex	%2- + 3-hex	$\%C_{12}$
0	100.0	-	-
15	3.0	54.2	44.8
30	1.0	49.9	49.1
45	0.6	43.6	55.8
90	0.6	42.5	56.9
180	0.5	40.9	58.6
181*	50.2	20.5	29.3
195	10.3	57.8	31.9
210	1.2	65.1	33.7
240	1.2	65.6	34.2
300	1.0	63.4	35.6

* After addition of further 1-hexene (15 ml)

Table 2.15 $[Ni(Nacac)_2]$: $AlEt_3$ = 1 : 1

Time(min)	%1-hex	%3-hex	%*tr*-2-hex	%*cis*-2-hex	$\%C_{12}$
0	100.0	-	-	-	-
10	97.5	0.4	1.1	1.0	-
40	89.1	2.8	4.7	3.5	-
120	78.4	4.8	10.5	6.3	-

Table 2.16 $[Ni(Nacac)_2]$: $AlEt_3$ = 1 : 4

Time(min)	%1-hex	%3-hex	%*tr*-2-hex	%*cis*-2-hex	$\%C_{12}$
0	100.0	-	-	-	-
10	2.0	19.4	58 3	20.3	-
20	1.9	19.6	58.9	19.6	-
180	1.5	19.7	59.3	19.4	-

Table 2.17 $[Ni(Nacac)_2]$: $AlEt_3$ = 1 : 10

Time(min)	%1-hex	%3-hex	%*tr*-2-hex	%*cis*-2-hex	$\%C_{12}$
0	100.0	-	-	-	-
30	1.0	20.5	62.7	16.8	-
60	1.0	20.7	62.7	16.6	-
120	0.9	20.8	62.7	16.6	-
300	1.1	20.7	62.7	16.5	-

Table 2.18 $[Ni(Nacac)_2]$: $AlEt_2Cl$ = 1 : 1

Time(min)	%1-hex	%3-hex	%*tr*-2-hex	%*cis*-2-hex	$\%C_{12}$
0	100.0	-	-	-	-
10	50.8	10.2	25.6	13.4	-
30	42.7	11.8	30.6	15.0	-
60	30.7	14.4	39.0	15.7	-
210	16.5	17.3	50.1	16.1	-

Table 2.19 $[Ni(Nacac)_2]$: $AlEt_2Cl$ = 1 : 10

Time(min)	%1-hex	%3-hex	%*tr*-2-hex	%*cis*-2-hex	$\%C_{12}$
0	100.0	-	-	-	-
10	50.8	9.9	25.9	13.4	-
40	41.7	11.2	31.4	15.7	-

Table 2.20 $[Ni(Nacac)_2]$: $Al_2Et_3Cl_3$ = 1 : 1

Time(min)	%1-hex	%3-hex	%*tr*-2-hex	%*cis*-2-hex	$\%C_{12}$
0	100.0	-	-	-	-
10	1.1	20.1	64.2	13.1	2.1
20	0.9	19.7	63.3	13.7	2.4
40	1.0	19.6	62.9	14.0	2.6
60	0.9	19.4	62.4	14.2	3.0

Table 2.21 $[Ni(Nacac)_2] : Al_2Et_3Cl_3 = 1 : 10$

Time(min)	%1-hex	%3-hex	%*tr*-2-hex	%*cis*-2-hex	$\%C_{12}$
0	100.0	-	-	-	-
30	0.9	17.8	57.5	16.1	7.6
60	0.8	18.0	57.6	16.0	7.5
120	0.8	17.9	57.6	16.2	7.4
300	0.9	18.0	57.6	15.8	7.5

Table 2.22 $[Ni(Nacac)_2] : AlEtCl_2 = 1 : 1$

Time(min)	%1-hex	%3-hex	%*tr*-2-hex	%*cis*-2-hex	$\%C_{12}$
0	100.0	-	-	-	-
10	1.7	18.8	58.8	17.5	3.5
20	1.8	18.5	57.4	18.5	3.7
40	1.7	18.5	57.3	18.8	3.6
60	1.6	18.5	57.4	18.5	3.5

Table 2.23 $[Ni(Nacac)_2] : AlEtCl_2 = 1 : 10$

Time(min)	%1-hex	%3-hex	%*tr*-2-hex	%*cis*-2-hex	$\%C_{12}$
0	100.0	-	-	-	-
10	1.0	13.7	38.2	10.9	35.2
20	0.9	13.2	38.5	10.9	36.9
40	0.8	13.1	38.1	10.9	37.3
60	0.8	12.7	36.5	10.8	38.8
120	0.7	12.1	36.4	10.6	40.0
180	0.7	12.0	36.5	10.7	40.2
330	0.6	11.6	34.7	10.7	42.3

Table 2.24 $[Ni(Sacac)_2]$: $AlEt_3$ = 1 : 1

Time(min)	%1-hex	%3-hex	%*tr*-2-hex	%*cis*-2-hex	$\%C_{12}$
0	100.0	-	-	-	-
60	100.0	-	-	-	-
120	100.0	-	-	-	-

Table 2.25 $[Ni(Sacac)_2]$: $AlEt_3$ = 1 : 10

Time(min)	%1-hex	%3-hex	%*tr*-2-hex	%*cis*-2-hex	$\%C_{12}$
0	100.0	-	-	-	-
10	13.8	17.0	54.8	14.4	-
30	11.3	17.9	55.5	15.5	-
90	11.5	17.9	55.0	14.3	-
270	9.9	18.0	56.0	16.1	-

Table 2.26 $[Ni(Sacac)_2]$: $AlEt_2Cl$ = 1 : 1

Time(min)	%1-hex	%3-hex	%*tr*-2-hex	%*cis*-2-hex	$\%C_{12}$
0	100.0	-	-	-	-
10	61.7	6.6	18.4	13.3	-
60	50.9	7.3	26.1	13.5	-
210	41.5	10.8	31.2	16.8	-

Table 2.27 $[Ni(Sacac)_2]$: $AlEt_2Cl$ = 1 : 10

Time(min)	%1-hex	%3-hex	%*tr*-2-hex	%*cis*-2-hex	$\%C_{12}$
0	100.0	-	-	-	-
30	15.7	17.7	51.4	15.2	-
60	10.4	18.5	53.5	17.6	-

Table 2.28 $[Ni(Sacac)_2]$: $Al_2Et_3Cl_3$ = 1 : 1

Time(min)	%1-hex	%3-hex	%*tr*-2-hex	%*cis*-2-hex	$\%C_{12}$
0	100.0	-	-	-	-
10	0.9	20.0	64.1	15.0	-
210	1.0	19.0	64.7	15.7	-

Table 2.29 $[Ni(Sacac)_2]$: $Al_2Et_3Cl_3$ = 1 : 10

Time(min)	%1-hex	%3-hex	%*tr*-2-hex	%*cis*-2-hex	$\%C_{12}$
0	100.0	-	-	-	-
10	1.0	19.6	62.6	16.8	-
120	0.9	19.7	62.9	16.4	-
210	1.0	19.9	63.7	15.5	-

Table 2.30 $[Ni(Sacac)_2]_3$: $AlEtCl_2$ = 1 : 1

Time(min)	%1-hex	%3-hex	%*tr*-2-hex	%*cis*-2-hex	$\%C_{12}$
0	100.0	-	-	-	-
20	1.1	19.8	59.6	17.4	2.0
60	1.0	19.9	60.0	16.9	2.2
120	1.0	20.3	60.8	16.6	2.3
300	0.9	20.3	61.0	16.1	2.7

Table 2.31 $[Ni(Sacac)_2]_3$: $AlEtCl_2$ = 1 : 10

Time(min)	%1-hex	%3-hex	%*tr*-2-hex	%*cis*-2-hex	$\%C_{12}$
0	100.0	-	-	-	-
10	2.0	9.7	31.2	7.9	49.2
20	1.1	9.6	29.8	7.2	50.5
40	1.1	10.3	31.2	7.2	50.3
120	1.0	10.6	32.1	7.6	49.9
330	1.0	10.0	30.1	6.8	52.1

Table 2.32 $[Ni(SacSac)_2]$: $AlEt_3$ = 1 : 1

Time(min)	%1-hex	%3-hex	%*tr*-2-hex	%*cis*-2-hex	$\%C_{12}$
0	100.0	-	-	-	-
10	100.0	-	-	-	-
30	100.0	-	-	-	-
60	100.0	-	-	-	-
300	100.0	-	-	-	-

Table 2.33 $[Ni(SacSac)_2]$: $AlEt_3$ = 1 : 10

Time(min)	%1-hex	%3-hex	%*tr*-2-hex	%*cis*-2-hex	$\%C_{12}$
0	100.0	-	-	-	-
20	96.3	0.8	2.4	0.4	-
30	92.4	1.5	4.4	1.7	-
90	88.7	2.1	6.1	3.7	-
270	81.0	3.1	9.1	6.8	-
2400	79.0	3.3	10.0	7.9	-

Table 2.34 $[Ni(SacSac)_2]$: $AlEt_2Cl$ = 1 : 1

Time(min)	%1-hex	%3-hex	%*tr*-2-hex	%*cis*-2-hex	$\%C_{12}$
0	100.0	-	-	-	-
10	90.3	2.0	5.8	1.9	-
30	88.5	2.3	7.0	2.2	-
120	84.8	2.8	8.4	4.0	-

Table 2.35 $[Ni(SacSac)_2]$: $AlEt_2Cl$ = 1 : 10

Time(min)	%1-hex	%3-hex	%*tr*-2-hex	%*cis*-2-hex	$\%C_{12}$
0	100.0	-	-	-	-
10	80.9	3.4	10.2	5.4	-
90	67.7	5.8	17.4	9.2	-
720	2.5	19.2	58.3	19.7	-
2160	1.5	20.0	60.1	18.1	-

Table 2.36 $[Ni(SacSac)_2]$: $Al_2Et_3Cl_3$ = 1 : 1

Time(min)	%1-hex	%3-hex	%*tr*-2-hex	%*cis*-2-hex	$\%C_{12}$
0	100.0	-	-	-	-
10	60.5	6.6	17.2	15.6	-
120	54.3	7.3	20.8	17.6	-

Table 2.37 $[Ni(SacSac)_2]$: $Al_2Et_3Cl_3$ = 1 : 10

Time(min)	%1-hex	%3-hex	%*tr*-2-hex	%*cis*-2-hex	$\%C_{12}$
0	100.0	-	-	-	-
10	3.9	19.0	61.0	16.0	-
250	1.0	20.0	62.7	16.3	-

Table 2.38 $[Ni(SacSac)_2]$: $AlEtCl_2$ = 1 : 1

Time(min)	%1-hex	%3-hex	%*tr*-2-hex	%*cis*-2-hex	$\%C_{12}$
0	100.0	-	-	-	-
10	85.1	3.2	9.9	2.0	-
120	85.0	3.6	9.4	2.0	-

Table 2.39 $[Ni(SacSac)_2]$: $AlEtCl_2$ = 1 : 10

Time(min)	%1-hex	%3-hex	%*tr*-2-hex	%*cis*-2-hex	$\%C_{12}$
0	100.0	-	-	-	-
10	10.4	19.4	56.3	13.8	-
60	1.1	20.7	62.3	15.9	-

2.4 DISCUSSION

2.4.1 Infrared Spectra

2.4.1.1 *Bis*(2,4-pentanedionato)copper(II), [Cu(acac)$_2$]

Of the three parent β-ketoenolates discussed (those of Ni(II), Cu(II) and Zn(II)), by far the most extensively reported infrared studies concern monomeric, square planar [Cu(acac)$_2$] [74]. On the basis of this structure, [Cu(acac)$_2$] may be assigned D_{2h} point group symmetry and two νM-O and three δO-M-O models are expected in the infrared spectrum. The frequencies and assignments are given in Table 2.2 and the spectra depicted in Fig. 2.6.

The results of the more detailed infrared studies appearing in the literature are summarised in Table 2.40.

As discussed in the Introduction, the controversy of the 1960's surrounding the assignment of νC=O and νC=C bands has been clearly resolved allowing firm assignment of the upper band (1577 cm^{-1}) to νC=O and the lower band (1527 cm^{-1}) to νC=C. A band occurs between these two stretching modes and, on the basis of its extreme sensitivity to γ-carbon deuteration [9], has been assigned to a combination band between infrared active and inactive C-H oop vibrations. The vibrations occurring at 1455 and 1415 cm^{-1} are undoubtedly C-H bending modes (δC-H). Based on their normal coordinate analyses, Nakamoto and Martell [8] and Mikami *et al.* [9] suggested that the upper band is coupled with νC=O, while on the grounds of metal [14] and ^{18}O-sensitivity [12], the lower band is also proposed as comprising some νC=O character. No two groups of authors appear to be in complete agreement, each acknowledging the existence of some νC=O character in this region (1470-1390 cm^{-1}). On the basis of the metal sensitivity observed in this work, νC=O character is attributed to the lower band (1415 cm^{-1}). Nakamura and Nakamoto [75] made a similar assignment on the same basis. Little controversy surrounds the assignment of the remaining vibrations above

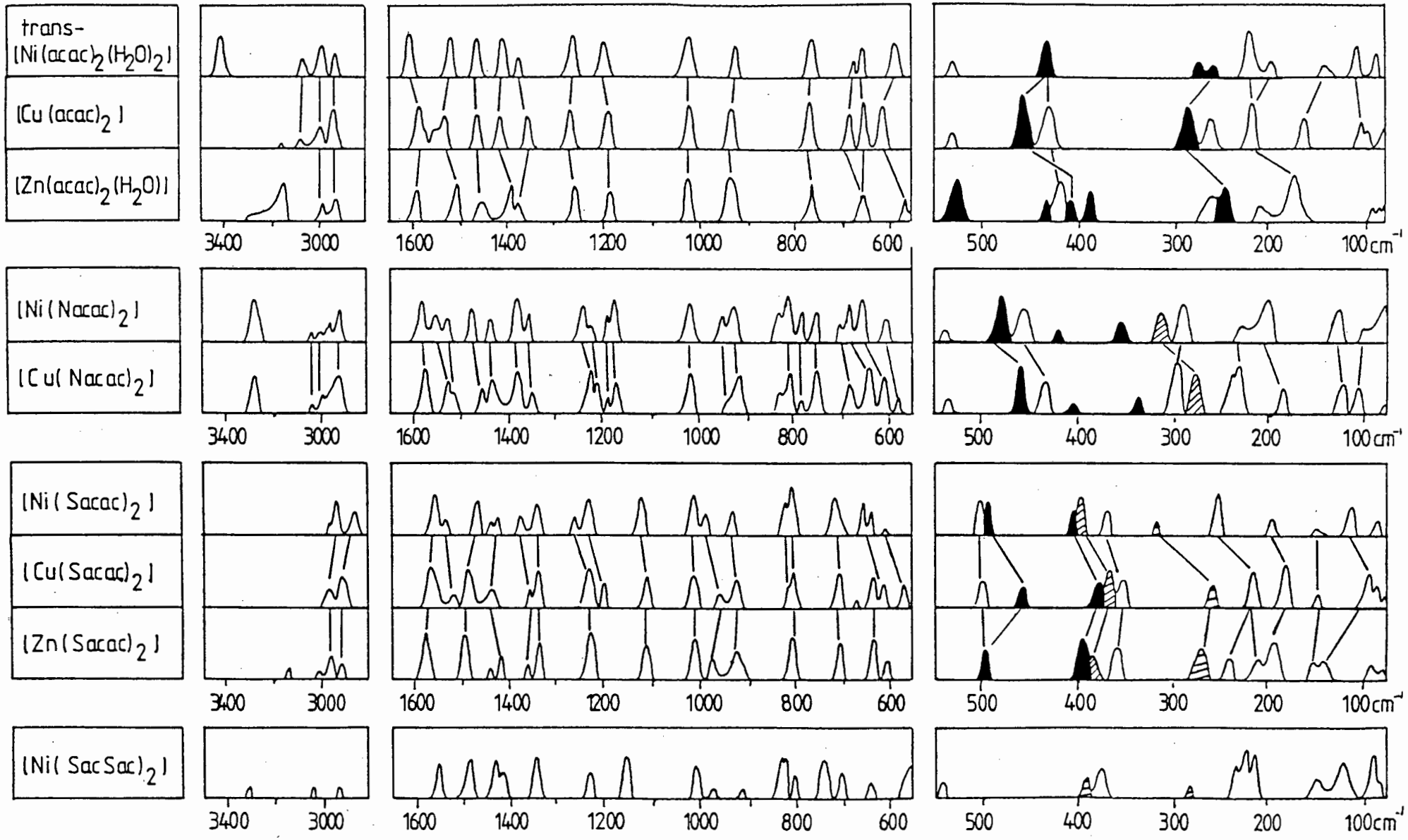

Figure 2.6 Infrared spectra of the acac, Nacac, Sacac and SacSac complexes.
Solid bands: νM-O, Shaded bands: νM-N or νM-S

Table 2.40 Infrared frequencies (cm^{-1}) and assignments for [$Cu(acac)_2$].

[$Cu(acac)_2$]	This work	Nakamoto [8]	Mikami [9]	Junge [12]	Vlckova [14]
3077	νC-H (γCH)		νC-H		νC-H
2988	-		$\nu_s CH_3$ ip		-
2977	-		$\nu_{as} CH_3$ ip		$\nu_{as} CH_3$
2974	νC-H (CH_3)		νCH_3		$\nu_{as} CH_3$
2923	-		νCH_3 oop		$\nu_s CH_3$
1578	νC=O	νC=C	νC=C + νC=O	ν_sC=O	ν_sC=O
1552	combination	νC=O	n.a.	-	δC-H oop
1530	νC=C	-	νC=O + νC=C	ν_{as}C=C=H + νC-C-H	ν_{as}C=C-C
1464	-	νC=O + δC-H	νC=O + δC-CH	-	$\delta_{as} CH_3$
1445	δC-H deg def	-	-	-	δ_{as}C=O
1430	-	-	δCH_3 oop	$\delta_{as} CH_3$	$\delta_{as} CH_3$
1415	δC-H deg def	δCH_3 deg def	$\delta_s CH_3$ ip	-	-
1403	-	-	$\delta_s CH_3$ip	ν_{as}C=O	$\delta_s CH_3$
1355	δC-H sym def	δCH_3 sym def	$\delta_s CH_3$	$\delta_s CH_3$	-
1340	-	-	$\delta_{as} CH_3$	-	-
1277	νC=C + νC-CH_3	νC=C + νC-CH_3	νC-CH_3 + δC-C-H	ν_sC=C-C	ν_sC=C-C
1189	δC-H ip	δC-H ip	δC-C-H	δC-C-H + ν_{as}C=O	δC-H ip
{1055}	-	-	$\rho_s CH_3$ ip	-	-
1020	ρCH_3	ρCH_3 oop	ρCH_3 ip	ρCH_3, δCH_3 oop	ρCH_3
{999}	-	-	ρCH_3 oop	-	-
938	νC-CH_3 +νC=O	νC-CH_3 +νC=O	νC=O +νC=C	complex	νC-CH_3
{895}	-	-	νC-CH_3 + νC=O	-	-
[825]	-	-	-	-	νC-CH_3
784	-	-	-	δC-H oop	δCH oop
780	δC-H oop	δCH oop	δCH oop	n.a.	δCH oop

Table 2.40 contd...

$[Cu(acac)_2]$	This work	Nakamoto [8]	Mikami [9]	Junge [12]	Vlckova [14]
685	ring def + νCu-O	ring def + νCu-O	ring def + νCu-O	ring def + $\nu C\text{-}CH_3$	ring ip
652	δC=C=C oop	$\delta C\text{-}CH_3$ + νCu-O	δC-C-C\O oop	δC=C-C oop	ring oop
614	ring def + νCu-O	n.a.	ring def + νCu-O	νCu-O	ring ip
[560]	$\delta C\text{-}CH_3$ + ring def	-	-	-	νCu-O
455	νCu-O	νCu-O	νCu-O	νCu-O + $\delta C\text{-}CH_3$	νCu-O
432	ring def	n.a.	ring def	n.a.	$\delta C\text{-}CH_3$ ip
[408]	-	-	-	-	$\delta C\text{-}CH_3$ oop
{373}	-	ring def	-		-
{320}	-	νCu-O	-		-
290	νCu-O	-	νCu-O		νCu-O
268	$\delta C\text{-}CH_3$ (+ νCu-O)	$\delta C\text{-}CH_3$	$\delta C\text{-}CH_3$ + νCu-O		$\delta C\text{-}CH_3$ ip
218	δO-Cu-O	-	δC-O + δCu-O		$\delta C\text{-}CH_3$ oop
{197}	-	ring def	-		
187	-		ring def		
167	δO-Cu-O		ring def		
104	ring def oop		$\delta C\text{-}CH_3$		
84	δO-Cu-O		δO-Cu-O		
74	lattice + δCH_3 oop		-		
60	lattice + δCH_3 oop		-		
{47}	-		δO-Cu-O		

ip = in-plane
oop = out-of-plane
def = deformation
s = symmetric
as = antisymmetric
n.a. = not assigned

{ } = calculated, not observed
[ ] = observed, not calculated

700 cm^{-1}. No certain assignment is given to the complex mode at 935 cm^{-1} which exhibits sensitivity to ^{13}C- and ^{18}O-labelling [12] as well as to metal ion substitution.

Assignment of the two νCu-O modes is facilitated by consideration of the results of metal isotope labelling [17]. Bands near 450 and 290 cm^{-1} are shifted most and are accordingly assigned to νCu-O. A lower frequency band (268 cm^{-1}), assigned to $\delta C\text{-}CH_3$ oop [8,14], is also shifted therefore implying coupling with νCu-O [9,75]. Of the three bands occurring between 700-600 cm^{-1}, those at 685 and 614 cm^{-1} shift on metal isotope and ^{18}O-labelling [12,17]. Both are assigned to ring deformations coupled with νCu-O [9]. The remaining band (650 cm^{-1}) is ^{13}C-sensitive [12] and is assigned to δC=C=C oop [9,12,14]. Although Vlckova *et al.* [14] assigned the band near 217 cm^{-1} to $\delta C\text{-}CH_3$ oop, observed metal isotope sensitivity suggests that assignment to δO-M-O is more appropriate.

The assignment of vibrations below 200 cm^{-1} is uncertain. Mikami *et al.* [9] suggested that bands above 100 cm^{-1} are oop ring deformations while those below 100 cm^{-1} are metal-oxygen bending modes. This is not in keeping with the general observation that the δO-M-O frequencies are roughly half those of νM-O. Vlckova *et al.* [14] suggested a reversal of these assignments which is consistent with the observations of Gillard *et al.* [76] who found the region from 400-120 cm^{-1} to be free of ring modes, but observed ring and methyl oop deformations below 120 cm^{-1}. Assignments in this study are made accordingly. The remaining bands are attributed to lattice vibrations.

2.4.1.2 Hydrated *Bis*(2,4-pentanedionato)nickel(II) and zinc(II), *trans*-$[Ni(acac)_2(H_2O)_2]$ and $[Zn(acac)_2(H_2O)]$

Certain inherent difficulties arise when comparing the infrared spectrum of $[Cu(acac)_2]$ with those of the nickel and zinc complexes. Two water molecules are *trans*-coordinated to the nickel [77] resulting in D_{2h} symmetry. One water molecule is coordinated to the zinc atom and the resulting complex has been shown crystallographically [78,79] to have approximately square-based pyramidal coordination and may therefore be

assigned to the C_{2v} point group. On the basis of these point groups, differing numbers of infrared-allowed M-L stretches may be expected. The square planar D_{2h} copper complex exhibited two νM-O bands while the D_{2h} nickel complex and C_{2v} zinc complex are expected to display three and five νM-O vibrations, respectively. Changes in band position are also expected due to mass and CFSE effects of the metal ions. In addition, a reduction in the coordination number is expected to cause vibrational shifts to higher frequencies [80].

The frequencies and proposed assignments are given in Table 2.2 and the spectra depicted in Fig. 2.6. Above 700 cm^{-1}, the spectra are comprised of ligand vibrations and comparison of the Ni(II) and Zn(II) complex spectra with that of Cu(II) is sufficient to allow an empirical assignment. An additional band at 1652 and 1615 cm^{-1} in the spectra of the Ni(II) and Zn(II) complexes, respectively, may be attributed to an H_2O bending vibration (δH-O-H) [81].

Below 700 cm^{-1}, the spectrum of *trans*-$[Ni(acac)_2(H_2O)_2]$ is similar to that of $[Cu(acac)_2]$ allowing for easy assignment of the bands in the 700-600 cm^{-1} region. The bands assigned to νCu-O at 454 and 288 cm^{-1} are shifted 27 and 33 cm^{-1} to 427 and 255 cm^{-1}, respectively, in the spectrum of the nickel complex. Such shifts are consistent with those previously observed [80] when changing from a four-coordinate to a six-coordinate complex. The greater shift of the lower frequency νM-O vibration was also observed by Nakamoto *et al.* [17] in their metal isotope labelling study. An additional band at 275 cm^{-1} (for which there is no analogue in the $[Cu(acac)_2]$ spectrum) may be assigned to the νNi-OH_2 mode.

Below 700 cm^{-1}, the spectrum of $[Zn(acac)_2(H_2O)]$ differs from those of the Ni(II) and Cu(II) species. A more complex array of bands is observed which is consistent with its lower C_{2v} symmetry. The ring deformations observed at 683 and 611 cm^{-1} for the Cu(II) complex are shifted to 653 and 570 cm^{-1}, respectively, in the spectrum of the zinc complex. These shifts are in agreement with the observed sensitivity of both of these bands to metal isotope labelling. The vibrations at 555, 433, 408, 388 and 239 cm^{-1} were observed to be those most sensitive to both $^{64,68}Zn$- and ^{18}O-labelling [13] and are therefore assigned to the five expected νZn-O modes. The largest shifts are observed for the

bands at 239 and 408 cm^{-1} indicating the greatest degree of vibrational purity. The band observed at 433 cm^{-1} exhibited greater sensitivity to metal isotope substitution than to ^{18}O-substitution resulting in its assignment to the νZn-OH_2 mode. The large difference in frequency between this vibration and the similarly assigned νNi-OH_2 mode observed at 275 cm^{-1} may be understood by considering the crystal structure of each complex. In the five coordinate zinc complex the Zn-OH_2 bond length is 2.00 Å [79], while the six-coordinate nickel complex has a Ni-OH_2 bond length of 2.14 Å [77]. The substantially shorter Zn-OH_2 value implies a stronger force constant and therefore a higher vibrational frequency. The bands observed at 421 and 210 cm^{-1} are relatively unshifted on isotopic labelling of the metal ion [13] and are assigned to oop ring deformations. A similar assignment is given to the band at 260 cm^{-1}, which was not observed by Niven *et al.* [13].

A direct comparison between the spectra of the acac complexes and those of the sulphur and nitrogen substituted derivatives is most clear for the complexes of copper, all of which are square planar. The most interesting region of the spectra is that below 700 cm^{-1} where the metal-ligand vibrations occur. This region is discussed with reference to the spectrum of $[Cu(acac)_2]$, prior to mentioning spectral differences above 700 cm^{-1} where absorptions are due to ligand vibrations.

2.4.1.3 The 4-Imino-2-pentanonate Complexes, $[M(Nacac)_2]$ (M = Ni, Cu)

Substitution of one oxygen atom of 2,4-pentanedione by the imino group, NH, leads to *trans*-square planar complexes $[M(Nacac)_2]$ [22,23,82]. These complexes have C_{2h} point group symmetry. This symmetry is lower than the D_{2h} symmetry of $[Cu(acac)_2]$, and these complexes are expected to exhibit two νM-L and five δL-M-L bands in their infrared spectra.

In the spectrum of $[Cu(Nacac)_2]$, five bands occur between 700 and 580 cm^{-1}. Only three occur in this region of the spectrum of the $[Cu(acac)_2]$ complex. The increased band multiplicity may be attributed to the lower symmetry of the $[M(Nacac)_2]$ complexes and consequent splitting of previously degenerate vibrations. The assignment of all

five bands as ring deformations is supported, not only by the analogous $[Cu(acac)_2]$ assignments, but by Gillard *et al.* [76] who attributed vibrations in this region exclusively to ring modes. Each of these bands is shifted between 15 and 50 cm^{-1} on substitution of nickel(II) for copper(II). Although ring modes are expected to be metal sensitive, these large shifts suggest coupling with νM-L, as observed for $[Cu(acac)_2]$. McGee and Walter [23] assigned the vibration observed at 617 cm^{-1} to a νM-L mode citing a similar assignment by Mikami *et al.* [9] and Junge and Musso [12] for $[Cu(acac)_2]$. However, Mikami *et al.* [9] assigned the band primarily to a ring deformation coupled with νCu-O, while Junge and Musso [12] did not extend their isotopic labelling study below 400 cm^{-1} and so did not observe the band near 300 cm^{-1} (subsequently assigned to νCu-O). The weak band observed near 550 cm^{-1} in the spectra of these Nacac complexes is assigned to a skeletal deformation as observed in the spectrum of the free ligand.

Below 500 cm^{-1}, $[Cu(acac)_2]$ and $[Cu(Nacac)_2]$ exhibit markedly similar infrared band patterns. The νM-L vibrations at 454 and 288 cm^{-1} in $[Cu(acac)_2]$ are observed at 463 and 277 cm^{-1} in the Nacac complex. In the square planar $[Ni(Nacac)_2]$ complex these bands are shifted to 481 and 315 cm^{-1}, respectively. The higher frequency vibration (481 cm^{-1}) is insensitive to nitrogen deuteration [23] and is therefore assigned to νNi-O and the band at 315 cm^{-1} to νNi-N. The relatively low intensity of the band at lower frequency is typical of νM-N modes [83]. Two very weak bands observed at 408 and 334 cm^{-1} for $[Cu(Nacac)_2]$ (for which no analogous $[Cu(acac)_2]$ bands exist) are shifted to 421 and 361 cm^{-1} when substituting nickel for copper. These two bands may be attributed to infrared forbidden νM-L modes which are observed due to lowering of the symmetry of the $[M(Nacac)_2]$ complexes. The skeletal deformations observed at 430 and 265 cm^{-1} for $[Cu(acac)_2]$ occur at 436 and 296 cm^{-1} in the spectrum of $[Cu(Nacac)_2]$. The sensitivity of the upper band to metal substitution implies strong coupling to the metal-ligand mode.

Below 250 cm^{-1}, assignment of δL-M-L at 228, 185 and 120 cm^{-1} for $[Cu(Nacac)_2]$ is readily made by comparison with $[Cu(acac)_2]$. The nickel complex is similar. The band at 230 cm^{-1} in the copper complex spectrum is unaffected by metal ion substitution and this supports its assignment

assignment on the basis of normal coordinate analysis to a $\tau C\text{-}CH_3$ torsional mode [23].

It is of interest to note that, if the νM-L assignments proposed above are correct, bands in the spectrum of the nickel complex are at higher frequencies than corresponding bands in the copper complex. In octahedral complexes the stability sequence Ni < Cu is usually observed because of the extra stabilisation which is conferred on the copper complex by JAHN-TELLER distortion [84]. However, in square planar symmetry, the expected stability sequence is Ni > Cu because the copper complex has an additional antibonding electron [85]. The νM-L frequency order for these complexes is Ni > Cu and this observation supports the proposed assignment.

2.4.1.4 The 4-Thioxo-2-pentanonate Complexes, $[M(Sacac)_2]$ (M = Ni, Cu, Zn)

The *cis*-square planar configuration of the nickel and copper complexes implies C_{2v} point group symmetry. Group Theory predicts sixty six infrared-active vibrations, of which four are νM-L modes. The zinc complex probably adopts a tetrahedral coordination geometry [28] and as such may be assigned C_2 symmetry. Of the eighty one infrared-active bands, four are expected to be νM-L modes.

Four ring deformations are observed between 700 and 570 cm^{-1} in the spectra of the square planar Sacac complexes. The lower three are shifted by metal ion substitution indicating possible coupling with νM-L vibrations. By contrast, a single broad peak occurs in the spectrum of $[Zn(Sacac)_2]$. However, shoulders on either side of the band indicate the presence of several nearly coincident vibrations.

A band occurs at very nearly 500 cm^{-1} in all three complexes. On the basis of a normal coordinate treatment [28], a split band at 498, 492 cm^{-1} in the spectrum of the nickel complex was assigned to $\delta C\text{-}CH_3$ + ring deformation. This assignment is reasonable so far as the 498 cm^{-1} component is concerned since this component is not shifted by metal ion substitution. However, the 492 cm^{-1} component shifts to 471 cm^{-1} on

substitution of copper for nickel and this suggests that it be correctly assigned to νM-O (probably coupled to δC-CH_3 [28]). The frequency order νNi-O > νCu-O would be anticipated for a band assigned to νM-O (or for that matter, to νM-S) for the reasons advanced above in the case of the Nacac complexes. In the tetrahedral zinc(II) complex, only one band occurs near 500 cm^{-1} and this is assigned to νZn-O + ring deformation + δC-CH_3 [30]. These assignments are at variance with the results of the normal coordinate analyses by Siiman *et al.* [28,30], which assigned a band at 648 cm^{-1} to νM-O. However, this band is less sensitive to metal substitution than those at lower frequencies. Assignment to an oop ring deformation which is coupled with νM-L is therefore preferred.

Both the nickel and copper complex spectra exhibit three bands between 410 and 360 cm^{-1}. The two upper bands at 409 and 396 cm^{-1} for the nickel complex are shifted to 387 and 379 cm^{-1}, respectively, on substituting nickel with copper. These bands are accordingly assigned to νM-O and νM-S, respectively. The lowest band at 373 cm^{-1} in the nickel complex is not as sensitive to metal substitution and is attributed to a ring deformation [28]. Only two bands are observed in this region of the $[Zn(Sacac)_2]$ spectrum, although a shoulder on the upper band indicates coincident vibrations. A weak band at 308 cm^{-1} in the spectrum of $[Ni(Sacac)_2]$, reported variously at 300 and 285 cm^{-1} by Siiman *et al.* [28,30], is strongly metal sensitive in the expected sequence Ni > Cu. It is assigned to νM-S due both to its low intensity and the fact that it is reasonably close to the calculated νNi-S frequency [30]. The band at 252 cm^{-1} in the spectrum of $[Ni(Sacac)_2]$ is assigned to δL-M-L. Although previously attributed to a stretching vibration [86], the occurrence of this band at approximately half the frequency of νM-O (492 cm^{-1}) supports this assignment. In addition, all four expected νM-L are already assigned. The weak band at 196 cm^{-1} is observed at 194 cm^{-1} in the Raman spectrum where it has been assigned as a further νNi-S mode [86]. However, substitution of copper for nickel causes the band to shift only 12 cm^{-1} and, in addition, the δS-Ni-S bands in the spectrum of $[Ni(SacSac)_2]$ occur near 200 cm^{-1}. For these reasons assignment to a metal-ligand bending mode is preferred.

The remaining vibrations below 200 cm^{-1} are assigned to δL-M-L and lattice modes with the exception of the band near 150 cm^{-1} which is

attributed to a ring deformation on the grounds of its insensitivity to metal substitution. This is consistent with the normal coordinate analysis of Siiman and Fresco [30]. The assignment of two bands at 396, 308 cm^{-1} and 379, 264 cm^{-1} in the spectra of the nickel and copper complexes, respectively, is consistent with the sequence Ni > Cu, expected for νM-S modes. These bands are also reasonably located at lower frequencies than the νM-O modes due to the greater mass of the sulphur atom as well as the fact that the M-O force constant is greater than the M-S force constant [28]. In the Zn(II) complex, the νZn-S bands occur at 386 and 274 cm^{-1}; the greater number of bending vibrations observed in this spectrum is consistent with the C_2 symmetry of the zinc complex.

2.4.1.5 *Bis*(2,4-pentanedithionato)nickel(II), [Ni(SacSac)$_2$]

The square planar nickel complex has D_{2h} point group symmetry and is therefore analogous to [Cu(acac)$_2$] for which two νM-L and three δL-M-L are expected. Assignment is also facilitated by the presence of only one type of metal-ligand mode (νNi-S).

Two ring deformation modes are observed at 648 and 556 cm^{-1}. While Siiman and Fresco [38] proposed that the band at 556 cm^{-1} is coupled with νM-S, the fact that the band is unshifted on metal ion substitution [38] implies that this is not the case. The region 550-440 cm^{-1}, where νM-O was observed for the [Ni(Nacac)$_2$] and [Ni(Sacac)$_2$] complexes, is free from bands.

The band at 390 cm^{-1} clearly qualifies for assignment to νNi-S. This is consistent with normal coordinate analyses performed for this square planar complex and its cobalt(II) analogue [36,38]. In addition, it supports assignment of the band at 396 cm^{-1} in [Ni(Sacac)$_2$] to νNi-S. Assignment of the band at 286 cm^{-1} to νNi-S is also consistent with these normal coordinate analyses. Similarly, the band at 374 cm^{-1} may be assigned to a ring deformation. The bands at 240, 227 and 216 cm^{-1} are clearly δS-Ni-S modes occurring at approximately half the frequency of the corresponding stretches. Their appearance at these frequencies supports the assignment of the 252 and 196 cm^{-1} vibrations in the

spectrum of the mixed donor atom complex, $[Ni(Sacac)_2]$, to bending modes rather than the previously proposed stretching bands *(vide infra)*. The vibration at 149 cm^{-1} is unshifted on changing from $[Ni(Sacac)_2]$ to $[Ni(SacSac)_2]$, further supporting its assignment to a ring deformation.

2.4.2 Spectra in the Mid-infrared Region

In the acac complex spectra, the presence of coordinated water in the nickel and zinc complexes yields νO-H bands near 3400 cm^{-1} (nickel) and 3300 cm^{-1} (zinc). The methyl groups give rise to νC-H bands within the range 3200-2900 cm^{-1} in all of the spectra. The stretches of the γ-methine groups are observed weakly above 3000 cm^{-1} [81]. In the Nacac complexes the single expected νN-H is a strong band near 3300 cm^{-1}.

In each complex two bands near 1580 and 1520 cm^{-1} are unambiguously assigned to νC=O and νC=C, respectively. These assignments are further supported by the shift of νC=C in the Sacac and SacSac complexes to 1490 cm^{-1} due to extensive coupling [30]. As expected, the νC=O band is absent from the spectrum of $[Ni(SacSac)_2]$. In addition, the presence of νC=O at values below 1650 cm^{-1} in the Sacac complexes implies that both the oxygen and sulphur atoms are coordinated to the metal ion, and the oxygen atom does not have the free character observed for the cadmium, silver and mercury complexes [35].

Bands which are unique to the spectra of the Nacac complexes are attributed to vibrations involving the nitrogen atom. The νC-N mode occurs near 1380 cm^{-1} which is similar to that found in the free ligand [87]. As expected, this band is absent from the acac complex spectra. The metal sensitive vibration near 1470 cm^{-1} is assigned to the δN-H ip mode, while a triplet between 830 and 750 cm^{-1} is assigned to δN-H oop. Extensive splitting of vibrations in the Nacac complex spectra may be attributed to their lower symmetry and to solid state effects [23].

For complexes of Sacac, Chaston *et al.* [33] assigned a band in the region 1270-1190 cm^{-1} to νC-S and tentatively assigned a band between 837 and 805 cm^{-1} to a coupled νC-S and δCH_3 mode. However, subsequent normal coordinate analyses on complexes of both the Sacac [28] and the

SacSac [36,38] ligands have shown the C-S stretching frequency to occur near 700 cm^{-1}. This is further supported by the assignment of νC-S in the region 850-550 cm^{-1} in dithiooxalato complexes [88,89], dithiooxamido complexes [90] and xanthato complexes [91]. Assignment of νC-S near 720 cm^{-1} is also supported by the observed shifts of 9 and 17 cm^{-1}, on substituting nickel with copper and zinc, respectively. This vibrational frequency is low for a carbon-sulphur double bond. However, bonding in the chelate ring of $[Ni(Sacac)_2]$ most resembles the resonance structure with a single C-S bond [30]. The band observed at 985 cm^{-1} in $[Ni(Sacac)_2]$ is shifted 25 cm^{-1} on substituting copper for nickel. This metal sensitivity may be due to extensive coupling to νC-S, as observed for vibrations near 1050 cm^{-1} in dithiooxalato [88] and SacSac complexes [38].

2.4.3 ^{1}H and ^{13}C NMR Spectra

The ^{1}H and ^{13}C NMR data are listed in Table 2.3, and are consistent with the four-coordinate structures that have been proposed earlier. Octahedral $[Ni(acac)_2(H_2O)_2]$ and square planar copper complexes are paramagnetic and as a result their spectra were not obtained.

Although the data have been used primarily to characterise the complexes, a few points of interest may be mentioned. Firstly, in the ^{1}H NMR spectra, the methine proton is most sensitive to metal ion and ligand donor atom substitution, whereas in the ^{13}C NMR, the methine carbon atom as well as the carbon atoms attached to the ligand donor atoms are sensitive to substitution. Secondly, the ^{1}H and ^{13}C resonances associated with the chelate ring are shifted considerably on ligand donor atom substitution and only slightly on metal ion substitution.

Finally, the complexes $[Ni(Nacac)_2]$ and $[Ni(Sacac)_2]$ have the possibility of existing as *cis*- or *trans*-isomers. However, it is concluded that either one isomer predominates at ambient temperature or that, as seen in similar systems [98], rapid exchange is taking place.

2.4.4 Catalysis

In this section, the catalytic activities of the four nickel complexes, $[Ni(acac)_2]_3$, $[Ni(Nacac)_2]$, $[Ni(Sacac)_2]$ and $[Ni(SacSac)_2]$, are discussed. The relative rates of the competing feed isomerisation and oligomerisation reactions and the selectivity of each system to linear products is ascertained. For clarity, the discussion of the various catalytic systems is divided into two sections: "chloride-free" and "chloride-containing" systems. The former employs $AlEt_3$ as co-catalyst and the effects of complex structure, co-catalyst concentration and 1-hexene concentration are investigated. In the "chloride-containing" systems, three co-catalysts are employed: $AlEt_2Cl$, $Al_2Et_3Cl_3$ and $AlEtCl_2$. It is therefore possible to study the effects of Lewis acid strength on the catalytic reaction.

Active oligomerisation reactions are only obtained in the presence of a co-catalyst, in this case, a Lewis acid. Prior to discussing the activity of the nickel catalysts, it is therefore necessary to establish that the reactions observed are not catalysed by the Lewis acid. At high temperatures and pressures, nickel has been shown to play the role of co-catalyst in the dimerisation of ethene by aluminium alkyls [92]. This reaction is unlikely, however, under the mild conditions in which the nickel-based catalysts are effective.

Under the rigidly anhydrous conditions used, none of the aluminium co-catalysts exhibit any isomerisation or oligomerisation activity in the absence of a nickel catalyst. However, for the stronger Lewis acids, $AlEtCl_2$ and $Al_2Et_3Cl_3$, the introduction of a trace amount of water leads to rapid and complete oligomerisation of the olefin. The products consist of approximately 60% dimer, 30% trimer and 10% tetramer with no significant shift of this distribution with time. In addition, changing from $AlEtCl_2$ to $Al_2Et_3Cl_3$ does not change the product distribution. In this reaction, the Lewis acids act as acid catalysts. The catalytic species is the superacid formed in the presence of a proton source, in this case water [59].

A comparison between the C_{12} products of the nickel catalysed and the acid catalysed oligomerisation shows them to be entirely different. The isomers formed during the former reaction have different retention times to the acid catalysed products. The fact that none of the acid catalysed C_{12} isomers are observed in the nickel catalysed reactions, implies that all activity is due to the active nickel species. The mechanism of acid catalysis (Fig. 1.4) proceeds *via* an unstable intermediate carbonium ion. This may undergo extensive rearrangement, thereby producing branched products with little selectivity [93]. The production of the two distinctive groups of dimers may also be due to the fact that internal olefins undergo acid catalysis more readily than α-olefins, whereas nickel catalysts preferentially oligomerise α-olefins.

It has been proposed that when a nickel catalyst is used, even in the presence of a large excess of Lewis acid, no "free acid" remains in the medium [55]. However, when water is introduced during nickel catalysed oligomerisation, acid catalysis is still observed.

2.4.4.1 "Chloride-free" Systems

Triethylaluminium, $AlEt_3$

A $[Ni(acac)_2]_3$ catalyst, used in conjunction with an equimolar amount of $AlEt_3$ co-catalyst, has been shown to be an active oligomerisation system [42]. The oligomerisation reaction is rapid (Fig. 2.7) and significant quantities of both dimer (C_{12}) and trimer (C_{18}) are formed. Figure 2.8 shows the proportions of the major C_{12} isomers recorded, the most abundant being the linear isomer, dodecene. Selectivity to the linear isomer is also exhibited in the C_{18} fraction. This is as predicted for systems in which a weak, halogen-free Lewis acid is used as co-catalyst [42,43,49]. Of the remaining three nickel complexes, $[Ni(Nacac)_2]$, $[Ni(Sacac)_2]$ and $[Ni(SacSac)_2]$, none is able to catalyse 1-hexene oligomerisation in the presence of an equimolar concentration of $AlEt_3$.

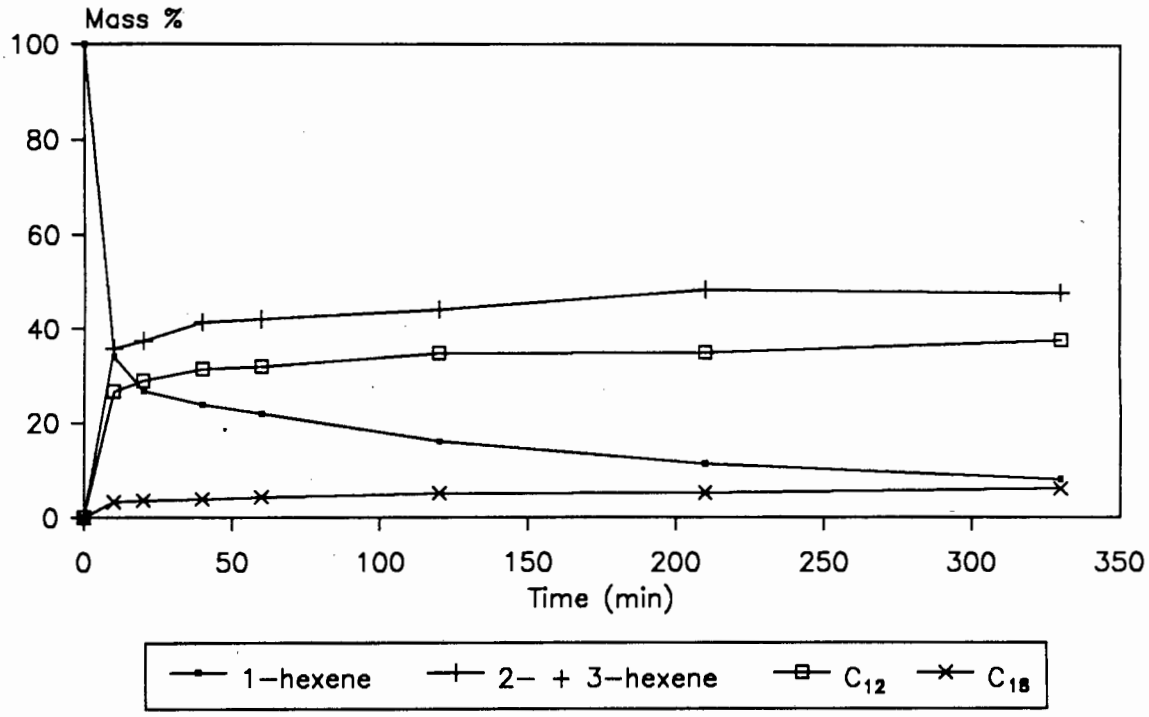

$[Ni(acac)_2]_3 : AlEt_3 = 1 : 1$

T = 40°C

Figure 2.7 Graph of conversion of 1-hexene with time.

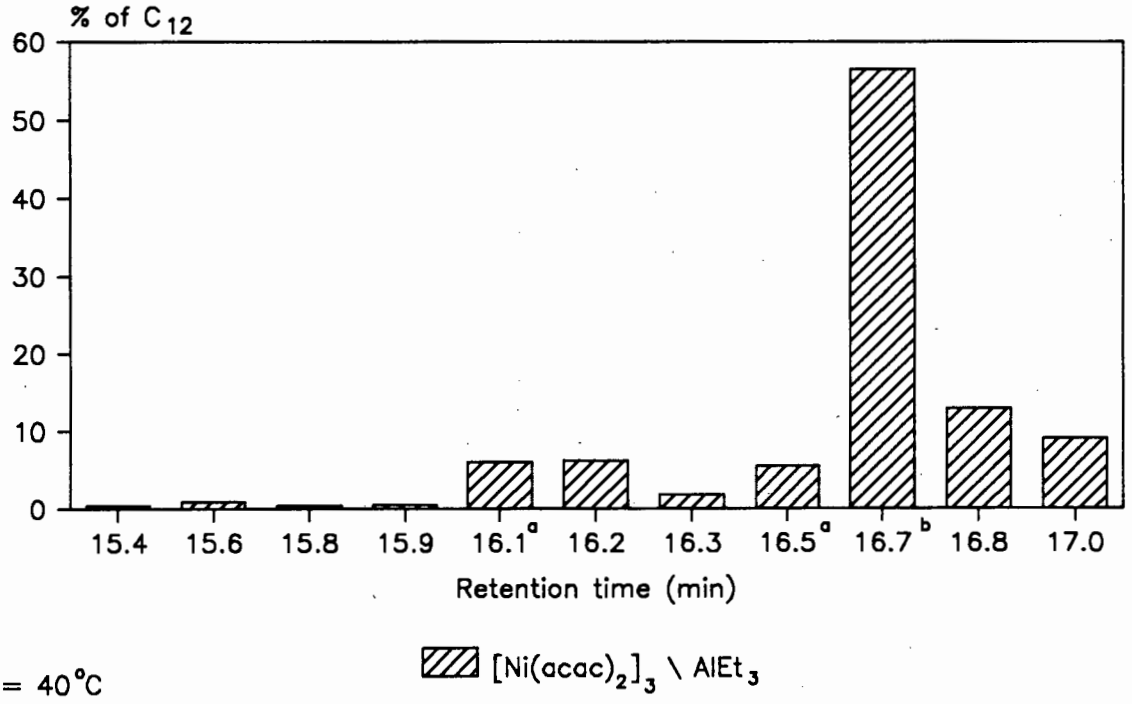

T = 40°C

Cat : Co–cat = 1 : 1

a = unresolved isomers, b = linear dodecene

Figure 2.8 Graph of distribution of dimer products.

Of the four catalytic systems tested above, only those employing the $[Ni(acac)_2]_3$ and $[Ni(Nacac)_2]$ complexes catalyse the isomerisation of 1-hexene. In the former system the reaction is rapid, while in the latter it is much slower. The products of the isomerisation are the *cis*- and *trans*-isomers of 2- and 3-hexene with no evidence of branched isomers. The identity of these isomers is proposed on the basis of their GC elution times and confirmed by ^{1}H and ^{13}C NMR of the fractionated product. Both Jones and Symes [42] and Keim *et al.* [43] have observed similar 1-hexene isomerisation reactions in which only internal isomers were formed. The rapid equilibration of the linear isomers is as expected for straight chain olefins in which the rate of successive double bond migration steps is not hindered by the presence of branching [55]. Isomerisation therefore occurs in a stepwise manner and at equilibrium the ratio of 1-hexene to 2- and 3-hexene is 1 : 79 : 19, respectively. This is similar for each oligomerisation system and is the same as the relative concentrations reported by Keim *et al.* [43]. For systems in which isomerisation of 1-hexene is rapid, the concentration of *cis*-2-hexene is observed to decrease with time. While the *cis*-isomer is initially formed, it rapidly isomerises to the more stable *trans*-isomer [94]. Although it has been proposed that the final isomer distribution approaches thermodynamic equilibrium [92], this is not entirely true. For example, at 25°C, 47% of a thermodynamic equilibrium mixture would be *trans*-2-hexene [95], while approximately 64% *trans*-2-hexene is present in the reaction mixtures at equilibrium. It is thus possible that the catalyst exerts some steric control over the isomerisation reaction.

The results depicted in Fig. 2.7 indicate what appears to be rapid deactivation of the dimerisation reaction. This is understood when considering that the rate of oligomerisation of internal olefins is generally much slower than that of α-olefins [92]. As is often the case for equilibrium mixtures of linear olefins, the α-olefin is only a minor component [92]. Once equilibrium is reached, the path of the oligomerisation reaction is therefore hindered by the limited availability of the reactive α-monomer. This is clearly seen from the results obtained when a further volume of 1-hexene is added to the reaction mixture after 3 hours of reaction (Fig. 2.9). The increase in the rate of oligomerisation shows that the system is still active and

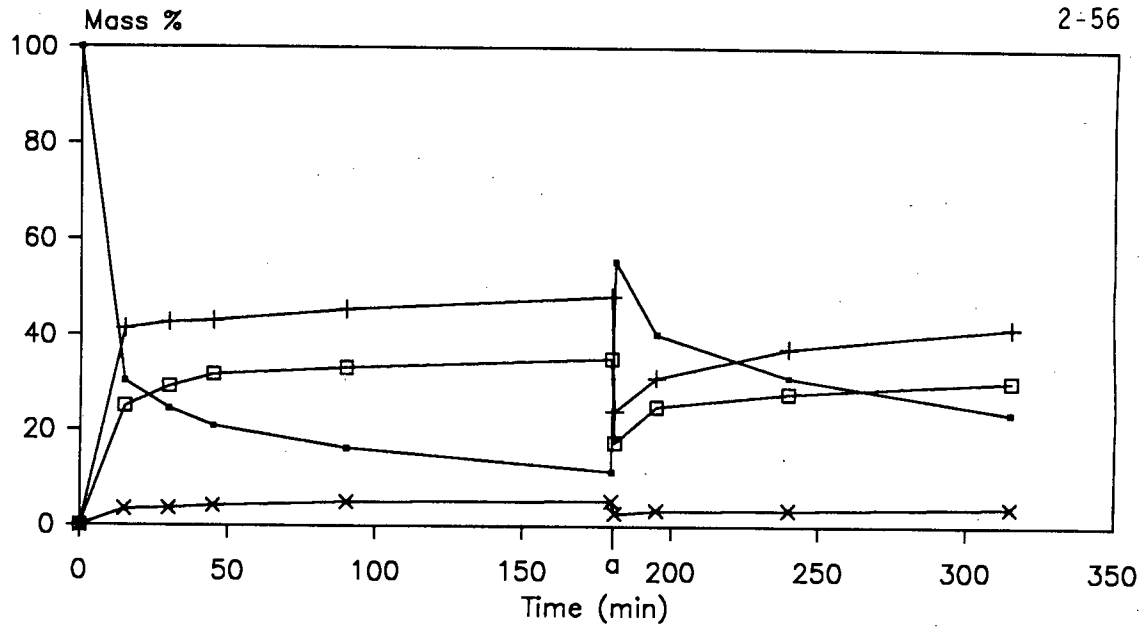

T = 40°C

$[Ni(acac)_2]_3$: $AlEt_3$ = 1 : 1

a = addition of further 1–hexene

Figure 2.9 Graph of the effect of addition of further 1-hexene after 3 hours of reaction.

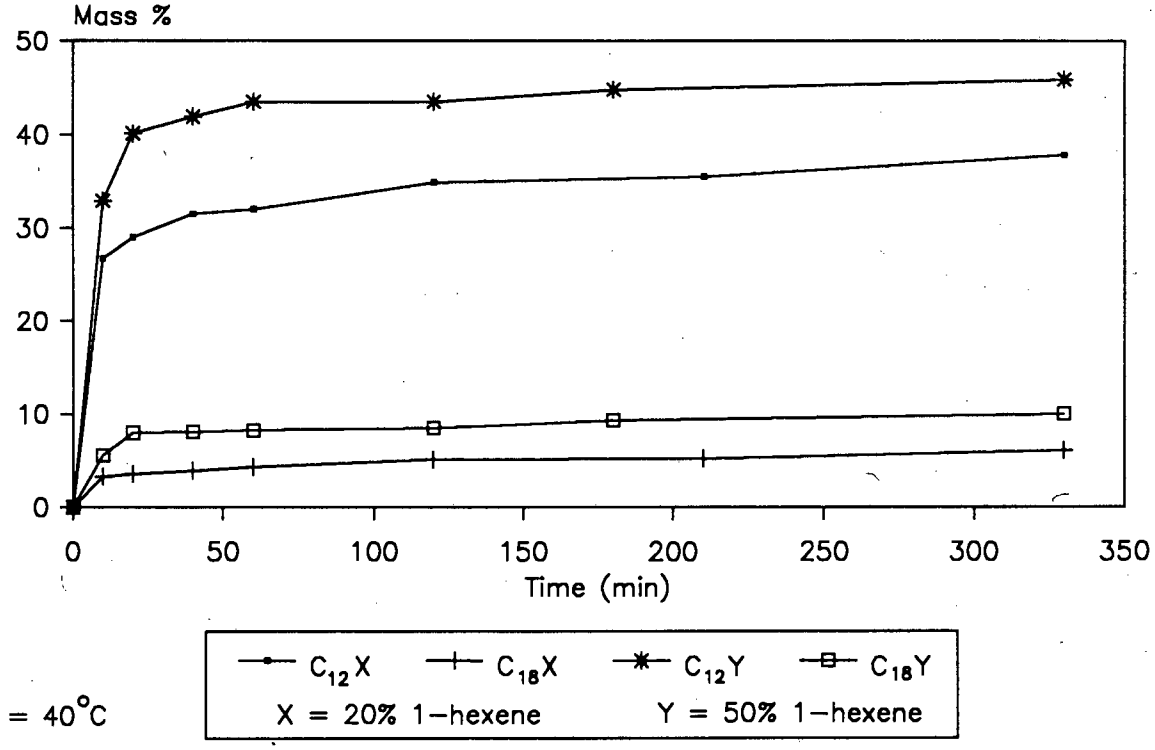

T = 40°C

$[Ni(acac)_2]_3$: $AlEt_3$ = 1 : 1

Figure 2.10 Graph of the effect of a change in feed concentration on the oligomerisation reaction.

implies that the decrease in the reaction rate is due, at least in part, to the low concentration of 1-hexene present.

By maintaining a constant volume, but increasing the concentration of 1-hexene from 20% v/v to 50% v/v in toluene, it is possible to observe the effect of 1-hexene concentration on the relative rates of oligomerisation and isomerisation. The increased feed concentration leads to significant enhancement of the oligomerisation reaction as well as an increase in trimerisation activity relative to that of dimerisation (Fig. 2.10). In addition, the isomerisation reaction is less active (Fig. 2.11). The fact that an increase in dielectric constant will lead to an increase in the rate of isomerisation relative to that of oligomerisation implies that when unisomerised products are required, solvent free systems should be used [55].

Finally, the effect of an increase in the concentration of the co-catalyst was investigated. The presence of a ten molar excess of co-catalyst relative to catalyst completely suppresses the oligomerisation reaction, irrespective of the nickel catalyst used. By contrast, the rate of the isomerisation reaction is increased for each catalyst. Figure 2.12 illustrates increasing isomerisation activity in the order:

$$[Ni(SacSac)_2] < [Ni(Sacac)_2] < [Ni(Nacac)_2] \sim [Ni(acac)_2]_3.$$

When a four molar excess of co-catalyst is used, $[Ni(acac)_2]_3$ is a more active isomerisation catalyst than $[Ni(Nacac)_2]$. Isomerisation activity therefore follows the order:

$$[Ni(SacSac)_2] < [Ni(Sacac)_2] < [Ni(Nacac)_2] < [Ni(acac)_2]_3.$$

2.4.4.2 "Chloride-containing" Systems

Diethylaluminium Chloride, $AlEt_2Cl$

In addition to being a stronger Lewis acid than $AlEt_3$, $AlEt_2Cl$ introduces chloride ions to the system. Of the four nickel catalysts

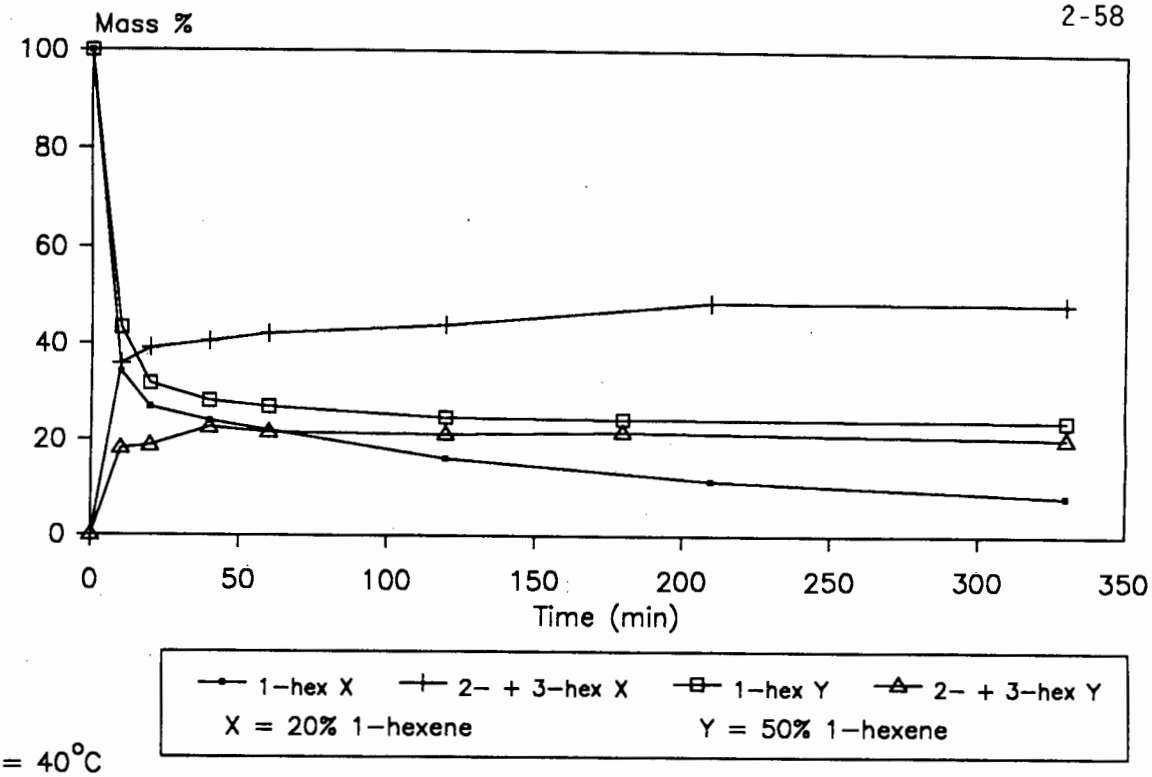

T = 40°C

$[Ni(acac)_2]_3$: $AlEt_3$ = 1 : 1

Figure 2.11 Graph of the effect of a change in feed concentration on the isomerisation reaction.

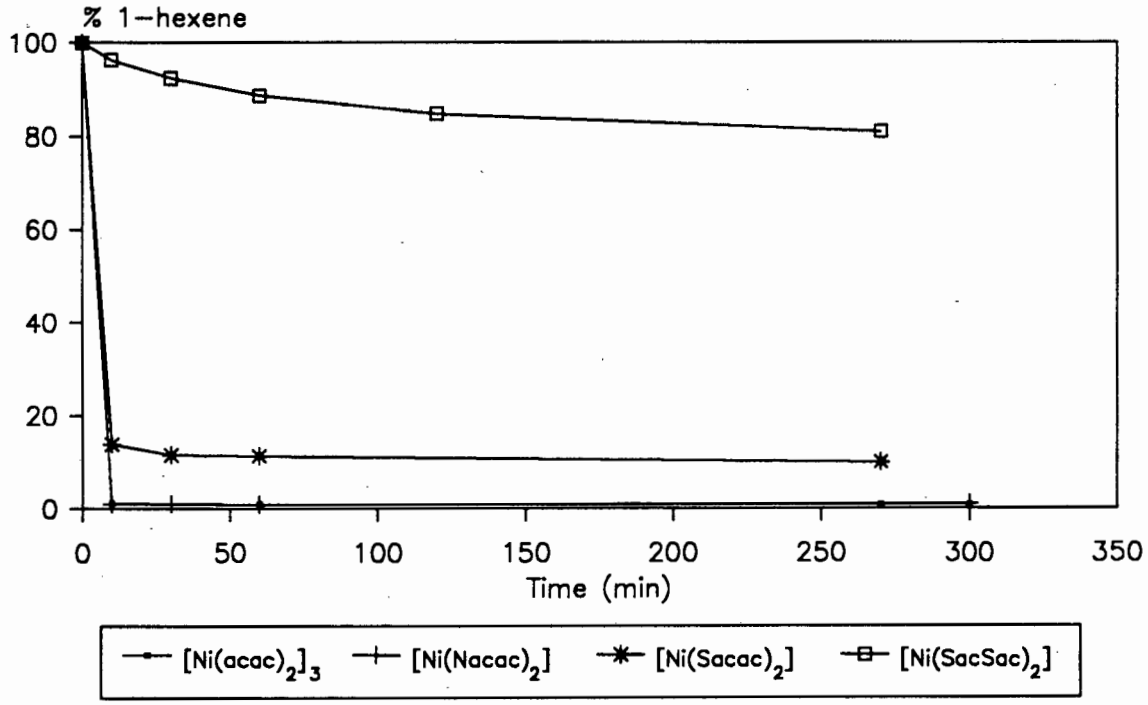

Cat : $AlEt_3$ = 1 : 10

T = 40°C

Figure 2.12 Graph of the effect of catalyst on 1-hexene isomerisation.

used in conjunction with an equimolar amount of $AlEt_2Cl$ co-catalyst, only the $[Ni(acac)_2]_3$ complex forms an active olefin oligomerisation system. However, only 4% of the olefin mass is dimerised (no higher oligomers form). Increasing to a ten molar excess of co-catalyst gives similar results.

In the presence of equimolar proportions of catalyst and co-catalyst, all the complexes are active isomerisation catalysts, with the relative activities depicted in Fig. 2.13. The order follows that observed above for systems employing the $AlEt_3$ co-catalyst. When the co-catalyst is present in a ten fold excess the isomerisation activity of each catalyst is increased while the order of activity remains unchanged.

Ethylaluminium Sesquichloride, $Al_2Et_3Cl_3$

Although $Al_2Et_3Cl_3$ is a strong Lewis acid, very little oligomerisation is observed. When using a 1 : 1 catalyst to co-catalyst ratio only the $[Ni(acac)_2]_3$ and $[Ni(Nacac)_2]$ complexes are active; each dimerises only 4% of the olefins present. On increasing the above ratio to 1 : 10, the oligomerisation activity of the above systems is only slightly enhanced, while $[Ni(Sacac)_2]$ and $[Ni(SacSac)_2]$ remain inactive.

By contrast, the rate of the isomerisation reaction is almost instantaneous for each nickel complex used at both 1 : 1 and 1 : 10 catalyst : co-catalyst ratios. The exception is the $[Ni(SacSac)_2]$ catalyst which exhibits low isomerisation activity at a 1 : 1 ratio. This is substantially increased at a 1 : 10 ratio.

Ethylaluminium Dichloride, $AlEtCl_2$

The $AlEtCl_2$ co-catalyst is the strongest Lewis acid used. In the presence of equimolar proportions of co-catalyst, each catalyst system exhibits low oligomerisation activity with the exception of the $[Ni(SacSac)_2]$ which is inactive. Increasing to a ten molar excess of co-catalyst enhances the dimerisation activity of each system while

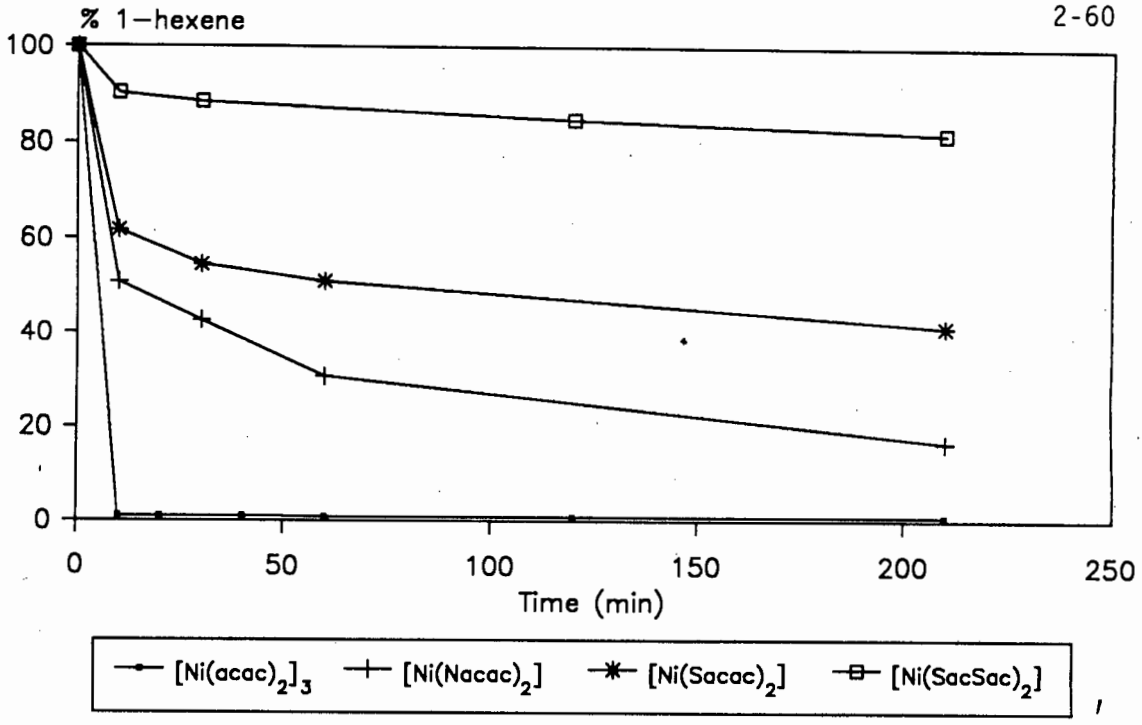

Cat : $AlEt_2Cl$ = 1 : 1

T = 40°C

Figure 2.13 Graph of the effect of catalyst on 1-hexene isomerisation.

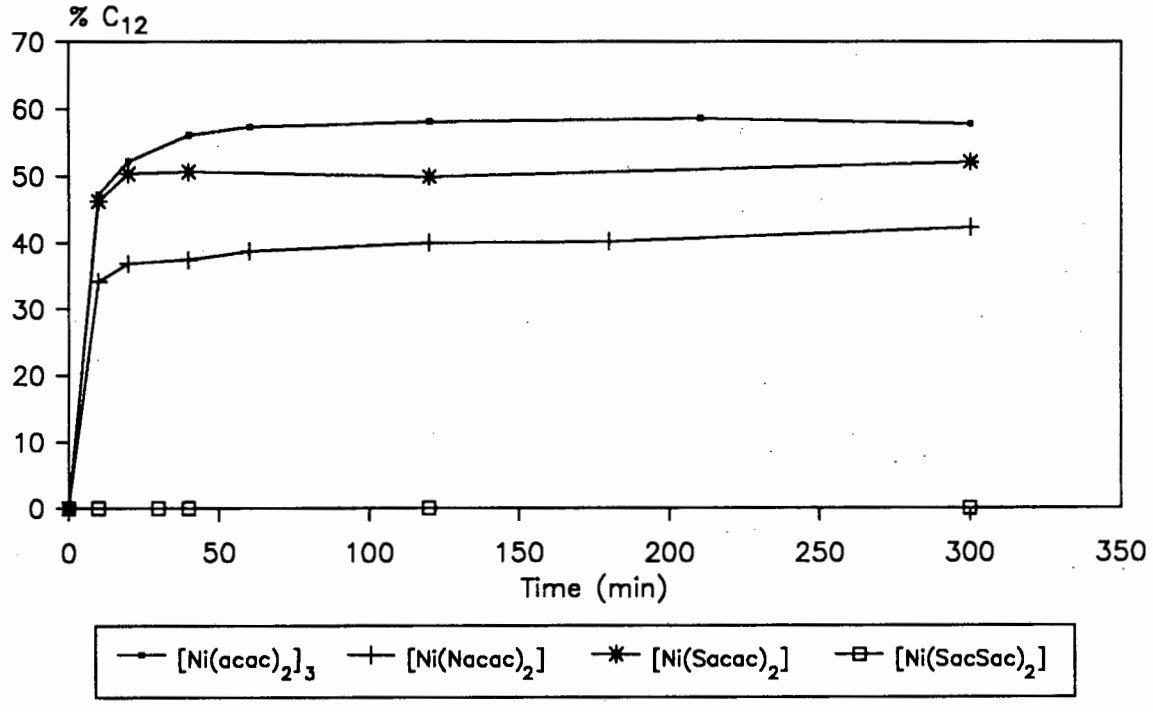

Cat : $AlEtCl_2$ = 1 : 10

T = 40°C

Figure 2.14 Graph of the effect of catalyst on 1-hexene dimerisation.

$[Ni(SacSac)_2]$ remains inactive (Fig. 2.14). The oligomerisation activity therefore increases in the order:

$$[Ni(SacSac)_2] << [Ni(Nacac)_2] < [Ni(Sacac)_2] < [Ni(acac)_2]_3.$$

The reduction in activity, illustrated by the levelling of the activity curves in Fig. 2.14, may be attributed to the limited quantity of 1-hexene remaining after isomerisation is complete. However, after further addition of 1-hexene very little dimerisation is observed, while isomerisation is again almost immediate (Fig. 2.15). It appears that, after 3 hours, the catalytic species responsible for dimerisation has deactivated.

Each of the above active nickel catalysts exhibits similar selectivity. Figure 2.16 shows the similarity in the distribution of dimer product. At no time are higher oligomers formed.

The isomerisation reaction is similar to that observed for the $Al_2Et_3Cl_3$ system in which isomerisation is instantaneous at both 1 : 1 and 1 : 10 catalyst to co-catalyst ratios. The $[Ni(SacSac)_2]$ catalyst system is again the exception and exhibits only subdued isomerisation activity.

2.4.4.3 Comparison of Relative Effects

Catalyst Effects

In the above systems employing a ten-fold excess of $AlEtCl_2$, dimerisation activity increases in the following order:

$$[Ni(SacSac)_2] << [Ni(Nacac)_2] < [Ni(Sacac)_2] < [Ni(acac)_2]_3.$$

In addition, the selectivity of the catalytic system is not influenced by the nickel complex. The linear dodecene only accounts for 10% of the C_{12} product. The uniformity in product distribution implies that the mechanism of oligomerisation is not affected by the type of nickel

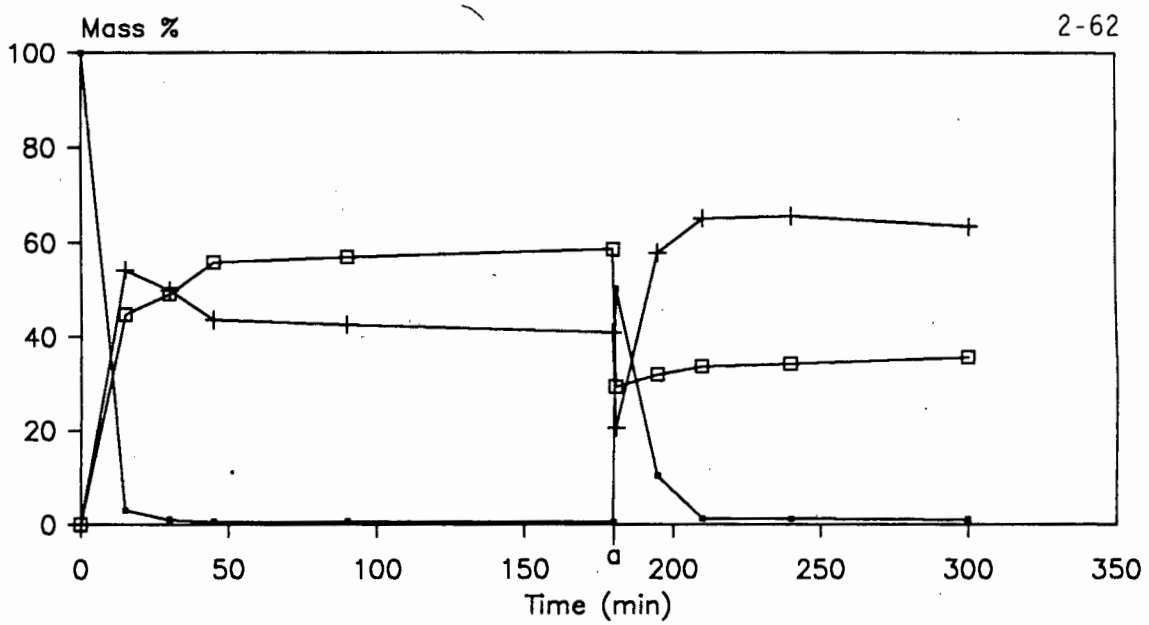

T = 40°C

$[Ni(acac)_2]_3$: $AlEtCl_2$ = 1 : 10

a = addition of further 1–hexene

Figure 2.15 Graph of the effect of addition of further 1-hexene after 3 hours of reaction.

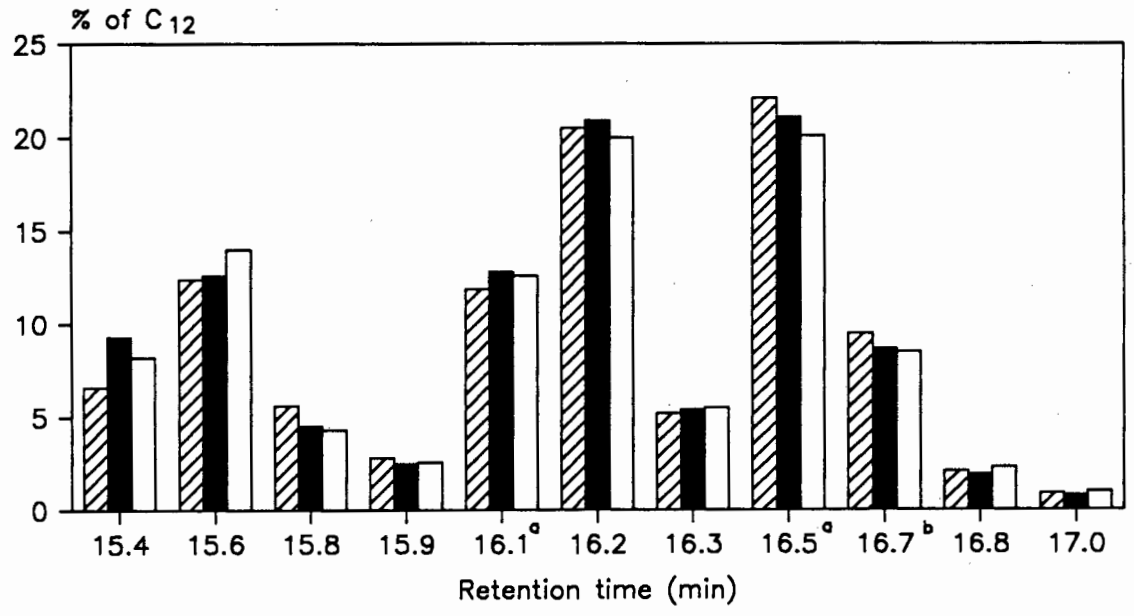

T = 40°C

Cat : $AlEtCl_2$ = 1 : 10

a = unresolved isomers, b = linear dodecene

Figure 2.16 Graph of the effect of catalyst on distribution of dimer products.

catalyst used, and that a similar active species has been formed in each case.

In the presence of equimolar quantities of $AlEt_2Cl$ and nickel, the isomerisation activity increases in the order: (Fig. 2.13)

$$[Ni(SacSac)_2] << [Ni(Sacac)_2] < [Ni(Nacac)_2] < [Ni(acac)_2]_3.$$

The selectivity of this reaction is also unaffected by the nickel catalyst used. For each system a similar equilibrium of C_6 isomers is obtained.

While reaction selectivity is independent of the nickel catalyst, the activity is markedly affected by a change in catalyst structure.

Each of the four catalysts used has a different structure. Dehydration of $[Ni(acac)_2(H_2O)_2]$ results in trimerisation of the nickel complex to form a species containing six coordinate Ni(II) centres [Fig. 2.17(a)]. The resulting chelate ring is stabilised by extensive electron delocalisation. The trimeric structure is retained in toluene solution [4].

Unlike $[Ni(acac)_2]_3$, $[Ni(Nacac)_2]$ has a *trans*-square planar structure [21] [Fig. 2.17(b)]. As for all square planar nickel species, the complex is diamagnetic. Although stable in organic solvents, $[Ni(Nacac)_2]$ is easily hydrolysed to $[Ni(acac)_2(H_2O)_2]$ in aqueous solution.

The $[Ni(Sacac)_2]$ species is also square planar but, unlike $[Ni(Nacac)_2]$, crystallographic studies have revealed a *cis*-conformation [Fig. 2.17(c)] [28]. Stability constant studies have shown that $[Ni(Sacac)_2]$ is more stable than the analogous $[Ni(acac)_2]_3$ complex [96].

Finally, the $[Ni(SacSac)_2]$ complex is a stable, square planar chelate [Fig. 2.17(d)] [37].

The only catalyst which exhibits no oligomerisation activity is $[Ni(SacSac)_2]$. It appears likely that enhanced activity is associated

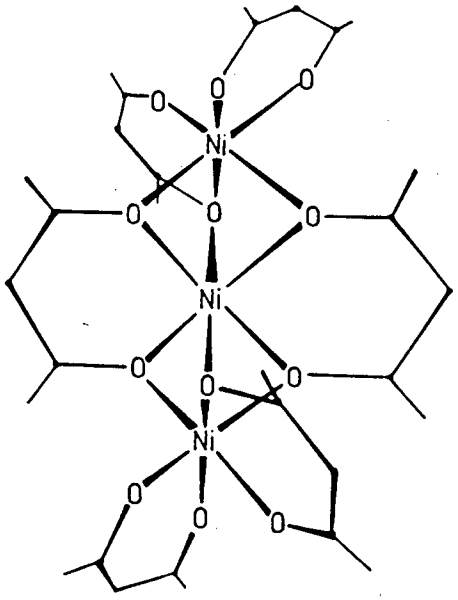

(a) $[Ni(acac)_2]_3$

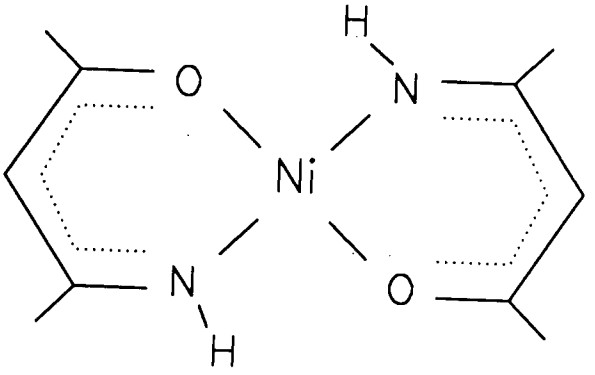

(b) $[Ni(Nacac)_2]$

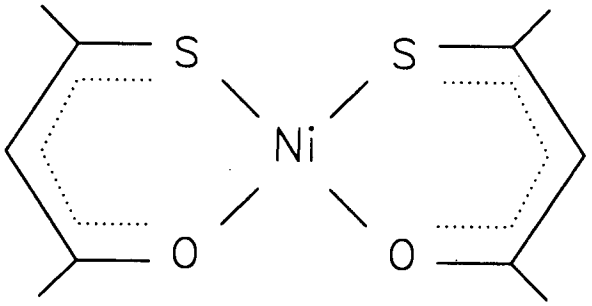

(c) $[Ni(Sacac)_2]$

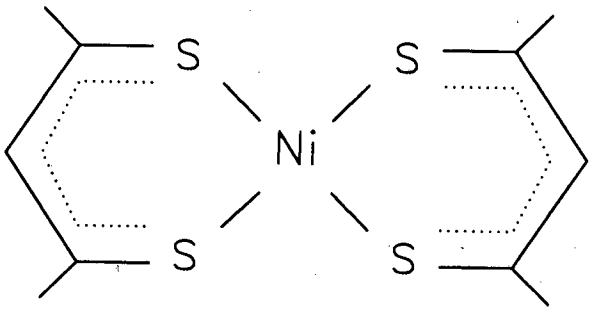

(d) $[Ni(SacSac)_2]$

Figure 2.17 Structures of nickel chelate catalysts.

with the presence of oxygen donor atoms on the chelating ligands. This is further supported by the fact that the catalyst with greatest activity, $[Ni(acac)_2]_3$, has the greatest number of oxygen donor atoms. In spite of the varied structures, the selectivity of each catalyst is similar, suggesting that the intact nickel complex does not influence the structure of the active species. This supports the proposal of Bogdanovic [48] in which all ligands are dissociated from the nickel centre and a halogen bridged dimer is the active species (Fig. 2.18).

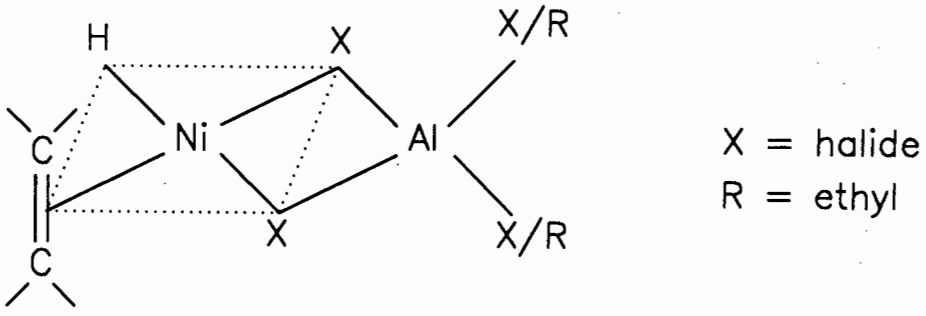

Figure 2.18 Proposed active nickel complex [48].

If this is the case, the chelating ligands play no direct role in the catalytic reaction. Rather, they influence the formation of the active species. The ease with which this species is formed may be linked to the stability of the nickel complex. Indeed, the system employing the $[Ni(Sacac)_2]$ complex exhibits lower activity than that with the less stable $[Ni(acac)_2]_3$ complex. In addition, the lack of activity observed for the $[Ni(SacSac)_2]$ complex, even in the presence of excess Lewis acid, may be understood when considering that $[Ni(SacSac)_2]$ is stable in boiling hydrochloric acid [36].

Co-Catalyst Effects

It is not possible to observe dimerisation trends at a 1 : 1 catalyst to co-catalyst ratio as the dimerisation reaction is insufficiently active for reliable product analysis. With the exception of $AlEt_3$, the dimerisation activity is enhanced at increased concentrations of co-catalyst.

The effect of a change in co-catalyst on dimerisation activity is best observed by considering the activity of $[Ni(acac)_2]_3$ in conjunction with a tenfold excess of Lewis acid (Fig. 2.19). Increased activity follows the order of increased Lewis acidity:

$$AlEt_3 < AlEt_2Cl < Al_2Et_3Cl_3 < AlEtCl_2.$$

This is contradictory to a previous report [55] in which activity increased in the following order:

$$AlEt_2Cl < AlEtCl_2 < Al_2Et_3Cl_3.$$

However, these results were obtained in a chlorobenzene medium.

The effect of changing the co-catalyst on the isomerisation reaction is best observed by studying the $[Ni(SacSac)_2]$ systems in which no oligomerisation occurs. Figure 2.20 shows the relative amounts of 1-hexene remaining unisomerised after ten minutes of reaction. For both a 1 : 1 and 1 : 10 catalyst to co-catalyst ratio, isomerisation activity increases in the order:

$$AlEt_3 < AlEt_2Cl < AlEtCl_2 < Al_2Et_3Cl_3.$$

In addition, isomerisation activity is enhanced by increasing the concentration of each co-catalyst. The fact that activity generally parallels Lewis acid strength and concentration may be understood in the light of the rôle of the co-catalyst to break the nickel-chelate bonds to form the active species. The selectivity of the isomerisation reaction remains unchanged when the Lewis acid is altered. The isomerisation mechanism is therefore independent of the co-catalyst [94].

Finally, the Lewis acid co-catalyst strongly influences the relative rates of the competing oligomerisation and isomerisation reactions. Once the olefin has inserted into the nickel-hydride bond, one of two processes can occur. The first is the insertion of a further olefin into the nickel-carbon bond to form a dimer product. This is known as

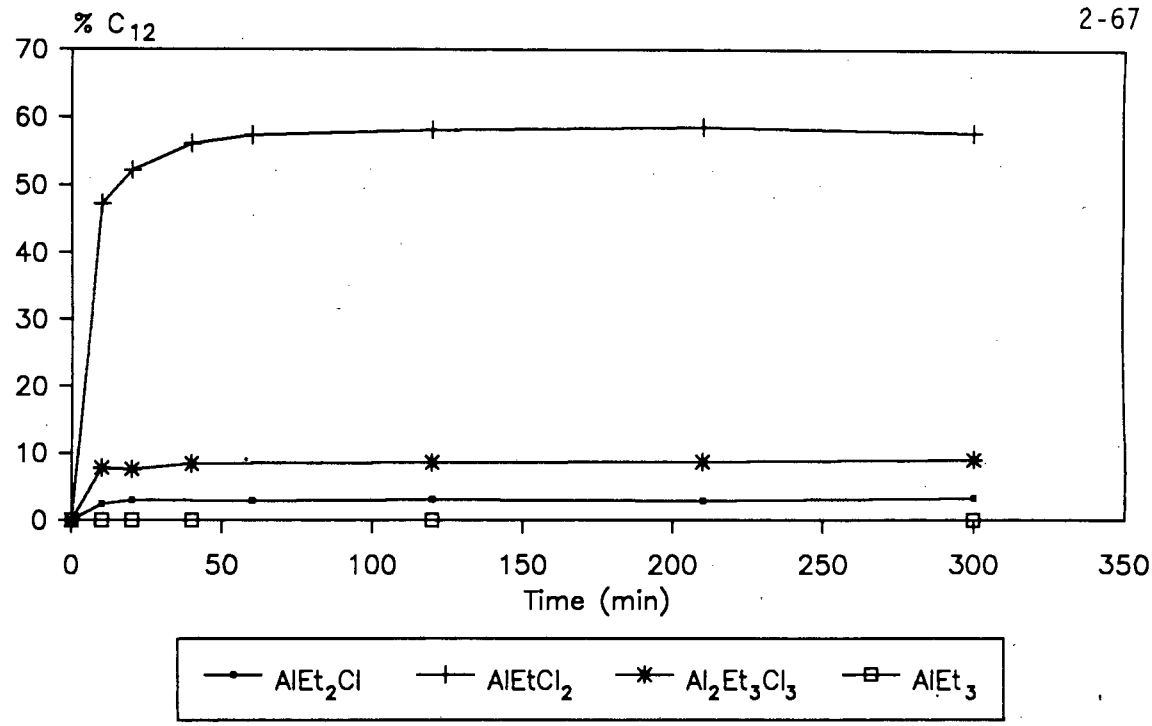

$[Ni(acac)_2]_3$: Co-cat = 1 : 10

T = 40°C

Figure 2.19 Graph of the effect of co-catalyst on 1-hexene dimerisation.

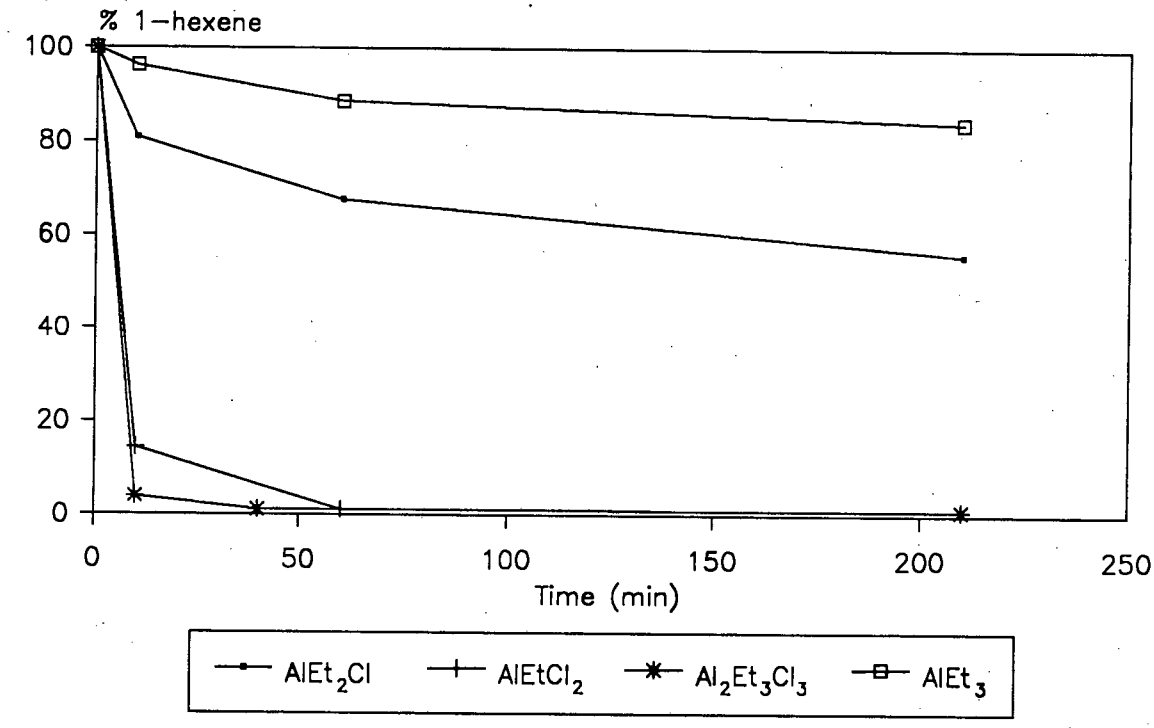

$[Ni(SacSac)_2]$: Co-cat = 1 : 10

T = 40°C

Figure 2.20 Graph of the effect of co-catalyst on 1-hexene isomerisation.

the propagation reaction. The second is the elimination of the olefin from the nickel complex which results in isomerisation. The final distribution of olefin products depends on the rate of the propagation reaction (k_p) relative to that of the elimination reaction (k_e). If $k_p >> k_e$, propagation is favoured and the products are mainly oligomers. If $k_p << k_e$, the isomerisation reaction dominates.

As has been previously reported [42], k_p is generally less than k_e. However, by changing the Lewis acid the relative rates of these reactions may be controlled. An increase in k_p relative to k_e parallels increasing Lewis acidity:

$$AlEt_3 < AlEt_2Cl < Al_2Et_3Cl_3 < AlEtCl_2.$$

Furthermore, increasing the concentration of the co-catalyst relative to that of the catalyst increases k_p *versus* k_e. This highlights the fact that the Lewis acid plays an integral role in the rate determining step of the reaction [59]. It is also a reason why many researchers use large molar excesses of co-catalyst [40,43,63-65].

The $[Ni(acac)_2]_3$ / $AlEt_3$ Catalytic System

Of all the catalytic systems studied, the $[Ni(acac)_2]_3$ complex, used in the presence of an equimolar concentration of $AlEt_3$, is unique. It differs from the other systems in the following ways:

(a) $k_p > k_e$,
(b) not only dimer, but trimer and some tetramer are formed at 40°C,
(c) the oligomeric products are predominantly linear (Fig. 2.21),
(d) the oligomerisation reaction is suppressed by excess of $AlEt_3$,
(e) the oligomerisation activity is less than that of the $[Ni(acac)_2]_3$ / $AlEtCl_2$ system (Fig. 2.22).

The unique selectivity and activity of this system implies the presence of a different active species from that discussed above. Two possible species have been postulated (Fig. 2.23):

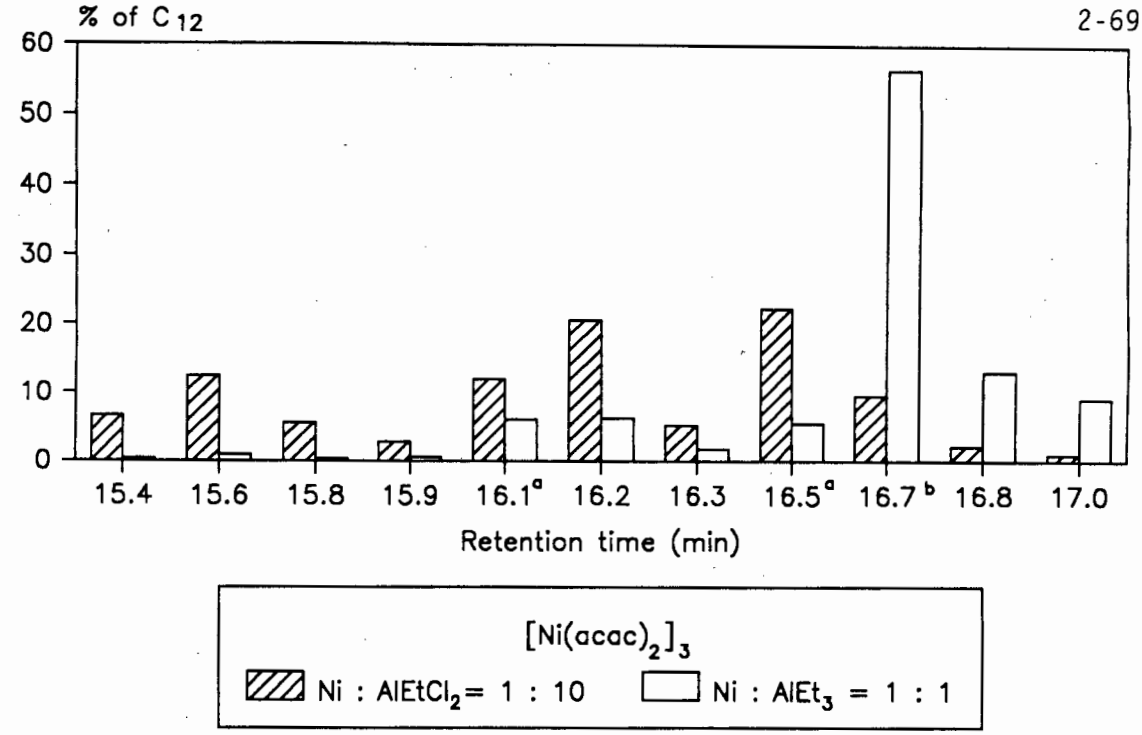

T = 40°C

a = unresolved isomers, b = linear dodecene

Figure 2.21 Graph of the effect of co-catalyst on dimer distribution.

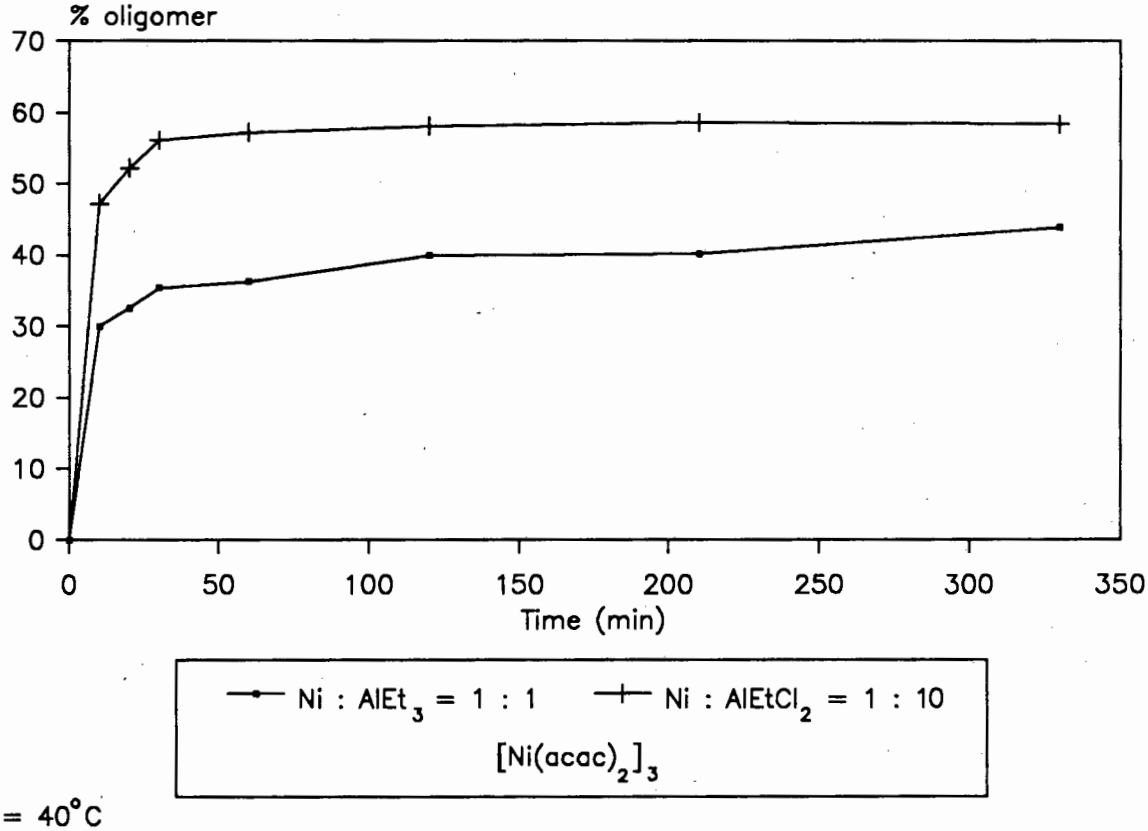

T = 40°C

Figure 2.22 Graph of the effect of co-catalyst on 1-hexene dimerisation.

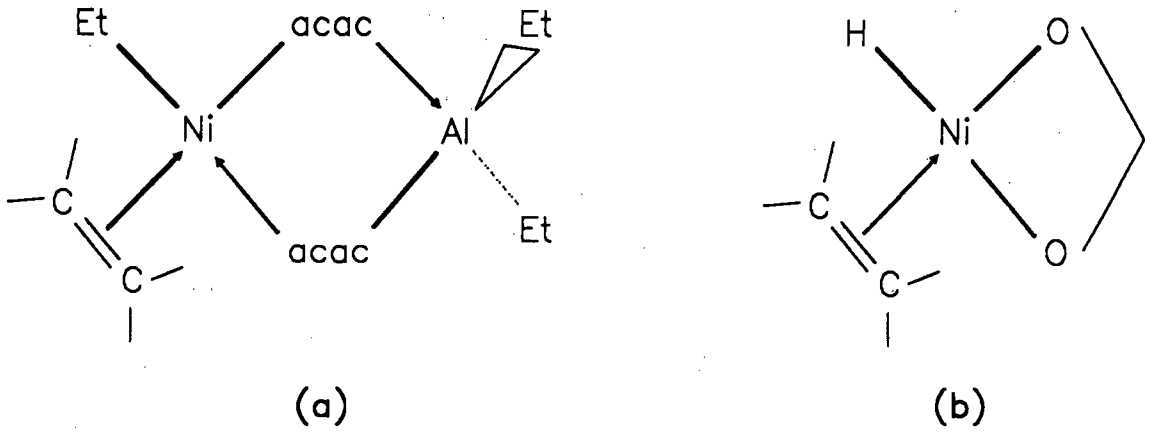

Figure 2.23 Proposed active species
(a) Jones and Symes [42]
(b) Keim *et al*. [44].

While (a) was specifically postulated for the $[Ni(acac)_2]_3$ / $AlEt_3$ system, (b) was proposed for a Lewis acid-free system or for any system in which a weak, halogen-free Lewis acid is used.

Formation of either of the above species involves the partial dissociation of the $[Ni(acac)_2]_3$ complex. This is possible with a weak co-catalyst such as $AlEt_3$ and may explain why increasing the strength or concentration of the Lewis acid prohibits formation of the active species. The inability of $[Ni(Nacac)_2]$, $[Ni(Sacac)_2]$ and $[Ni(SacSac)_2]$ to form the above proposed complex may be due to the different bonding capabilities of the O, N and S atoms. For example, the Lewis acids used are "hard" acids and will therefore readily bind to oxygen which is also a "hard" acid [97]. Both nitrogen and sulphur are "softer" than oxygen and bonding to the aluminium species is therefore not as favourable.

REFERENCES

1. J.L. Burdett and M.T. Rodgers, J. Amer. Chem. Soc., **86** (1964) 2105.

2. G.T. Morgan and H.W. Moss, J. Chem. Soc., **105** (1914) 189.

3. C.M. Harris and S.E. Livingstone, in "Chelating Agents and Metal Chelates", (1964), Academic Press, New York, p. 100.

4. J.P. Fackler, Progr. Inorg. Chem., **7** (1966) 361.

5. J. Lecomte, Disc. Faraday Soc., **9** (1950) 125.

6. C. Duval, R. Freymann and J. Lecomte, Bull. Chem. Soc. France, **19** (1952) 106.

7. L.J. Bellamy and R.F. Branch, J. Chem. Soc., (1954) 4491.

8. K. Nakamoto and A.E. Martell, J. Chem. Phys., **32** (1960) 588.

9. M. Mikami, I. Nakagawa and T. Shimanouchi, Spectrochim. Acta., **23A** (1967) 1037.

10. G.T. Behnke and K. Nakamoto, Inorg. Chem., **6** (1967) 433.

11. S. Pinchas, B.L. Silver and I. Laulicht, J. Chem. Phys., **46** (1967) 1506.

12. H. Junge and H. Musso, Spectrochim. Acta, **24A** (1968) 1219.

13. M.L. Niven and D.A. Thornton, Spectrosc. Lett., **13** (1980) 419.

14. B. Vlckova, B. Strauch and M. Horak, Coll. Czech. Chem. Comm., **50** (1985) 306.

15. K. Nakamoto, P.J. McCarthy and A.E. Martell, J. Amer. Chem. Soc., **83** (1961) 1272.

16. K. Nakamoto, P.J. McCarthy, A. Ruby and A.E. Martell, J. Amer. Chem. Soc., **83** (1961) 346, 1066.

17. K. Nakamoto, C. Udovich and J. Takemoto, J. Amer. Chem. Soc., **92** (1970) 3973.

18. W.O. George, Spectrochim. Acta, **27A** (1971) 265.

19. A. Combes and C. Combes, Bull. Chem. Soc. France, **7** (1892) 778.

20. R.D. Archer, Inorg. Chem., **2** (1963) 292.

21. C.E. Gurr, Inorg. Chem., **3** (1964) 614.

22. H.F. Holtzclaw, J.P. Collman and R.M. Alire, J. Amer. Chem. Soc., **80** (1958) 1100.

23. T.J. McGee and J.L. Walter, Spectrosc. Lett., **11** (1978) 765.

24. E. Fromm and P. Ziersch, Chem. Ber., **39** (1906) 3599.

25. S.K. Mitra, J. Indian Chem. Soc., **10** (1933) 71.

26. J. Sieler, P. Thomas and E. Uhlemann, Zeit. Chem., **7** (1967) 243.

27. E.A. Shugam, L.M. Shkol'nikova and S.E. Livingstone, Zhur. Struk. Khim., **8** (1967) 550.

28. O. Siiman, D.D. Titus, C.D. Cowman, J. Fresco and H.B. Gray, J. Amer. Chem. Soc., **96** (1974) 2353.

29. A. Ouchi, M. Hyodo and Y. Takahashi, Bull. Chem. Soc. Japan, **40** (1967) 2819.

30. O. Siiman and J. Fresco, J. Chem. Phys., **54** (1971) 734.

31. O. Siiman and J. Fresco, J. Chem. Phys., **54** (1971) 740.

32. A. Fredga and A. Brandstrom, Ark. Kemi., **1** (1949) 197.

33. S.H.H. Chaston, S.E. Livingstone, T.N. Lockyer, V.A. Pickles and J.S. Shannon, Aust. J. Chem., **18** (1965) 673.

34. R.K.Y. Ho, S.E. Livingstone and T.N. Lockyer, Aust. J. Chem., **18** (1965) 1929.

35. S.H.H. Chaston and S.E. Livingstone, Aust. J. Chem., **20** (1967) 1065.

36. C.G. Barraclough, R.L. Martin and I.M. Stewart, Aust. J. Chem., **22** (1969) 891.

37. R. Beckett and B.F. Hoskins, J. Chem. Soc. Dalton, (1974) 622.

38. O. Siiman and J. Fresco, Inorg. Chem., **8** (1969) 1846.

39. D.A. Thornton, Coord. Chem. Rev., in press (1990).

40. J. Ewers, Angew. Chem. Int. Edit., **5** (1966) 584.

41. J.R. Jones, J. Chem. Soc. C, (1971) 1117.

42. J.R. Jones and T.J. Symes, J. Chem. Soc. C, (1971) 1124.

43. W. Keim, B. Hoffman, R. Lodewick, M. Peuckert, G. Schmitt, J. Fleischhauer and U. Meier, J. Mol. Catal., **6** (1979) 79.

44. W. Keim, A. Behr and G. Kraus, J. Organomet. Chem., **251** (1983) 377.

45. G. Henrici-Olivé and S. Olivé, Angew. Chem. Int. Edit., **14** (1975) 104.

46. K.J. Cavell and A.F. Masters, J. Chem. Res., (1983) 72.

47. K.J. Cavell and A.F. Masters, Aust. J. Chem., **39** (1986) 1129.

48. B. Bogdanovic, Adv. Organomet. Chem., **17** (1979) 105.

49. K. Zhou, Z. Gao and W. Keim, Proc. VIIIth International Congress on Catalysis, Berlin, **V** (1984) 429.

50. W. Keim, F.H. Kowaldt, R. Goddard and C. Kruger, Angew. Chem. Int. Edit., **17** (1978) 466.

51. W. Keim, Ann. N.Y. Acad. Sci., **415** (1983) 191.

52. M. Peuckert and W. Keim, Organometallics, **2** (1983) 594.

53. K.A.O. Starzewski and J. Witte, Angew. Chem. Int. Edit., **24** (1985) 7.

54. W. Keim *et. al.*, (1972), US Patents 3 635 937, 3 644 563, 3 647 914, 3 647 915, 3 686 159.

55. G. Lefebvre and Y. Chauvin, in "Aspects of Homogeneous Catalysis", (1970), Carlo Manfredi, Milan, p. 107.

56. W.C. Drinkard and R.V. Lindsey, German Patent, 1,808,434 (1969); Chem. Abs., **71** (1969) 70093.

57. D.L. Thorn and L. Hoffman, J. Amer. Chem. Soc., **100** (1978) 2079.

58. O.T. Onsager, H. Wang and U. Blindheim, Helv. Chim. Acta., **52** (1969) 230.

59. O.T. Onsager and J.E. Johansen, Chem. Met. Car. Bond, **3** (1985) 205.

60. Shell Oil Company, US Patent, 3 355 510 (1965).

61. W. Keim, A. Behr and M. Roper, in "Comprehensive Organometallic Chemistry", (1982), Pergamon Press, New York, p. 371.

62. M. Born, Y. Chauvin, G. Lefebvre and N. Phung, C.R. Acad. Sci., Paris, **268C** (1969) 1600.

63. R. de Haan and J. Dekker, J. Catal., **44** (1976) 15.

64. G. Henrici-Olivé and S. Olivé, Trans. Met. Chem., **1** (1976) 109.

65. H. van Zwet, R.S. Bauer and W. Keim, German Patent, 2,062,293 (1971), Chem. Abs., **75** (1971) 98942.

66. P. Cossee, J. Catal., **3** (1964) 80.

67. O.T. Onsager, H. Wang and U. Blindheim, Helv. Chim. Acta, **52** (1969) 196.

68. G. Hata and A. Miyaka, Chem. Ind., (1967) 921.

69. V.P. Yurev, G.A. Gailyunas, F.G. Yusupova, G.V. Nurtdinova, E.S. Monakhova and G.A. Tolstikov, J. Organomet. Chem., **169** (1979) 19.

70. R.G. Charles and M.A. Pawlikowski, J. Phys. Chem., **62** (1958) 440.

71. G.J. Bullen, R. Mason and P.J. Pauling, Nature, **189** (1961) 291.

72. R. Mayer, G. Hiller, M. Nitzschke and J. Jentzsch, Angew. Chem. Int. Edit., **2** (1963) 370.

73. T-M. Hseu, D.F. Martin and T. Moeller, Inorg. Chem., **2** (1963) 587.

74. L. Dahl, Mol. Phys., **5** (1962) 153 and references cited therein.

75. Y. Nakamura and K. Nakamoto, Inorg. Chem., **14** (1975) 63.

76. R.D. Gillard, H.G. Silver and J.L. Wood, Spectrochim. Acta, **20** (1964) 63.

77. H. Montgomery and E.C. Lingafelter, Acta Cryst., **17** (1964) 1481.

78. E.L. Lippert and M.R. Truter, J. Chem. Soc., (1960) 4996.

79. H. Montgomery and E.C. Lingafelter, Acta Cryst., **16** (1963) 748.

80. A.T. Hutton and D.A. Thornton, J. Mol. Struct., **39** (1977) 33.

81. K. Nakamoto, in "Infrared and Raman Spectra of Inorganic and Coordination Compounds." 4th Ed., (1986), Wiley-Interscience, New York.

82. R.F. Jameson and R.D. Peacock, J. Chem. Soc., (1969) 2453.

83. L.G. Hulett and D.A. Thornton, J. Inorg. Nucl. Chem., **35** (1973) 2661.

84. D.A. Thornton, Coord. Chem. Rev., **55** (1984) 113.

85. R.D. Hancock and D.A. Thornton, J. S. Afr. Chem. Inst., **23** (1970) 71.

86. O. Siiman, Inorg. Chem., **19** (1980) 2889.

87. T.J. McGee and J.L. Walter, Spectrosc. Lett., **10** (1977) 831.

88. D. Coucouvanis, N.C. Baenziger and S.M. Johnson, J. Amer. Chem. Soc., **95** (1973) 3875.

89. D. Coucouvanis and D. Piltingsrud, J. Amer. Chem. Soc., **95** (1973) 5556.

90. H.O. Desseyn, W.A. Jacob and M.A. Herman, Spectrochim. Acta, **25A** (1969) 1685.

91. G.W. Watt and B.J. McCormick, Spectrochim. Acta, **21** (1965) 753.

92. P.W. Jolly and G. Wilke, in "The Organic Chemistry of Nickel", (1975), Academic Press, New York.

93. W.O. Haag and H. Pines, J. Amer. Chem. Soc., **82** (1960) 2488.

94. H. Kanai, J. Chem. Soc. Chem. Commun., (1972) 203.

95. S.J. Brown, L.M. Clutterbuck, A.F. Masters, J.I. Sachinidis and P.A. Tregloan, Appl. Catal., **48** (1989) 1.

96. S.H.H. Chaston and S.E. Livingstone, Aust. J. Chem., **19** (1966) 2035.

97. R.G. Pearson, J. Chem. Ed., **45** (1968) 581.

98. J.P. Fackler and A.F. Masters, Inorg. Chim. Acta., **39** (1980) 111.

CHAPTER 3

PHOSPHINE COMPLEXES

3.1 INTRODUCTION

In 1857 the first phosphine complexes, formed between triethylphosphine and platinum and gold, were discovered [1]. Since then the chemistry of the coordination complexes of transition metal ions and phosphines has been increasingly investigated.

This interest stems from the novel properties of phosphine ligands. As early as the 1930's Jensen [2] showed that tertiary phosphines would stabilise metals in unusual oxidation states. In addition, phosphine ligands initiated the move of complex chemistry out of aqueous solution and into organic solvents where their complex compounds were found to be ideal for the study of the properties of metal atoms in a non-aqueous environment. Out of this evolved polymerisation, hydrogenation and carbonylation catalysts, the development of alkyl and aryl complexes of transition metals and much of the vast organometallic chemistry of the transition metals.

The ability of phosphines to ligate most metals, and some non-metals may be attributed to the fact that these ligands have vacant *d*-orbitals which may form a "dative π-bond" with a filled metal *d*-orbital, in addition to the ligand-metal σ-bond [3]. Much controversy has surrounded the degree of this π-backbonding which may accompany the σ-donation [4].

Of the tertiary phosphine complexes of nickel, the most widely studied are those of general formula $[Ni(PR_3)_2X_2]$ (R = alkyl or aryl; X = anionic ligand). Complexes of aryldialkyl- and trialkylphosphines exhibit planar, diamagnetic geometry both in the solid state and in solution and are usually red or yellow in colour. Triarylphosphines form paramagnetic blue or green complexes and generally have tetrahedral structures. This pattern also holds for tricyclohexylphosphine which produces planar complexes. For diarylalkylphosphine complexes, appreciable amounts of both isomers are present under similar conditions.

3.1.1 Infrared Studies

Throughout the 1960's the far-infrared spectra of complexes of general formula $[M(PR_3)_2X_2]$ received extensive interest [5-10]. Authors used the number and position of νM-P [10] or νM-X [5] modes to predict whether complexes were tetrahedral or *cis*- or *trans*-square planar [8].

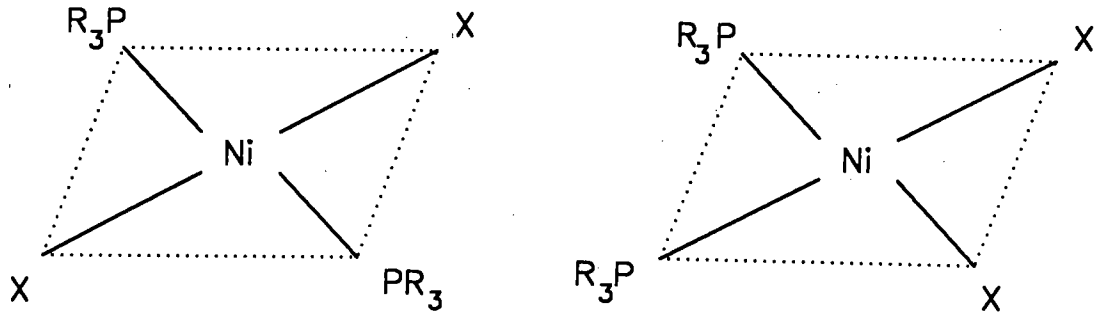

Figure 3.1 (a) *trans*-$[M(PR_3)_2X_2]$ (b) *cis*-$[M(PR_3)_2X_2]$

For *trans*-square planar complexes [Fig. 3.1(a)] which have C_{2h} point group symmetry, group theory predicts one νM-X and one νM-P infrared active vibration (both asymmetric). The point group of analogous *cis*-complexes [Fig. 3.1(b)] is C_{2v} for which four infrared active vibrations, two νM-X and two νM-P, are expected. Furthermore, the νM-X modes for *trans*-complexes are expected at higher frequency than for *cis*-complexes. This frequency difference is due to the presence of the phosphine ligands *trans* to the anion in the *cis*-complexes. This *trans* effect is the propensity for phosphines to weaken metal-ligand σ-bonds *trans* to the phosphine. Similarly, for the complexes in Fig. 3.1, νM-P vibrations will generally occur at higher frequency in *the cis*- than in the *trans*-complexes. For tetrahedral complexes of C_{2v} symmetry, two νM-X and two νM-P bands are expected to be infrared active. However, the vibrational frequencies of the νM-P bands are lower than for the square planar complexes which may be indicative of weaker M-P bonds [8].

Although there has been general agreement as regards assignment of νM-X, until 1970 the νM-P mode was assigned empirically and assignments ranged from 460-90 cm^{-1}. In 1970 a metal isotope labelling study by Shobatake and Nakamoto [11] showed that only two bands were significantly shifted

in each spectrum. For *trans*-square planar $[Ni(PEt_3)_2Cl_2]$ (Et = C_2H_5), the bands at 403 and 273 cm^{-1} were shifted on $^{58,62}Ni$-substitution. The higher frequency vibration was assigned to νNi-Cl, as it was absent from the spectrum of the bromo complex, and the lower to νNi-P. Previously, νNi-P had been assigned to the band at 415 cm^{-1} [5,10]. Labelling with ^{62}Ni also led to the reassignment of νNi-X and νNi-P in *cis*-square planar complexes [12].

By contrast, the results of a similar labelling study carried out on the tetrahedral $[Ni(PPh_3)_2X_2]$ complexes (Ph = C_6H_5) [5] led to assignments which were in complete agreement with those previously made [6,8].

Reaction of the above diphosphine-dihalide complexes of nickel with $[NiL_2]$ (L = SacSac or Sacac) leads to disproportionation and formation of square planar complexes of the type $[NiL(PR_3)X]$ [13]. Although the structures of some such complexes have been determined [13,14,15], no systematic study has been made of their infrared spectra. These spectra are of interest due to the presence of four different metal-ligand stretching modes.

In this Chapter, several of the above complexes have been prepared. By varying the β-ketoenolate ligand, the tertiary phosphine ligand and the halide anion, it is possible to make a systematic study of the far-infrared spectra and assign the metal-ligand modes in what would otherwise be a complex situation.

3.1.2 Catalysis

When phosphine ligands are introduced into a nickel catalysed oligomerisation reaction, significant rate enhancement occurs [16,17]. In addition, there is a change in oligomerisation activity, isomer selectivity and isomerisation activity. This phosphine effect was revealed by Wilke and Bogdanovic for the complex π-$C_3H_5NiX.PR_3$ activated by aluminium chloride [18].

The degree of oligomerisation may be controlled by varying the phosphine ligand [19,20]. The highest selectivity for dimerisation of ethene

(>98%) has been achieved using a less bulky phosphine such as a PMe_3-modified catalyst (Me = CH_3). With $P(i\text{-Pr})(t\text{-Bu})_2$ (Pr = C_3H_7, Bu = C_4H_{10}), 50% of the product consisted of tetramers and higher oligomers [21]. The phosphine controls the relative rates of propagation by olefin insertion (k_p) and elimination (k_e). This control parallels the increasing steric demands rather than the basicity of the phosphines. The decrease of the k_e/k_p ratio with increasing steric demand can be explained by assuming that the elimination reaction involves a penta-coordinate nickel hydride intermediate having two olefins simultaneously coordinated to the metal atom. With increasing size, the complexed phosphine would suppress the formation of such higher coordination species, thus suppressing the elimination step [21].

In addition to controlling the degree of oligomerisation, the k_e/k_p ratio affects olefin isomerisation [22]. Using a catalyst modified by PMe_3 (for which the elimination reaction is rapid relative to propagation), rapid double bond isomerisation may occur without significant dimerisation. On the other hand, catalysts with low k_e/k_p ratios are able to dimerise and oligomerise olefins without extensive isomerisation. Investigations [21] have indicated that the isomerisation activity of modified catalysts decreases in the order:

$$PMe_3 > PPh_3 > PEt_3 \sim P(n\text{-Bu})_3 > P(i\text{-Pr})_3 \sim PCx_3 \qquad (Cx = C_6H_{11}).$$

This order supports predictions made on the basis of decreasing k_e/k_p. Isomerisation has also been found to be olefin dependent [19]. An interesting example of selectivity control in isomerisation reactions is the selective formation of *cis*-2-butene from 1-butene by a PPh_3-modified catalyst [23].

Possibly the most important parameter controlled by phosphines is the distribution of product isomers. The influence of phosphines on the distribution of the C_6 isomers obtained from propene dimerisation has received much interest [16,22].

The scheme for propene dimerisation is similar to that presented earlier for 1-hexene dimerisation (Fig. 1.7). In the first step the nickel hydride catalyst adds across the double bond of propene to give either

an *n*-propyl or isopropyl nickel complex. The insertion of the second propene molecule into the metal-carbon bond results in four possible intermediates. β-Elimination of the nickel hydride and subsequent isomerisation reduces the final product composition to 3-hexene, 2-methyl-2-pentene and 2,3-dimethylbutene.

The first insertion step of the dimerisation is largely independent of the nature of the phosphine and 70 to 80% of the isopropyl nickel complex is formed. An exception is the case of the extremely bulky ligand P(*i*-Pr)(*t*-Bu)$_2$, where the direction of addition is altered to favour the less sterically demanding *n*-propyl product [24]. The changes in composition of the propene dimers are mainly associated with changes in the second insertion step. Some phosphine ligands hinder, through steric interference, the preferred Ni→C$_2$ addition [25] forcing a highly selective Ni→C$_1$ addition.

The composition of the dimer obtained using a phosphine-free catalyst system was similar to that obtained with a PPh$_3$-modified catalyst (20% *n*-hexene, 75% methylpentene, 5% dimethylbutene). The use of alternative phosphine-modified catalysts has made it possible to decrease the yield of hexene and methylpentene from 21.6 to 0.1% and from 76.9 to 19.0%, respectively, while increasing the dimethylbutene yield from 4.5 to 80.9% [21].

Both steric and electronic (ligand basicity) arguments have been used to explain the selectivity influence of tertiary phosphine ligands [16,21,22], although no one argument may completely explain the effect. Onsager and Johansen [16] have given a detailed review of the mechanism of phosphine participation in the oligomerisation reaction. They concluded that the influence of such ligands on the selectivity of nickel catalysed propene dimerisation is predominantly a steric effect although more information on the influence of soft PR$_3$ ligands is necessary before electronic effects may be neglected.

Many conflicting reports are available on the optimisation of the phosphine to nickel ratio. For example, the oligomerisation of ethene with a P(*t*-Bu)$_3$-modified catalyst (P:Ni = 1:1) produced oligomers as well as a small amount of polyethylene, while, when a four-fold excess

of $P(t\text{-}Bu)_3$ was used, only polyethylene was formed [22]. Some authors have found that addition of more than molar amounts of phosphine deactivates the catalyst [26] probably due to coordination at the free coordination site [22]. By contrast, several successful catalytic systems have used an excess of phosphine [17,27,28]. Examples of chelating phosphines which deactivate catalytic systems have been published [22,29] as well as papers in which active nickel-diphosphine chelate complexes are used [30,31]. A possible reason for the addition of an excess of phosphine is the ability of the phosphine to bond to the aluminium species present. It has been shown that the resulting complex is inactive [32]. In the presence of a P:Al ratio of more than one, some free phosphine exists in equilibrium with the aluminium-phosphine complex. However, it has been proposed that, at a molar ratio P:Al > 8:1, catalytic activity is almost completely absent, possibly due to blocking of the free coordination site [16].

Of the nickel β-ketoenolate type complexes studied in Chapter 2, the dimerisation activity of both $[Ni(acac)_2]_3$ and $[Ni(Nacac)_2]$ complexes in the presence of phosphines has been reported. Ewers [17], using a $[Ni(acac)_2]_3$ / $Al_2Et_3Cl_3$ system, added a sixteen molar excess of PPh_3 relative to nickel and recorded dimerisation activity of 5.7×10^5 moles of propene per mole of nickel in two hours. Henrici-Olivé and Olivé [33] found that, while $[Ni(Nacac)_2]$ is inactive in the presence of a twenty-fold excess of $AlEt_2Cl$, the addition of $P(i\text{-}Pr)_3$ activated the system. Unlike any of the other systems which they tested, the products of this dimerisation reaction were predominantly 2,3-dimethylbutenes.

When generating the phosphine-modified catalyst *in situ*, the number of phosphine ligands and their mode of coordination to the nickel ion is uncertain. To overcome this problem, Cavell and Masters [34] prepared, isolated and characterised phosphine-nickel complexes prior to observing their catalytic activity. They found that, in conjunction with a thirty molar excess of $AlEt_2Cl$ co-catalyst, complexes of general formula $[Ni(SacSac)(PR_3)Cl]$ (R = Ph, Bu, Et) were active oligomerisation catalysts. Propene dimerisation activities depended on the phosphine used and ranged from 3500 to 25000 moles of propene per mole of nickel per hour. The products were mainly dimers although by altering the temperature the degree of oligomerisation could be controlled [35]. For

each catalyst system studied, the rate of olefin isomerisation was faster than that of the oligomerisation reaction [36]. In addition to being active propene dimerisation catalysts, complexes of this type have been used successfully to oligomerise ethene and butene [35,37].

In this Chapter, the catalytic oligomerisation activity of several nickel-phosphine complexes, based on those prepared by Cavell and Masters, has been tested. Factors that have been investigated are the effect of changing the Lewis acid, phosphine, chelating ligand and halogen on the oligomerisation reaction. In addition, the selectivity influence of the phosphine ligand on the dimer product distribution, as well as the degree of oligomerisation, has been observed.

3.2 EXPERIMENTAL

3.2.1 Preparation of Complexes of the Type $[Ni(PR_3)_2X_2]$

The following complexes were prepared:

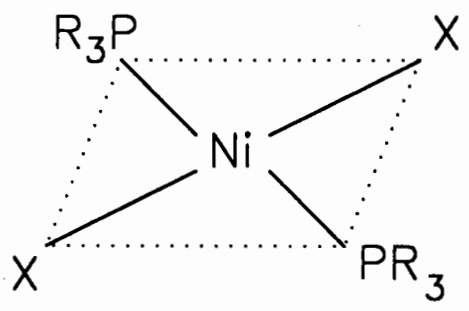

R = Ethyl (Et)
Methyl (Me)
Cyclohexyl (Cx)
Phenyl (Ph)

X = Chloride (Cl)
Bromide (Br)
Iodide (I)
Isothiocyanate (NCS)

Each complex was prepared using deoxygenated, analytical reagent grade solvents under a nitrogen atmosphere using standard Schlenk techniques. Once isolated, products were dried immediately under reduced pressure over P_2O_5.

3.2.1.1 $[Ni(PEt_3)_2Cl_2]$

Successful preparation was achieved following the method of Jensen *et al.* [38]. $NiCl_2.6H_2O$ (10 mmol) was dissolved in warm ethanol (25 ml) and PEt_3 (20 mmol) was added. Red crystals were precipitated immediately. The solution was filtered and the crystals washed with ethanol. No further purification was necessary.

3.2.1.2 $[Ni(PEt_3)_2Br_2]$

Hydrated nickel bromide (10 mmol) was dissolved in warm ethanol (35 ml) and PEt_3 (20 mmol) was added. The solution was concentrated and red-brown crystals were precipitated. The product was filtered and washed with cold ethanol. No further purification was necessary.

3.2.1.3 $[Ni(PEt_3)_2I_2]$

$[Ni(PEt_3)_2Br_2]$ (10 mmol) was dissolved in a minimum of ethanol. A saturated solution of NaI in ethanol (10 ml) was added. The solution changed from brown to dark green. The ethanol was removed under reduced pressure and benzene (20 ml) was added to the remaining solid. The solution was filtered to remove the sodium salt and the filtrate evaporated to dryness. Recrystallisation from ethanol gave pure, brown crystals.

3.2.1.4 $[Ni(PEt_3)_2(NCS)_2]$

$[Ni(PEt_3)_2Br_2]$ was dissolved in a minimum of ethanol and a saturated solution of NaSCN in ethanol (10 ml) was added. The solution was stirred until the colour changed from brown to bright yellow. The ethanol was removed under reduced pressure and the residue taken up in benzene (20 ml). The solution was filtered and the filtrate evaporated to dryness. Recrystallisation from ethanol gave pure, orange-yellow crystals.

3.2.1.5 $[Ni(PMe_3)_2Cl_2]$

$NiCl_2.6H_2O$ (10 mmol) was dissolved in a minimum of warm ethanol and the flask placed in liquid nitrogen. To this, a flask containing PMe_3 (20 mmol in the form of its silver iodide salt) was connected and the system evacuated. Gentle heating of the silver salt led to the release of PMe_3 which condensed into the nickel solution. The ethanolic solution was then allowed to come to room temperature and was stirred and the volume gradually reduced over two hours. The resulting crystals were filtered and washed with cold ethanol. No further purification was necessary.

3.2.1.6 $[Ni(PCx_3)_2Cl_2]$

$NiCl_2.6H_2O$ (10 mmol) was dissolved in warm ethanol (25 ml) and a solution of PCx_3 (20 mmol) in ethanol (25 ml) was added. Fine, pink

crystals were precipitated and these were filtered off and washed with ethanol. No further purification was necessary.

3.2.1.7 $[Ni(PPh_3)_2Cl_2]$

The reported method of Venanzi [39] was followed. A solution of PPh_3 (20 mmol) in glacial acetic acid (25 ml) was added to a solution of $NiCl_2.6H_2O$ (10 mmol) in water (2 ml) and glacial acetic acid (50 ml). A dark green precipitate resulted which, when left to stand overnight in contact with its mother liquor, gave blue-black crystals. Subsequent filtration, washing with warm glacial acetic acid and drying, yielded the pure complex.

3.2.2 Preparation of Complexes of the Type $[NiL(PR_3)X]$

The following complexes were prepared:

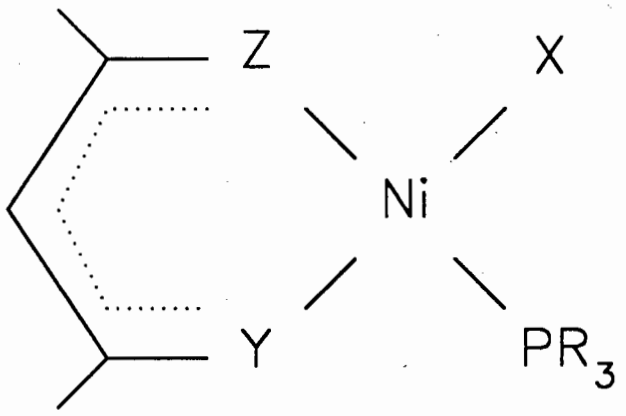

Y = Z = S (SacSac)
Y = S, Z = O (Sacac)

R = Et, Me, Cx, Ph

X = Cl, Br, I, NCS

The general method reported by Fackler and Masters [13] was used. Each preparation was carried out using deoxygenated, analytical reagent grade solvents under a nitrogen atmosphere using standard Schlenk techniques. Once isolated, products were dried under reduced pressure over silica gel.

3.2.2.1 [Ni(SacSac)(PR_3)X] (R = Et, Me, Cx; X = Cl, Br, I)

[Ni(SacSac)$_2$] (1.5 mmol), prepared as described in 2.2.1.10, and [Ni(PR_3)$_2X_2$] (1.5 mmol), prepared as described above, were dissolved in benzene (40 ml) and refluxed for three hours. The solution was filtered while hot and the solvent removed under reduced pressure. The solid which remained was recrystallised from acetone to yield pure, black-brown crystals.

3.2.2.2 [Ni(Sacac)(PEt_3)X] (X = Cl, Br, I)

The method outlined in 3.2.2.1 was followed using [Ni(Sacac)$_2$] (1.5 mmol), prepared previously in 2.2.1.5, in place of [Ni(SacSac)$_2$].

3.2.2.3 [Ni(SacSac)(PEt_3)(NCS)]

[Ni(SacSac)(PEt_3)Br] (1.5 mmol), prepared as described in 3.2.2.1, was dissolved in acetone and a saturated solution of NaSCN in acetone (15 ml) was added. The resulting solution was stirred until it became bright orange in colour. The acetone was removed under reduced pressure and the solid residue taken up in benzene. The resulting solution was filtered and the filtrate evaporated to dryness. Recrystallisation from acetone yielded pure red crystals.

3.2.2.4 [Ni(Sacac)(PEt_3)(NCS)]

The method outlined in 3.2.2.3 was followed substituting [Ni(Sacac)(PEt_3)Br] for [Ni(SacSac)(PEt_3)Br].

3.2.2.5 [Ni(SacSac)(PPh_3)Cl]

[Ni(SacSac)$_2$] (1.5 mmol), prepared as described in 2.2.1.10, and [Ni(PPh_3)$_2Cl_2$] (1.5 mmol), prepared as described in 3.2.1.9, were dissolved in benzene and refluxed for ten hours. The solution was

filtered while hot and the solvent removed from the filtrate under reduced pressure. The oily residue was taken up in a minimum of acetone. Slow addition of heptane yielded black crystals. The complex was recrystallised several times in this fashion before pure crystals were obtained.

3.2.3 Crystal Structure Determination of [Ni(Sacac)(PEt_3)Cl]

A single crystal, suitable for X-ray analysis, was obtained by recrystallisation from acetone-heptane. The structure determination was carried out by Dr M. L. Niven of the Department of Chemistry, University of Cape Town. The structure was solved by location of the nickel atom in a Patterson map. All remaining non-hydrogen atoms were located in subsequent difference Fouriers. In the final refinements all non-hydrogen atoms were modelled anisotropically. The methylene and methine hydrogens were placed in calculated positions at 1.00 Å from their parent carbons with a single isotropic temperature factor. A weighting scheme was applied and further omission of some ten reflections was carried out to improve the model of the structure. The final residual electron density map was smooth except near the chlorine (0.22-0.29 Å) where residual peaks, attributable to inadequate modelling of the thermal motion of the Cl, remained.

3.2.4 Catalytic Experiments

The catalytic runs were carried out under the same conditions, and products were analysed using the same techniques, as described in section 2.2.2.

3.3 RESULTS

3.3.1 Analytical Data

Table 3.1 Analytical data for the complexes $[Ni(PR_3)_2X_2]$.

Compound	Calculated			Found		
	%C	%H	%N	%C	%H	%N
$[Ni(PEt_3)_2Cl_2]$	39.4	8.3	-	39.9	8.4	-
$[Ni(PEt_3)_2Br_2]$	31.7	6.6	-	31.6	6.4	-
$[Ni(PEt_3)_2I_2]$	26.3	5.5	-	26.3	5.5	-
$[Ni(PEt_3)_2(NCS)_2]$	40.8	7.3	6.8	40.8	7.2	6.8
$[Ni(PMe_3)_2Cl_2]$	25.6	6.5	-	25.6	6.1	-
$[Ni(PCx_3)_2Cl_2]$	62.6	9.6	-	63.1	9.6	-
$[Ni(PPh_3)_2Cl_2]$	66.1	4.6	-	66.0	4.2	-

Table 3.2 Analytical data for the complexes $[Ni(L)(PR_3)X]$.

Compound	Calculated			Found		
	%C	%H	%N	%C	%H	%N
$[Ni(SacSac)(PEt_3)Cl]$	38.5	6.5	-	38.7	6.3	-
$[Ni(Sacac)(PEt_3)Cl]$	40.3	6.8	-	40.3	6.6	-
$[Ni(SacSac)(PEt_3)Br]$	34.0	5.7	-	34.1	5.6	-
$[Ni(Sacac)(PEt_3)Br]$	35.5	6.0	-	35.4	6.0	-
$[Ni(SacSac)(PEt_3)I]$	30.4	5.1	-	30.7	5.1	-
$[Ni(Sacac)(PEt_3)I]$	31.5	5.2	-	31.9	5.3	-
$[Ni(SacSac)(PEt_3)(NCS)]$	39.3	6.1	3.8	39.7	6.3	3.8
$[Ni(Sacac)(PEt_3)(NCS)]$	41.2	6.3	4.0	40.5	6.2	4.0
$[Ni(SacSac)(PMe_3)Cl]$	31.9	5.4	-	31.9	5.1	-
$[Ni(SacSac)(PCx_3)Cl]$	54.6	8.0	-	54.6	8.1	-
$[Ni(SacSac)(PPh_3)Cl]$	56.6	4.5	-	57.1	4.2	-

3.3.2 Infrared Results

Table 3.3 Mid-infrared spectra of the complexes $[Ni(SS)(PR_3)X]$ and their precursors. (SS = SacSac)

PEt_3	$[Ni(SS)_2]$	$[Ni(PEt_3)_2X_2]$				$[Ni(SS)(PEt_3)X]$				
		X=Cl	Br	I	NCS	X=Cl	Br	I	NCS	Assignment
	3030					3027	3031	3032	3030	νC-H (γCH)
2998						2984				
		2963	2959	2957	2957	2962	2959	2959	2960	νCH_3(as)
						2944				νCH_3
	1220	2929	2928	2927	2928	2929	2927	2925	2930	νCH_2(as)
2900		2908	2905	2903	2903	2915	2912	2912	2905	νCH_2(s)
2845		2875	2870	2868	2872	2868	2870	2869	2874	νCH_3(s)
					2096				2098	νC≡N
	1552					1569	1569	1567	1566	combination
						1517	1518	1514	1524	
	1491					1485	1482	1483	1486	νC=C
1465										
1458		1451	1457	1455	1455	1449	1456	1455	1454	δCH_3(as)
		1448	1448	1447	1444				1448	
1423		1420	1422	1422	1422	1414	1425	1424	sh	δCH_2(as)
		1409	1408	1407	1411	1407	1409	1408	1412	
1380						1376	1375	1375	1377	δCH_3(s)
		1375	1377	1376	1377	1363	1363	1363	1367	
	1348					1356	1350	1350	1354	
	1312					1309	1313	1314	1315	δCH_3(s)
	1289					1289			1295	
							1293	1293	1264	
1245		1248	1246	1245	1253	1256	1250	1247	1254	ωCH_2
1231		1240	1235	1233	1234	1235	1235	1233	1242	τCH_2
	1229					1226	1229		1230	νC-C + νC-CH_3
1183										δCH(ip)
	1156					1156	1160	1159	1159	δCH(ip)
									1042	
1043		1027	1028	1026	1033	1037	1035	1034	1034	ρCH_3 + νC-C
1023						1026				
	1009	1011	1008	1010	1007	1004	1014	1012	1012	ρCH_3
1003		1000	1000	1000	999		1000	1000	1000	ρCH_3 + νC-C

Table 3.3 contd.

PEt_3	$[Ni(SS)_2]$	$[Ni(PEt_3)_2X_2]$				$[Ni(SS)(PEt_3)X]$				Assignment
		X=Cl	Br	I	NCS	X=Cl	Br	I	NCS	
975		984	984	981	980	985		980		νC-C + ρCH_3
	979					sh	978	975	978	ρCH_3 + νC-S
									956	
					930				930	2δN-CS
									860	
					859				839	νS-CN
	826					825	832	833	830	ρC-H(oop)
	801					800	804	804	803	
765							768	768		ρCH_2
748		761	760	757	761	756	758	757	766	
	747					737	740	738	751	νC-S
717		725	719	714	728	721	723	719	737	νC-P(as)
		705	705	705	706		708	705	697	νC-S
690										νC-P(as)
670		674	677	676	679	673	682	680	674	
	648					645			648	ring def + νNi-S
625		628	630	628	627	626	631	628	618	
619										νC-P(s)
600										
	556					554	555	555	555	$\delta C-CH_3$ + ring def

as = antisymmetric, s = symmetric

ip = in-plane, oop = out-of-plane

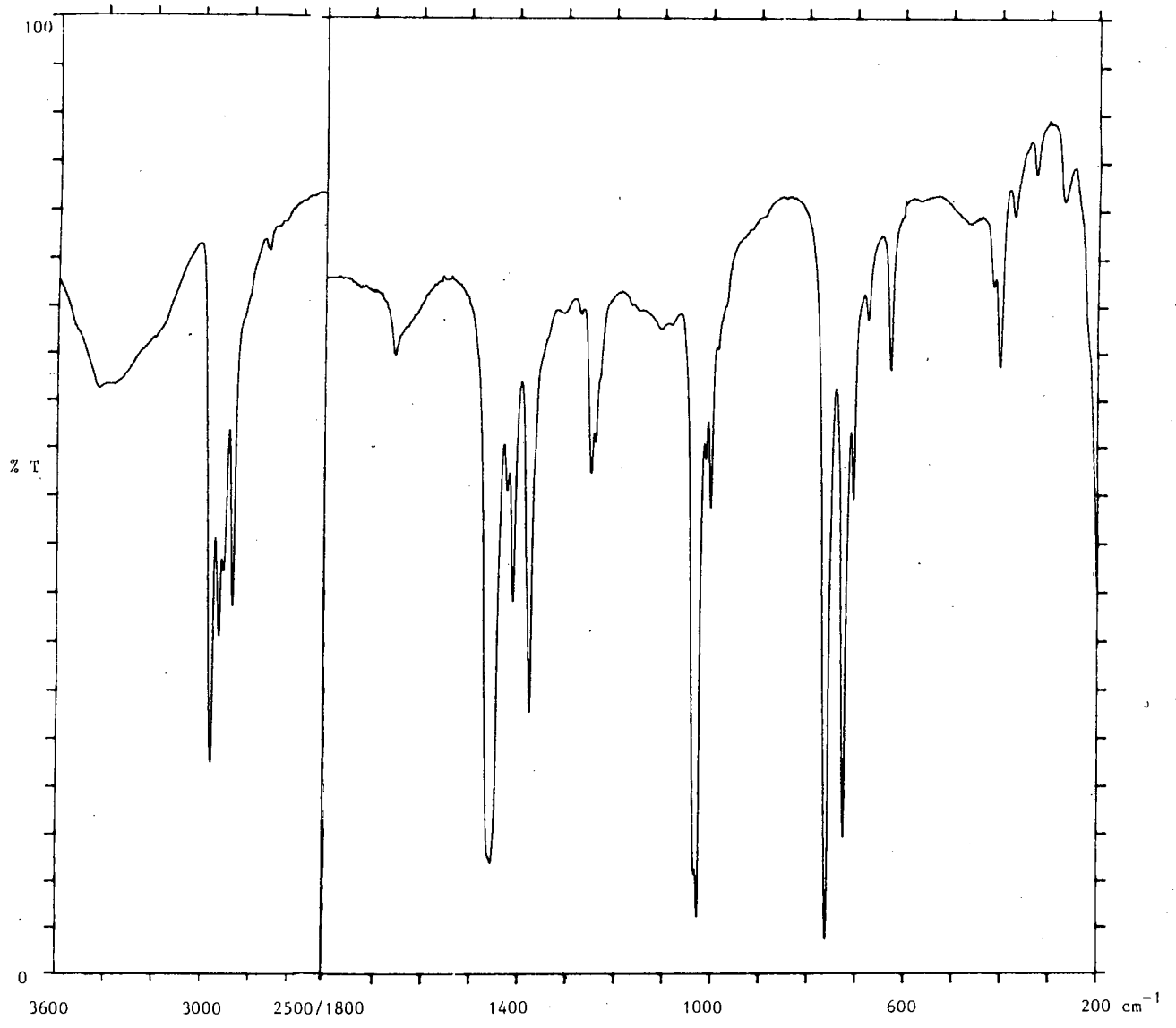

Figure 3.2 Mid-infrared spectrum of $[Ni(PEt_3)_2Cl_2]$.
HCBD: 3600-2500 cm^{-1}, Nujol: 1800-200 cm^{-1}

Table 3.4 Mid-infrared spectra of the complexes [Ni(SA)(PEt_3)X] and their precursors, (SA = Sacac).

PEt_3	$[Ni(SA)_2]$	$[Ni(PEt_3)_2X_2]$				[Ni(SA)(PEt_3)X]				Assignment
		X=Cl	Br	I	NCS	X=Cl	Br	I	NCS	
	3010				2984					νC-H (γCH)
	2978					2965	2965	2963	2964	
2998		2963	2959	2957	2957	2958	2957			νCH_3(as)
	2911	2932	2928	2927	2928	2930	2928	2926	2933	νCH_2(as)
2900		2908	2905	2903	2903	2906	2905	sh	2902	νCH_2(s)
2845		2875	2870	2868	2872	2869	2872	2870	2876	νCH_3(s)
					2096				2100	νC≡N
	1565					1571	1578	1572	1567	νC=O
	1520									combination
	1474					1480	1471	1465	1474	νC=C
1468										δCH_3(as)
1458		1451	1457	1455	1455	1451	1457	sh	1453	
		1448	1448	1447	1444					
	1440						1440	1441	1442	δCH(as)
1423		1420	1422	1422	1422					δCH_2(as)
	1420					1416	1417	sh	1412	δCH(as)
		1409	1408	1407	1411	1409	1410	1409	(1412)	δCH_3(s)
1380		1375	1377	1376	13771376		1375	1375	1378	
	1371					1350	1359	1355	sh	
	1338					1338	1344	1341	1345	
1245		1248	1246	1245	1253	1257	1262	1255	1266	ωCH_2
1231		1240	1235	1233	1234	1238	1243	1241	1251	τCH_2
	1234									νC-C + νC-CH_3
	1227					1226	1232	1231	1231	
1183						1150	1150	1150	1160	δCH(ip)
	1117					1109	1115	1113	1113	
									1046	ρCH_3 + νC-C
1043		1027	1028	1026	1033	1037	1041	1034	1036	
1023						1026	1032		1022	
	1016	1011	1008	1010	1007	1004	1014	1012	1012	ρCH_3
1003		1000	1000	1000	999					ρCH_3 + νC-C

Table 3.4 contd.

PEt_3	$[Ni(SA)_2]$	$[Ni(PEt_3)_2X_2]$				$[Ni(SA)(PEt_3)X]$				Assignment
		X=Cl	Br	I	NCS	X=Cl	Br	I	NCS	
975		984	984	981	980	985	985	980	987	νC-C + ρCH_3
	985					973	976	972	980	ρCH_3 + νC-S
									956	2δNCS
					930				936	
	935					931	934	933	(936)	νC-CH_3 + νC=O
					859				834	νS-CN
	813									δCH(oop)
	809					800	807	810	801	
765									768	ρCH_2
748		761	760	757	761	757	759	759	751	
	720					713	711	709	717	νC-S
717		725	719	714	728	722	725	721	740	
690		705	705	705	706	703	692		700	νC-P(as)
670		674	677	676	679	673	673	680	673	
659										
	672									ring def
	662									ring def +
	642					641	645	642	647	νNi-S/O
	620					sh	635			
625		628	630	628	627	627	627	629	620	
619										νC-P(s)
600										

as = antisymmetric, s = symmetric

ip = in-plane, oop = out-of-plane

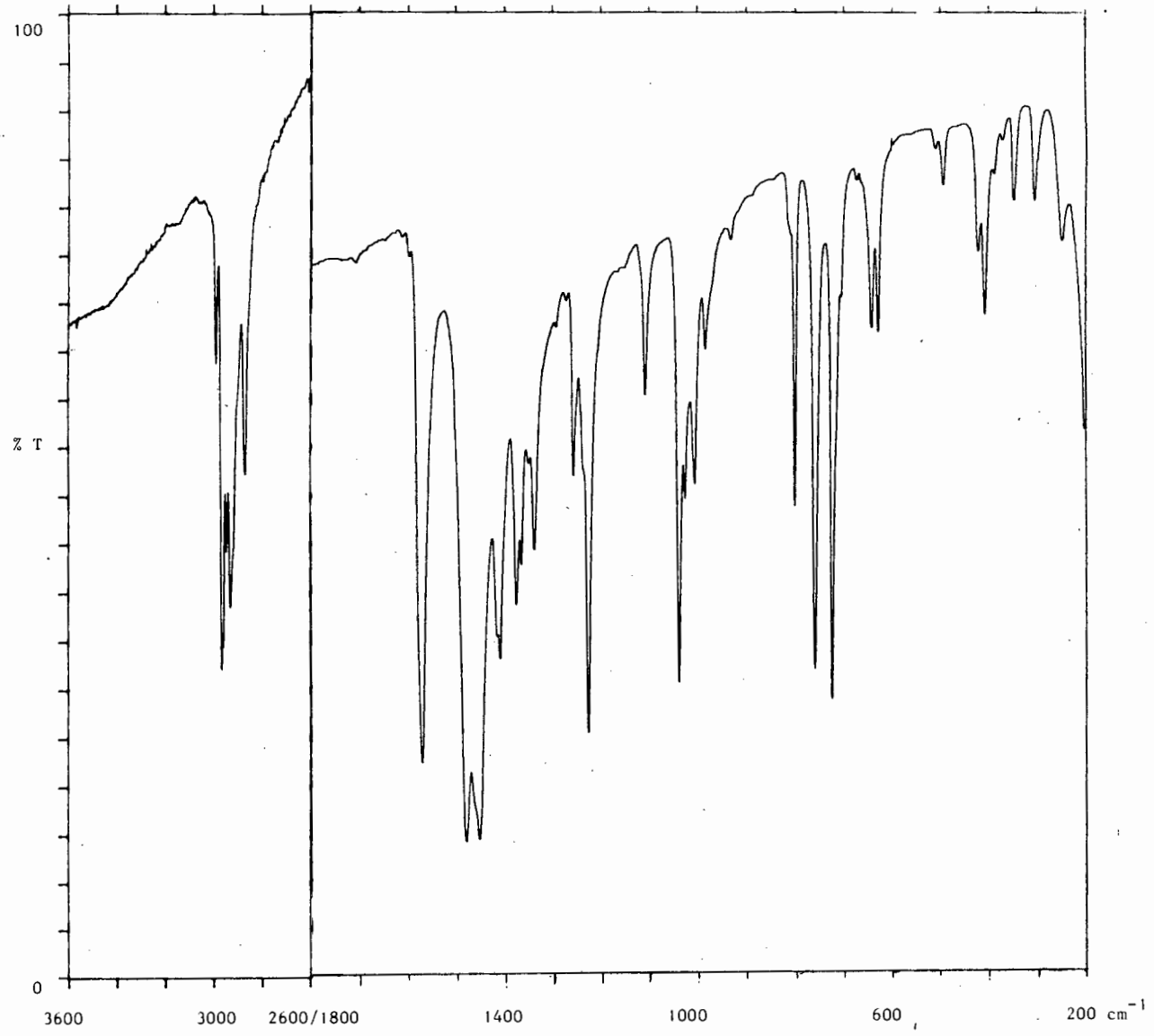

Figure 3.3 Mid-infrared spectrum of [Ni(Sacac)(PEt_3)Cl].
HCBD: 3600-2600 cm^{-1}, Nujol: 1800-200 cm^{-1}

Table 3.5 Far-infrared spectra (cm^{-1}) of the complexes $[Ni(SacSac)_2]$, $[Ni(PR_3)_2Cl_2]$ and $[Ni(SacSac)(PR_3)Cl]$.

$[Ni(SacSac)_2]$	$[Ni(PR_3)_2Cl_2]$				$[Ni(SacSac)(PR_3)Cl]$				Assignment
	R = Me	Et	Cx	Ph	Me	Et	Cx	Ph	
			488	496			495	497	phosphine ligand
			450				475	477	
			439	445			453	457	
			429	439			439	431	
			414	420			395	421	
		416	406	397		415	410	402	
	405	402	386	340	327	333	334	332	νNi-Cl
				304					
390					380	381	381	381	νNi-S
374					367	361	360	358	δCCS
	362	373			353	(361)	(360)	(358)	phosphine ligand
		329		263				275	
284					274	288	275	290	νNi-S
	275	270	277	188	250	256	252	249	νNi-P
				163					
	249		234	248					phosphine ligand
240									
227					228	234	226	226	δNi-S
216						203	207	202	
		254	220	217	(228)	(234)	(226)	(226)	phosphine ligand
	218	185	sh	(188)	187	182	192	197	δCPC
	sh	198	191	(163)	165	170	177	175	δNi-Cl
149					135	144	143	146	πCCS
	145	165	156	144					δP-Ni-P
	115	114	121	120	115	111	110	111	δNi-P
		101	108	108		sh	98	105	
122									δNi-S
98	76	84	91	95		81	82	84	lattice + δCH_3
82	66	72	76		73	72	77	79	
	52		59	60	53		54	55	

Table 3.6 Far-infrared spectra (cm^{-1}) of the complexes $[NiL_2]$, *trans*-$[Ni(PR_3)_2X_2]$ and $[NiL(PR_3)X]$ [L = SacSac (SS), Sacac (SA)].

$[Ni(SS)_2]$	[Ni(SacSac)(PEt_3)X]				*trans*-$[Ni(PEt_3)_2X_2]$				[Ni(Sacac)(PEt_3)X]				*cis*-$[Ni(SA)_2]$	Assignment
X =	Cl	Br	I	NCS	Cl	Br	I	NCS	Cl	Br	I	NCS		
									509	508	507	518	498	$\delta C\text{-}CH_3$ + δring
									493	488	488	492	492	νNi-O
				464				466				465		δNCS
	415	417	416	433	416	414	411	425	421	423	424	437		δCCP
	334	311	250	315	402	336	260	316	347	329	255	322		νNi-X
													409	νNi-O
	382	380	379	386					408	403	402	412		δCCP
390	362	359	356	sh					389	390	386	390	396	νNi-S
374		372	373	370					374	374	372	377	373	δCCS
		(372)	(373)	(370)	373	374	377	375	(374)	(374)	(372)	(377)		δCCP
	(334)	332	330	336	329	328	331	329	(347)	(329)	324	(322)		δCCP
286	288	285	286	292									308	νNi-S
							309							
	256	242	240	232	271	263	251	243	305	296	293	312		νNi-P
									258	250	(255)	251	252	δNi-O
240									246					δNi-S
227	234	(242)	(240)	(217)					235	230	230	231	196	
					257	251	235	(243)	213	224	212	sh		δCCP
216	203	205	205	204										δNi-S
	170	165	154	157	198	152	143	142	170	155	153	155		δNi-X
	182	174	184	192	185	188	184	188	185	180	185	180		δCPC
					165	171	162	161						δP-Ni-P
149	144	144	146	144					124	sh	117	140	149	πCCS
122		124	124	sh									112	δNi-S
95														
					114		113							δNi-P
	111	105	103	111	101	102	92	112	116	116	106	112		
	80		73		sh	80	77	80	66	93	94	74	84	lattice + πCH_3
82	72	80	64	72	72	62	65	60	54	73	62	55	53	

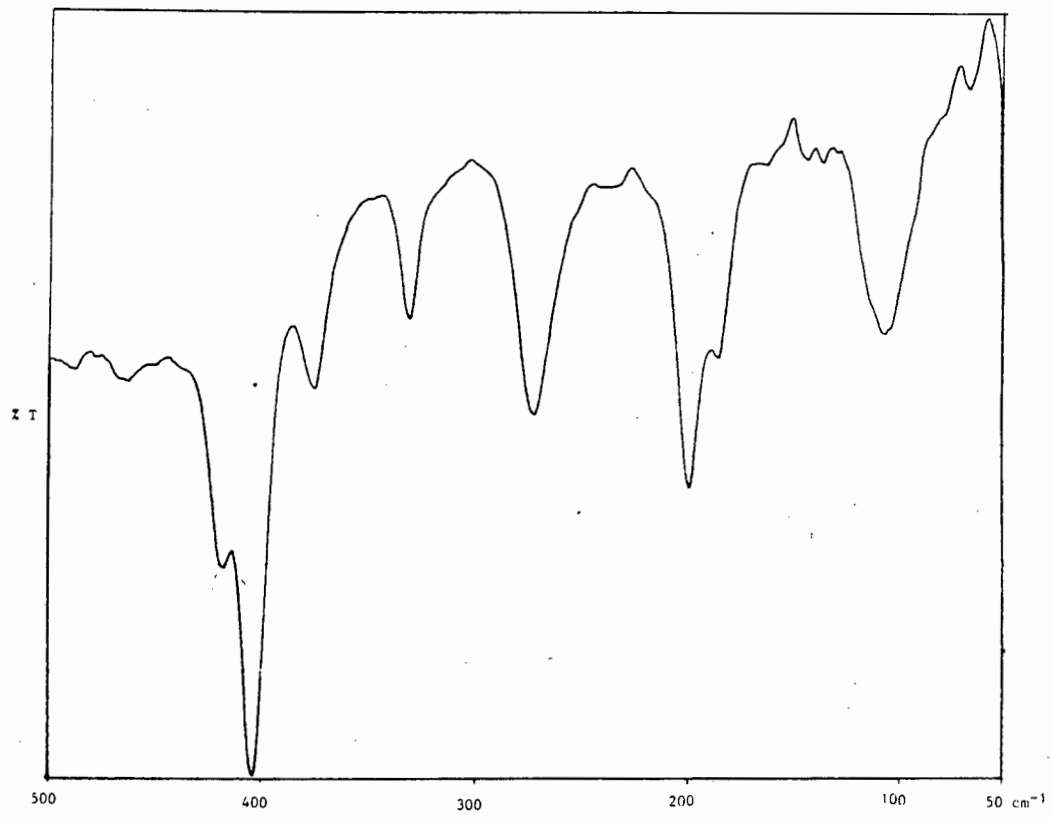

Figure 3.4 Far-infrared spectrum of $[Ni(PEt_3)_2Cl_2]$.

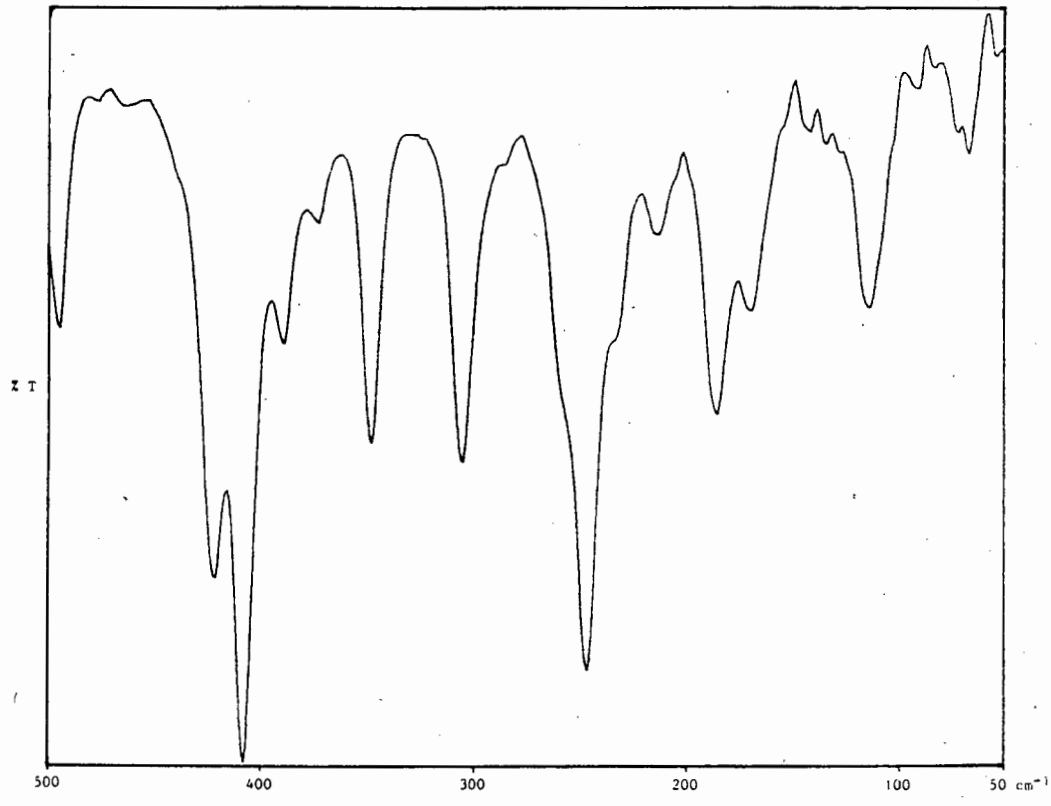

Figure 3.5 Far-infrared spectrum of $[Ni(Sacac)(PEt_3)Cl]$.

3.3.3 ^{1}H and ^{13}C NMR Results

All spectra were run at ambient temperature (25°C) using $CDCl_3$ as lock and solvent.

Table 3.7 ^{1}H and ^{13}C NMR data (ppm) for the complexes *trans*-$[Ni(PEt_3)_2X_2]$.

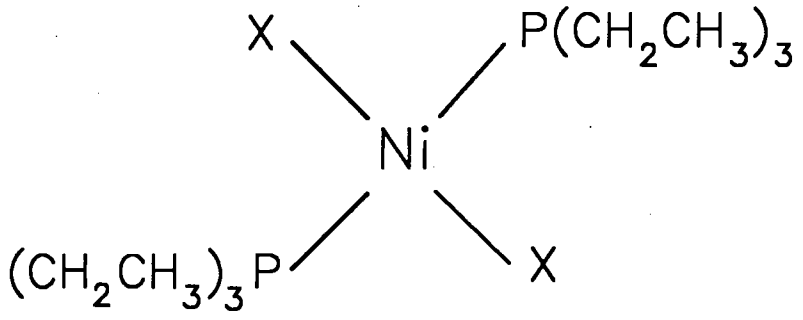

	^{1}H NMR		^{13}C NMR		
X	CH_3	CH_2	CH_3	CH_2	NCS
Cl	1.31(t)	1.67(q)	8.27	13.38	
Br	1.30(t)	2.02(q)	8.51	15.83	
I	1.28(t)	2.82(q)	10.36	22.16	
NCS	1.31(t)	1.68(q)	7.94	14.31	146.43

(t) = triplet, (q) = quartet

Table 3.8 ^{1}H and ^{13}C NMR data (ppm) for the complex *trans*-$[Ni(PMe_3)_2Cl_2]$.

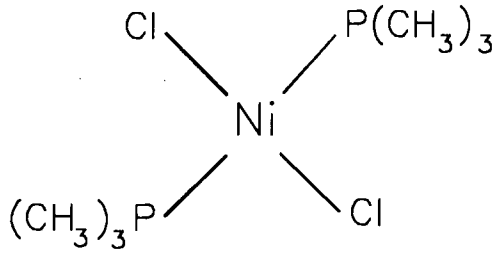

^{1}H NMR		^{13}C NMR	
CH_3	1.27	CH_3	12.01

Table 3.9 ^{1}H and ^{13}C NMR data (ppm) for the complex $[Ni(PCx_3)_2Cl_2]$.

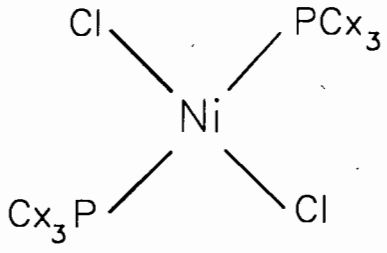

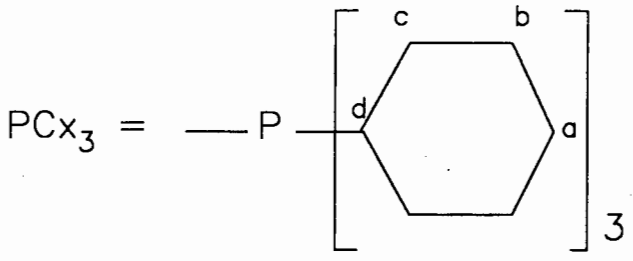

^{1}H NMR		^{13}C NMR	
C^aH_2	1.36(m)	C^a	26.61
C^bH_2*	1.91(m)	C^{b*}	27.86
C^cH_2*	2.11(m)	C^{c*}	30.01
C^dH	2.42(m)	C^d	32.39

(m) = multiplet

* - resonances may be interchanged

Table 3.10 ^{1}H and ^{13}C NMR data (ppm) for the complexes $[Ni(SacSac)(PEt_3)X]$.

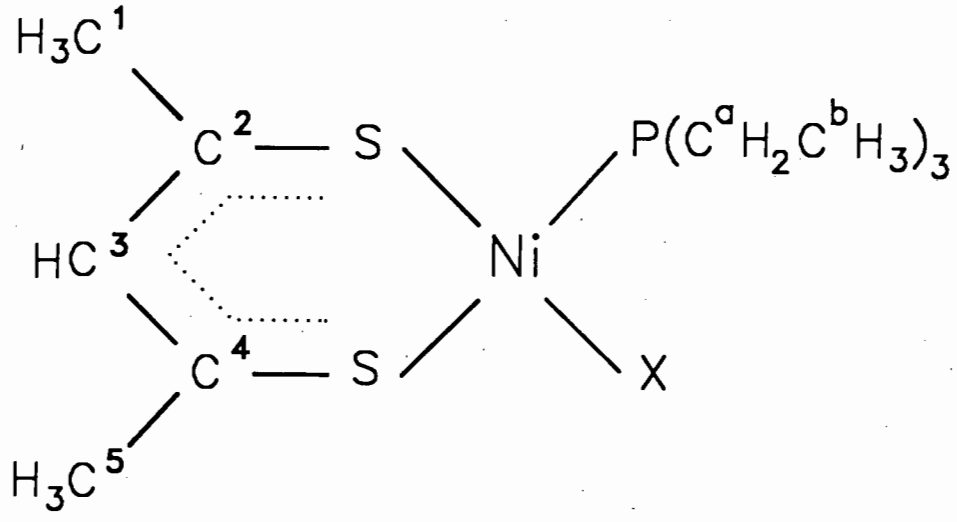

X	^{1}H NMR				
	C^bH_3	C^aH_2	C^1H_3	C^5H_3	C^3H
Cl	1.23(m)	1.80(m)	2.35	2.35	7.10
Br	1.27(m)	1.90(m)	2.41	2.41	7.12
I	1.24(m)	2.05(m)	2.42	2.42	7.12
NCS	1.33(m)	1.80(m)	2.40	2.49	7.38

X	^{13}C NMR							
	C^a	C^b	C^5	C^2	C^3	C^4	C^1	NCS
Cl	13.3(d)^x	8.05	32.54(d)^y	n.o.	131.00	n.o.	31.76	
Br	14.5(d)^x	8.25	32.54(d)^y	n.o.	130.47	n.o.	32.30	
I	16.7(d)^x	8.34	32.94	n.o.	129.22	n.o.	32.61	
NCS	13.7(d)^x	8.00	32.75(d)^y	176.66	131.55	187.19	31.76	140.66

n.o. = not observed

(d) = doublet, (m) = multiplet

x - $^{1}J_{PC}$: Cl = 26.5 Hz, Br = 25.5 Hz, I = 28.0 Hz, NCS = 25.8 Hz

y - $^{4}J_{PC}$ ~ 8.7 Hz

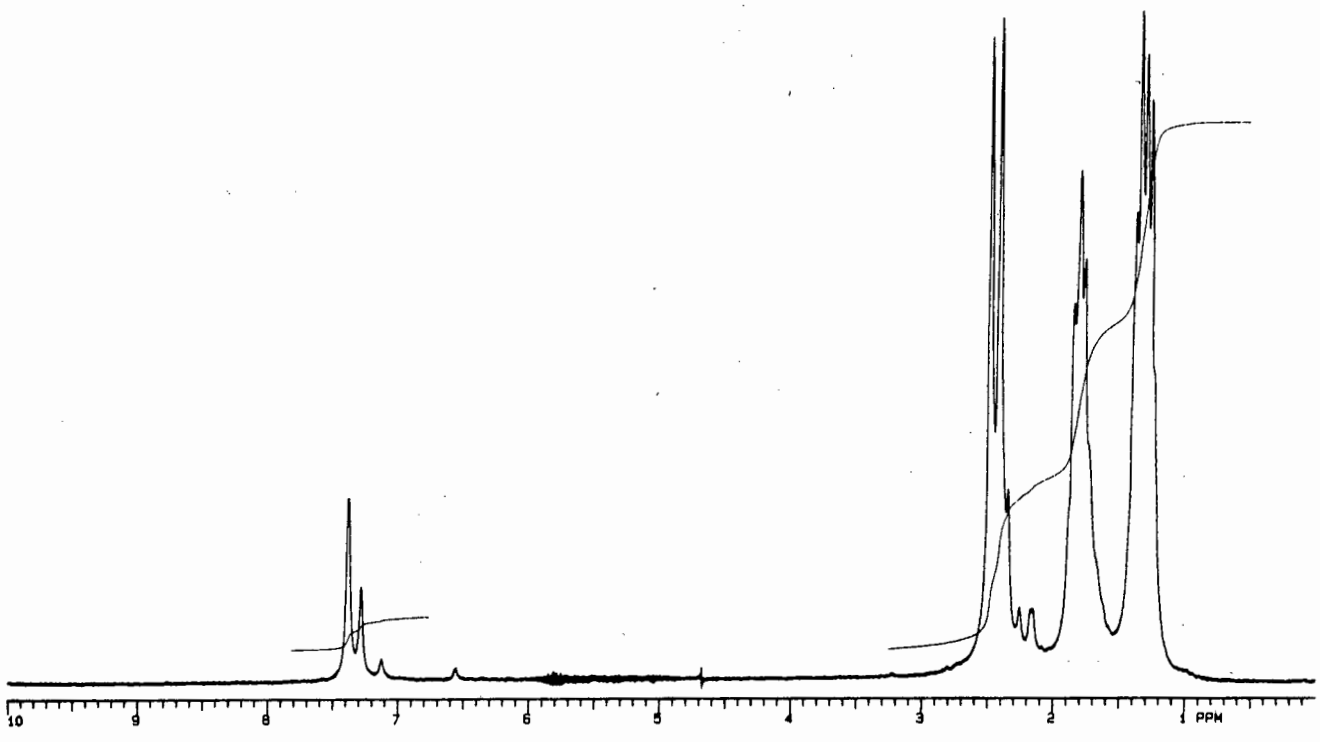

Figure 3.6(a) ^{1}H NMR spectrum of [Ni(SacSac)(PEt_3)(NCS)], (0-10 ppm).

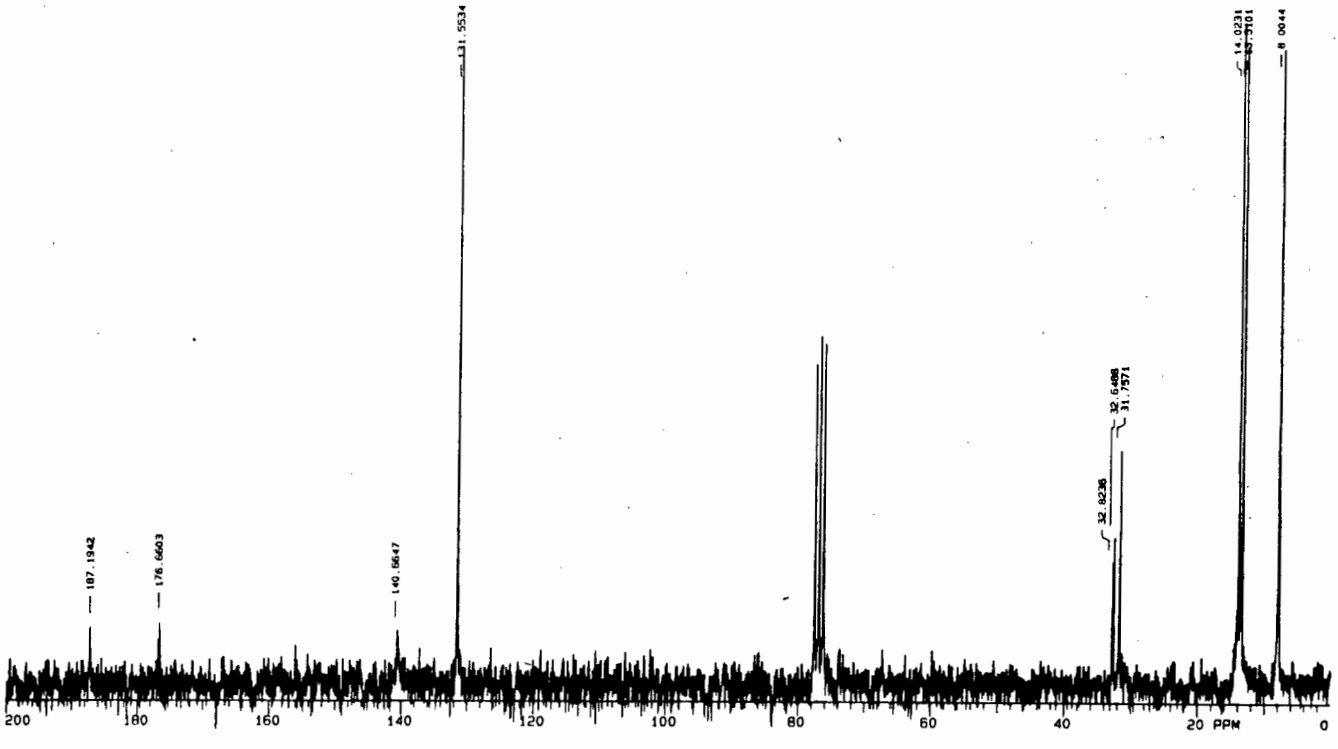

Figure 3.6(b) ^{13}C NMR spectrum of [Ni(SacSac)(PEt_3)(NCS)], (0-200 ppm).

Table 3.11 ^{1}H and ^{13}C NMR data (ppm) for the complexes $[Ni(Sacac)(PEt_3)X]$.

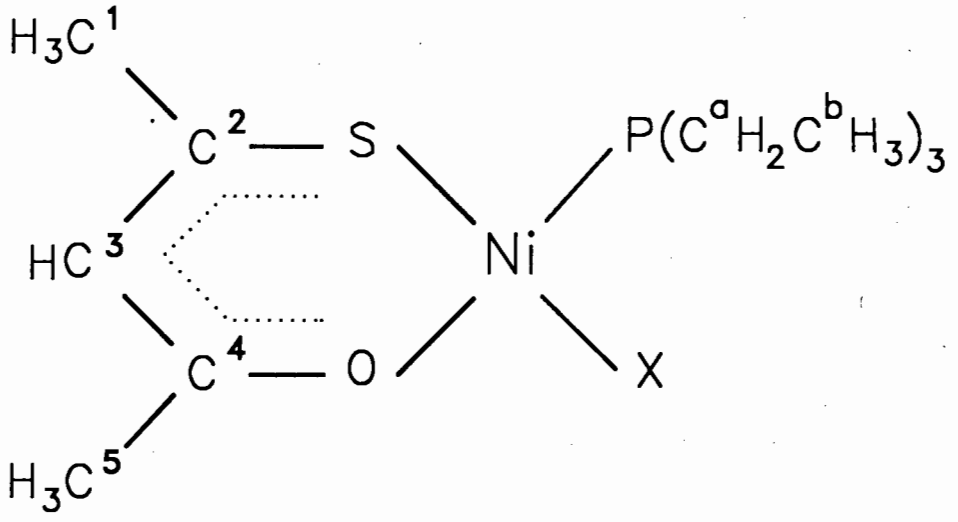

X	^{1}H NMR				
	C^bH_3	C^aH_2	C^5H_3	C^1H_3	C^3H
Cl	1.26(m)	1.64(m)	2.20	2.07	6.45
Br	1.27(m)	1.73(m)	2.22	2.08	6.45
I	1.28(m)	1.84(m)	2.23	2.05	6.35
NCS	1.34(m)	1.64(m)	2.24	2.14	6.55

X	^{13}C NMR							
	C^a	C^b	C^5	C^2	C^3	C^4	C^1	NCS
Cl	14.6(d)^x	8.13	29.35	n.o.	118.48	n.o.	29.22	
Br	15.7(d)^x	8.19	29.92	174.28	117.90	189.55	29.31	
I	18.0(d)^x	8.50	29.92	178.25	117.06	188.91	29.36	
NCS	14.3(d)^x	7.92	29.03	173.82	118.90	190.85	28.97	138.73

n.o. = not observed

(d) = doublet, (m) = multiplet

x - $^{1}J_{PC}$: Cl = 30.0 Hz, Br = 30.0 Hz, I = 28.0 Hz, NCS = 29.0 Hz

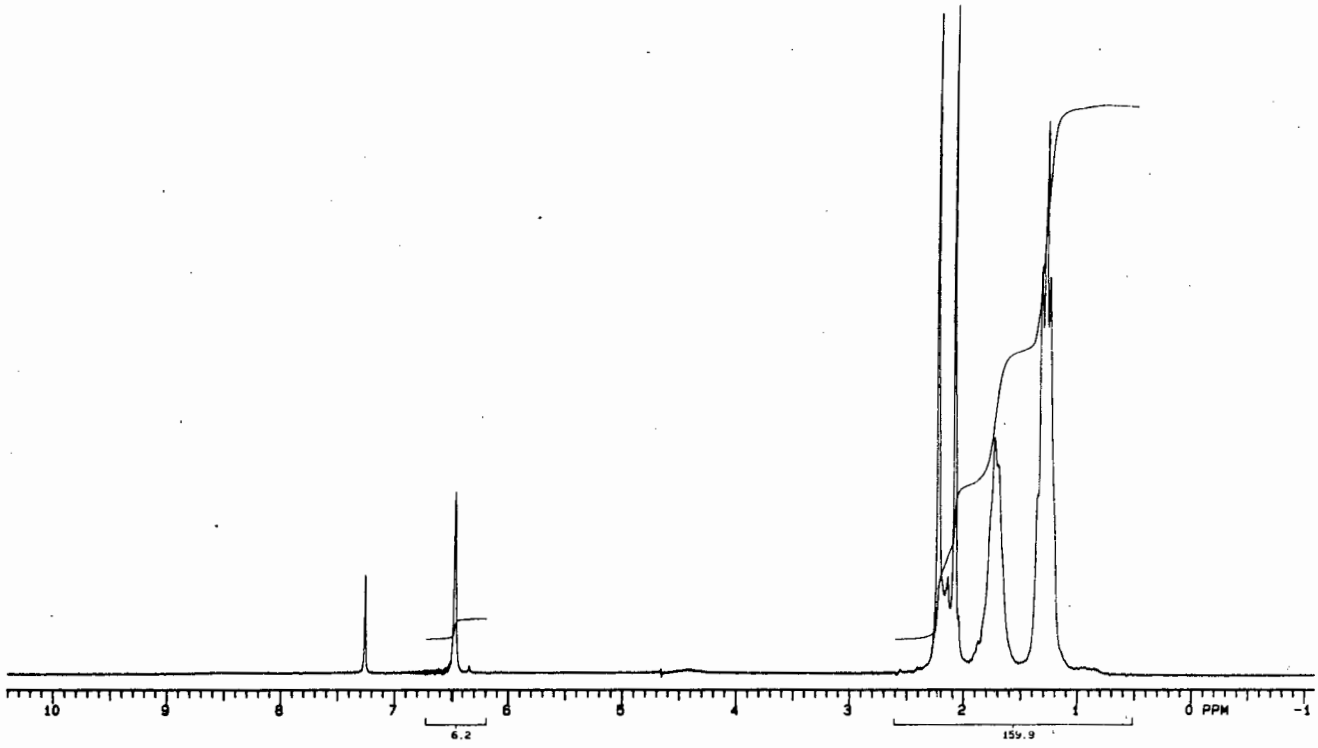

Figure 3.7(a) ^{1}H NMR spectrum of [Ni(Sacac)(PEt_3)Br], (0-10 ppm).

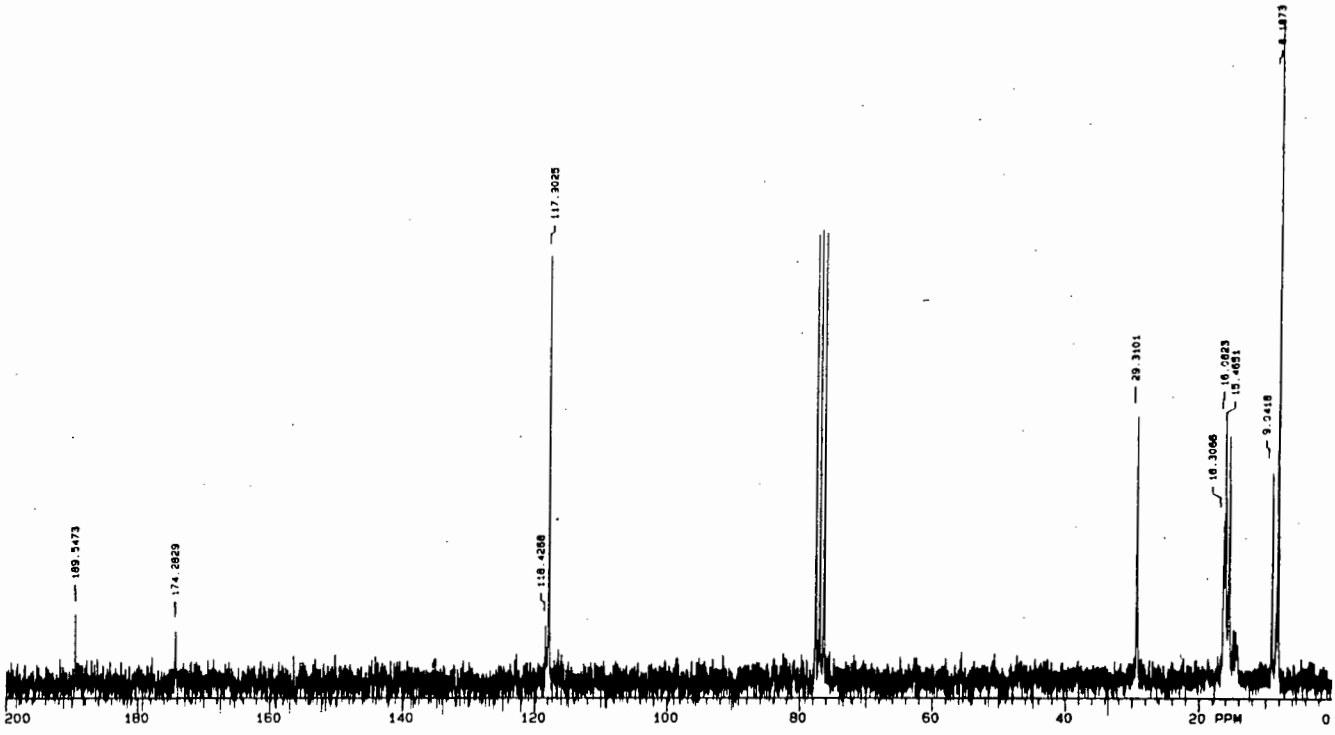

Figure 3.7(b) ^{13}C NMR spectrum of [Ni(Sacac)(PEt_3)Br], (0-200 ppm).

Table 3.12 ^{1}H and ^{13}C NMR data (ppm) for the complex [Ni(SacSac)(PMe_3)Cl].

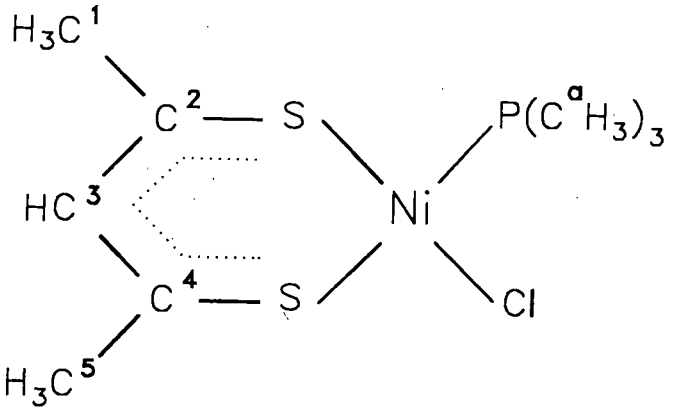

^{1}H NMR		^{13}C NMR	
C^aH_3	1.45(d)[x]	C^a	12.75(d)[y]
C^1H_3	2.36	C^1	31.76
		C^2	n.o.
C^3H	7.32	C^3	131.25
		C^4	n.o.
C^5H_3	2.40	C^5	32.60

n.o. = not observed

(d) = doublet

x - $^{1}J_{HP}$ = 2.71 Hz

y - $^{4}J_{CP}$ = 9.31 Hz

Table 3.13 ^{1}H and ^{13}C NMR data (ppm) for the complex [Ni(SacSac)(PCx_3)Cl].

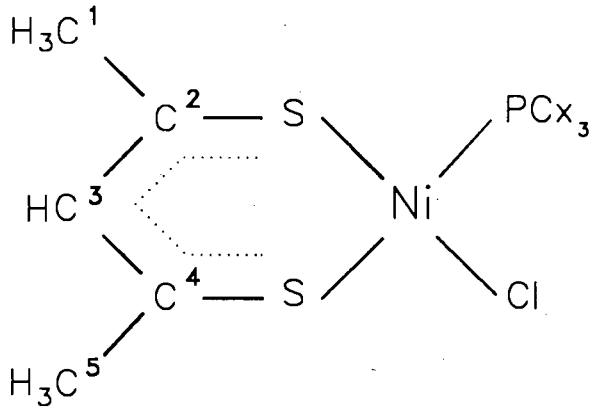

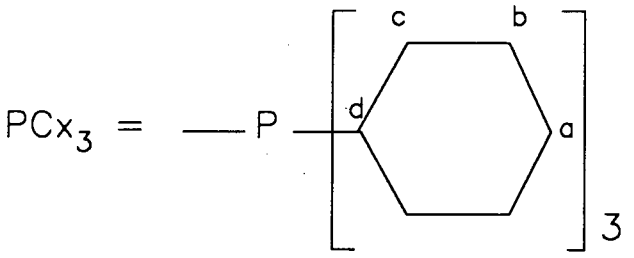

^{1}H NMR		^{13}C NMR	
Cx	1.2-2.2 (m)	C^{a}	26.29
		C^{b*}	29.29
		C^{c*}	27.63(d)^{x}
		C^{d}	32.50(d)^{y}
$C^{1}H_3$, $C^{5}H_3$	2.28	C^{1}	32.01
		C^{2}	n.o.
$C^{3}H$	7.25	C^{3}	129.65
		C^{4}	n.o.
		C^{5}	32.08

n.o. = not observed
(d) = doublet, (m) = multiplet
x* - $^{2}J_{CP}$: Cl = 10.4 Hz
y - $^{1}J_{CP}$ = 18.8 Hz
* - resonances may be interchanged

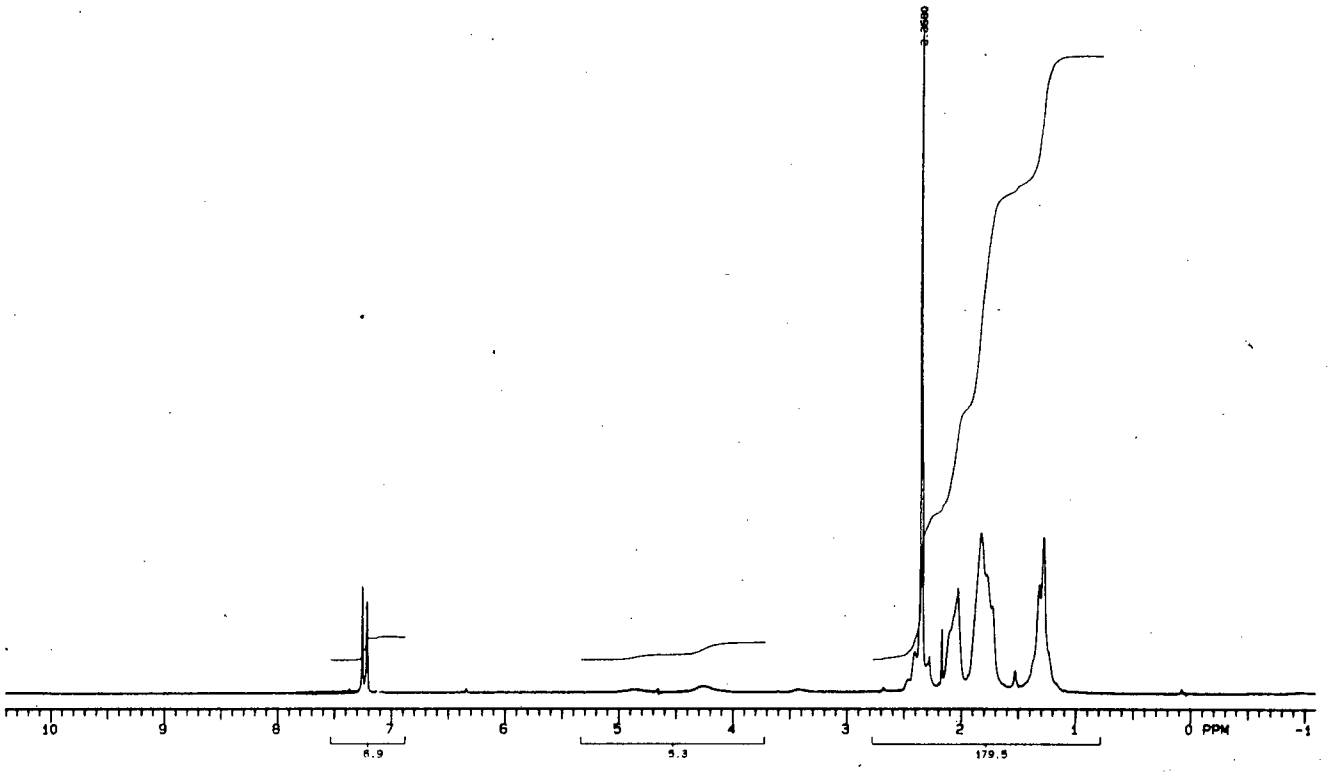

Figure 3.8(a) ^{1}H NMR spectrum of [Ni(SacSac)(PCx_3)Cl], (0-10 ppm).

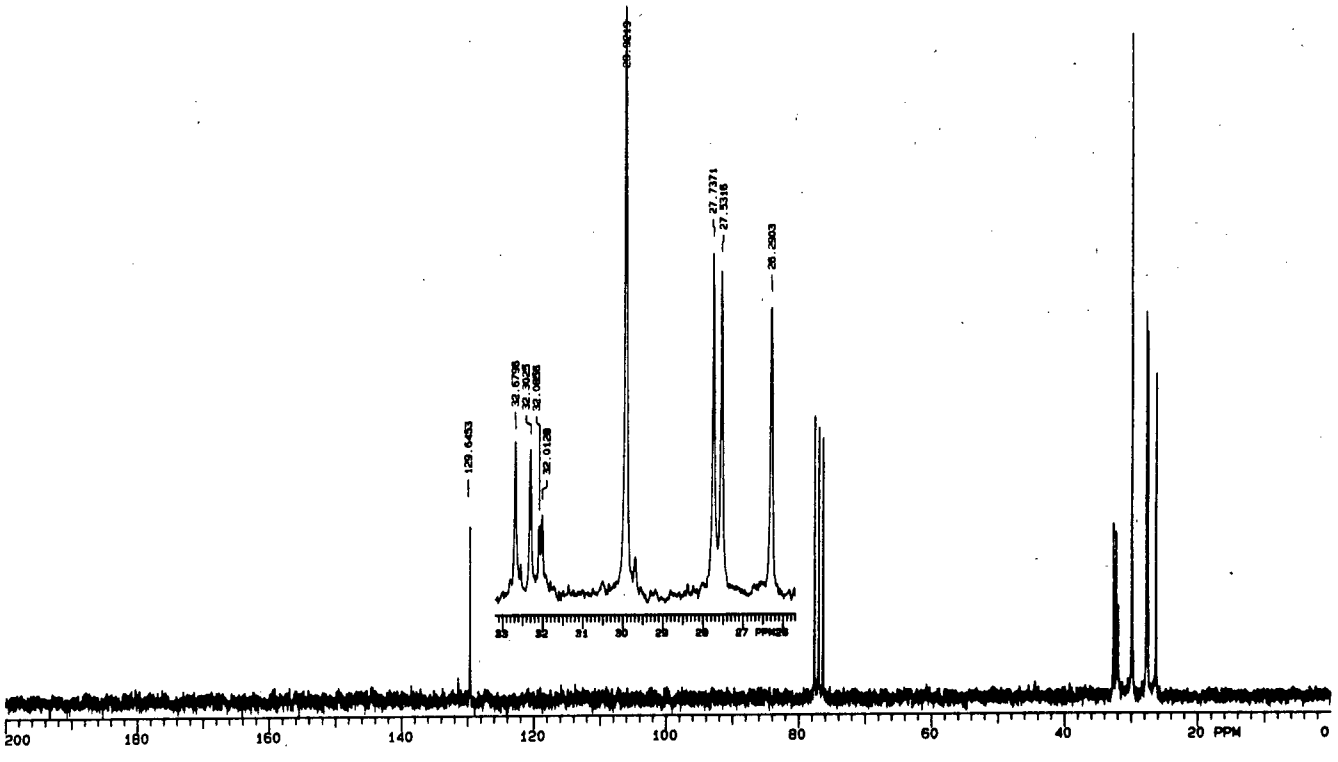

Figure 3.8(b) ^{13}C NMR spectrum of [Ni(SacSac)(PCx_3)Cl], (0-200 ppm).

Table 3.14 ^{1}H and ^{13}C NMR data (ppm) for the complex [Ni(SacSac)(PPh_3)Cl].

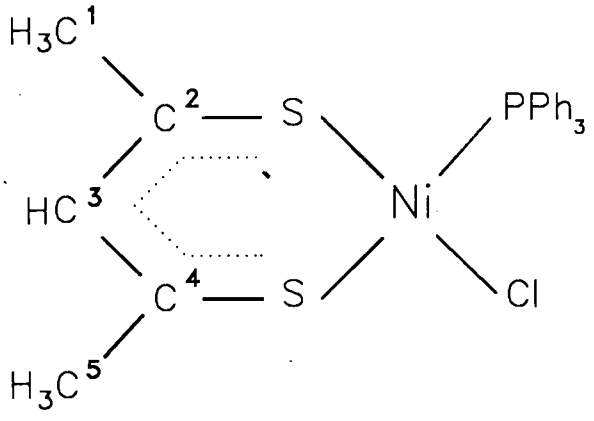

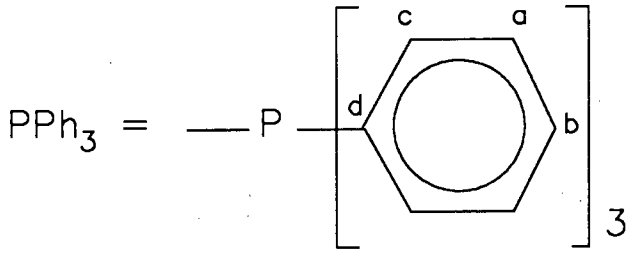

^{1}H NMR		^{13}C NMR	
Ph	7.4-7.9 (m)	C^a	128.13(d)[x]
		C^b	130.53
		C^c	135.04(d)[y]
		C^d	n.o.
C^1H_3, C^5H_3	2.28	C^1, C^5	31.56
		C^2, C^4	n.o.
C^3H	obscured	C^3	130.84

n.o. = not observed

(d) = doublet, (m) = multiplet

x - $^{3}J_{CP}$ = 10.2 Hz

y - $^{2}J_{CP}$ = 9.8 Hz

3.3.4 Crystal Structure Results

Complete details of the structure can be found in Appendix II.

Table 3.15 Crystal data and final refinements for [Ni(Sacac)(PEt_3)Cl]*.

Molecular formula	$C_{11}H_{22}OSPClNi$
Molar mass (g mol^{-1})	327.50
Space group	$P_{21/n}$
a (Å)	7.644(4)
b (Å)	18.005(8)
c (Å)	11.021(3)
β (°)	96.17(3)
V ($Å^3$)	1508(5)
Dc (gcm^{-3}) (for Z = 4)	1.44
F(000)	688
μ(Mo-K_α) (cm^{-1})	16.89
Crystal dimensions (mm)	0.45 x 0.45 x 0.50
Crystal stability (%)	1.2
$R = \Sigma\|\|F_o\| - \|F_c\|\| / \Sigma\|Fo\|$	0.056
$R_w = \Sigma w^{1/2}\|\|F_o\| - \|F_c\|\| / \Sigma w^{1/2}\|Fo\|$	0.069
Weighting	$(\sigma^2F + 0.01F^2)^{-1}$
$S = \Sigma w\|\|F_o\| - \|F_c\|\| /$ N-NP	0.98

* M.L. Niven, personal communication

Table 3.16 Selected molecular parameters for [Ni(Sacac)(PEt_3)Cl]*.

Bond lengths (Å)	Ni(1)-P(1)	2.185(1)
	Ni(1)-Cl(1)	2.245(1)
	Ni(1)-S(1)	2.125(1)
	Ni(1)-O(1)	1.893(4)
	P(1)-C(111)	1.822(5)
	P(1)-C(211)	1.837(5)
	P(1)-C(311)	1.821(5)
	S(1)-C(1)	1.717(5)
	C(3)-O(1)	1.254(6)
Bond angles (°)	Cl(1)-Ni(1)-P(1)	85.6(1)
	S(1)-Ni(1)-P(1)	91.2(1)
	O(1)-Ni(1)-Cl(1)	87.2(1)
	O(1)-Ni(1)-S(1)	96.0(1)
	S(1)-Ni(1)-Cl(1)	176.3(1)
	O(1)-Ni(1)-P(1)	172.7(1)

* M.L. Niven, personal communication

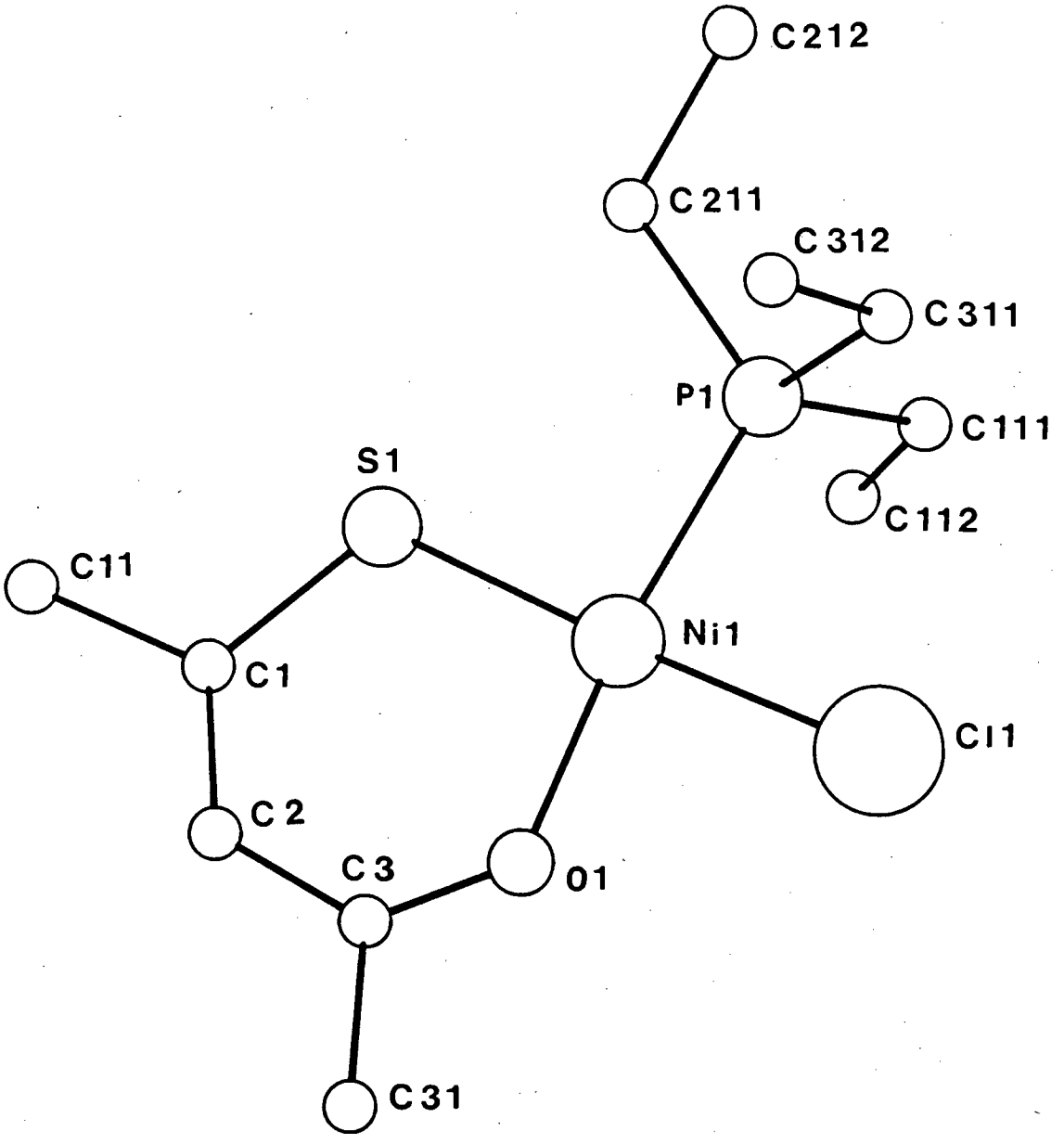

Figure 3.9 Diagram of the structure of [Ni(Sacac)(PEt_3)Cl].

3.3.5 Catalytic Run Data

Each of the Tables below represents the data accumulated by gas-liquid chromatographic analysis of the liquid samples taken at various time intervals during a catalytic run. The catalyst, co-catalyst and relative molar amounts of each are given above each Table. Unless otherwise stated, the values are expressed as a percentage of the total mass of olefins present in the sample.

Table 3.17 [Ni(SacSac)(PEt_3)Cl] : $AlEt_3$ = 1 : 1

Time(min)	%1-hex	%3-hex	%*tr*-2-hex	%*cis*-2-hex	$\%C_{12}$	$\%C_{18}$
0	100.0	-	-	-	-	-
10	82.9	8.7	3.5	4.9	-	-
20	75.9	8.7	9.9	5.5	-	-
60	68.0	6.6	16.1	9.4	-	-
210	62.6	8.8	19.3	9.3	-	-

hex = hexene
tr = *trans*

Table 3.18 [Ni(SacSac)(PEt_3)Cl] : $AlEt_3$ = 1 : 10

Time(min)	%1-hex	%3-hex	%*tr*-2-hex	%*cis*-2-hex	$\%C_{12}$	$\%C_{18}$
0	100.0	-	-	-	-	-
10	5.5	14.3	68.1	12.1	-	-
20	4.0	14.5	68.2	13.3	-	-
60	2.1	15.1	69.0	13.9	-	-
210	1.5	15.2	69.3	14.0	-	-

Table 3.19 [Ni(SacSac)(PEt_3)Cl] : $AlEtCl_2$ = 1 : 1

Time(min)	%1-hex	%3-hex	%*tr*-2-hex	%*cis*-2-hex	$\%C_{12}$	$\%C_{18}$
0	100.0	-	-	-	-	-
10	15.9	8.7	63.5	10.9	-	-
60	5.0	14.4	67.1	13.5	-	-
210	4.1	14.1	67.1	14.7	-	-

Table 3.20 [Ni(SacSac)(PEt_3)Cl] : $AlEtCl_2$ = 1 : 10

Time(min)	%1-hex	%3-hex	%*tr*-2-hex	%*cis*-2-hex	$\%C_{12}$	$\%C_{18}$
0	100.0	-	-	-	-	-
10	0.8	7.6	35.4	8.8	44.6	2.8
20	0.8	6.7	30.2	7.2	51.2	3.9
40	0.7	6.1	27.5	6.5	53.5	5.7
60	0.7	5.5	24.6	6.3	58.0	4,9
120	0.7	5.3	25.2	5.8	59.0	5.4
210	0.7	5.2	23.4	5.6	59.0	6.1

Table 3.21 [Ni(Sacac)(PEt_3)Cl] : $AlEtCl_2$ = 1 : 10

Time(min)	%1-hex	%3-hex	%*tr*-2-hex	%*cis*-2-hex	$\%C_{12}$	$\%C_{18}$
0	100.0	-	-	-	-	-
10	0.8	7.8	32.5	8.0	48.7	2.2
20	0.8	7.2	31.4	7.2	50.5	2.9
40	0.7	6.2	28.0	6.6	55.4	3.1
60	0.7	6.2	26.8	6.4	55.7	4.2
120	0.7	5.8	25.8	6.1	57.2	4.4
210	0.7	5.6	25.2	6.0	58.0	4.5

Table 3.22 [Ni(SacSac)(PEt_3)Br] : $AlEtCl_2$ = 1 : 10

Time(min)	%1-hex	%3-hex	%*tr*-2-hex	%*cis*-2-hex	$\%C_{12}$	$\%C_{18}$
0	100.0	-	-	-	-	-
10	0.8	10.1	27.7	8.0	50.1	2.9
20	0.7	9.8	27.4	7.8	52.3	3.8
40	0.6	8.3	23.2	6.6	57.6	3.9
60	0.6	7.8	22.0	6.3	59.1	4.0
120	0.6	7.5	21.4	6.1	59.1	4.8
210	0.6	6.9	19.6	5.6	62.3	5.5

Table 3.23 [Ni(SacSac)(PMe_3)Cl] : $AlEtCl_2$ = 1 : 10

Time(min)	%1-hex	%3-hex	%*tr*-2-hex	%*cis*-2-hex	$\%C_{12}$	$\%C_{18}$
0	100.0	-	-	-	-	-
10	1.5	13.9	58.0	15.6	6.0	0.7
20	1.3	14.8	56.3	16.4	7.4	1.0
40	1.2	14.8	56.8	16.3	9.1	1.2
60	1.2	14.6	55.4	15.6	11.5	1.5
180	1.1	14.9	55.3	15.5	12.0	1.6

Table 3.24 [Ni(SacSac)(PCx_3)Cl] : $AlEtCl_2$ = 1 : 10

Time(min)	%1-hex	%3-hex	%*tr*-2-hex	%*cis*-2-hex	$\%C_{12}$	$\%C_{18}$
0	100.0	-	-	-	-	-
10	1.3	12.1	50.0	12.9	22.6	1.3
20	0.9	11.9	49.7	12.4	23.5	1.6
40	0.8	11.5	50.0	12.3	23.5	1.9
60	0.8	11.3	49.9	11.9	24.0	2.0
120	0.8	11.2	49.7	11.8	24.4	2.2
210	0.8	10.4	47.2	11.1	27.8	2.8

Table 3.25 [Ni(SacSac)(PPh_3)Cl] : $AlEtCl_2$ = 1 : 10

Time(min)	%1-hex	%3-hex	%*tr*-2-hex	%*cis*-2-hex	$\%C_{12}$	$\%C_{18}$
0	100.0	-	-	-	-	-
10	1.4	13.0	54.9	15.2	15.5	-
20	1.4	12.5	53.8	15.0	17.3	-
40	1.4	12.0	51.0	14.0	21.4	-
60	1.2	11.5	49.3	13.8	24.2	-
120	1.0	11.5	47.8	12.7	26.9	-

3.4 DISCUSSION

3.4.1 Infrared Spectra

3.4.1.1 Mid-Infrared Spectra (4000-500 cm^{-1})

Tables 3.3 and 3.4 list the frequencies and assignments of the mid-infrared vibrations of complexes of general formula PEt_3 [40,41,42], $[NiL_2]$ (Chapter 2), $[Ni(PEt_3)_2X_2]$ and $[NiL(PEt_3)X]$ (L = SacSac, Sacac; X = Cl, Br, I, NCS).

$[Ni(PEt_3)_2X_2]$

The mid-infrared region of the complexes $[Ni(PEt_3)_2X_2]$ has received limited attention. However, the analogous Pd and Pt complexes have previously been discussed [40,43]. On the basis of the reported infrared [41] and Raman [40] spectra of PEt_3, the C-H stretching frequencies of the ethyl groups in $[Ni(PEt_3)_2X_2]$ may be readily assigned to bands above 2000 cm^{-1}, while the C-H bending modes occur within the range 1460-1370 cm^{-1}. Two bands observed near 1246 and 1235 cm^{-1} in the spectra of these complexes are clearly of similar origin to those at 1245 and 1231 cm^{-1} in the spectrum of the free ligand and may be assigned to ωCH_2 and τCH_2 modes, respectively [40]. This is consistent with similarly assigned bands for compounds in which ethyl groups are bonded to S or Si [44]. For ethyl derivatives of phosphorus, arsenic or antimony, bands in the region 1100-900 cm^{-1} are usually attributed to ρCH_2 and νC-C modes [45]. However, calculations using compounds in which ethyl groups are bonded to Si have shown that these vibrations are comprised of motions of the whole ethyl group [44]. These include changes of the H-C-C, H-C-H and H-C-P bond angles as well as stretching of the C-C bond.

There is some disagreement concerning the assignment of the νP-C modes. In his study of the PEt_3 ligand, Green [40] assigned two bands at 765 and 748 cm^{-1} to ρCH_2 modes and the four bands at 717, 690, 670 and

619 cm^{-1} to νC-P modes. This is supported by comparison with similar ligands such as PMe_3, $PMeCl_2$ [40] and P_2Et_4 [46], as well as νC-Si in compounds with an Et-Si bond and νC-S in compounds with an Et-S bond [47]. Furthermore, for the complex $[Ni(PMe_3)_4]$, νP-C was assigned to bands at 694 and 650 cm^{-1} [48]. However, in the complexes $[M(PMe_3)_2X_2]$ (M = Pd, Pt; X = Cl, Br, I), νP-C was consistently assigned to bands in the region 750-680 cm^{-1} [7,9,43] and in the complexes $[Pt(PEt_3)_2X_2]$ (X = Cl, I), νP-C was assigned to a vibration at 765 cm^{-1} (also observed for the free ligand) and the ρCH_2 mode to vibrations of lower frequency [45]. This was based on the observation that when P is replaced by As or Sb, the band at 765 cm^{-1} disappears. In this work, assignments follow those of the free ligand and the normal coordinate analysis of Loutellier *et al.* [48], where the CH_2 rocking modes are at higher frequency than the P-C stretching vibrations. Without more extensive isotopic labelling or normal coordinate studies, no completely unambiguous assignments may be made. For the free ligand, the presence of seven νP-C modes may be due to rotation about the P-C bond giving rise to several spectroscopically unique isomers [47]. The fact that only four νP-C vibrations are observed for $[Ni(PEt_3)_2X_2]$ may be attributed to restrictions placed on the conformation of PEt_3 when bonded to nickel.

$[NiL(PEt_3)X]$ (L = SacSac, Sacac; X = Cl, Br, I, NCS)

Assignment of the mid-infrared spectra of these complexes is made straightforwardly by comparison with the spectra of their synthetic precursors. The frequency shifts of the ligand (L) vibrations on changing from $[NiL_2]$ to the $[NiL(PEt_3)X]$ complexes are consistent with the crystal structures of the latter complexes [13]. The C=S and C=C bonds are shorter in $[NiL_2]$ than in the $[NiL(PEt_3)Cl]$ complexes, resulting in shifts of these stretching vibrations to higher frequencies in the $[NiL_2]$ complex spectra. Similarly, in $[Ni(Sacac)_2]$, the C=O bond is longer than in $[Ni(Sacac)(PEt_3)Cl]$ and νC=O is therefore observed at a lower frequency in the $[Ni(Sacac)_2]$ spectrum. In the spectra of the complexes $[NiL(PEt_3)(NCS)]$, $\nu C{\equiv}N$ is near 2100 cm^{-1} while the νS-CN mode occurs at 859 cm^{-1} indicating bonding of NCS through N [49,50]. The

2δNCS overtones are observed in the range 960-860 cm^{-1}, and the νC-S mode is observed in the range 860-830 cm^{-1}.

3.4.1.2 Far-Infrared Spectra (500-50 cm^{-1})

$[Ni(PEt_3)_2X_2]$ (X = Cl, Br, I, NCS)

The far-infrared spectra over the range 500-50 cm^{-1} are depicted in Fig. 3.10. The frequencies and assignments for the complexes *trans*-$[Ni(PEt_3)_2X_2]$, taken from the empirical study of Fergusson *et al.* [51], the $^{58,62}Ni$-labelling studies of Nakamoto *et al.* [11,12,52] and the present work, are given in Table 3.26. According to the D_{2h} point group symmetry, only one νNi-X and one νNi-P are expected.

The only complex to exhibit a band within the range 550-425 cm^{-1} is the isothiocyanate derivative. This unique band, at 466 cm^{-1}, is clearly the δNCS mode confirmed by the appearance of its overtone 2δNCS at 930 cm^{-1}. The relatively intense 2δNCS overtone is often observed in isothiocyanate complexes such as $[Ni(aniline)_2(NCS)_2]$ [53] (the overtone is present as a very strong band at 960 cm^{-1} in the spectrum of NaSCN).

One of the complicating features of the infrared spectra of metal-PEt_3 complexes is the occurrence of no less than five δCCP bands. However, they are consistent in their position in numerous triethylphosphine complexes near 415, 375, 360, 330 and 250 cm^{-1} (the band near 360 cm^{-1} is not always observed). The identity of some of these modes has been established by their insensitivity to $^{58,62}Ni$-substitution [11,12,52].

The νNi-X modes are identified as strongly $^{58,62}Ni$-sensitive bands at 403 and 338 cm^{-1} for X = Cl, Br, respectively. The νNi-I mode in the spectrum of $[Ni(PEt_3)_2I_2]$ has been assigned to the moderately strong band at 309 cm^{-1}. However, assignment of the band at 260 cm^{-1} to νNi-I is preferred, since this assignment gives a νNi-I/νNi-Cl frequency ratio of 0.64 whereas the band at 309 cm^{-1} gives a value of 0.77. Clark [54] considers a value of 0.62 as diagnostically typical. The νNi-P bands are at 271, 263 and 251 cm^{-1} for X = Cl, Br, I, respectively. They have

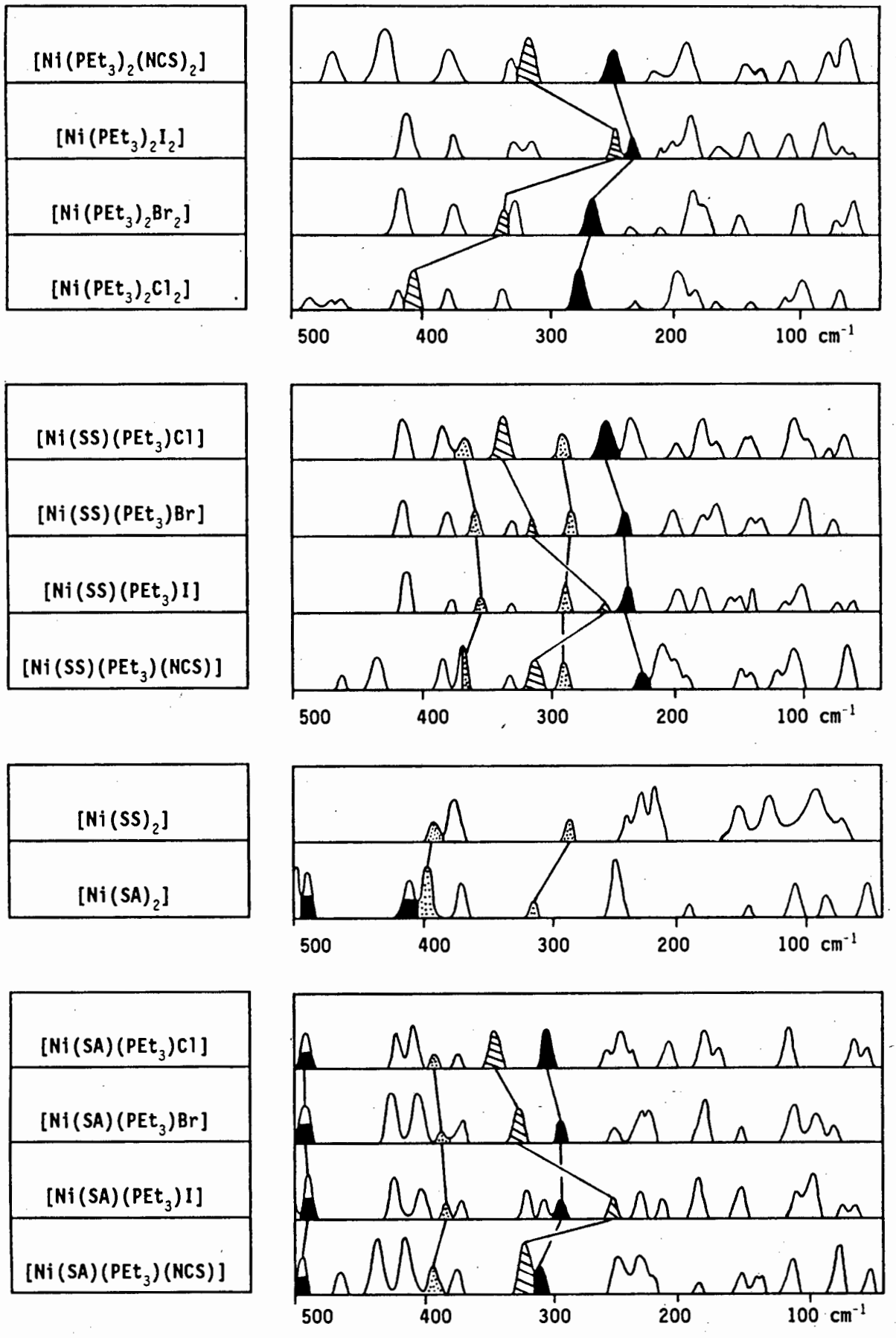

Shaded bands: νNi-X, Solid bands: νNi-P,
Dotted bands: νNi-S, Half-shaded bands: νNi-O

Figure 3.10 Far-infrared spectra of the complexes $[Ni(PEt_3)X_2]$, $[NiL(PEt_3)X]$ and $[NiL_2]$. [L = SacSac (SS), Sacac (SA)]

Table 3.26 Far-infrared spectra (cm^{-1}) of the complexes *trans*-$[Ni(PEt_3)_2X_2]$: A comparison of the data from three studies.

Fergusson and Heveldt [51]			Nakamoto *et al.* [11,12]		This work				Assignment
X = Cl	Br	I	Cl	Br	Cl	Br	I	NCS	
								466	δNCS
			417(0)	414(1.2)	416	414	411	425	δCCP
403	338	307	403(6.7)	338(10.5)	402	336	260	316	νNi-X
375	378	377	373(-0.1)	374(1.1)	373	374	377	375	δCCP
365		359							δCCP
324	327	329	329(-0.5)	328(0.5)	329	328	331	329	δCCP
							309		
270	263	253	273(5.9)	265(4.7)	271	263	251	243	νNi-P
249	253				257	251	235	(243)	δCCP
199	191	184	200(0.8)	190(0.7)	185	188	184	188	δNi-P-C / δCPC
185	151	142	187(-0.2)	155(1.5)	198	152	143	142	δX-Ni-X
164					165	171	162	161	δP-Ni-P
					114		113		δP-Ni-P
109	106	95	107(-0.7)	106(-0.4)	101	102	92	112	πNi-P-C
					72	80	73	80	lattice + πCH_3
47		50				62	63	68	lattice + πCH_3

Figures in parentheses indicate shifts on $^{58,62}Ni$-substitution

been identified by their sensitivity towards $^{58,62}Ni$-substitution. It is interesting to note that νNi-P undergoes a stepwise reduction in frequency as the halide becomes softer. The increased covalency in the Ni-X bonds is apparently accomplished at the expense of the electron density in the Ni-P bonds. Bands near 200 cm^{-1}, which are moderately sensitive to $^{58,62}Ni$-substitution, have been assigned to δC-P-C bending modes, while bands near 185, 155 and 115 cm^{-1} (for X = Cl, Br, I, respectively) have been assigned to δX-Ni-X modes in view of their sensitivity to the nature of X and their moderate sensitivity towards $^{58,62}Ni$-substitution. However, the band at 185 cm^{-1} is relatively unshifted on $^{58,62}Ni$-substitution, while the band at 198 cm^{-1} is shifted -0.8 cm^{-1}. Their assignments are therefore reversed in this study. Bands near 10Q cm^{-1}, which are slightly $^{58,62}Ni$-sensitive, are assigned to δP-Ni-P bending modes and bands of lower frequency to πNi-P-C oop bends and lattice modes.

[NiL(PR_3)X] (L = SacSac, Sacac; R = Me, Et, Cx, Ph; X = Cl, Br, I, NCS)

When the assignments given above are extended to the complexes [NiL(PEt_3)X], the additional complexity resulting from the Ni-O and Ni-S bands causes greater ambiguity in the assignments. The complexes are square planar and the C_s point group symmetry implies the presence of four metal-ligand stretching modes; νNi-X, νNi-P and two νNi-L. Furthermore, significant shifts are expected for certain metal-ligand bands due to the presence of tertiary phosphines and sulphur donor ligands which exert a strong *trans* influence [55].

Assignments are facilitated by first considering the spectra of the complexes [Ni(SacSac)(PR_3)Cl] and their synthetic precursors [Ni(PR_3)$_2$$Cl_2$] and [Ni(SacSac)$_2$] (Fig. 3.11, Table 3.5). The strong νNi-Cl band, near 400 cm^{-1} for the complexes *trans*-[Ni(PR_3)$_2$$Cl_2$], is observed near 330 cm^{-1} for the complexes [Ni(SacSac)(PR_3)Cl]. This shift to lower frequency is due to the presence of Cl *trans* to an S of the SacSac ligand. Such a large shift is not anticipated for νNi-P, as in both types of complex it is *trans* to a ligand with a strong *trans*-effect. Indeed, it occurs near 270 cm^{-1} for *trans*-[Ni(PR_3)$_2$$Cl_2$] and near 250 cm^{-1} for the complexes [Ni(SacSac)(PR_3)Cl]. An exception to the

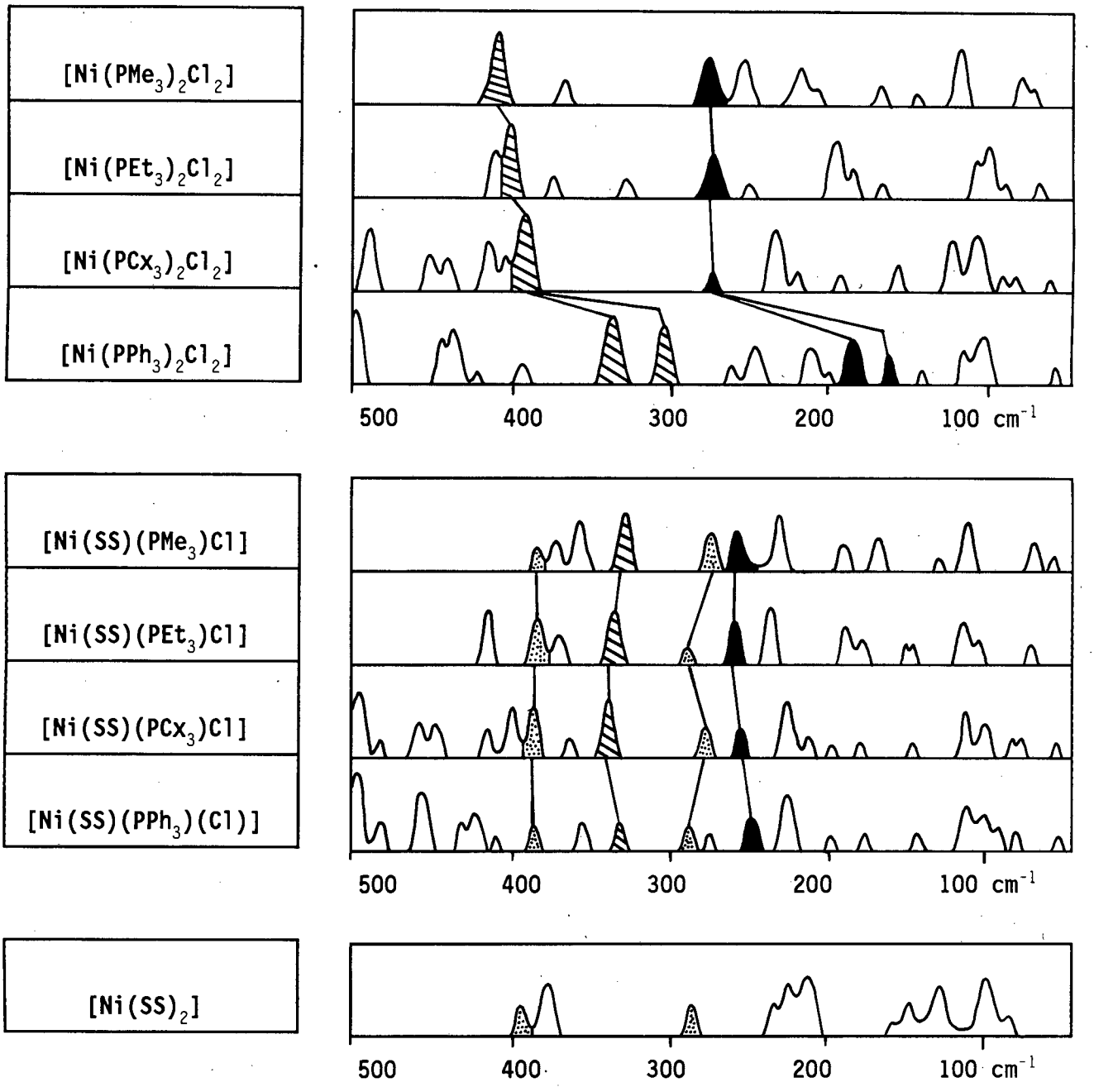

Shaded bands: νNi-X, Solid bands: νNi-P, Dotted bands: νNi-S

Figure 3.11 Far-infrared spectra of the complexes $[Ni(PR_3)_2Cl_2]$ and $[Ni(SS)(PR_3)Cl]$. (SS = SacSac)

above is the complex $[Ni(PPh_3)_2Cl_2]$ which is tetrahedral (C_{2v} point group symmetry). Two νNi-P and two νNi-Cl are expected and, in a $^{58,62}Ni$-substitution study [11], four bands were observed to move on isotopic substitution. The upper two, at 341 and 305 cm^{-1}, were absent from the spectra of both the bromo analogue and the PPh_3 ligand and were accordingly assigned to νNi-Cl. The bands at lower frequency (188 and 163 cm^{-1}) were therefore assigned to νNi-P.

The νNi-S bands are observed near 380 and 280 cm^{-1}, near their positions in the spectrum of $[Ni(SacSac)_2]$, while δNi-S bands occur near 220 and 200 cm^{-1}. The δNi-Cl modes, observed near 200 cm^{-1} for the complexes *trans*-$[Ni(PR_3)_2Cl_2]$, are shifted to lower frequency in the spectra of $[Ni(SacSac)(PR_3)Cl]$, occurring near 170 cm^{-1}, *i.e.* at approximately half the frequency of νNi-Cl. It has been proposed that the band near 200 cm^{-1} in the $[Ni(PEt_3)_2Cl_2]$ complex spectrum be attributed to δNi-P-C [51]. However, it is probably more correct to assign this mode to the band near 115 cm^{-1}, where it lies at lower wavenumber than δNi-Cl. Finally, below 100 cm^{-1}, the vibrations are assigned to lattice modes, in some cases probably coupled with δCH_3 oop.

The assignments given above may be extended to the complexes $[Ni(SacSac)(PEt_3)X]$ (Fig. 3.10, Table 3.6). Changing X dramatically shifts the νNi-X modes which are observed at 311, 250 and 316 cm^{-1} for X = Br, I and NCS, respectively. As for the chloro complex, the *trans*-effect of the SacSac ligand causes the νNi-X bands to occur at lower frequency than in the spectra of the complexes $[Ni(PEt_3)_2X_2]$, although this shift is not as marked as for X = Cl. The δNi-X modes are observed at 165, 154, and 157 cm^{-1} for X = Br, I and NCS, respectively. The two νNi-S bands are relatively unshifted by X-substitution and occur near 380 cm^{-1} and 290 cm^{-1} for each complex. As for *trans*-$[Ni(PEt_3)_2X_2]$, νNi-P undergoes a stepwise reduction in frequency as the halide gets softer and is observed at 256, 242, 240 and 232 cm^{-1} for X = Cl, Br, I and NCS, respectively.

The added complexity of the spectra of the complexes $[Ni(Sacac)(PEt_3)X]$ arises from the presence of both Ni-O and Ni-S bands. Unlike $[Ni(Sacac)_2]$, for which two νNi-O and two νNi-S are observed, only one of each is expected in the $[Ni(Sacac)(PEt_3)X]$ spectra. These occur near

490 cm^{-1} (νNi-O) and 400 cm^{-1} (νNi-S), corresponding to the bands at 492 and 396 cm^{-1}, respectively, for $[Ni(Sacac)_2]$. The remaining two bands, observed at 409 and 308 cm^{-1} for $[Ni(Sacac)_2]$, are absent. The crystal structure determination of the complex $[Ni(Sacac)(PEt_3)Cl]$ (detailed in 3.3.4) has shown that the chlorine atom is *trans* to the S atom. νNi-Cl is therefore expected, and is indeed observed, at lower frequency than for $[Ni(PEt_3)_2Cl_2]$. The νNi-Cl mode, at 347 cm^{-1} in this Sacac complex, is at lower frequency in the corresponding SacSac complex, suggesting that the Sacac ligand exerts a lesser *trans* influence. Similarly, νNi-X for X = Br, I and NCS occurs at 329, 255 and 322 cm^{-1}, respectively; each of which is at higher frequency than in the corresponding SacSac complex. The substitution of oxygen for sulphur *trans* to the PEt_3 ligand reduces the *trans* effect and causes νNi-P to appear at higher frequency in the Sacac complex spectra. This vibration is therefore observed at 305, 296, 293 and 312 cm^{-1} for X = Cl, Br, I and NCS, respectively. This is consistent with the length of the Ni-P bond which is 2.232 Å in the complex $[Ni(SacSac)(PEt_3)Cl]$ [13] and only 2.185 Å in $[Ni(Sacac)(PEt_3)Cl]$. The remaining bending vibrations are assigned as for the SacSac complexes with δNi-O and δNi-S modes observed near 250 and 230 cm^{-1}, respectively, and δNi-X modes assigned to bands at 170, 155, 153 and 155 cm^{-1} for X = Cl, Br, I and NCS, respectively.

3.4.2 ^1H and ^{13}C NMR Spectra

The ^1H NMR and ^{13}C NMR data for complexes of the type $[Ni(PEt_3)_2X_2]$ are represented in Table 3.7. In each ^1H NMR spectrum, two multiplets are observed due to proton coupling. The CH_3 resonance is therefore divided into a triplet and the CH_2 resonance into a quartet. The ^{13}C NMR spectra contain two singlets. Coupling to the phosphorus atom is not observed in either spectrum. Neither the NMR spectra of the complex $[Ni(PMe_3)_2Cl_2]$ (Table 3.8) nor those of the complex $[Ni(PCx_3)_2Cl_2]$ (Table 3.9) show evidence of phosphorus coupling, although extensive proton coupling gives rise to several multiplets in the ^1H NMR spectrum of the latter complex.

The NMR data of the complexes [Ni(SacSac)(PEt_3)X] are given in Table 3.10. In the ^1H NMR spectrum both the CH_3 and CH_2 resonances of the phosphine ligand are split into multiplets due to the combined effects of proton and phosphorus coupling. With the exception of the complex for which X = NCS, the CH_3 resonances of the chelating ligand are magnetically equivalent. This equivalence has been explained in terms of a rapid phosphine or halide exchange mechanism [13]. The fact that separate CH_3 resonances are distinct when X = NCS suggests that halide exchange is responsible for this coalescence. In the ^{13}C NMR spectra, the effects of phosphorus coupling are observed. The CH_2 resonance of the phosphine ligand is therefore split as is the downfield resonance of the CH_3 groups on the chelating ligand. This ^4CP coupling has been observed previously [13], and may be attributed to the CH_3 *trans* to the phosphine. For X = Cl, the CH_3 resonances of the SacSac ligand have been observed to coalesce at 298K, becoming a broad singlet. ^1H NMR signals coalesce at lower temperatures than ^{13}C NMR signals and this explains why, for the ^1H NMR, a single resonance occurs.

The NMR data of the complexes [Ni(Sacac)(PEt_3)X] are represented in Table 3.11. The spectra are similar to those of the corresponding SacSac complexes. However, the presence of hetero chelating atoms excludes the possibility of equivalent CH_3 resonances at elevated temperatures. Furthermore, there is no evidence of splitting in the methyl resonance *trans* to the phosphine ligand.

For the complex [Ni(SacSac)(PMe_3)Cl] (Table 3.12), phosphorus coupling is evident in both the ^1H and ^{13}C NMR, where the phosphine methyl resonance is split. In addition, in the ^{13}C NMR spectrum, the resonance of the methyl on the SacSac ligand which lies *trans* to the phosphine is split.

The NMR spectra of the complex [Ni(SacSac)(PCx_3)Cl] (Table 3.13) are also similar to those of the corresponding PEt_3 complexes. The methyl resonances of the SacSac ligand are present as a single peak in the ^1H NMR but are split in the ^{13}C spectrum although there is no evidence of phosphorus coupling. Two of the cyclohexyl resonances are split. The first may be attributed to C^d closest to the phosphorus atom and the

second to either C^b or C^c as it is possible for both ^2CP and ^3CP coupling to occur [38].

The NMR data of the [Ni(SacSac)(PPh_3)Cl] complex (Table 3.14) are also similar to those of the corresponding PEt_3 complex. In both the ^1H and ^{13}C NMR spectra, the methyl groups of the chelate ligand are observed as a singlet.

3.4.3 Catalysis

The phosphine-modified catalysts studied in this section are square planar and of general formula:

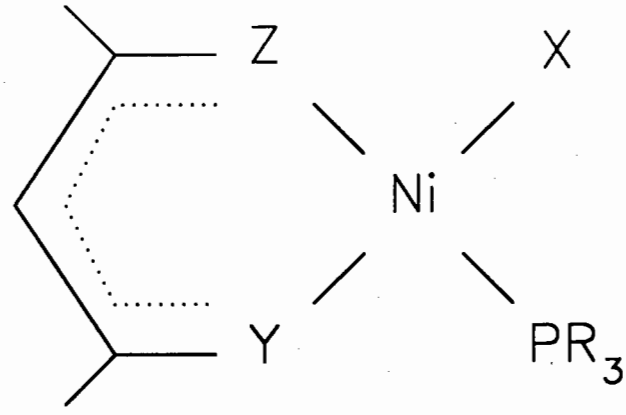

Z = Y = S (SacSac)
Z = O, Y = S (Sacac)

R = Ph, Cx, Et, Me

X = Cl, Br

By altering the phosphine as well as the halogen and the chelating ligand, their influences on the isomerisation and oligomerisation reactions may be ascertained.

3.4.3.1 Effect of the Lewis Acid

$AlEt_3$

In the presence of $AlEt_3$ as co-catalyst, at a Ni:Al of either 1:1 or 1:10, [Ni(SacSac)(PEt_3)Cl] is inactive as an oligomerisation catalyst. Only isomerisation is observed. The use of the chloride-free $AlEt_3$ co-

catalyst may, in fact, be negated due to the presence of a chloride ion in the system. The nickel may catalyse a halide substitution to form a weak chloride-containing Lewis acid [16]:

$$AlEt_3 + R\text{-}Cl \xrightarrow{Ni} AlEt_2Cl + R\text{-}Et.$$

$AlEtCl_2$

Based on the results obtained in Chapter 2, $AlEtCl_2$ was selected as the most effective chloride-containing co-catalyst. When $AlEtCl_2$ is employed in the same molar ratio as the nickel complex, [Ni(SacSac)(PEt_3)Cl], only isomerisation of 1-hexene occurs. The reaction is complete after only ten minutes. The equilibrium proportion of the hexene isomers is similar to that obtained for the phosphine-free systems (1-hexene : 2-hexene : 3-hexene = 1 : 80 : 19). In the presence of a ten molar excess of the same co-catalyst, significant dimerisation activity and instantaneous isomerisation activity are observed (Fig. 3.12). Few higher oligomers are formed. The dimerisation activity dramatically exceeds that of the inactive [$Ni(SacSac)_2$] / 10 $AlEtCl_2$ system studied in Chapter 2.

3.4.3.2 Effect of the Chelating Ligand

In the presence of a ten molar excess of $AlEtCl_2$ as co-catalyst, replacement of the SacSac ligand by a Sacac ligand to form the complex [Ni(Sacac)(PEt_3)Cl] has little effect on dimerisation rate or activity (Fig. 3.13). This is in sharp contrast to the previously tested [$Ni(SacSac)_2$] and [$Ni(Sacac)_2$] systems, in which only the latter is active as a dimerisation catalyst. In addition, changing the chelating ligand has little influence on catalyst selectivity (Fig 3.14). Linear dodecene accounts for only 5% of the dimer formed. The phosphine-containing complex catalyst, [Ni(Sacac)(PEt_3)Cl], is also markedly more active than the [$Ni(Sacac)_2$] precursor (Fig. 3.13).

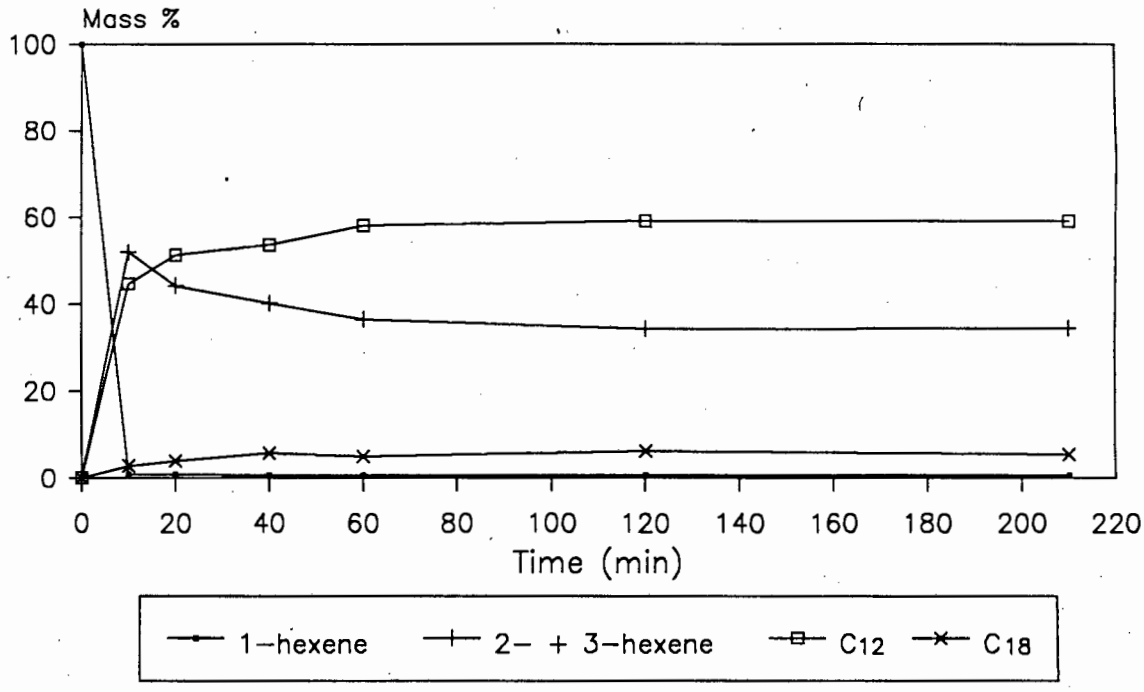

$[Ni(SacSac)(PEt_3)Cl] : AlEtCl_2 = 1 : 10$

$T = 40^{\circ}C$

Figure 3.12 Graph of the conversion of 1-hexene with time.

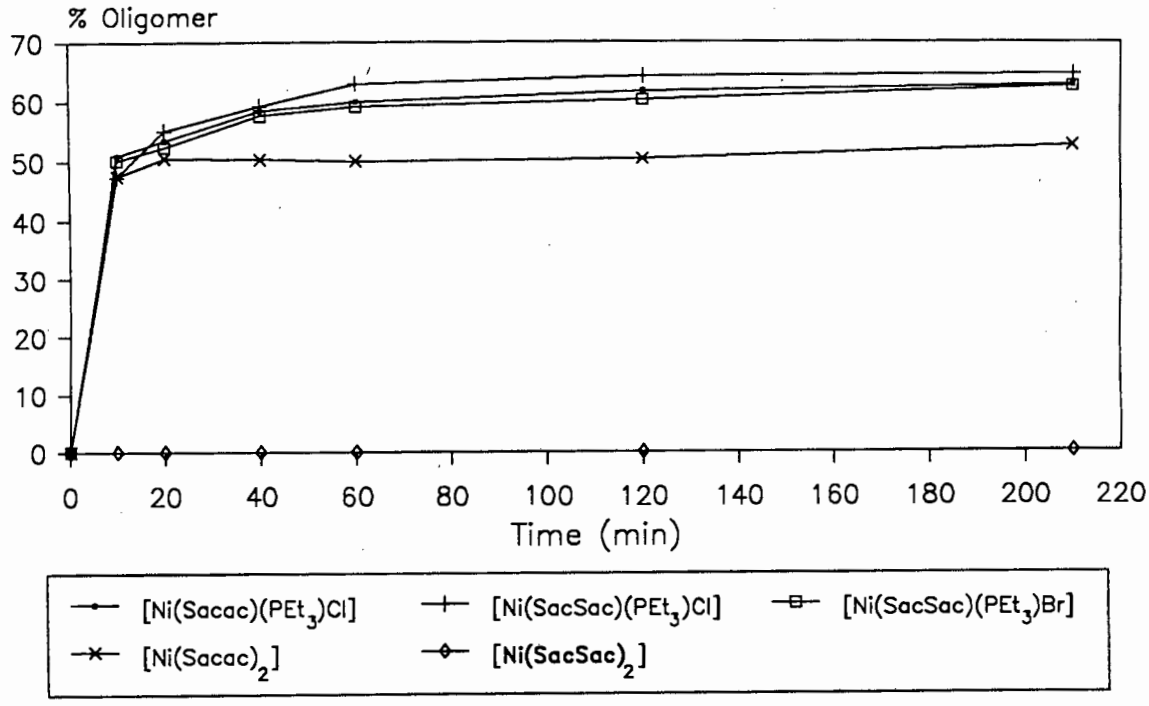

T = 40°C

Ni : $AlEtCl_2$ = 1 : 10

Figure 3.13 Graph of the effect of a change in chelating ligand and halide anion on the dimerisation reaction.

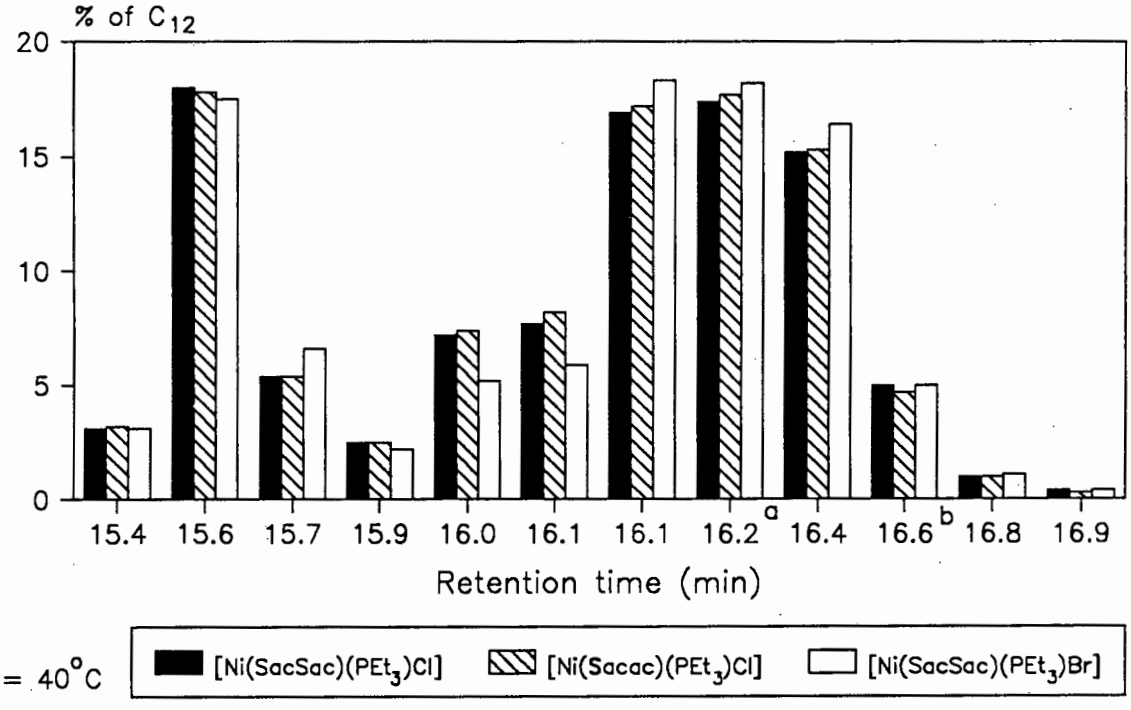

T = 40°C

Ni : $AlEtCl_2$ = 1 : 10

a = unresolved isomers b = linear dodecene

Figure 3.14 Graph of the effect of a change in chelating ligand and halide anion on the distribution of dimer products.

3.4.3.3 Effect of the Halide Anion

When the chloride ion in [Ni(SacSac)(PEt_3)Cl] is replaced by a bromide ion, neither the dimerisation nor the oligomerisation rate or activity is significantly affected (Fig. 3.13). The selectivity of the system also remains unchanged (Fig. 3.14). It appears likely that, in solution, the bromide ion may be replaced by a chloride ion due to the large excess of chloride ions present in the reaction mixture.

3.4.3.4 Effect of the Phosphine Ligand

Dimerisation

When a ten-fold excess of $AlEtCl_2$ co-catalyst is present, substitution of PEt_3 in [Ni(SacSac)(PEt_3)Cl] by PMe_3, PCx_3 or PPh_3 leads to a decrease in the dimerisation activity (Fig. 3.15). The decrease in activity follows the order:

$$PEt_3 > PCx_3 \sim PPh_3 > PMe_3.$$

This variation in activity is more marked than on changing the chelate ligand. The PMe_3-modified catalyst exhibits low oligomerisation activity which may be attributed to the high isomerisation activity of PMe_3-modified systems [21]. With the exception of the PMe_3-modified system, the effect of the phosphine ligands appears to be a mainly steric phenomenon. To date, there has been no systematic study of the effect of phosphines on catalytic activity and it is possible that trends vary from system to system. For example, Cavell and Masters [34] observed that [Ni(SacSac)(PPh_3)Cl] is a more active propene dimerisation catalyst than the analogous PEt_3 complex. In addition, they report a short half-life for the former catalyst, while in the PPh_3 system used in this study, prolonged catalyst lifetime is observed. These apparent contradictions may be due to the use of different reaction temperatures (-15°C *versus* 40°C), different co-catalysts ($AlEt_2Cl$ *versus* $AlEtCl_2$) or different feeds (propene *versus* 1-hexene). Indeed, temperature variation has been shown to influence phosphine-modified, nickel catalysed reactions [21]. When considering the effect of a change in

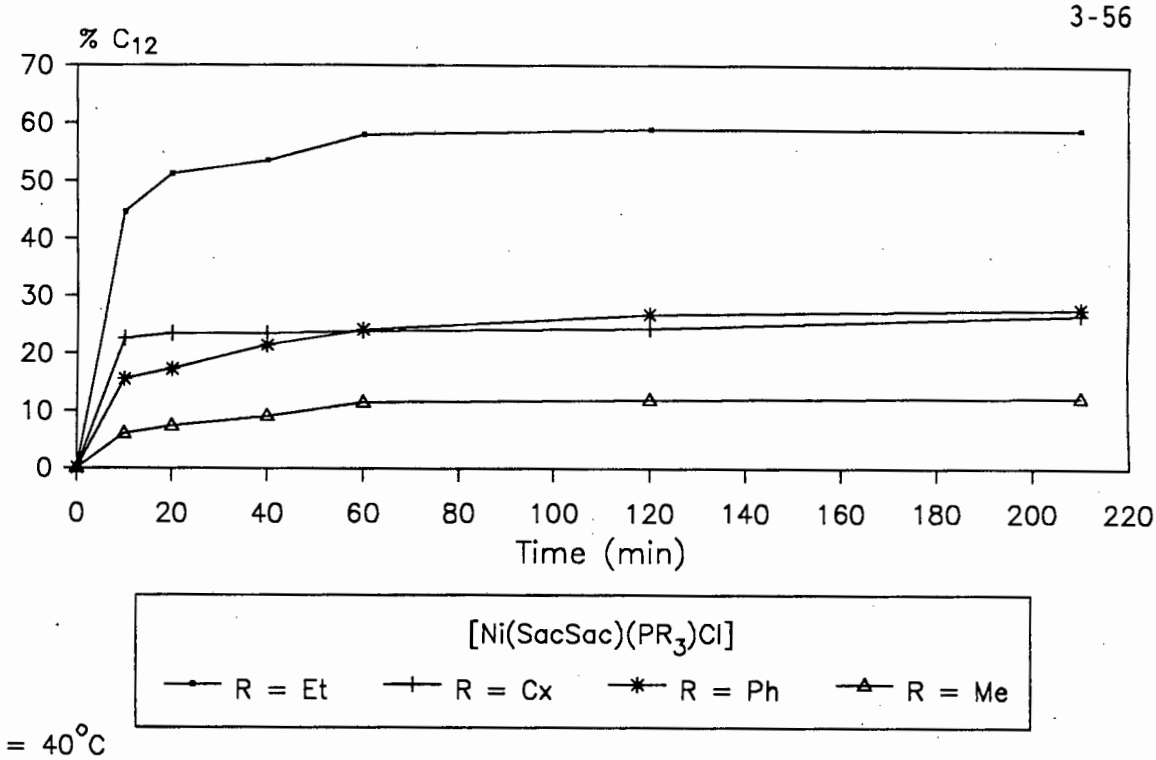

T = 40°C

Ni : $AlEtCl_2$ = 1 : 10

Figure 3.15 Graph of the effect of a change in phosphine ligand on the dimerisation reaction.

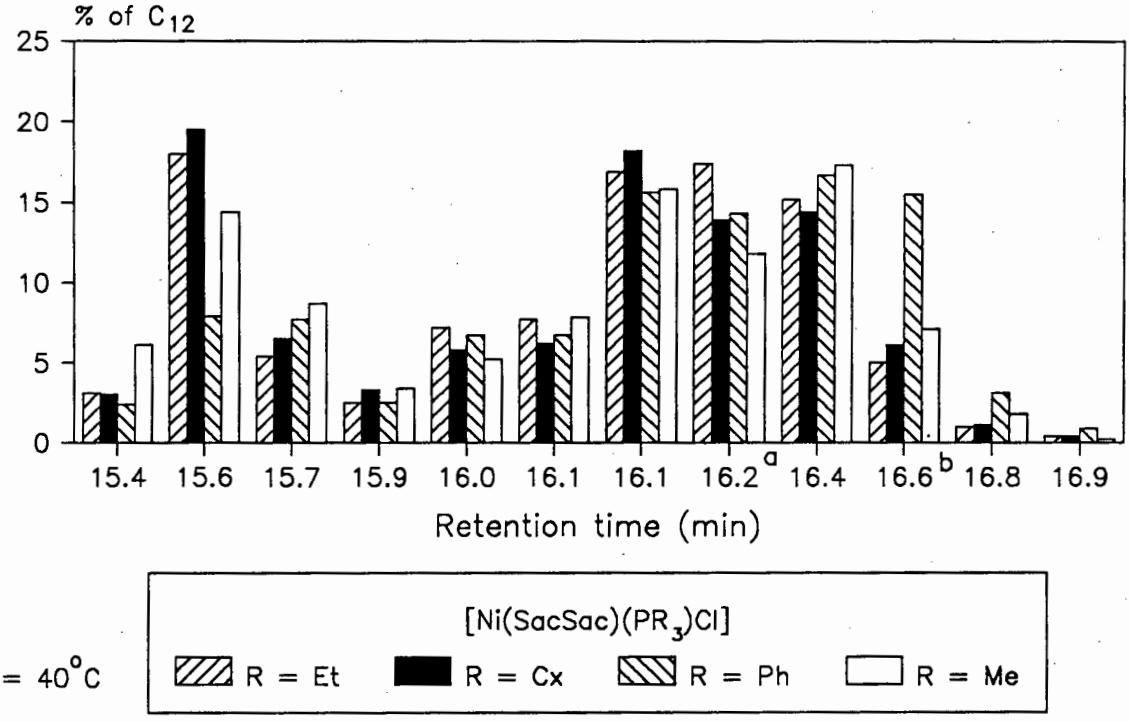

T = 40°C

Ni : $AlEtCl_2$ = 1 : 10

a = unresolved isomers b = linear dodecene

Figure 3.16 Graph of the effect of a change in phosphine ligand on the distribution of dimer products.

reacting monomer, 1-hexene may be subject to increased steric restriction relative to the propene molecule. This is supported by the observation that propene oligomerisation catalysed by [Ni(SacSac)(PPh_3)Cl], yielded only dimeric products in spite of its high activity [34]. It is also well established that 1-hexene is a less active monomer than propene [56].

Isomerisation

In each system the isomerisation reaction is almost instantaneous and similar equilibrium concentrations of the hexene isomers are established. It has been proposed that phosphines with low steric requirements effectively increase the isomerisation rate [22]. For propene isomerisation the rate is reported to decrease in the order:

$$PMe_3 > PPh_3 > PEt_3 > PCx_3 \quad [21].$$

In fact, using a PMe_3-modified catalyst (for which the elimination reaction is rapid, $k_e >> k_p$) double bond isomerisation may occur without significant dimerisation. An instance has also been recorded in which, with correct temperature control, 1-hexene has been selectively isomerised to the corresponding β-olefins. This may be the reason why the PMe_3-modified system used above exhibits only limited dimerisation activity.

Selectivity

Although the selectivity control exerted by phosphines on the propene dimerisation reaction has received much attention [16,22], the effect on the selectivity of the 1-hexene dimerisation reaction has not been reported. For propene dimerisation, the PPh_3-modified catalyst exhibits similar selectivity to the unmodified catalyst. By contrast, for 1-hexene dimerisation, the C_{12} isomer distribution in the PPh_3-modified system differs significantly from that of the unmodified catalyst. The same is true of the PMe_3-, PEt_3- and PCx_3-modified systems (Fig. 3.16). Of the four phosphine-modified systems, the PPh_3 system produces the

greatest amount of linear dimer. This is consistent with the trend observed for propene dimerisation where PMe_3-, PEt_3- and PCx_3-modified catalysts produce less hexene than the PPh_3-modified system [21].

The ability of a phosphine ligand to control selectivity in olefin oligomerisation reactions, while a chelating ligand exerts little influence, may be understood by considering the proposed active species (Fig. 3.17).

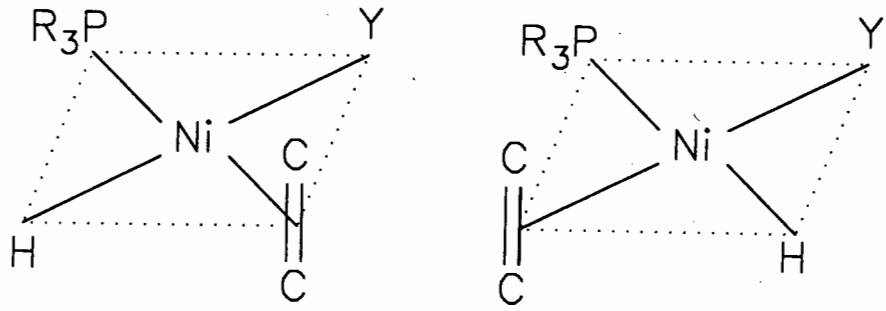

Y = Lewis acid complex

Figure 3.17 Active species for phosphine-modified catalysts [21].

While the phosphine ligand remains coordinated in the active complex, the chelating ligand is dissociated from the nickel. The phosphine ligand may therefore exert both steric and electronic influences on the active species, thereby directly influencing the dimerisation reaction and catalyst selectivity.

3.4.4 Crystal Structure of [Ni(Sacac)(PEt_3)Cl]

Crystals of [Ni(Sacac)(PEt_3)Cl] are monoclinic and the Ni has square planar coordination. The Cl atom is *trans* to the sulphur of the Sacac ligand. This structure may be understood by considering the relative "hardness" or "softness" of the ligands. For example, the "soft"

sulphur and phosphine donor ligands favour the position *trans* to the "harder" oxygen and chloro ligands.

Table 3.27 lists some bond lengths and angles of the above complex and others similar to it.

The Ni-P and Ni-Cl bonds in the complexes C, D and E are longer than average Ni-P and Ni-Cl bonds in four-coordinate planar nickel complexes [15]. This may be attributed to the strong *trans* influence of the sulphur atoms and is supported by the fact that, in [Ni(Sacac)(PEt_3)Cl], the Ni-P bond, which is *trans* to O, is significantly shorter than in complexes C, D and E. The length of the Ni-P bond in the complex [Ni(Sacac)(PEt_3)Cl] [2.185(1) Å] approaches that of Ni-P in [Ni(acac)(PPh_3)Et] [2.137(4) Å] [59] and [Ni(acac)(PCy_3)Me] (2.159 Å) [60]. This is consistent with the greater π-bond character in the Ni-S bond than the Ni-O bond. The long Ni-P and Ni-Cl bonds may be the reason why, in the NMR spectra, ligand exchange is observed [13]. The *trans* influence of the phosphine ligands is also evident in the complexes C, D and E, where Ni-S_1 (*trans* to P) is longer than Ni-S_2 (*trans* to Cl). The reduced *trans* influence of the PBu_3 ligand is reflected in the shorter Ni-S_1 (relative to complex C) [15].

The replacement of SacSac with Sacac in the complex [NiL(PEt_3)Cl] has little effect on the bond angles. Furthermore, the S-Ni-S and O-Ni-S angles are similar to those in the precursor complexes, [Ni($SacSac)_2$] and [Ni($Sacac)_2$], respectively.

Table 3.27 Bond lengths (Å) and angles (θ) for the complexes $[NiL_2]$ and $[NiL(PR_3)Cl]$. L = SacSac, aSacSac[a], Sacac; R = Et, Bu

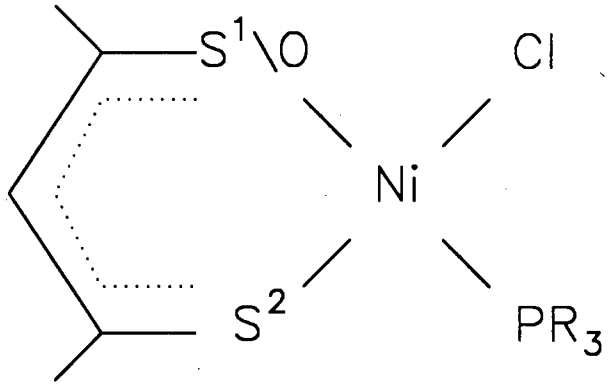

Compound	Bond Length (Å)[b]				
	Ni-Cl	Ni-P	Ni-S^1	Ni-S^2	Ni-O
A $[Ni(SacSac)_2]$			2.156(1)		
B *cis*-$[Ni(Sacac)_2]$			2.142(2)		1.880(4)
C $[Ni(SacSac)(PEt_3)Cl]$	2.206(2)	2.232(2)	2.154(2)	2.108(2)	
D $[Ni(aSacSac)(PEt_3)Cl]$	2.208(2)	2.234(2)	2.127(2)	2.083(2)	
E $[Ni(SacSac)(PBu_3)Cl]$	2.216(3)	2.237(3)	2.138(3)	2.097(3)	
F $[Ni(Sacac)(PEt_3)Cl]$	2.245(1)	2.185(1)		2.125(1)	1.893(4)

Compound	Bond Angle (θ)[b]				
	S-Ni-S[c]	O-Ni-S[c]	O/S-Ni-Cl	S-Ni-P	Cl-Ni-P
A $[Ni(SacSac)_2]$	97.20(4)				
B *cis*-$[Ni(Sacac)_2]$		96.2(1)			
C $[Ni(SacSac)(PEt_3)Cl]$	97.9(1)		85.6(1)	91.4(1)	85.2(1)
D $[Ni(aSacSac)(PEt_3)Cl]$	96.8(1)		86.2(1)	90.7(1)	86.9(1)
E $[Ni(SacSac)(PBu_3)Cl]$	98.6(1)		85.4(1)	89.5(1)	86.8(1)
F $[Ni(Sacac)(PEt_3)Cl]$		96.0(1)	87.2(1)	91.2(1)	85.6(1)

a aSacSac = 3-allylpentane-2,4-dithionato ion
b numbers in parentheses are estimated standard deviations
c X-Ni-Y angles where X and Y belong to the same ligand
References are: A [57]; B [58]; C [13]; D [14]; E [15]; F this work

REFERENCES

1. A.W. Hoffman, Justus Liebigs Annalen der Chemie, **103** (1857) 357.

2. K.A. Jensen, Z. anorg. Chem., **229** (1936) 265.

3. J. Chatt, Nature, **165** (1950) 637;
   J. Chatt and A.A.J. Williams, J. Chem. Soc., (1951) 3061.

4. J.G. Verkade, Coord. Chem. Rev., **9** (1972) 1.

5. G.E. Coates and C. Parkin, J. Chem. Soc., (1963) 421.

6. J. Bradbury, K.P. Forest, R.H. Nuttall and D.W.A. Sharp, Spectrochim. Acta, **23A** (1967) 2701.

7. R.J. Goodfellow, J.G. Evans, P.L. Goggin and D.A. Duddell, J. Chem. Soc. A, (1968) 1604.

8. P.M. Boorman and A.J. Carty, Inorg. Nucl. Chem. Lett., **4** (1968) 101.

9. P.J.D. Park and P.J. Hendra, Spectrochim. Acta, **25A** (1969) 227, 909.

10. P.L. Goggin and R.J. Goodfellow, J. Chem. Soc. A, (1966) 1462.

11. K. Shobatake and K. Nakamoto, J. Amer. Chem. Soc., **92** (1970) 3332.

12. C. Udovich, J. Takemoto and K. Nakamoto, J. Coord. Chem., **1** (1971) 89.

13. J.P. Fackler and A.F. Masters, Inorg. Chim. Acta, **39** (1980) 111.

14. K.J. Cavell, D.G. Hay, A.F. Masters and G.A. Williams, Aust. J. Chem., **37** (1984) 273.

15. K.J. Cavell, D.G. Hay, A.F. Masters and G.A. Williams, Aust. J. Chem., **38** (1985) 369.

16. O.T. Onsager and J.E. Johansen, Chem. Met. Car. Bond, **3** (1985) 205.

17. J. Ewers, Angew. Chem. Int. Edit., **5** (1966) 584.

18. G. Wilke and B. Bogdanovic, Angew. Chem. Int. Edit., **5** (1966) 151.

19. G. Lefebvre and Y. Chauvin, in "Aspects of Homogeneous Catalysis" (1970), Carlo Manfredi, Milan, p. 107.

20. G. Henrici-Olivé and S. Olivé, in "Coordination and Catalysis", (1977), Verlag Chemie, Weinheim, p. 134.

21. B. Bogdanovic, Adv. Organomet. Chem., **17** (1979) 105.

22. B. Bogdanovic, B. Henc, H.G. Karmann, H-G. Nüssel, D. Walter and G. Wilke, Ind. Eng. Chem., **62** (1970) 34.

23. H. Kanai, J. Chem. Soc. Chem. Communs., (1972) 203.

24. H. Bönnemann, C. Grard, W. Kopp and G. Wilke, Proc. 23rd Int. Congr. Pure Appl. Chem., **6** (1971) 265.

25. G. Henrici-Olivé and S. Olivé, Top. Curr. Chem., **67** (1976) 107.

26. W. Keim, Angew. Chem. Int. Edit., **17** (1978) 466.

27. R. De Haan and J. Dekker, J. Catal., **44** (1976) 15.

28. G. Hata and A. Miyaka, Chem. Ind. London, (1967) 921.

29. J. Chatt and F.A. Hart, J. Chem. Soc., (1960) 1378.

30. Y. Inoue, T. Kagawa, Y. Uchida and H. Hashimoto, Bull. Chem. Soc. Japan, **45** (1972) 1996.

31. K.J. Cavell and A.F. Masters, Aust. J. Chem., **39** (1986) 1129.

32. P.W. Jolly, in "Comprehensive Organometallic Chemistry", **5** (1982) Pergamon Press, New York, p. 615.

33. G. Henrici-Olivé and S. Olivé, Trans. Met. Chem., **1** (1976) 109.

34. K.J. Cavell and A.F. Masters, J. Chem. Res., (1983) 72.

35. S.J. Brown and A.F. Masters, J. Organomet. Chem., **367** (1989) 371.

36. S.J. Brown, L.M. Clutterbuck, A.F. Masters, J.I. Sachinidis and P.A. Tregloan, Appl. Catal., **48** (1989) 1.

37. S.J. Brown, A.F. Masters and M. Vender, Polyhedron, **7** (1988) 2009.

38. K.A. Jensen, P.H. Nielsen and C.T. Pedersen, Acta Chem. Scand., **17** (1963) 1115.

39. L.M. Venanzi, J. Chem. Soc., (1958) 719.

40. J.H.S. Green, Spectrochim. Acta, **24A** (1968) 137.

41. M. Baudler and H. Grundlach, Naturwiss., **42** (1955) 152.

42. H.D. Kaesz and F.G.A. Stone, Spectrochim. Acta, **15** (1959) 360.

43. D.A. Duddell, P.L. Goggin, R.J. Goodfellow, M.G. Norton and J.G. Smith, J. Chem. Soc. A, (1970) 545.

44. S.E. Rudakova and Y.A. Pentin, Opt. Spectroscopy, **18** (1965) 339, **20** (1966) 353 and **21** (1966) 240.

45. K.A. Jensen and P.H. Nielsen, Acta Chem. Scand., **17** (1963) 1875.

46. E. Steger and K. Stopperka, Chem. Ber., **94** (1961) 3029.

47. D.W. Scott and J.P. McCullough, J. Amer. Chem. Soc., **80** (1958) 3554.

48. A. Loutellier, M. Trabelsi and M. Bigorgne, J. Organomet. Chem., **133** (1977) 201.

49. J. Lewis, R.S. Nyholm and P.W. Smith, J. Chem. Soc., (1961) 4590.

50. A Sabatini and I. Bertini, Inorg. Chem., **4** (1965) 959.

51. J.E. Fergusson and P.F. Heveldt, Inorg. Chim. Acta, **31** (1978) 145.

52. J.T. Wang, C. Udovich, K. Nakamoto, A. Quattrochi and J.R. Ferraro, Inorg. Chem., **9** (1970) 2675.

53. C. Engelter and D.A. Thornton, J. Mol. Struct., **33** (1976) 119.

54. R.J.H. Clark, Spectrochim. Acta, **21** (1965) 955.

55. M.M. Jones, in "Elementary Coordination Chemistry", (1964) Prentice-Hall Inc., New Jersey, p. 221.

56. V.P. Yurev, G.A. Gailyunas, F.G. Yusupova, G.V. Nurtdinova, E.S. Monakhova and G.A. Tolstikov, J. Organomet. Chem., **169** (1979) 19.

57. R. Beckett and B.F. Hoskins, J. Chem. Soc. Dalton, (1974) 62.

58. O. Siiman, D.D. Titus, C.D. Cowman, J. Fresco and H.B. Gray, J. Amer. Chem. Soc., **96** (1974) 2353.

59. F.A. Cotton, B.A. Frenz, and D.L. Hunter, J. Amer. Chem. Soc., **96** (1974) 4820.

60. B.L. Barnett and C. Krüger, J. Organomet. Chem., **42** (1972) 169.

CHAPTER 4

ETHYLENEDIAMINE COMPLEXES

4.1 INTRODUCTION

4.1.1 Infrared Spectroscopy

Coordination complexes involving the ethylenediamine ligand (en) of the type believed to be $[Ni(en)_nX_2]$ were first prepared by Werner in 1899 [1] at the inception of coordination chemistry. Since then a vast number of publications have appeared studying both the ligand and its complexes. The infrared and Raman spectra have received much attention, yet to date there is still only limited agreement between authors regarding vibrational assignments. This is probably due to the lack of systematic studies to be found in the literature. An investigation of the assignment problem based on ligand and metal ion isotopic labelling and metal ion substitution has therefore been undertaken. Of additional interest are the effects of a change of anion on the metal complex spectra.

4.1.1.1 The Ethylenediamine Ligand

The infrared spectra of the free ethylenediamine ligand have been the subject of several reports in which the spectra have been used as a diagnostic tool in determining the conformation (*cis*, *trans* or *gauche*) of the free ligand. The *cis*-form belongs to the point group C_{2v} and the *trans*-and *gauche*-forms to the point groups C_{2h} and C_2, respectively.

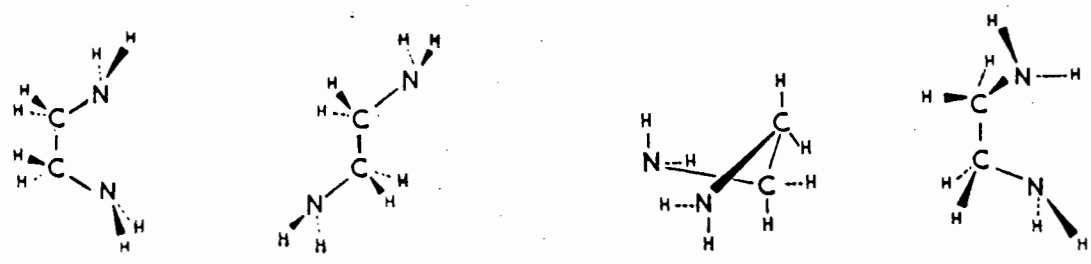

cis *trans* *gauche*

Figure 4.1 The *cis*, *trans* and *gauche* conformations of ethylenediamine.

On the basis of these point groups different numbers of infrared allowed bands are expected. Several spectroscopic studies of the free ligand and its amino-deuterated derivative, while providing reproducible band assignments, did not resolve the question of ligand conformation [2,3]. Nakamoto [4] reported that the *trans*-form is excluded in the free ligand due to the observation of coincident infrared and Raman bands and suggested that steric repulsion may exclude the *cis*-form due to ligand instability. Sabatini and Califano [2] studied the polarised spectra of the ethylenediamine ligand. They proposed a *cis*-structure as only three NH_2 and three CH_2 stretching vibrations are observed (the fourth stretch is infrared forbidden in C_{2v} symmetry). However, they also found evidence of two CH_2 rocking modes, one of which should be inactive for the C_{2v} point group. In addition, a Raman band is observed at 186 cm^{-1} and assigned to a skeletal torsion. A corresponding band appears at 125 cm^{-1} for *gauche*-dichloroethane [5]. Diot and Theophanides [3], while suggesting the existence of the *cis*-conformer on the basis of selection rules, also observed a disturbing splitting of the Raman bands, indicative of the presence of other isomers. Further doubt arises when cognisance is taken of the numerous complexes studied by X-ray methods which generally exist in the *gauche*-form [6-9]. It eventually took the electron diffraction data of Yokozeki and Kuchitsu [10] to show that the free ligand did indeed exist in the *gauche*-form. A subsequent vibrational assignment based on this information [11] showed remarkable agreement to earlier work which is based on the selection rules for the *cis*-conformers.

4.1.1.2 Coordination Complexes of Ethylenediamine

The configuration of en when coordinated to metals is of interest in coordination chemistry. Early infrared data suggested that the complexed ligand assumed a *gauche*-conformation [12]. However, the coupling of the CH_2 rocking mode (previously used as a diagnostic tool) with the NH_2 rocking and C-N stretching modes in the metal complex spectra have prevented extensive use of this method. The existence of the *gauche*-conformer has since been established by X-ray analysis of several complexes involving chelating ethylenediamine ligands [6-9]. It

is well known that for *tris*-complexes, the complexed ethylenediamine ligands may exist as either *lel* or *ob* conformers [13].

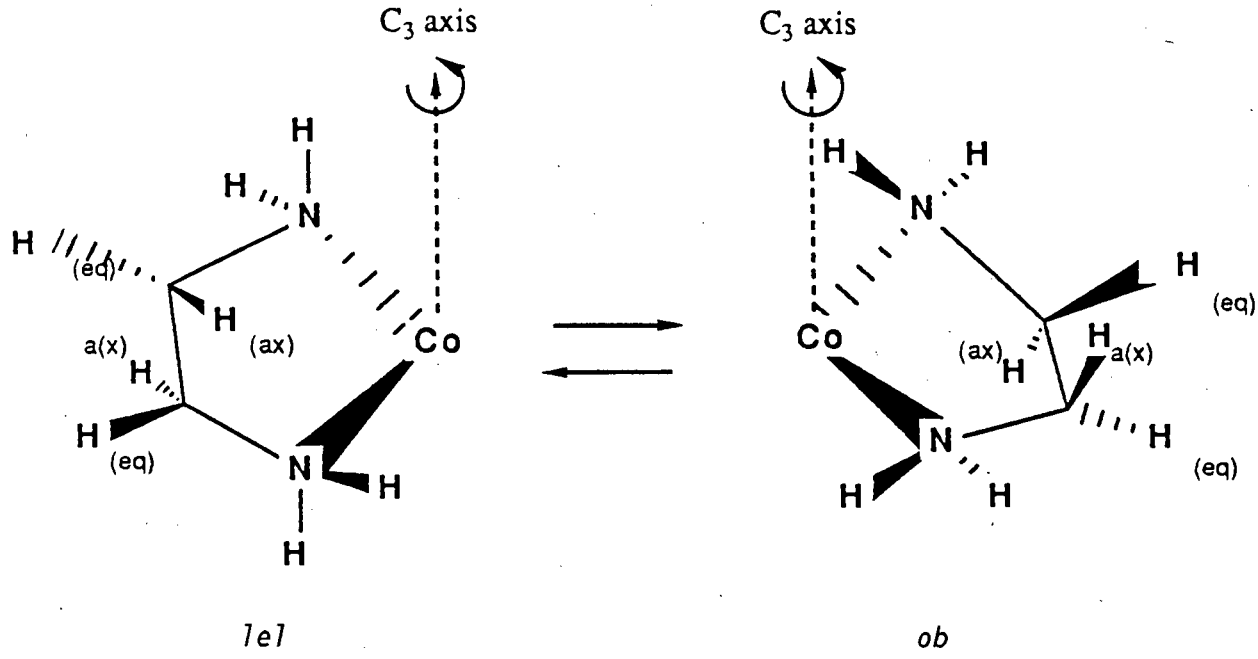

Figure 4.2 Possible conformations of complexed en ligands.

Based on metal ion size, it is probably safe to assume that all divalent transition metal complexes are lel_3 (all three ligands take up the *lel* conformation). For example, the relatively small cobalt(III) ion has a lel_3 conformation [14] and hence the larger divalent ions are probably lel_3, but with more of a trigonal twist.

There is still considerable confusion in the literature as to the frequency of the metal-nitrogen stretching modes (νM-N) in complexes of en. Several of the earlier reports assigned bands above 500 cm^{-1} to νM-N [15-17]. Durig *et al.* [18] suggested that the νPd-N modes in divalent palladium complexes of en are found between 520 and 430 cm^{-1}. This infers that first row divalent transition metal-nitrogen modes may be expected below 500 cm^{-1}. Krishnan and Plane [19] examined both the infrared and Raman spectra of complexes of en with zinc(II), cadmium(II) and mercury(II), and assigned a band near 400 cm^{-1} to νM-N. Gabelica [20], in his extensive study of *tris*(ethylenediamine) complexes and their amino-deuterated analogues, assigned νM-N to a similar band near

400 cm^{-1}. In a study of *bis*(ethylenediamine)chromium(II), spectra were recorded above 450 cm^{-1} and no νM-N were assigned, implying that these modes lie below 450 cm^{-1} [21]. It would appear that more recent studies favour lower values of νM-N. However, even when νM-N is assigned at low frequencies, inconsistencies still arise. For example, in their normal coordinate treatment of the $[M(en)_2]^{2+}$ ion, Omura *et al.* [22] assigned the νCu-N stretching modes at 472 and 412 cm^{-1}. Contrarily, applying the metal isotope technique to analogous complexes, Lever and Mantovani [23] assigned νCu-N vibrations in the range 420-360 cm^{-1}.

On reviewing the assignments of these metal-nitrogen stretching vibrations, it is alarming to see the large frequency range proposed for these normal modes. It is anticipated that the above modes would lie at similar or perhaps slightly lower energies than the corresponding modes in metal-ammonia complexes, since the effective mass of the nitrogen atom has been increased while the force constant, although slightly increased on chelation [19], is relatively unchanged. For the hexaamine complexes of the first row transition metals, these modes lie between 350 and 300 cm^{-1} and for the tetraamines near 400 cm^{-1} [24]. Metal-nitrogen stretches are generally expected near or below these values and certainly not above 500 cm^{-1}. Complicating factors in νM-N assignment arise due to the NH_2 rocking mode as well as the skeletal ring mode, both of which fall in this low frequency region and may be coupled with νM-N [2,21]. An additional complication arises as the νM-N is generally very weak [25] and in several earlier investigations these bands have been missed entirely.

The most thorough infrared investigations have been carried out on *tris*(ethylenediamine) trivalent metal complexes [26-33]. These include detailed infrared and Raman work by Gouteron [26,27] on Co(III), Rh(III) and Cr(III) complexes as well an in-depth ligand isotopic labelling study of $[Rh(en)_3]^{3+}$ by Borch *et al.* [28-30], which led to a complete normal coordinate treatment of this ion and seven isotopically labelled species [28]. By comparison, studies of analogous divalent metal complexes are few. Krishnan and Plane [19] assigned the spectra of *tris*-complexes of Zn(II), Cd(II) and Hg(II) and more recently Gabelica [20] studied the vibrations of $[M(en)_3]^{2+}$ (M = Zn, Cd, Fe, Ni, Co, Mn) and some of their amino-deuterated analogues. However, there has been

no systematic study of the effects of metal ion substitution across a transition series [34] and no multiple isotope labelling study of these divalent complexes to assist the vibrational assignment.

Unlike the analogous *tris*-complexes, the most studied *bis*-en complexes are of Cu(II) [36-41] and Pd(II) and Pt(II) [15,22,42-45] with a wide range of anions. Changing the anion has been found to profoundly influence the structure of such complexes. In addition to extensive vibrational studies, the copper ion, $[Cu(en)_2]^{2+}$, has been the subject of two normal coordinate analyses [22,40]. The Cu(II) and analogous Ni(II) complexes represent two of only three examples of the application of metal isotope labelling to metal complexes of en [37,46]. Relative to copper, the *bis*(ethylenediamine)nickel(II) ion has barely been studied [36,46,47]. With complex anions such as AgI_2^-, BF_4^-, ClO_4^-, PF_6^- and NO_3^-, the *bis*(ethylenediamine) complexes of both Cu(II) and Ni(II) have simple monomeric square planar structure and these compounds may be correctly formulated $[M(en)_2]X_2$ [36,37,44,46,48]. However, with the monoatomic halide anions, the structures are markedly different. The copper complexes are *trans*-tetragonal six-coordinate monomers with weak axial copper halide bonding [36], while the nickel complexes are six-coordinate *cis*-octahedral dimers with both bridging covalent and anionic halides [46,49].

There is little literature available on the vibrational band assignments of *mono*(ethylenediamine) complexes of divalent metals. This is not surprising when considering the structural diversity of these complexes. For example, Iwamoto and Schriver [50] detected three different types of $[Zn(en)Cl_2]$ by vibrational spectroscopy. The discovery of the structural peculiarity of $[M(en)Cl_2]$ (M = Zn, Cd, Hg) dates back to the report by Newman and Powell [51] in which a *trans*-C_{2h} configuration was proposed due to the simplicity of the spectra in comparison to those of other ethylenediamine chelate complexes. This proposal was supported by Raman spectroscopy [19]. The zinc complexes, $[Zn(en)X_2]$, are thought to comprise polymeric chains $-ZnX_2$-en-ZnX_2-en- in which the bridging en takes the *trans*-form. The Zn(II) ion therefore has an effective octahedral symmetry with the octahedron being completed by weak bonding between Zn and the NH_2 groups from neighbouring en molecules [19,50-52]. The Ni(II) and Cu(II) complexes are unlike the zinc complexes. The

copper complexes with this formulation are known to be tetragonally distorted six-coordinate polymeric species, with both terminal and *trans*-axially bridging Cu-X bonds [53,54]. The only isotopic labelling study of *mono*(ethylenediamine) complexes is a $^{63,65}Cu$, amino-deuteration study of $[Cu(en)X_2]$ [36]. Although no X-ray data is available, it has been suggested that the complexes of $[Ni(en)X_2]$ formulation are probably polymeric octahedral [52]. Their spectra have not previously been reported.

In this Chapter, the complexes $[M(en)_3]X_2$ (M = Mn, Fe, Co, Ni, Cu, Zn) (X = SO_4, Cl, Br, I) have been prepared and their infrared spectra in the range 4000-50 cm^{-1} reported. On the basis of ligand and metal ion isotopic labelling, as well as the effects of metal ion substitution, it is possible to reach reasonable assignments for all observed bands. The spectra of the *tris*(ethylenediamine)Cu(II) complex is of particular structural interest in view of the expectation of JAHN-TELLER distortion in this compound.

In addition, the preparation and infrared spectra of complexes of nominal formula $[M(en)_2X_2]$ and $[M(en)X_2]$ (M = Ni, Cu, Zn) (X = Cl, Br, I) are reported. The assignment of ligand modes and, where structural similarities allow, certain metal sensitive vibrations is made by comparison with the *tris*-complexes. Furthermore, metal ion substitution effects are of use where several compounds in a series are successfully prepared. As for the complex $[Cu(en)_3]^{2+}$, the band splitting which may occur due to tetragonal distortion in copper(II) complexes is of particular interest.

4.1.2 Homogeneous Catalysis

To date there are no published investigations of the catalytic oligomerisation properties of nickel complexes of ethylenediamine.

The en ligand is neutral and as such forms a variety of complexes with divalent nickel. In each complex, anions are necessary to balance the charge on the nickel. These may be either coordinated to the metal or present as counterions outside the coordination sphere. The structural

diversity of the resulting complexes lends itself to an investigation of the effect of a structural change on the catalytic reaction. Three complexes of varying structure have been selected; $[Ni(en)Cl_2]$, $[Ni(en)_2Cl_2]$ and $[Ni(en)_3]Cl_2$. None exhibit square planar configuration believed to be necessary for the formation of an active oligomerisation catalyst.

4.2 EXPERIMENTAL

4.2.1 Preparation of Complexes

All solvents used were analytical reagent grade. The zinc isotopes were purchased as the sulphate salts from Prochem and the isotopically labelled ligands from Merck, Sharpe and Dohme isotopes.

Once isolated, complexes were dried over silica gel under reduced pressure and complex purity subsequently ascertained using microanalysis (C,H,N).

4.2.1.1 *Tris*(ethylenediamine)metal(II) Sulphates $[M(en)_3]SO_4$ M = Mn, Fe, Co, Ni, Cu, Zn

The metal(II) sulphate (2 mmol), dissolved in a minimum of water, was added to excess anhydrous en (8 mmol). Precipitation of the complex was usually immediate but, where necessary, was facilitated by addition of ethanol. The crystals were filtered and washed well with ethanol and finally ether to remove traces of free en.

To prevent oxidation of the metal ion, complexes of manganese and iron were prepared under oxygen-free conditions using standard Schlenk techniques.

4.2.1.2 *Tris*(ethylenediamine)zinc(II) Sulphates

A variety of isotopically labelled zinc complexes were prepared. Metal labelling included both ^{64}Zn and ^{68}Zn isotopes and ligand labelling took the form of the methylene-deuterated (en-C_2D_4), amino-deuterated (en-N_2D_4) and ^{15}N (en-^{15}N) isotopes. The deuterated ligands were in the form of the free base, while the ^{15}N-labelled compound was in the form of a dihydrochloride salt. Subsequent release of the base from the salt (see 4.2.3) was therefore necessary prior to reaction.

The zinc(II) sulphate (0.5 mmol) was dissolved in a minimum of water. For the complexes involving the zinc isotopes, excess en (3 mmol) was added causing immediate product precipitation. For complexes of the labelled ligand, four molar equivalents of ligand were added and subsequent addition of ethanol caused complex precipitation. The products were isolated by vacuum filtration and washed with ethanol. Where necessary, complexes were purified by dissolution in a minimum of water, addition of a small amount of en (labelled where necessary) and finally, precipitation by slow addition of ethanol.

4.2.1.3 *Tris*(ethylenediamine-C_2D_4)metal(II) Sulphates $[M(en\text{-}C_2D_4)_3]SO_4$ M = Mn, Fe, Co, Ni, Cu, Zn

A general method, similar to that used previously, was followed. The metal(II) sulphate (0.5 mmol), dissolved in a minimum of water, was added to anhydrous en (2 mmol). If precipitation was not immediate, it was facilitated by addition of ethanol. The pure complexes were isolated by vacuum filtration and washed with ethanol. To prevent oxidation of the manganese and iron salts to trivalent species, preparation was carried out under oxygen-free conditions using Schlenk techniques.

The en ligand decomposes slowly once exposed to air and is thus best stored in the form of the dihydrochloride salt. To liberate en, the dihydrochloride salt was dissolved in water and passed through an anion exchange resin (Amberlite IRA 400) in the hydroxide form. Resulting anion exchange led to the release of the free base, which was eluted with distilled water. This ligand was subsequently reacted with the required metal ion under dilute conditions and the water removed on a rotary evaporator until complex precipitation occurred. In some cases, precipitation was facilitated by the addition of ethanol.

4.2.1.4 *Tris*(ethylenediamine)metal(II) Halides

$[M(en)_3]Cl_2$ M = Mn, Fe, Co, Ni, Cu, Zn

The metal(II) chloride (2 mmol), dissolved in a minimum of water, was added to anhydrous en (8 mmol). Addition of acetone led to complex precipitation. Subsequent vacuum filtration and washing with acetone led to isolation of the pure complexes. Due to sensitivity to oxidation, the manganese, iron and cobalt complexes were prepared under nitrogen using deoxygenated solvents and Schlenk techniques.

Preparation of the copper complex led to the formation of an oil. Crystallisation was effected by successive additions of dry acetone and vigorous scratching. Once crystals were obtained, they were filtered immediately, washed once with dry ether and immediately dried. Within a short time of exposure to the atmosphere the blue complex lost a ligand and became purple $[Cu(en)_2Cl_2]$.

$[M(en)_3]X_2$ M = Ni, Cu, Zn X = Br, I

Complex preparation was as for $[M(en)_3]Cl_2$ above, but metal(II) bromide and metal(II) iodide salts were substituted where appropriate.

4.2.1.5 *Bis*(ethylenediamine)metal(II) Halides

$[Ni(en)_2X_2]$ X = Cl, Br, I

Nickel(II) halide (1 mmol) was dissolved in a minimum of warm methanol. Ethylenediamine (1.8 mmol) was added and, where not immediate, precipitation was facilitated by addition of acetone. The product was filtered and washed with acetone.

$[Cu(en)_2X_2]$ X = Cl, Br, I

Copper(II) halide (1 mmol) was dissolved in a minimum of warm methanol and en (2.2 mmol) was added. Precipitation was immediate. The product was filtered and washed with acetone. Preparation of $[Cu(en)_2I_2]$ was

achieved by addition of excess saturated NaI (aq) to an aqueous solution of $[Cu(en)_2Br_2]$.

$[Zn(en)_2X_2]$ X = Cl, Br, I

Several preparative attempts were made, all of which proved unsuccessful:

a) $[Zn(en)_3]X_2$ (2 mmol) and ZnX_2 (1 mmol) were mixed in methanolic solution. Gentle warming led to the formation of $[Zn(en)_3]X_2$. Addition of acetone to effect precipitation also led to this product.
b) ZnX_2 (5 mmol) was dissolved in water. HX (10 mmol) was added followed by en (10 mmol). The resulting precipitate was again $[Zn(en)_3]X_2$.
c) ZnX_2 (1 mmol) was dissolved in a minimum of warm methanol. Addition of en (2 mmol) led to slow precipitation of $[Zn(en)_3]X_2$.

4.2.1.6 *Mono*(ethylenediamine)metal(II) Halides

$[Ni(en)X_2]$ X = Cl, Br

Nickel(II) halide (2 mmol) was dissolved in a minimum of warm methanol and en (1.8 mmol) was added. Precipitation was immediate and the product was filtered and washed with acetone. Attempts to prepare $[Ni(en)I_2]$ were unsuccessful and led to precipitation of $[Ni(en)_2I_2]$.

$[Cu(en)X_2]$ X = Cl, Br, I

Copper(II) halide (2 mmol) was dissolved in a minimum of warm methanol. Ethylenediamine (2.2 mmol) was added. Precipitation was immediate and the product was filtered and washed with acetone. Precipitation of the iodide complex was immediate on addition of excess saturated NaI (aq) to an aqueous solution of $[Cu(en)Br_2]$.

$[Zn(en)X_2]$ X = Cl, Br, I

The method of Krishnan and Plane [19] was used. Zinc(II) halide (2 mmol) was dissolved in a minimum of water. Concentrated HCl (0.3 ml) was added followed by en (2 mmol). The white precipitate was isolated by filtration and washed with acetone.

4.2.2 Homogeneous Catalytic Runs

The procedure followed was as for the homogeneous catalytic experiments described in 2.2.2.

The selected complexes were insoluble in toluene. The catalysts were therefore slurried in the dry solvent. Subsequent addition of the co-catalyst caused dissolution of the nickel complex and a yellow-orange solution resulted. When an $AlEt_3$ co-catalyst was employed, no catalyst dissolution was observed.

4.3 RESULTS

4.3.1 Analytical Data

Table 4.1 Analytical data for *tris*(ethylenediamine) complexes.

Complex	Calculated			Found		
	%C	%H	%N	%C	%H	%N
$[Mn(en)_3]SO_4$	21.73	7.30	25.37	21.50	7.05	25.15
$[Co(en)_3]SO_4$	21.47	7.23	25.07	21.35	7.05	24.85
$[Fe(en)_3]SO_4$	21.46	7.20	25.04	21.60	7.30	25.20
$[Cu(en)_3]SO_4$	21.20	7.13	24.73	21.05	7.05	24.50
$[Ni(en)_3]SO_4$	21.45	7.23	25.09	21.55	7.15	25.05
$[Zn(en)_3]SO_4$	21.09	7.09	24.60	21.00	7.05	24.45
$[Zn(en\text{-}^{15}N)_3]SO_4$	20.72	6.97	24.17	20.25	6.60	23.55
$[^{64}Zn(en)_3]SO_4$	21.17	7.12	24.70	21.25	7.20	24.65
$[^{68}Zn(en)_3]SO_4$	20.93	7.04	24.41	21.00	7.10	24.40
$[Zn(en\text{-}N_2D_4)_3]SO_4$	20.37	6.85	23.76	20.25	6.75	23.55
$[Zn(en\text{-}C_2D_4)_3]SO_4$	20.37	6.85	23.76	20.40	6.80	23.60
$[Mn(en\text{-}C_2D_4)_3]SO_4$	20.99	7.05	24.49	20.00	7.05	23.20
$[Co(en\text{-}C_2D_4)_3]SO_4$	20.74	6.97	24.20	20.60	7.20	23.90
$[Ni(en\text{-}C_2D_4)_3]SO_4$	20.76	6.97	24.22	20.70	7.20	24.20
$[Cu(en\text{-}C_2D_4)_3]SO_4$	20.48	6.87	23.89	20.45	7.15	23.70
$[Mn(en)_3]Cl_2.H_2O$	22.23	8.10	25.93	22.05	8.40	25.70
$[Fe(en)_3]Cl_2$	23.47	7.89	27.38	23.00	7.70	26.90
$[Co(en)_3]Cl_2$	23.23	7.82	27.10	23.35	7.85	26.80
$[Ni(en)_3]Cl_2$	23.25	7.82	27.13	23.25	7.85	27.00
$[Cu(en)_3]Cl_2$	22.89	7.70	26.71	22.90	7.90	26.45
$[Zn(en)_3]Cl_2$	22.76	7.66	26.55	22.80	8.00	26.60
$[Ni(en)_3]Br_2$	18.07	6.07	21.08	17.75	5.50	20.55
$[Cu(en)_3]Br_2$	17.85	5.99	20.83	18.50	5.70	21.05
$[Zn(en)_3]Br_2$	17.77	5.97	20.73	17.50	6.50	20.35
$[Ni(en)_3]I_2$	14.62	4.91	17.06	14.30	4.95	16.70
$[Zn(en)_3]I_2$	14.43	4.84	16.83	14.35	4.90	16.75

Table 4.2 Analytical data for *bis*(ethylenediamine) complexes.

Complex	Calculated			Found		
	%C	%H	%N	%C	%H	%N
$[Ni(en)_2Cl_2]$	19.23	6.45	22.43	19.30	6.50	22.30
$[Cu(en)_2Cl_2]$	18.86	6.33	22.01	18.80	6.70	21.80
$[Ni(en)_2Br_2]$	14.18	4.76	16.55	14.20	4.70	16.55
$[Cu(en)_2Br_2]$	13.98	4.69	16.31	14.00	4.85	15.70
$[Ni(en)_2I_2]$	11.10	3.72	12.95	11.10	3.80	12.90
$[Cu(en)_2I_2]$	10.98	3.69	12.81	11.10	3.70	12.85

Table 4.3 Analytical data for *mono*(ethylenediamine) complexes.

Complex	Calculated			Found		
	%C	%H	%N	%C	%H	%N
$[Ni(en)Cl_2]$	12.66	4.23	14.77	13.20	4.60	14.80
$[Cu(en)Cl_2]$	12.34	4.15	14.40	12.50	3.95	14.00
$[Zn(en)Cl_2]$	12.23	4.10	14.27	12.30	4.20	14.40
$[Ni(en)Br_2]$	8.62	2.89	10.06	8.75	3.25	9.80
$[Cu(en)Br_2]$	8.47	2.85	9.89	8.55	2.85	9.85
$[Zn(en)Br_2]$	8.42	2.83	9.82	8.70	2.80	9.60
$[Cu(en)I_2]$	6.36	2.14	7.42	6.40	2.20	7.35
$[Zn(en)I_2]$	6.33	2.13	7.39	6.30	2.15	7.35

4.3.2 Infrared Data

Table 4.4 Frequency and shift data (cm^{-1}) for the isotopically substituted derivatives of $[Zn(en)_3]SO_4$.

Zn	^{64}Zn	^{68}Zn	^{15}N ($\Delta\nu$)	N_2D_4($\Delta\nu$)	C_2D_4($\Delta\nu$)	Assignment
3290	3282	3283(0)	3285(5)	2476(814)	3293(0)	νN-H
3161	3166	3162(4)	3158(3)	2335(826)	3161(0)	
2955		2954	2954(1)	2954(1)	2200(755)	
2924	2925	2925	2924	2924(0)	2180(744)	νC-H
2860	2861	2880	2880	2878(0)	2070(790)	
1592	1592	1592	1589(3)	1202(390)	1592(0)	δNH_2 (scissor)
1463	1462	1462	1462	1462(0)	1307(155)	δCH_2 (scissor)
1451	1451	1452	1451(0)	1453(0)	1275(178)	
1389	1387	1389	1387(2)	1368(21)	1202(187)	ωCH_2
1373	1375	1375	1370(3)	1368(5)	1202(171)	
1337	1336	1337	1334(3)	1355(0)	1155(182)	τCH_2
1272	1272	1272	1271(1)	1272(0)	1070(202)	τCH_2 + ωNH_2
1115sh	1115sh	1115sh	1115(0)	1007(108)	1107(8)	ωNH_2
1091	1088	1092	1093	1090	1094	ν_3 $SO_4^=$
1040	1039	1037(2)	1032(8)	1033(7)	1034(6)	
					928(112)	νC-N + νC-C
1013	1009	1010	1000(13)	886(127)	863(150)	
871	871	871	864(7)	811(60)	836(35)	ρCH_2 + ρNH_2
				772(99)	772(99)	
					670(15)	
685	688	685(3)	683(2)	585(100)	648(37)	ρNH_2
611	610	610	610	611	610	ν_4 $SO_4^=$
522	522	522	519(3)	472(5)	453(69)	ring def
495	495	495	493(2)	425(70)	439(56)	(+ νZn-N?)
440	440	440	441	440	masked	ν_2 $SO_4^=$
405	405	405	394(11)	375(30)	397(8)	νZn-N
291	292	290(2)	284(7)	275(16)	287(4)	νZn-N
228	229	227(2)	224(4)	214(14)	221(7)	δN-Zn-N
194	197	194(3)	193(1)	186(8)	191(3)	δN-Zn-N
104sh		107sh		110sh	104sh	lattice + δN-Zn-N
99	99	96	95	90	99	lattice

() Figures in parentheses are the shifts observed on isotopic labelling

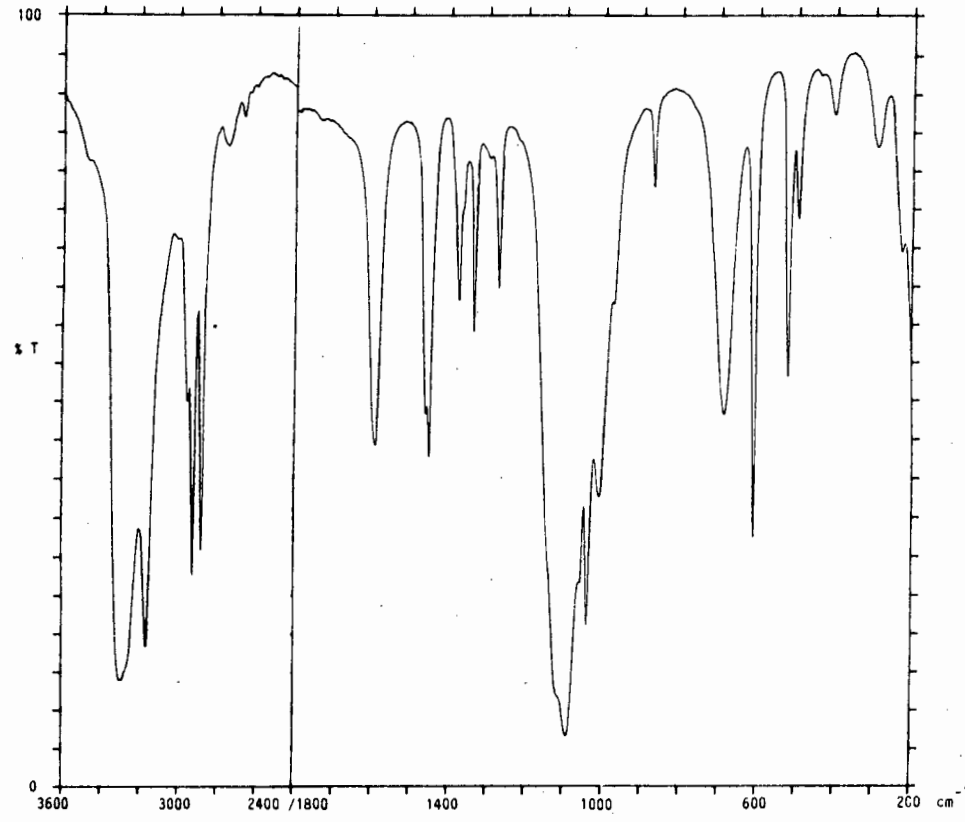

Figure 4.3 Mid-infrared spectrum of $[Zn(en)_3]SO_4$.
HCBD: 3600-2400cm^{-1}, Nujol: 1800-200cm^{-1}

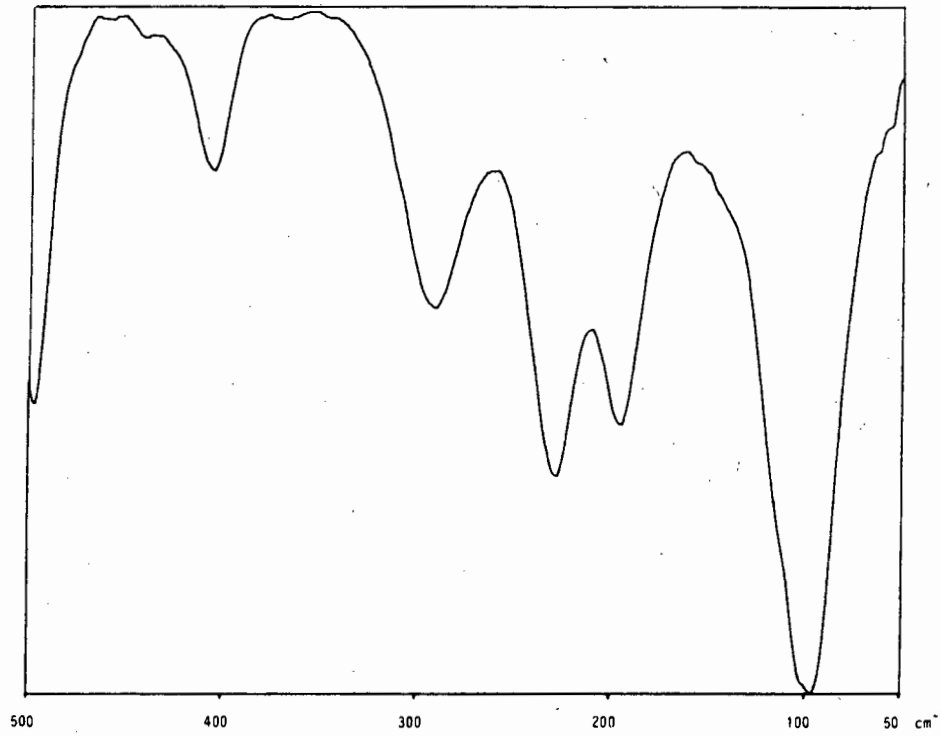

Figure 4.4 Far-infrared spectrum of $[Zn(en)_3]SO_4$.

Table 4.5 Frequencies (cm^{-1}) and assignments for the complexes $[M(en)_3]SO_4$.

M=Mn	Fe	Co	Ni	Cu	Zn	Assignment
3279	3287	3296	3278	3242	3290	νN-H
3158	3156	3160	3164	3138	3161	
2924	2924	2922	2923	2927	2924	νC-H
2879	2881	2870	2880	2890	2860	
1593	1591	1592	1591	1594	1592	δNH_2 (scissor)
1462	1461	1461	1461	1462	1463	δCH_2 (scissor)
1452	1450	1450	1451	1451	1451	
1389	1389	1390	1390	1388	1389	ωCH_2
1357	1370				1373	
1336	1336	1336	1335	1335	1337	τCH_2
1273	1273	1273	1272	1275	1272	τCH_2 + ωNH_2
1115sh	1115sh	1115sh	1115sh	1115sh	1115sh	τNH_2
1091	1089	1091	1091	1077	1091	ν_3 $SO_4^=$
1036	1036	1036	1035	1040	1040	
1014	1014	1015	1020sh		1013	νC-N + νC-C
972	973	973	975	975	972	
867	870	871	873	874	871	ρCH_2 + ρNH_2
				849		
667	680	688	706	733	685	ρNH_2
				690		
609	609	610	611	611	611	ν_4 $SO_4^=$
513(65)	519(67)	525(69)	533(73)	537(78)	522(69)	ring def
489(54)	494(56)	500(59)	507(61)	510(72)	495(56)	
444	443	444	442	440	440	ν_2 $SO_4^=$
391(3)	397(6)	402(6)	410(5)	485(26)	405(8)	
				346(7)		νM-N
303(5)	321(8)	319(7)	334(6)	404(8)	291(4)	
				270(25)		
263(+6)	272(1)	299(11)				
213(6)	220(5)	228(8)	238(8)	270(25)	228(7)	
184(+7)	198(2)	205(5)	220(0)	225(8)	194(3)	δN-M-N
110(5)	112(3)	117(4)	128(4)		104(1)	lattice
89	85	110	103	89	99	

() Figures in parentheses represent the shifts observed on C_2D_4-labelling

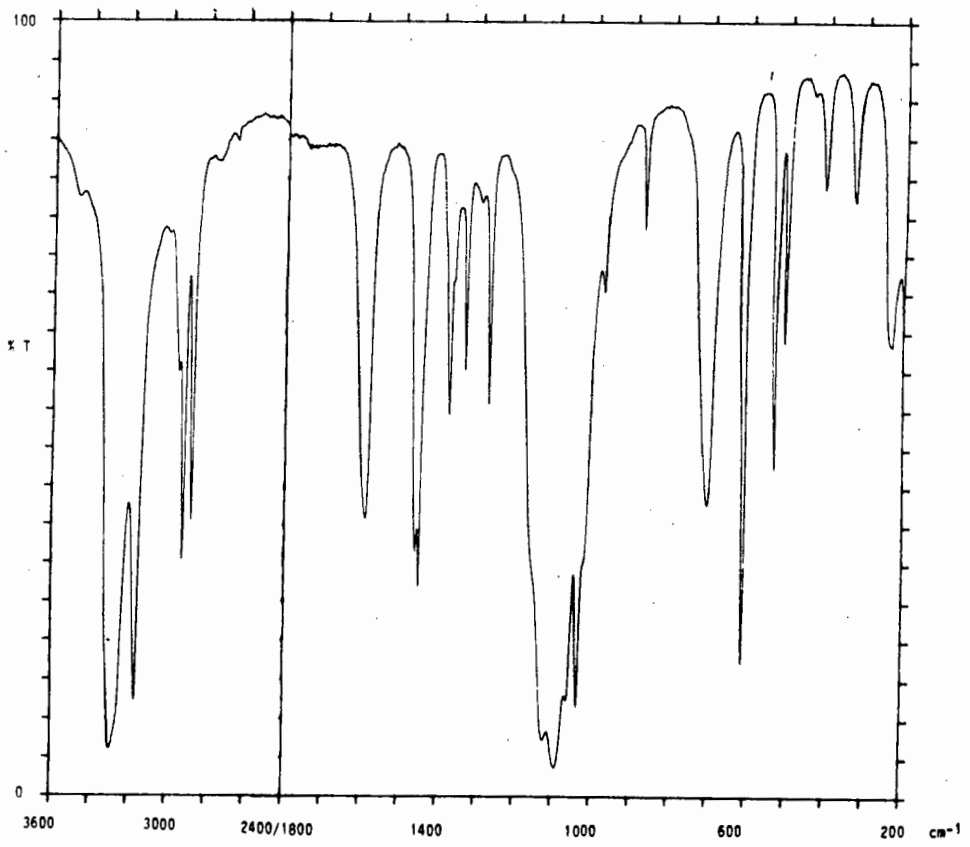

Figure 4.5 Mid-infrared spectrum of $[Ni(en)_3]SO_4$.
HCBD: 3600-2400cm^{-1}, Nujol: 1800-200cm^{-1}.

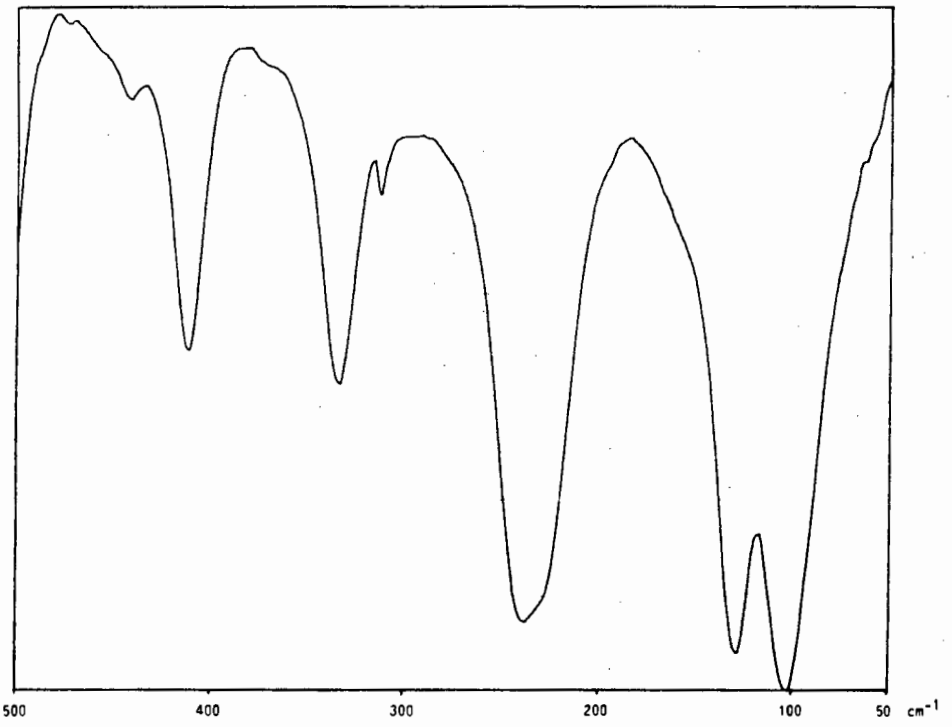

Figure 4.6 Far-infrared spectrum of $[Ni(en)_3]SO_4$.

Table 4.6 Frequencies (cm^{-1}) and assignments for the complexes $[M(en)_3]X_2$.

X = Cl						Assignment
M=Mn	Fe	Co	Ni	Cu	Zn	
3331	3320					
3277	3282	3282	3292	3305	3291	νN-H
3235	3240	3240	3243	3233	3243	
3162	3145	3158	3171	3133	3160	
2947	2947	2949	2947	2943	2948	νC-H
2885	2876	2884	2886	2879	2885	
1619	1602	1601	1605	1601	1600	δNH_2 (scissor)
1585	1588	1588	1590	1590	1587	
			1461	1471		δCH_2 (scissor)
1456	1455	1455	1455	1455	1456	
1393	1388	1391	1391	1388	1391	$\omega CH_2 + \omega NH_2$
1370	1365	1365	1368	1365	1369	
1326	1329	1328	1327	1327	1328	τCH_2
1292	1296	1297	1297	1294	1295	ωNH_2
1275	1272	1274	1274	1273	1275	
1146	1148	1149	1152	1158	1145	
1106	1108	1101	1111	1099	1108	τNH_2
1090	1092		1091		1093	
1066	1069	1067	1075	1065	1067	
1020	1018	1024	1028	1040	1023	νC-N
997		1010	1016	994	1000	
975	978	979	983	968	979	
				950		νC-C
870	870	871	876	869	871	
858	860	860	864	853	860	
		759	775		750sh	ρCH_2
720		718	720	718	720	
688	701					
622	633	648	663	685	641	ρNH_2
				655	582	
				570		
502	508	516	523	525	512	ring def
481	486	493	499	487	488	
380	390	397	403	471	400	
				343		νM-N
294	307	309	324	402	292	
				272		
253	265	277	284	300	275	
211	212	221	234	240	227	δN-M-N
175	192	194	200	211	190	
143	148	132	141	152	135	
110	110	112	120	126	109	
89		98	101	95	90	lattice
79	82		79		80	

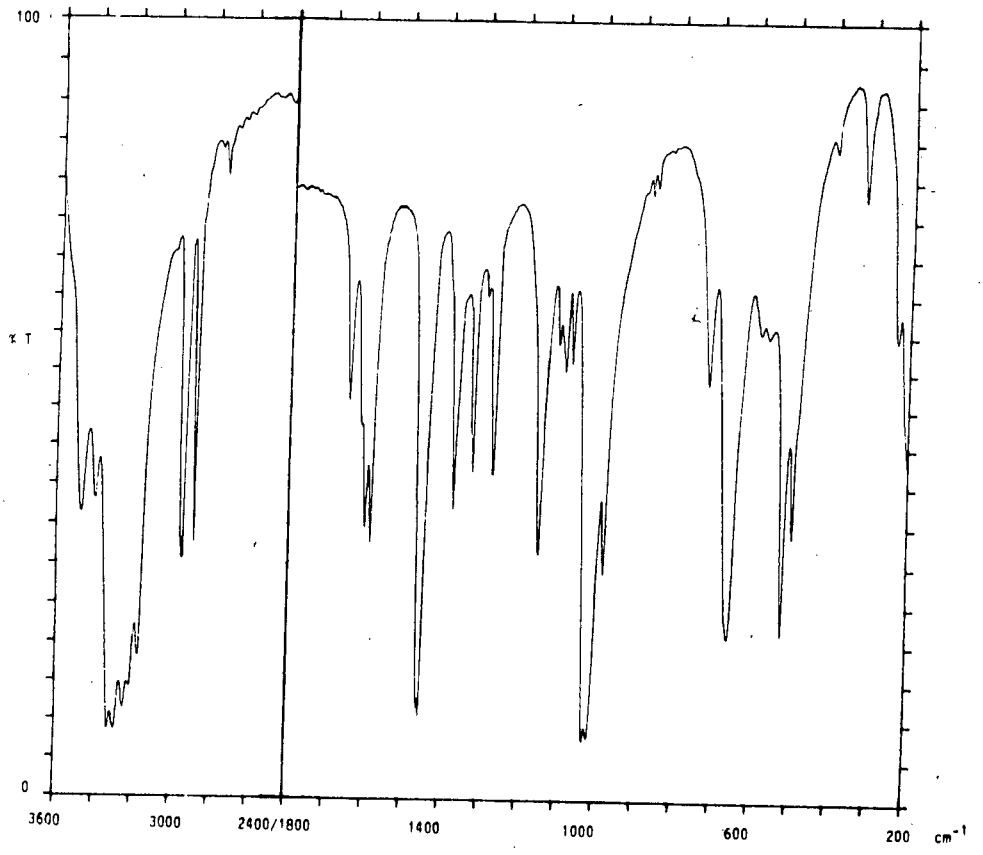

Figure 4.7 Mid-infrared spectrum of $[Ni(en)_3]Cl_2$.
HCBD: 3600-2400cm^{-1}, Nujol: 1800-200cm^{-1}

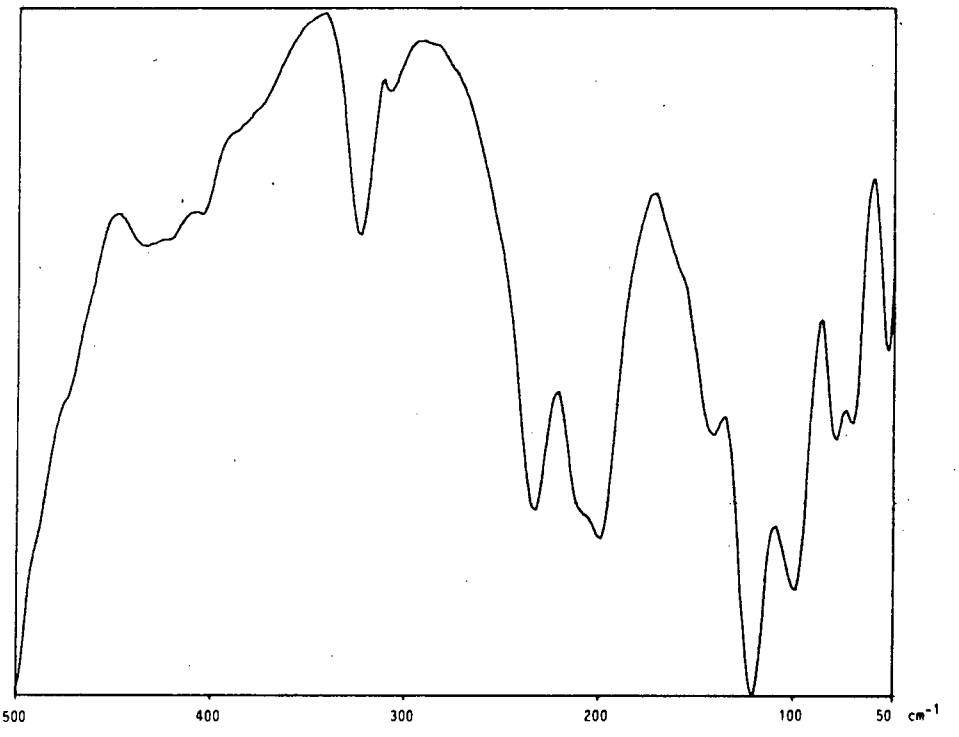

Figure 4.8 Far-infrared spectrum of $[Ni(en)_3]Cl_2$.

Table 4.7 Frequencies (cm^{-1}) and assignments for the complexes $[M(en)_3]X_2$.

X = Br			X = I		Assignment
M=Ni	Cu	Zn	M=Ni	Zn	
3333	3347	3330	3382	3391	
3282	3213	3276	3290	3295	νN-H
			3253	3233	
3159	3124	3156	3151	3149	
2947	2948	2953	2934	2933	νC-H
2882	2870	2880	2882	2881	
1584	1580	1586	1570	1567	δNH_2 (scissor)
				1466	δCH_2 (scissor)
1455	1453	1455	1458	1456	
1391	1389	1394	1394	1396	ωCH_2
1366	1365	1369	1370	1371	
1326	1325	1329	1327	1328	τCH_2
			1275	1274	ωNH_2
1152	1155	1142	1147	1129	τNH_2
1099	1100	1101	1107	1105	
1072	1065	1066	1066	1058	νC-N
1026	1042	1010	1021	1016	
976	971	977	971	994	νC-C
	950	950		963	
872	864	870	877		ρCH_2
862	849	864	865	864	
720	718	720	720	720	
660		658	660	641	ρNH_2
	639	638	626	611	
520	523	518	509	493	ring def
494	479	505	499	478	
400	451	400	401	395	
	342				
326	401	339	325	284	νM-N
	320				
302	(342)	279	290	(284)	
	270				
228	235	230	239	219	
208	222	223	200	200	δN-M-N
172	200	191			
149	157	175	142	140	
130		122	134	122	
105	123	101	122	94	lattice
	81	71	66	60	

Table 4.8 Frequencies (cm^{-1}) and assignments for the complexes $[M(en)_2X_2]$, (X = Cl, Br, I).

M = Ni			M = Cu			
X=Cl	Br	I	X=Cl	Br	I	Assignments
3330	3327	sh	3307	3307	3340	
3295	3281	3291	3284		3283	νN-H
3238	3250	3228	3219	3217	3210	
sh	3192					
3153	3151	3141	3144	3135	3120	
3117	3123					
2954	2956	2955	2966	2958	2960	
2937	2941	2930	2951	2941	2939	νC-H
2877	2878	2875	2886	2881	2881	
1594	sh	sh				δNH_2 (scissor)
1587	1581	1572	1588	1583	1574	
1464	1463	1463	1471	1470		
1454	1456	1454	1452	sh	1455	δCH_2 (scissor)
1443	1443	1442	1446	1449	1447	
1393	1390	1384	1390	1392	1391	ωCH_2
1373	1368	1366	1368	1363	1358	
1330	1326	1322				τCH_2
1323	1319	1314	1319	1320	1316	
1291	1289	1280				$\omega NH_2 + \tau CH_2$
1275	1272	1271	1273	1275	1272	
1146	1140	1138	1156	1163	1160	ωNH_2
sh	sh	sh	1110	1101	1095	τNH_2
1097	1095	1091	1084	1083		
		1075	1066	1070	1069	
1035	1030 br	1027	1038 br	1032 br	1030	νC-N
1019		1019	994	973	sh	and νC-C
982	979	965	965	962	963	
sh	967					

sh = shoulder br = broad

Table 4.8 contd...

M = Ni			M = Cu			
X=Cl	Br	I	X=Cl	Br	I	Assignments
879	877	877	884	886	876	
870	868	sh	880	881		ρCH_2
862	860					
669	676	659	724	721	700	
sh	655	645	670	667	673	ρNH_2
611	608	sh	626	sh	621	
575	575	576				
521	520	508	534	529	527	ring def
511	510	sh	sh		520	
425	433	442	463	459	461	νM-N + ring def
353	357	351	407	404	400	
314	310	316	360	350	340	νM-N
302	292	297	326	325	317	
274	273	274	298	290	287	νM-N + νM-X
239	229	224				
232	224	218	235	221	208	
199	206	197	180	178	169	δN-M-N
			145	147	143	
160	152	128				νM-X bridging
136	116	101				
			116	105	84	νM-X terminal
102	101	84				δX-M-X
86	82	74	98	74	73	
78	73	68			54	lattice
67	56					

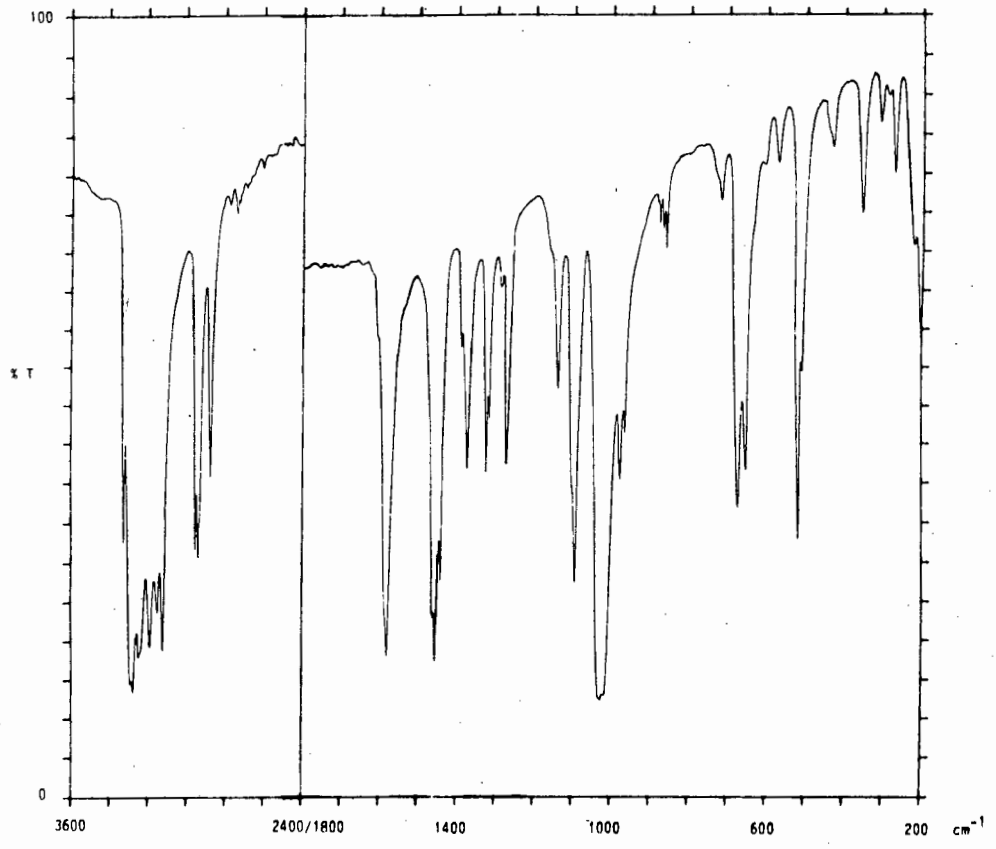

Figure 4.9 Mid-infrared spectrum of $[Ni(en)_2Br_2]$.
HCBD: 3600-2400cm^{-1}, Nujol: 1800-200cm^{-1}

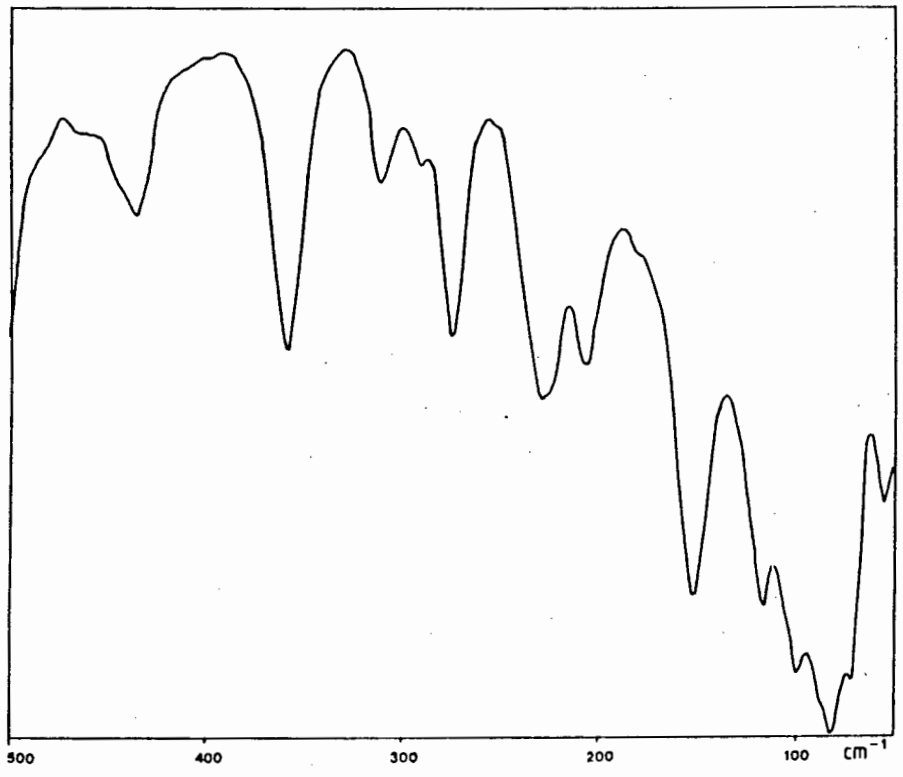

Figure 4.10 Far-infrared spectrum of $[Ni(en)_2Br_2]$.

Table 4.9 Frequencies (cm^{-1}) and assignments for the complexes $[M(en)X_2]$, (X = Cl, Br, I).

M = Ni		M = Cu			M = Zn			
X=Cl	Br	X=Cl	Br	I	X=Cl	Br	I	Assignments
3342	3328	3297	3292	3284	3284	3281	3254	
3271	3259	3232	3225	3214	3227	3219	3201	νN-H
3141	3132	3118	3109	3121	3149	3107	3109	
					3128			
					2990		2984	
2953	2951	2966	2968	2960	2976	2968	2962	νC-H
2936	2935	2935	2941	2940	2952	2944	2938	
2877	2877	2879	2884	2882	2887	2885	2880	
1586	1585			sh	1590			
		1570	1568	1572	1573	1562	1566	δNH_2 (scissor)
1571	1566		sh	sh	1566			
		1467	1467	1463	1463	1462	1460	
1450	1450	1455	1452	1455	1453	1449	sh	δCH_2 (scissor)
1443	1443	1447	1448	1447				
1383	1384	1386	1385	1391				ωCH_2
1362	1362	1359	1358	1358	1375	1372	1372	
1319	1317	1306	1304	1313	1336	1334	1334	τCH_2
1274	1273	1270		1272	1183	1181		ωNH_2 and τCH_2
				1267				
1145	1148	1126	1119	1163	1127	1126	1132	τNH_2
1102	1103	1099	1095	1099	sh		sh	
1076	1077	1074	1074	1084	1060	1055		
1052	1055	1044	1036	1035				νC-N
1007	1008	1015	1013	1013	1008	997	1009	and νC-C
961	963	974	971	963	987	983	sh	
874	872	872	867	876		852		ρCH_2
863	862				760	764	785	

sh = shoulder

Table 4.9 contd...

M = Ni		M = Cu			M = Zn			
X=Cl	Br	X=Cl	Br	I	X=Cl	Br	I	Assignments
697	691	680	670	686				
					656	648	639	
		625	630	622	632			ρNH_2
			623		620	612	sh	
					609	597	590	
528	528	529	525	528				ring def
	sh			508				
455	455	476	470	467	477	472	474	νM-N
					466	461	sh	+ ring def
364	362	374	367	401	320	313	268	νM-N
		316	319	315	283	283	257	
		281	300	294				νM-N + δN-M-N
276	277	263	275	270	219	217	221	δN-M-N
							189	
225	216	216	197	179			164	νM-X terminal
175	159	188	162	142	190	143	128	
					128	127		νZn-N---Zn
137	130	142	126	105				νM-X bridging
117	103	114	102	84				
					101	90	114	δX-M-X
104	(103)	97			92	89		
87	83	80	77	72	74	79	66	lattice
	69		69sh					
53					56	57	52	

sh = shoulder

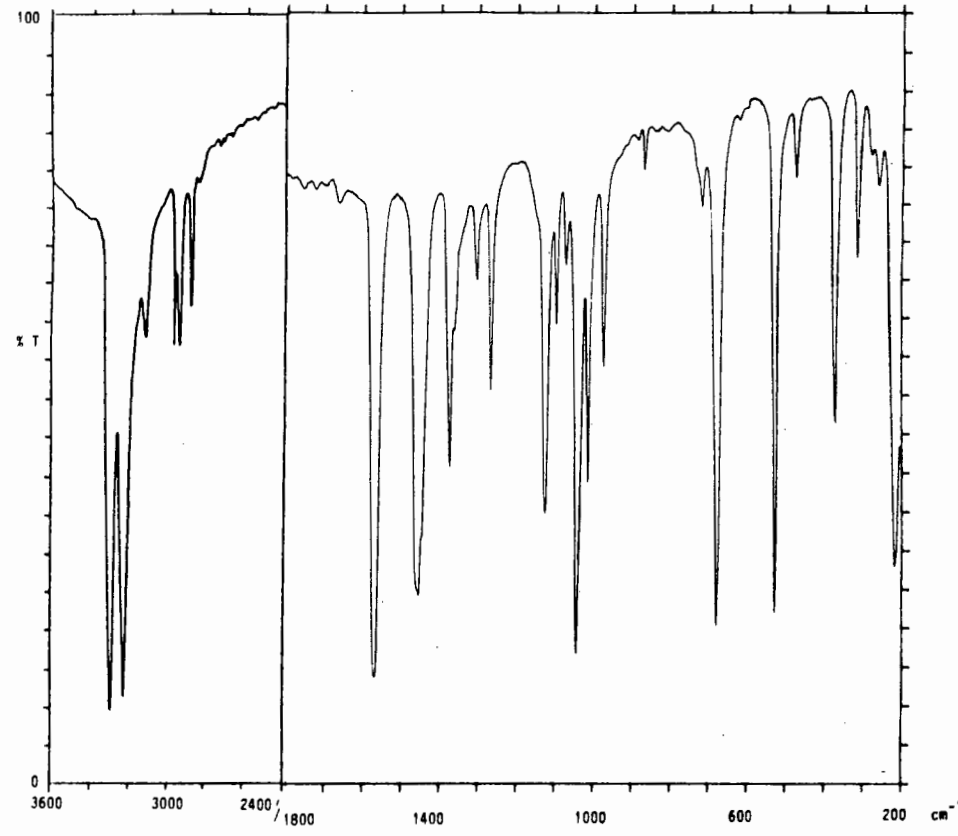

Figure 4.11 Mid-infrared spectrum of $[Cu(en)Cl_2]$.
HCBD: 3600-2400cm^{-1}, Nujol: 1800-200cm^{-1}

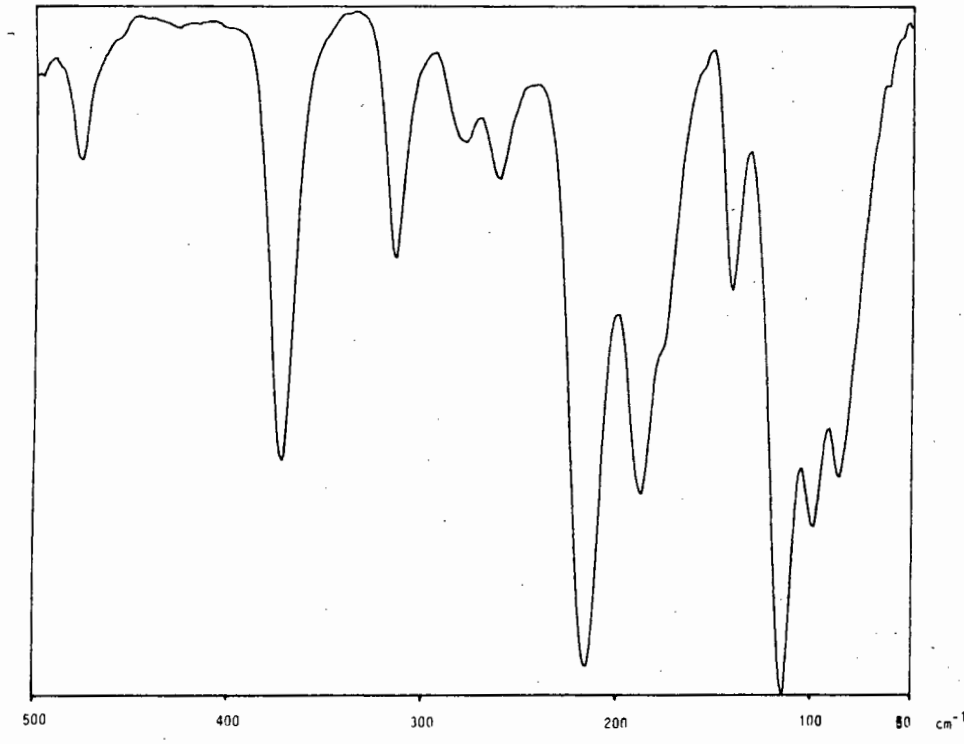

Figure 4.12 Far-infrared spectrum of $[Cu(en)Cl_2]$.

4.3.3 Catalytic Run Data

Each of the Tables below represents the data accumulated by gas-liquid chromatographic analysis of the liquid samples taken at various time intervals during the catalytic run. The catalyst, co-catalyst and relative molar amounts of each are given above each Table. Each % value is expressed as a percentage of the total mass of olefins present in the sample.

Table 4.10 $[Ni(en)Cl_2]$: $AlEt_3$ = 1 : 1

Time(min)	%1-hex	%3-hex	%*tr*-2-hex	%*cis*-2-hex	$\%C_{12}$
0	100	-	-	-	-
10	100	-	-	-	-
300	100	-	-	-	-

hex = hexene
tr = *trans*

Table 4.11 $[Ni(en)Cl_2]$: $AlEt_2Cl$ = 1 : 10

Time(min)	%1-hex	%3-hex	%*tr*-2-hex	%*cis*-2-hex	$\%C_{12}$
0	100.0	-	-	-	-
10	1.3	16.5	65.7	16.5	-
40	1.2	16.7	65.2	16.9	-
1140	1.2	17.0	64.7	17.2	-

Table 4.12 $[Ni(en)Cl_2]$: $Al_2Et_3Cl_3$ = 1 : 10

Time(min)	%1-hex	%3-hex	%*tr*-2-hex	%*cis*-2-hex	$\%C_{12}$
0	100.0	-	-	-	-
10	1.1	17.6	57.9	15.0	8.3
30	1.0	16.1	53.4	13.8	15.7
60	0.9	14.0	44.8	11.7	28.6
240	0.5	8.7	26.8	7.1	56.9
720	0.4	6.5	19.6	5.2	68.3

Table 4.13 $[Ni(en)Cl_2]$: $AlEtCl_2$ = 1 : 10

Time(min)	%1-hex	%3-hex	%*tr*-2-hex	%*cis*-2-hex	$\%C_{12}$
0	100.0	-	-	-	-
20	1.3	13.8	48.4	10.3	26.0
60	0.8	11.3	37.5	8.7	41.4
120	0.6	8.9	29.4	7.2	53.9
180	0.5	8.4	29.4	7.2	57.4
300	0.3	6.9	22.1	5.9	64.7
720	0.3	5.4	16.2	4.4	73.7

Table 4.14 $[Ni(en)_2Cl_2]$: $AlEtCl_2$ = 1 : 10

Time(min)	%1-hex	%3-hex	%*tr*-2-hex	%*cis*-2-hex	$\%C_{12}$
0	100.0	-	-	-	-
30	1.3	15.7	62.5	16.6	3.0
210	1.2	14.1	55.2	14.6	14.5
330	1.1	13.6	51.7	13.8	19.3
1140	0.9	11.5	42.4	11.4	32.5

Table 4.15 $[Ni(en)_3]Cl_2$: $AlEtCl_2$ = 1 : 10

Time(min)	%1-hex	%3-hex	%*tr*-2-hex	%*cis*-2-hex	$\%C_{12}$
0	100.0	-	-	-	-
10	1.9	18.3	60.6	16.6	2.5
30	1.9	18.3	60.6	16.0	2.5
120	1.7	17.4	57.4	15.1	7.6
720	0.8	10.4	31.1	9.1	51.8
2160	0.4	8.0	23.9	5.9	61.5

4.4 DISCUSSION

4.4.1 Infrared Spectroscopy

4.4.1.1 *Tris*(ethylenediamine) Complexes

Assignments Based on Isotopic Labelling

The spectra of the complex $[Zn(en)_3]SO_4$ and its ^{64}Zn-, ^{68}Zn-, ^{15}N-, N_2D_4- and C_2D_4-labelled derivatives are depicted in Fig. 4.13 and the frequency and shift data are reported in Table 4.4.

Based on D_3 point group symmetry, the normal infrared-active modes for the $[Zn(en)_3]^{2+}$ cation are as depicted in Table 4.16. In addition, one can expect to observe the internal modes of the sulphate ion. It is possible to reach reasonable assignments for all of these bands on the basis of the multiple isotopic labelling employed (Table 4.4). Assignment of the N-H and C-H stretching vibrations is facilitated by the knowledge that these vibrations invariably occur in the 3500-3000 cm^{-1} and 3000-2800 cm^{-1} regions, respectively [4]. The N-H stretching vibrations (νN-H) are shifted to 2500-2300 cm^{-1} in the N-deuterated complexes. The average value for the ratio (νN-H/νN-*D*) of 1.35 is in reasonable agreement with the value of 1.37 calculated by the simple harmonic oscillator approximation. The average (νC-H/νC-*D*) value of 1.37 is also consistent with this approximation.

In some cases, for example the NH_2 and CH_2 scissoring modes, a clearcut assignment results. Thus the band at 1592 cm^{-1} shifts 3 and 390 cm^{-1} to lower wavenumbers on ^{15}N- and N_2D_4-labelling, respectively, but is not shifted at all on C_2D_4-labelling. This band is therefore firmly assigned to the NH_2 scissoring mode. By contrast, the bands at 1463 and 1451 cm^{-1} do not shift at all on ^{15}N- and N_2D_4-labelling, but move 155 and 178 cm^{-1}, respectively, to lower frequencies on C_2D_4-labelling: this is clearly a CH_2 scissoring mode. It is also useful when assigning ligand vibrations, to compare the spectra of the complexes to that of the free ligand. The modes involving carbon are not expected to shift

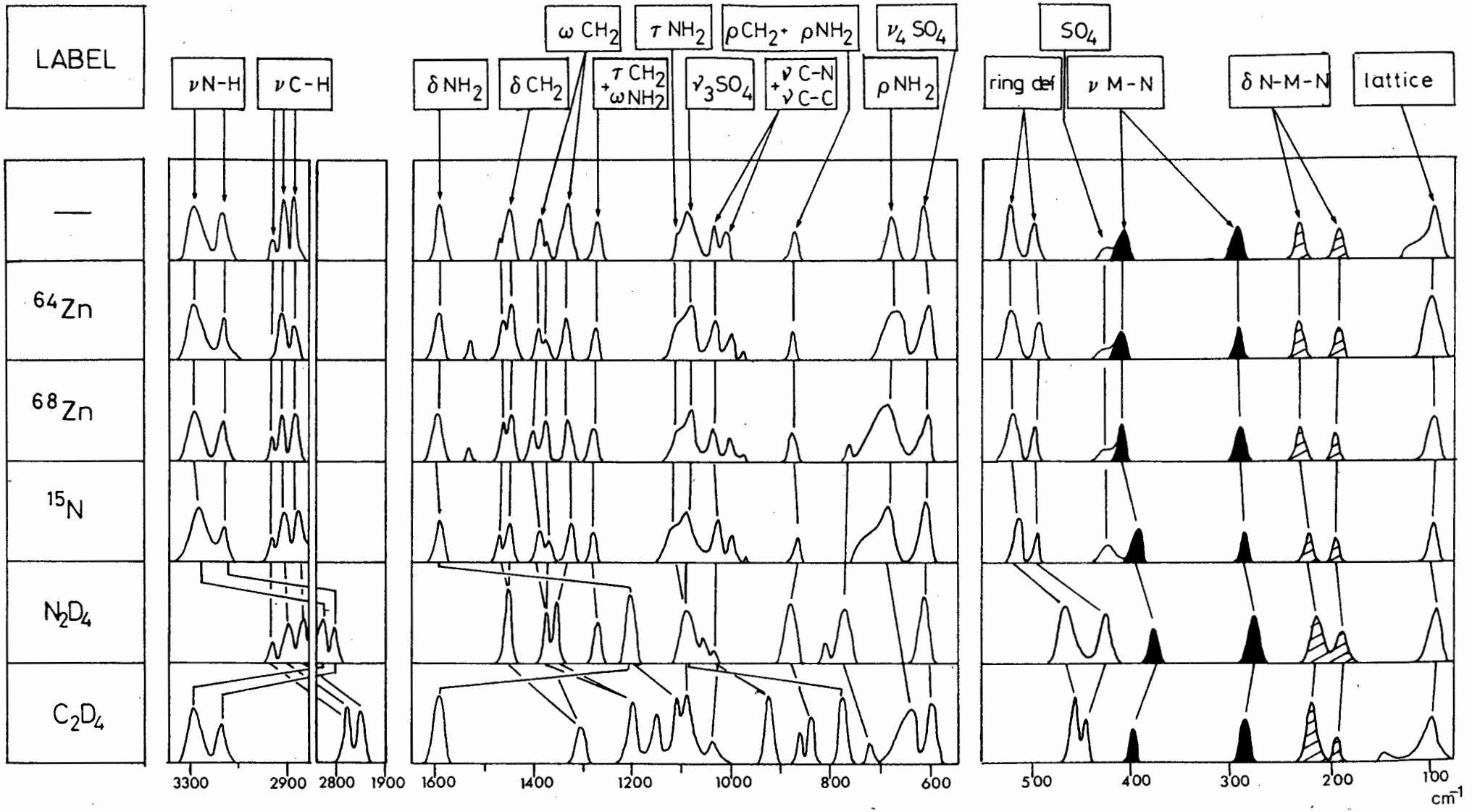

Figure 4.13 Infrared spectra of the labelled complexes $[Zn(en)_3]SO_4$.

Table 4.16 Normal i.r.-active internal ligand and metal-ligand modes for the cation $[Zn(en)_3]^{2+}$ with D_3 point group symmetry.

Mode	I.r. active species
νN-H stretch	$2A_2 + 4E$ (6)
νC-H stretch	$2A_2 + 4E$ (6)
δNH_2 scissor	$A_2 + 2E$ (3)
δCH_2 scissor	$A_2 + 2E$ (3)
ωNH_2 wag	$A_2 + 2E$ (3)
ωCH_2 wag	$A_2 + 2E$ (3)
τNH_2 twist	$A_2 + 2E$ (3)
τCH_2 twist	$A_2 + 2E$ (3)
ρNH_2 rock	$A_2 + 2E$ (3)
ρCH_2 rock	$A_2 + 2E$ (3)
νM-N stretch	$A_2 + 2E$ (3)
νC-N stretch	$A_2 + 2E$ (3)
νC-C stretch	E (1)
δNCCN chelate def	$2A_2 + 4E$ (6)
δN-M-N bend	$A_2 + 2E$ (3)
	$17A_2 + 25E$ (52)

as much on chelation as those involving nitrogen [55]. A clear example is that of the vibrationally pure scissoring modes. Relative to reported values for the free ligand [11], the NH_2 scissor shifts 25 cm^{-1} on chelation, while the analogous CH_2 mode is shifted only 4 cm^{-1}. In many instances for these complexes of en, the effects of vibrational coupling become evident. For example, the band at 1389 cm^{-1} shifts on ^{15}N-, N_2D_4- and C_2D_4-labelling and is therefore assigned to a CH_2 wag coupled with an NH_2 deformation. The νC-N and νC-C modes are approximately coincidental at 1040 cm^{-1} since the band is slightly shifted on ^{15}N- and N_2D_4-labelling and it splits into two components on C_2D_4-labelling one of which is unshifted (νC-N) and the other shifted 112 cm^{-1} to lower frequency (νC-C). The absence of a shift in νC-N on C_2D_4-labelling was also noted by Berg and Rasmussen [43]. The lower skeletal stretch is assigned to νC-N on the basis of its sensitivity to ^{15}N-labelling and the similarly large shifts observed on both N_2D_4- and C_2D_4-labelling. These observed shifts in skeletal stretches are consistent with those calculated by Borch *et al.* [28].

The ν_3 and ν_4 sulphate bands are expected [56], and occur, at 1091 and 611 cm^{-1} where they are readily recognised by their complete insensitivity to all types of isotopic labelling. The CH_2 rocking mode at 871 cm^{-1} is overlaid by the NH_2 rock and the band is split into two components on both N_2D_4- and C_2D_4-labelling. The band at 685 cm^{-1}, assigned to an NH_2 rock, is observed to shift 100 cm^{-1} on N-deuteration. However, the observed sensitivity to C-deuteration is indicative of coupling with a CH_2 mode. This extensive coupling of the rocking modes has been well documented [28-30]. The bands at 522 and 495 cm^{-1} are probably chelate ring deformations since they are sensitive to all types of labelling. The large observed shifts on C_2D_4-labelling, 69 and 56 cm^{-1}, respectively, precludes their assignment to νM-N vibrations as previously reported [16,47]. However, in view of their metal sensitivity, they may well be vibrationally coupled with νM-N. The shifts which occur on replacement of ^{64}Zn by ^{68}Zn are small. However, all the bands which do shift are consistent with the assignments proposed on the basis of the other types of labelling employed and on the effects of metal ion substitution. Thus a shift of 4 cm^{-1} is exhibited by νN-H, a shift of 3 cm^{-1} by the NH_2 rock and a shift of 2 or 3 cm^{-1} by both νZn-N and δN-Zn-N. The calculated shift of νZn-N for

metal isotope substitution is approximately 4 cm^{-1}. The small observed shifts may be attributed to the vibrational impurity of the bands.

The Effects of Metal Ion Substitution

Previous work in this laboratory [34] has shown that bands which have been assigned to metal-ligand stretching modes (on the basis of other techniques) display, practically without exception, the maximum sensitivity towards metal ion substitution. The spectra of the complexes of a series of first row transition metal ions are depicted in Fig. 4.14 and the frequency and shift data are reported in Table 4.5.

It is clear that almost every band below 750 cm^{-1} is metal sensitive in the crystal field stabilisation energy (CFSE) sequence: Mn < Fe < Co < Ni > Cu > Zn. Some of the bands in the copper complex spectrum do not follow this sequence and this may be attributed to tetragonal distortion of the complex. It is now well recognised that a vibration identified as νM-L will undoubtedly be coupled with other vibrations occurring in the neighbouring spectral region, namely δN-M-N and chelate ring deformations. The resulting bands are expected to have a significant degree of mixed character [25,32,43-46]. However, the two which exhibit maximum sensitivity to ^{15}N- and N_2D_4-labelling (and to metal ion substitution) are those near 400 and 300 cm^{-1}. In addition, there are no bands in this region in the spectrum of the free ligand [11]. These bands are therefore assigned to two of the three infrared-active νM-N modes expected in terms of the D_3 point group symmetry of the complexes. The third is probably one of the bands within the range 540-470 cm^{-1} which is coupled with one of the chelate ring deformations. The assignment of the band at 300 cm^{-1} is at odds with the work of Gabelica [20] in which he assigned this band to the first δN-M-N.

The bands near 870 and 670 cm^{-1}, assigned as NH_2 rocking modes, are as metal sensitive, if not more so, than the assigned νM-N. Many metal complexes with amine ligands (ammonia, aniline *etc.*) show a similar effect, namely that the shift on changing the metal ion is greater for the band assigned to an NH_2 rock than for those assigned to metal-nitrogen vibrations [57-61].

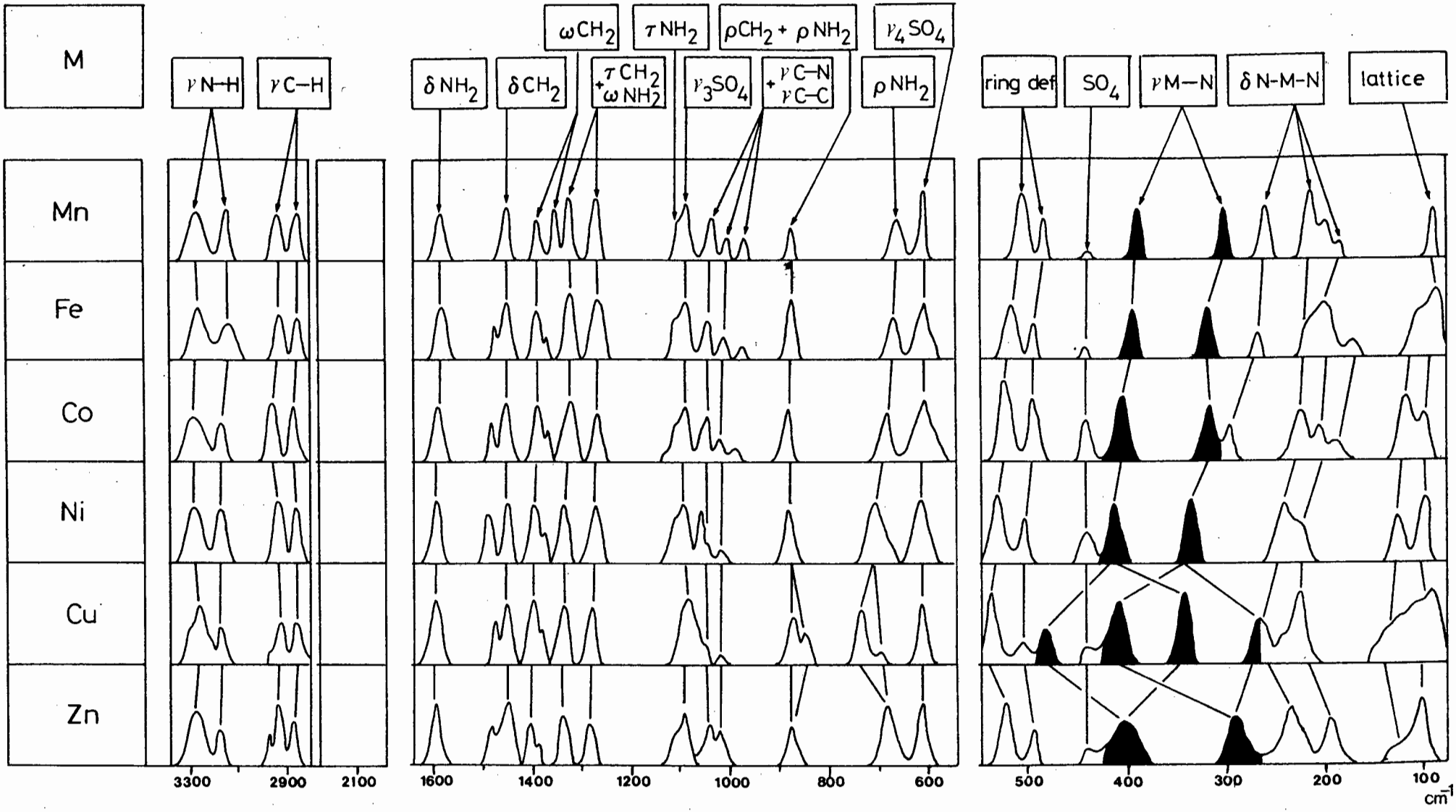

Figure 4.14 Infrared spectra of the complexes $[M(en)_3]SO_4$.

There are two bands near 200 cm^{-1} which exhibit metal sensitivity in the sequence Mn < Fe < Co < Ni > Cu > Zn, but to a lesser extent than the νM-N modes. These are undoubtedly two of the three δN-M-N bands expected for the D_3 molecule. They are also shifted by ^{15}N-, N_2D_4- and C_2D_4-labelling but, as has been noted by Saito *et al.* [62], their sensitivity is lower than that of the corresponding stretching modes. A third δN-M-N vibration is only observed in the Mn, Fe and Co complexes and is probably coincident with other bands in the remaining complex spectra. The bracketed shift data in Table 4.5 serve to illustrate the sensitivity of all the lower vibrations (including those assigned to metal-nitrogen modes) to C_2D_4-labelling. This is again indicative of coupling to chelate ring modes.

The Spectrum of the Cu(II) Complex in Relation to JAHN-TELLER Distortion

It is now well established [30] that splitting of a metal-ligand stretching vibration is an extremely sensitive indicator of axial elongation of an octahedral molecule leading to tetragonal distortion. The infrared spectrum of $[Cu(en)_3]SO_4$ is therefore of great interest since it will afford evidence of similar distortion which is expected to arise from the JAHN-TELLER effect, thereby disturbing the D_3 symmetry. Furthermore, the most sensitive index of the distortion will be the vibrationally purest νCu-N band and the observation of band splitting will therefore also assist in solving the assignment problem. By comparison with the preceding Ni(II) complex and the succeeding Zn(II) complex, the splitting in the Cu(II) complex is considered to be as indicated in Fig. 4.14. The bands near 400 cm^{-1} and 300 cm^{-1} exhibit splitting of similar magnitude ($\Delta\nu$ = 139, 134 cm^{-1}, respectively) and this is consistent with the observed shifts on ^{15}N-, N_2D_4- and C_2D_4-labelling, which are also similar in magnitude for both bands. The additional splitting observed for the NH_2 rocking modes and the ring deformations in the region 570-480 cm^{-1} is also indicative of a decrease in the symmetry of the molecule caused by distortion of the bonds as well as possible coupling to metal-nitrogen vibrations [63].

In view of the evidence of distortion in the $[Cu(en)_3]SO_4$ spectrum, it is surprising to find that a crystal structure determination [64]

reveals that all Cu-N bond lengths are very nearly identical. It is pointed out, however, that since the molecule is found, crystallographically, to have large thermal parameters, there may be some justification for assuming the existence of a dynamic JAHN-TELLER effect. Nevertheless, considering that the much more rigid ligand 2,2′-bipyridine is capable of accommodating static tetragonal distortion in $[Cu(bipy)_3](ClO_4)_2$ [65], one would anticipate that the relatively flexible en ligand would be better able to expand its bite to yield a tetragonal $[Cu(en)_3]^{2+}$ cation.

The two bands near 200 cm^{-1}, assigned (as a result of the isotopically labelled spectra) to δN-M-N modes, also shift in the sequence Mn < Fe < Co < Ni > Cu > Zn, but the metal sensitivity is smaller than that of the two stretching modes and there is little evidence of band splitting in the spectrum of the Cu(II) complex. These observations are consistent with their assignment to δN-M-N.

The Effects of Changing the Anion

The infrared spectra of the complexes $[M(en)_3]X_2$ (M = Mn, Fe, Co, Ni, Cu, Zn) (X = Cl, Br, I) are depicted in Fig. 4.15 and the frequency data and assignments are reported in Table 4.6 and 4.7. The formulae of the complexes suggest that the structures are of regular six-coordinate D_3 symmetry except for the copper complex which is tetragonally distorted. As expected, the metal(II) chloride, bromide and iodide complexes are very similar to one another and are also similar to the sulphate spectra. However, a larger number of bands are observed for the halides relative to the analogous sulphate complexes. While this may be attributed in part to the unmasking of several vibrations in the absence of the strong sulphate modes, band multiplicity does appear to increase. For example, where only two νN-H modes are observed in the sulphate complex spectra, all four expected vibrations are observed for the halide complexes. It has been proposed that observed spectral differences on changing the anion are not satisfactorily justified by the hydrogen bonding of the amino-hydrogen to the anion [16], but should rather be attributed to minor changes in crystal structure. Allen and Senoff [55] take this further by

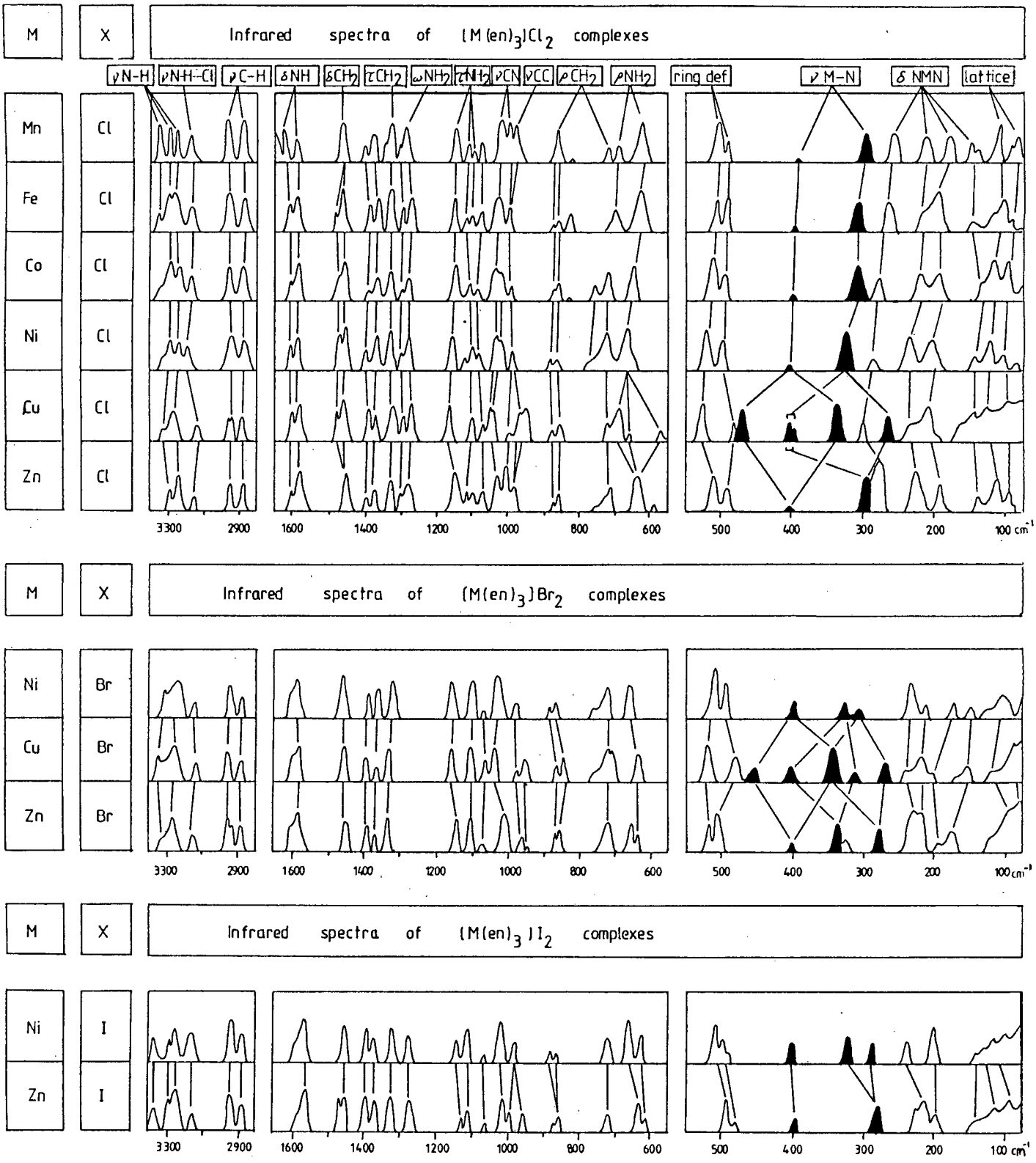

Figure 4.15 Infrared spectra of the complexes $[M(en)_3]X_2$.

proposing that halide salts have similar crystal structures, which are different to those complexes with a relatively large anion. However, there is no X-ray structural evidence for such proposals and it is possible that site and factor group considerations may account for observed differences.

Another notable difference between the halide and sulphate spectra is the appearance of NH_2 twisting modes near 1100 and 1090 cm^{-1} as well as an additional skeletal stretching vibration at 1067 cm^{-1}. These three bands were previously obscured by a ν_3 sulphate mode. In addition, the CH_2 and NH_2 rocking modes are no longer coincidental: the NH_2 rocking modes are observed at lower frequencies than the CH_2 modes. This is in agreement with the normal coordinate treatment of Borch *et al.* [28]. Further support for these assignments is the splitting of the lower NH_2 rocking mode near 680 cm^{-1} for both the chloride and bromide complexes of copper as observed for the copper sulphate complex.

These observed differences do not, however, complicate the vibrational assignments of the halide complexes which are readily made by comparison with the sulphate complexes. Moreover, the splitting of the νCu-N bands observed for the halide complexes of copper(II) is very similar to that observed for the sulphate complexes, indicative of a similar degree of tetragonal distortion. The values of νM-N for the species $[M(en)_3]^{2+}$ are summarised in Table 4.17. It may be mentioned here that, for the metal halide complexes, the νM-N band of higher frequency (near 400 cm^{-1}) is less intense than in the metal sulphate complexes. Furthermore, in the spectra of metal(II) bromide or iodide complexes, an additional metal-sensitive band near 300 cm^{-1} (which is split into two components in the copper(II) spectrum) is observed. This is assigned as the third infrared-active νM-N expected for the D_3 symmetry of the species $[M(en)_3]^{2+}$.

4.4.1.2 *Bis*(ethylenediamine) Complexes, $[M(en)_2X_2]$ (M = Cu, Ni)

The infrared spectra are depicted in Fig. 4.16 and the frequency and assignment data are recorded in Table 4.8. Above 600 cm^{-1}, where vibrations are due to the en ligand, the spectra are markedly similar to

Table 4.17 Values of νM-N (cm^{-1}) and isotopically-induced shifts ($\Delta\nu$) for all complexes $[M(en)_3]X_2$ which have been studied.

M =	Mn	Fe	Co	Ni	Cu	Zn
X = Cl[a]	380	390	397	403	471 343	400(6, 20, 6)[b]
	294	307	309	324	402 272	292(8, 34, 0)[b]
X = Br[a]				400	451 342	400
				326	401 320	339
				302	(342) 270	279
X = I[a]				401 325		395 284
X = $\frac{1}{2}SO_4$[a]	391	397	402	410	485 346	405(11, 30, 8)[b]
	303	321	319	334	404 270	291(7, 16, 4)[b]
X = $\frac{1}{2}S_2O_3$[20]	390 303[d]	397 317[d]	403 315[d]	410(31)[c] 329(13)[cd]		404(27)[c] 283(14)[cd]

[a] This work

[b] Figures in parentheses denote the isotopically-induced shifts to lower frequencies ($\Delta\nu$) induced by ^{15}N-labelling, N_2D_4-labelling and C_2D_4-labelling, respectively

[c] Shift ($\Delta\nu$) on N_2D_4-labelling

[d] Assigned by the authors to δN-M-N [20]

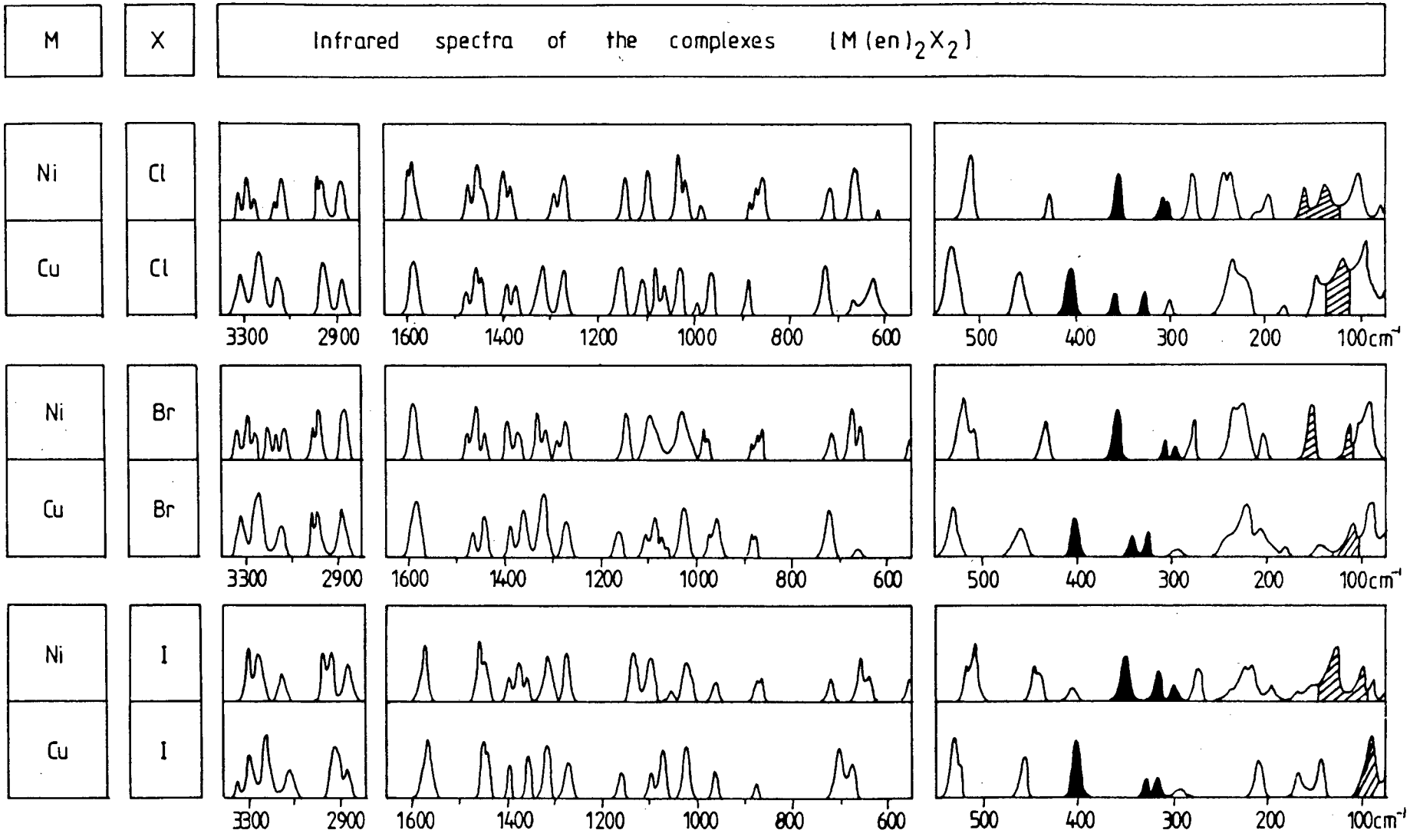

Figure 4.16 Infrared spectra of the complexes $[M(en)_2X_2]$, M = Ni, Cu; X = Cl, Br, I.
Solid bands = νM-N, Shaded bands = δN-M-N

those of the *tris*-complexes. The likeness is such as to allow for a band-for-band comparison and assignments are readily made in this way. It is of interest, however, to mention certain assignments which have caused controversy. The first disagreement arose over the assignment of two bands, one near 1320 cm^{-1} and one at ~1270 cm^{-1}. Earnshaw *et al.* [21], Watt and Klett [15] and Gabelica [38] assigned the NH_2 wagging mode to the upper frequency, while Berg and Rasmussen [43] ascribed the band near 1270 cm^{-1} to this vibration and the band near 1320 cm^{-1} to a CH_2 twisting mode. The band near 1270 cm^{-1} was assigned by Gabelica [38] and Watt and Klett [15] to a CH_2 twist. Based on the isotopic labelling of the *tris*-complexes and in agreement with a recently published normal coordinate analysis [40], it appears reasonable to assign the band at 1320 cm^{-1} to a predominantly CH_2 mode and that near 1270 cm^{-1} to an NH_2 wagging mode extensively coupled with a CH_2 twisting mode.

There is also confusion associated with the correct assignment of the vibration occurring near 870 cm^{-1}. Due to its insensitivity to deuteration, several authors have assigned the band to the CH_2 rocking mode [38,49]. Diaz *et al.* [40], in their normal coordinate treatment, assigned the band to a νC-C mode and the band at 970 cm^{-1} to the CH_2 rocking mode. On the basis of the above labelling study as well as the more extensive normal coordinate analysis of Borch *et al.* [28], the band at 870 cm^{-1} is assigned to the CH_2 rocking vibration. This is also in agreement with the analogous rocking mode in the free ligand. These discrepancies aside, there is largely agreement between authors. However, the most interesting bands are found below 600 cm^{-1} where vibrations sensitive to both metal and halide substitution occur.

The Complexes Trans-*$[Cu(en)_2X_2]$ (X = Cl, Br, I)*

The copper complex spectra will be discussed prior to those of the nickel as extensive work has already been published regarding their vibrational assignment. These studies include metal isotope labelling [37], ligand deuteration [36], normal coordinate analysis [40] as well as other techniques [21,22]. The majority of the more sophisticated studies refer to the square planar species $[Cu(en)_2]^{2+}$ (formed in the

presence of large anions) rather than the six-coordinate *trans*-tetragonal complexes discussed here. Substituting alternative halogens (X = Cl, Br, I) does not significantly alter the band pattern, indicating that all three complexes have similar structures.

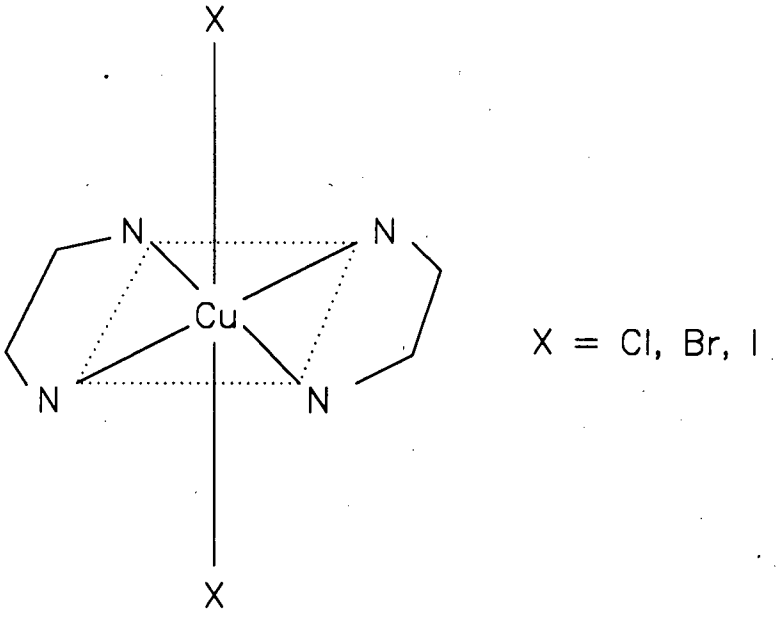

Figure 4.17 Tetragonally distorted $[Cu(en)_2X_2]$ complex.

The doublet near 530 cm^{-1} is assigned to a ring deformation on the grounds of its shift of 22 cm^{-1} in the spectrum of $[Cu(en\text{-}N_2D_4)_2Cl_2]$ [36] and its insensitivity towards halide substitution. This is consistent with a similar assignment given to the corresponding band in the spectra of $[Cu(en)_3]^{2+}$ complexes. The band near 460 cm^{-1} is also assigned to a skeletal mode but, in view of its low sensitivity to N-deuteration of en [36] and its significant metal-sensitivity in the sequence Ni < Cu, it is probably coupled with νCu-N. This would be consistent with the potential energy distribution of the corresponding band in the normal coordinate analysis of $[Cu(en)_2](PF_6)_2$ which is comprised of 70% νCu-N + 30% chelate ring deformation [40].

The bands near 400 and 320 cm^{-1} are confidently assigned to νCu-N modes in view of their sensitivities towards nickel substitution, N-deuteration of en ($\Delta\nu$ = 13 cm^{-1} for the chloro complex [36]) and $^{63,65}Cu$-labelling ($\Delta\nu$ = 2 cm^{-1} for the chloro complex [37]). This assignment is also consistent with the normal coordinate analysis of $[Cu(en)_2]^{2+}$ which

indicates a potential energy distribution comprising 70-80% νCu-N for the bands in this region [40]. In addition to the two νCu-N bands mentioned, a weak band occurs near 340 cm^{-1}. Since this band shifts slightly with a change in halogen (X), it is assigned to a coupled νCu-X mode. The weak bands observed near 290 cm^{-1} are assigned to the coupled vibration, νCu-N + δN-Cu-N, as proposed for a similar band (ν_7) at 290 cm^{-1} in the normal coordinate analysis of $[Cu(en)_2]^{2+}$ [40].

Four bands occur in the range 250-140 cm^{-1} and are assigned to predominantly δN-Cu-N modes. The first two of these bands may be coupled with νCu-X in view of slight X-sensitivity. The first strongly X-sensitive band in the spectra occurs between 116 and 84 cm^{-1}. This is assigned to νCu-X. The low frequency is reasonable in relation to the weak *trans*-axial Cu-X bonding in the JAHN-TELLER distorted molecule.

The Complexes $[Ni(en)_2X_2]$ (X = Cl, Br, I)

In the presence of large anions, *bis*(ethylenediamine)nickel(II) are diamagnetic square planar complexes of formula $[Ni(en)_2]^{2+}$. With simple monoatomic anions such as the halides studied here, the complexes are paramagnetic, six-coordinate dimers formulated $[Ni_2(en)_4X_2]X_2$ with both *cis*-bridging and anionic halides.

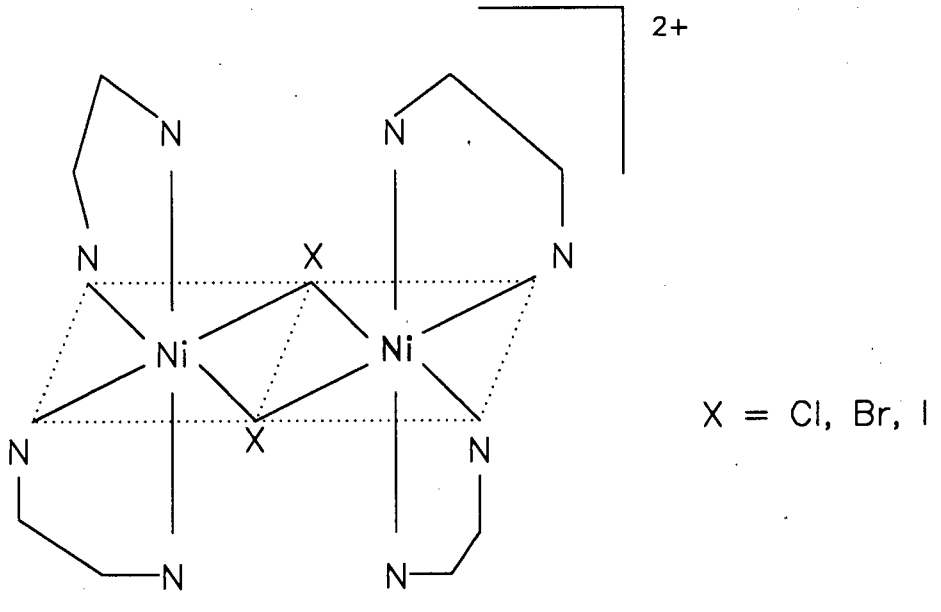

Figure 4.18 *Cis*-octahedral $[Ni(en)_2X_2]X_2$ complex.

Spectral band assignments above 550 cm^{-1} are made by comparison with the previously discussed copper complexes. There is considerable similarity, with the most notable difference being the increased band multiplicity due to the lower symmetry of the *cis*-dimeric nickel complex [46]. For example, additional N-H stretching and NH_2 scissoring vibrations are observed as well as two additional bands in the 1325 and 1290 cm^{-1} region. The observed metal-sensitivity of the bands in the 720-600 cm^{-1} region, which are invariably assigned to the NH_2 rocking modes, is in accordance with the previous observation that in many metal complexes with amine ligands, the NH_2 rocking modes are as sensitive to metal ion substitution as the M-N stretching vibrations.

The diamagnetic square planar $[Ni(en)_2X_2]$ complexes give rise to a ring deformation mode near 500 cm^{-1} and a νNi-N mode near 395 cm^{-1} [36]. The νNi-N bands are expected to lie below those of νCu-N in the $[Cu(en)_2X_2]$ complexes [34,38]. Bands sensitive to metal isotope labelling have been observed near 350 and 300 cm^{-1} in the complexes $[Ni(en)_2X_2]$ and have, on this basis, been assigned to νNi-N [38]. This work entirely supports these earlier assignments since the chelate ring and νNi-N modes are found to be practically insensitive to the nature of the halogen. Likewise, the band at 275 cm^{-1} in $[Ni(en)_2Cl_2]$ is sensitive to ^{62}Ni isotope substitution ($\Delta\nu$ = 4 cm^{-1} [46]) but is unshifted by halogen substitution. This band is therefore assigned to δN-M-N, probably coupled with νNi-N as proposed for the $[Cu(en)_2X_2]$ complexes [40]. On similar grounds, the assignment δN-Ni-N is proposed for the doublet at 239, 232 cm^{-1}. Furthermore, the band near 200 cm^{-1} is practically halogen-insensitive and is therefore also assigned to a mode in which δN-Ni-N predominates. The isotopic labelling study [46] was not extended below 200 cm^{-1} but the bands at 160 and 136 cm^{-1} in the spectrum of $[Ni(en)_2Cl_2]$ are both sensitive towards halide substitution and are therefore assigned to bridging νNi-Cl. The frequencies are reasonable in relation to the reported frequencies of bridging νM-Cl bands in first transition series metal(II) complexes [66]. A further X-sensitive band occurs at 102 cm^{-1} in the spectrum of $[Ni(en)_2Cl_2]$ and is assigned to the δCl-Ni-Cl mode.

4.4.1.3 *Mono*(ethylenediamine) Complexes, $[M(en)X_2]$

The infrared spectra are depicted in Fig. 4.19 and the frequencies are listed in Table 4.9. The copper complexes with a single coordinated ethylenediamine ligand are six-coordinate polymeric species, with both terminal and *trans*-axially bridging halide atoms [53,54].

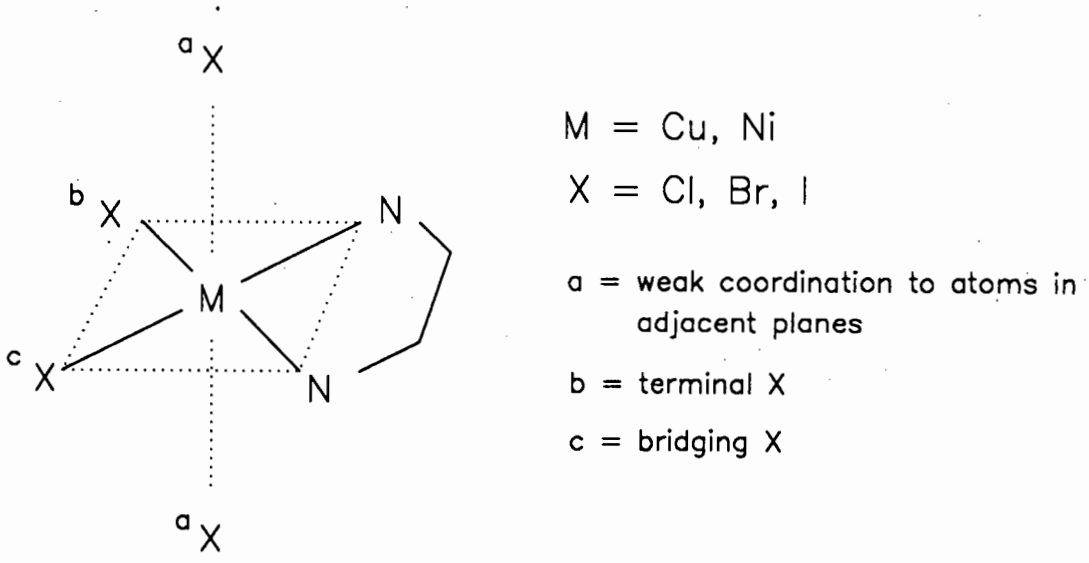

Figure 4.20 Polymeric $[M(en)X_2]$ complexes.

In the complex with X = Cl, the Cu-Cl bond lengths are 2.3 Å (terminal) and 2.9 Å (bridging), thus indicating tetragonal distortion [54]. In view of the long axial Cu-Cl distances, νCu-Cl (bridging) is anticipated at very low frequency and νCu-Br and νCu-I even lower.

The tetragonally distorted six-coordinate symmetry is sufficiently similar to the $[Cu(en)_3]X_2$ and particularly to the $[Cu(en)_2X_2]$ species to expect an analogous band pattern above 600 cm^{-1}. This is indeed the case, allowing band assignments in this region. From the foregoing examination of the copper(II) complex spectra, the ring modes are readily identified near 530 and 470 cm^{-1}, the latter of which is coupled with a Cu-N stretching frequency. The νCu-N modes are observed near 370 and 320 cm^{-1}. The latter bands exhibit shifts of between 1 and 2.5 cm^{-1} on $^{63,65}Cu$-labelling and shifts of between 6 and 13 cm^{-1} on N_2D_4-labelling in the complexes with X = Cl and Br [36]. The band near 300 cm^{-1} is assigned to the coupled νCu-N + δN-Cu-N mode on the basis of the normal

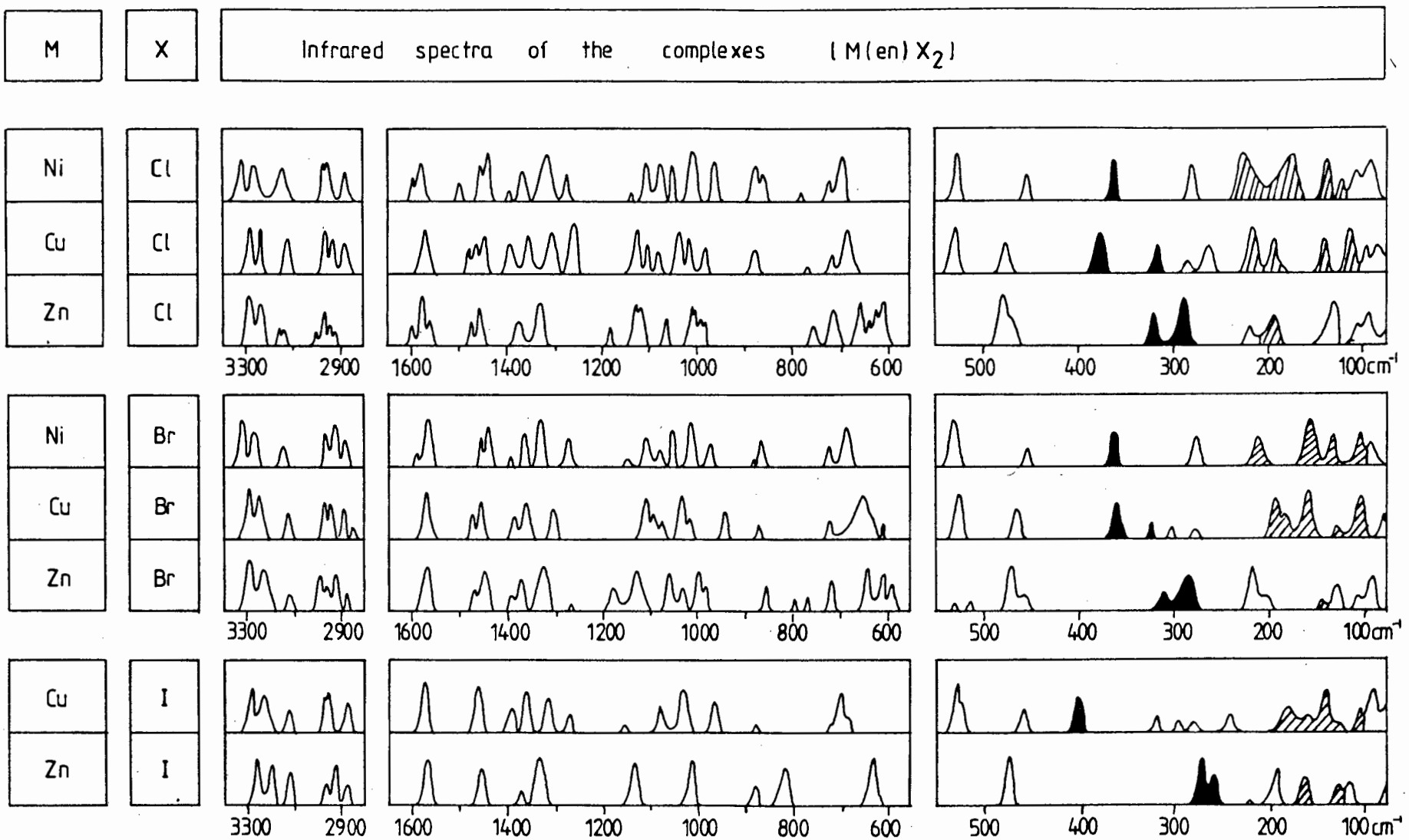

Figure 4.19 Infrared spectra of the complexes $[M(en)X_2]$, M = Ni, Cu, Zn; X = Cl, Br, I.
Solid bands = νM-N, Shaded bands = δN-M-N.

coordinate analysis of $[Cu(en)_2](PF_6)_2$ [40]. However, this band is anomalous in respect of its apparent insensitivity to $^{63,65}Cu$-labelling in the chloro complex but not in the bromo complex [37].

The first vibration to show marked X-sensitivity is that at 216 cm^{-1} in the spectrum of $[Cu(en)Cl_2]$. This feature, together with its sensitivity to $^{63,65}Cu$-labelling but not to N-deuteration [37], enables it to be firmly assigned to νCu-Cl (terminal). The band at 188 cm^{-1} is also X-sensitive and therefore receives the same assignment although the labelling study was not extended below 200 cm^{-1}.

The pair of X-sensitive bands within the range 145-80 cm^{-1} is assigned to the νM-X (bridging) mode and the bands at 97, 77 and 72 cm^{-1} in the complexes with X = Cl, Br and I, respectively, are assigned to the δX-Cu-X mode.

An interesting feature of the complexes $[Cu(en)X_2]$ is the relatively high value of νCu-N in $[Cu(en)I_2]$. The frequencies are 374, 367 and 401 cm^{-1} for the complexes with X = Cl, Br and I, respectively. Although the crystal structure of $[Cu(en)I_2]$ has not been determined, it seems likely that the size of the iodide ion does not permit Cu-I-Cu bridging of the type exhibited by $[Cu(en)Cl_2]$ and $[Cu(en)Br_2]$. The resulting further weakening of the Cu-I bond would yield stronger Cu-N bonding in this complex as is evident from the higher νCu-N frequency.

The Complexes $[Ni(en)X_2]_n$ (X = Cl, Br)

It has been suggested that the *mono*(ethylenediamine) complexes of Ni(II) are probably polymeric octahedral [52]. That their spectra are similar to those of the copper complexes $[Cu(en)X_2]$ is certainly in accordance with this proposal. There is evidence of less band-splitting in the spectra of the nickel complexes which is also consistent with the possibility that these compounds (unlike the copper complexes) may not be tetragonally distorted. On the basis of this structure, the assignments proposed are shown in Table 4.9. Their spectra have not previously been reported.

The Complexes $[Zn(en)X_2]$ (X = Cl, Br)

Finally, the $[Zn(en)X_2]$ complexes are completely unlike the analogous copper and nickel species as the en takes up the *trans*-configuration and bridges two zinc atoms. The Zn-X bands are therefore all terminal. The final structure is six-coordinate due to weak bonding between the zinc ion and adjacent NH_2 groups [19,50-52].

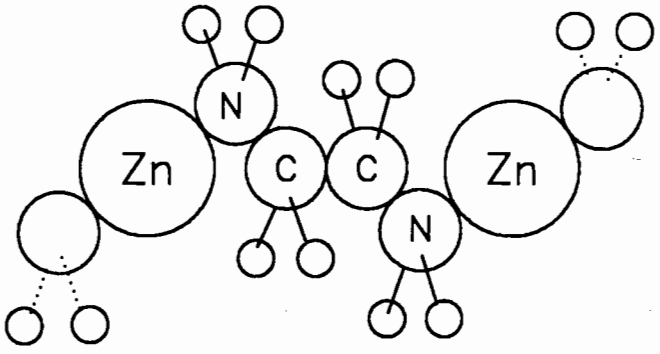

Figure 4.21 *Trans*-bridging en in the complex $[Zn(en)X_2]$.

The local C_{2h} symmetry of *trans*-ethylenediamine is supported by the infrared and Raman spectra of $[Zn(en)Cl_2]$ and $[Zn(en)Br_2]$ [19] as all bands in the infrared are excluded from the Raman spectra.

There are supposedly three forms of $[Zn(en)Cl_2]$. The spectrum recorded in this study is similar to that reported by Iwamoto and Shriver [50] (to 400 cm^{-1}) for form (iii) of $[Zn(en)Cl_2]$ and to those reported by Krishnan and Plane [19] (to 250 cm^{-1}) for $[Zn(en)Cl_2]$ and $[Zn(en)Br_2]$. It is clear from the spectra that the structures are very different from those of the Cu(II) and Ni(II) complexes. Furthermore, the spectrum of $[Zn(en)I_2]$, which has not previously been reported, differs from those of the chloride and bromide complexes, and will be discussed separately.

The deformation band, which has thus far appeared near 525 cm^{-1} in all en complexes studied above, is no longer present indicating the absence of a chelate ring. The skeletal mode near 470 cm^{-1} (which is independent of ring formation) is present. This band is considered to contain a contribution from coupled νM-N which is probably responsible for its variable position (within the range 500-425 cm^{-1}) in all the en complexes. The νZn-N vibration occurs at 315 and 285 cm^{-1} for the

chloride and bromide complexes, respectively. It is, as expected, halide-independent. This feature discounts its assignment to νZn-Cl by Krishnan and Plane [19] who did not examine the spectrum of $[Zn(en)Br_2]$. The band at 219 cm^{-1} is probably the δN-Zn-N mode since it is independent of X, while that at 190 cm^{-1} is shifted to 143 cm^{-1} on substitution of Cl by Br and is therefore assigned to νZn-X. The rather low values of Zn-X support the proposal that Zn(II) is in an essentially six-coordinate environment. The band at 128 cm^{-1}, which is independent of X, may be associated with Zn-N bonding to neighbouring molecules and is effectively a lattice mode.

The spectrum of $[Zn(en)I_2]$ is of interest since the structure of this molecule clearly differs from those of the corresponding chloride and bromide complexes. The spectrum is very simple comprising only eight bands over the range 500-50 cm^{-1}. The absence of the band near 525 cm^{-1} implies the absence of the chelate ring (of the type comprising both N-atoms of a single en molecule bonded to a single zinc ion). The only bands which present themselves for possible assignment to νZn-N are those at 268, 257 cm^{-1}. Based on the spectra of the above chloro and bromo complexes, their position is indicative of bridging en. The νZn-I (terminal) vibrations occur at 164 and 128 cm^{-1}, while the band at 114 cm^{-1} is probably δI-Zn-I or δN-Zn-I. The relatively high values of these iodide bands may be associated with a lower coordination number of zinc thus implying stronger Zn-X bonds. If these assignments are correct (and taking into account the simplicity of the spectrum) the most probable structure is $I_2Zn(\mu\text{-en})_2ZnI_2$ with two bridging en molecules linking two tetrahedral zinc ions.

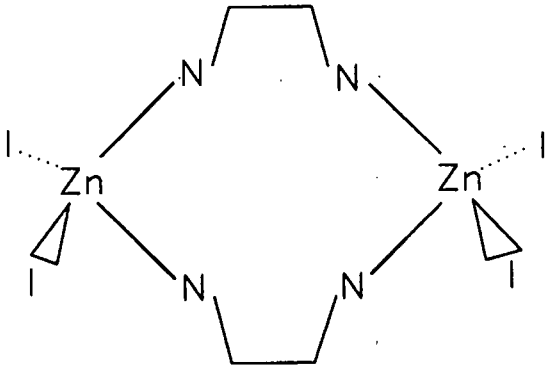

Figure 4.22 Proposed structure of $[Zn(en)I_2]$.

4.4.2 Catalysis

The results of the catalytic experiments are summarised in Tables 4.10-4.15. The series of experiments shows the effect of a change in co-catalyst and a change in catalyst on the dimerisation and isomerisation activity and dimerisation selectivity.

4.4.2.1 Co-Catalyst Effects

A single catalyst, $[Ni(en)Cl_2]$, was tested with four alternative co-catalysts; $AlEt_3$, $AlEt_2Cl$, $Al_2Et_3Cl_3$, $AlEtCl_2$.

The system in which equimolar proportions of $[Ni(en)Cl_2]$ and $AlEt_3$ are present exhibits no oligomerisation or isomerisation activity. This may be ascribed to the fact that the catalyst does not dissolve under the prevailing conditions thereby preventing the formation of a homogeneous active species.

The remaining three co-catalysts were present in a ten molar excess over the catalyst. In each case dissolution of the nickel complex occurred on addition of the co-catalyst.

Dimerisation

Of the three catalytic systems, only those with the $Al_2Et_3Cl_3$ and $AlEtCl_2$ co-catalysts actively dimerise 1-hexene (no higher oligomers are formed). The $[Ni(en)Cl_2]$ / $AlEtCl_2$ system is initially the more active of the two, although after 30 minutes the dimerisation rate is similar to that of the $[Ni(en)Cl_2]$ / $Al_2Et_3Cl_3$ system (Fig. 4.23). The differing initial reaction rate may be due to the weaker $Al_2Et_3Cl_3$ co-catalyst taking longer to form the necessary active complex. Once the active species is formed, however, the reaction proceeds independently of the co-catalyst. It appears that the stronger the Lewis acid, the greater the catalytic dimerisation activity. Activity therefore increases in

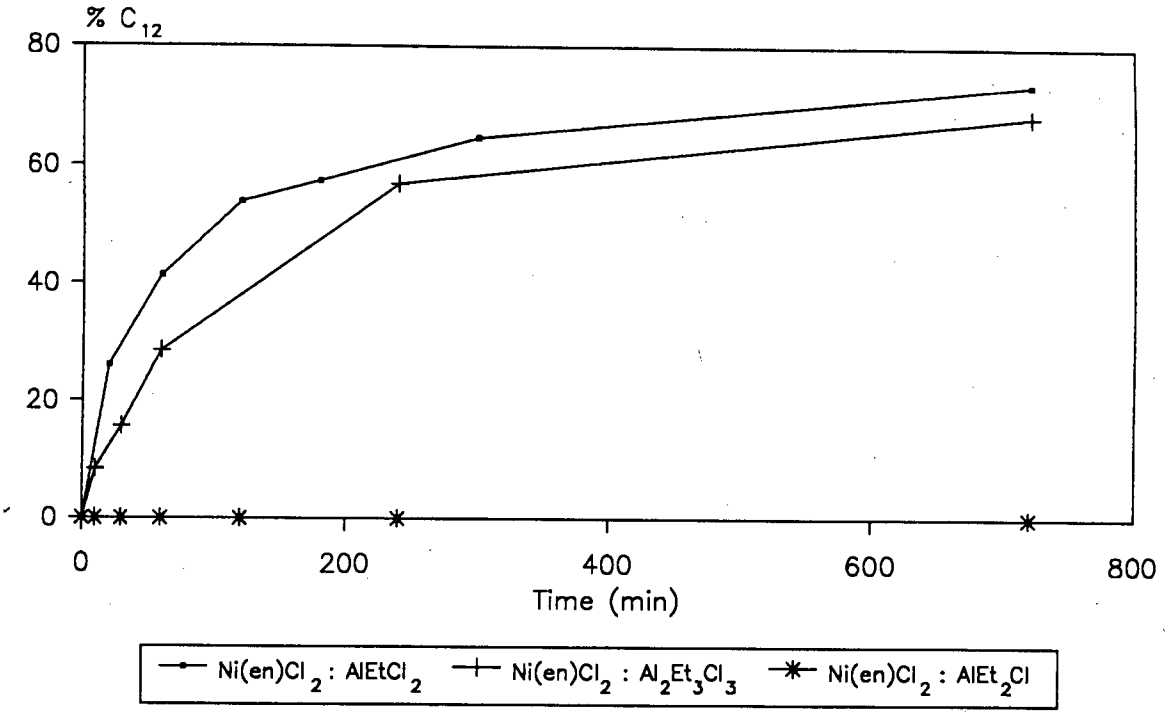

Cat : Co–cat = 1 : 10

T = 40°C

Figure 4.23 Graph of the effect of co-catalyst on dimerisation activity.

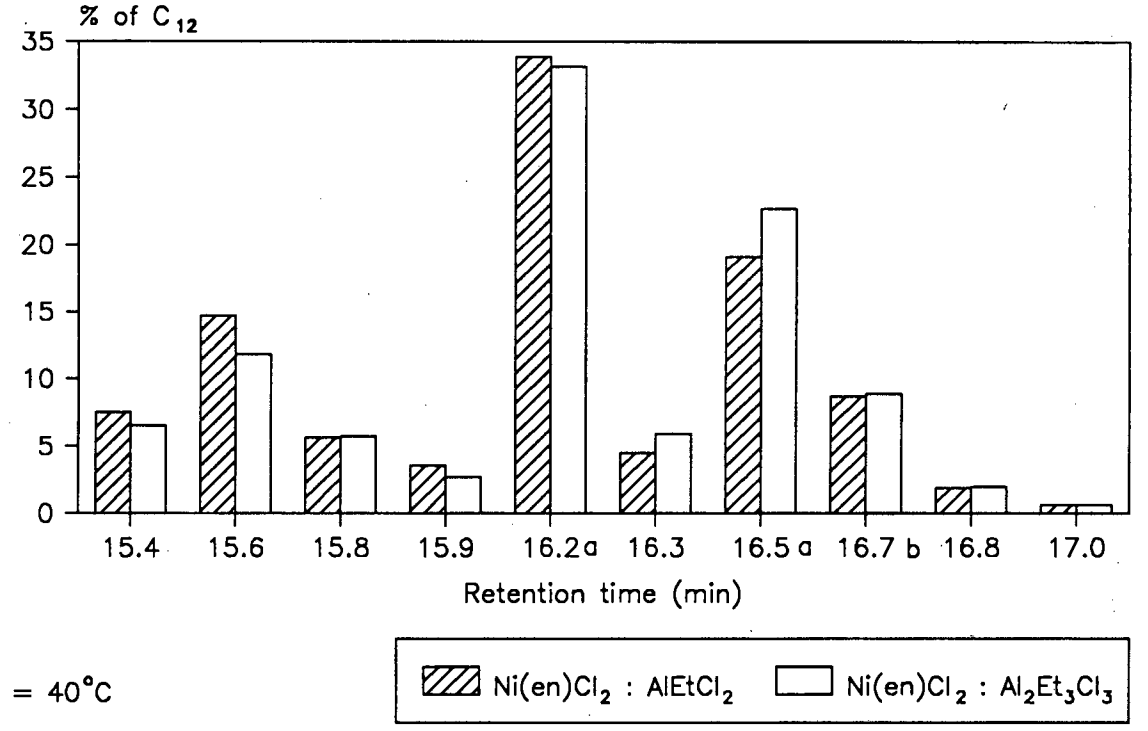

T = 40°C

Cat : Co–cat = 1 : 10

a = unresolved isomers b = linear dodecene

Figure 4.24 Graph of the effect of co-catalyst on selectivity.

the following order:

$$AlEt_3 << AlEt_2Cl < Al_2Et_3Cl_3 < AlEtCl_2.$$

Isomerisation

In conjunction with a ten molar excess of any of the three chloride-containing Lewis acids ($AlEt_2Cl$, $Al_2Et_3Cl_3$, $AlEtCl_2$), $[Ni(en)Cl_2]$ catalyses the isomerisation of 1-hexene to internal olefins. In each case the reaction is almost instantaneous and an equilibrium isomer concentration is rapidly established. The relative concentrations of the 1-hexene to 2- and 3-hexene remain constant thereafter at 1 : 83 : 16. This implies that either all the isomers are dimerised at the same rate, or that 1-hexene only is dimerised and the equilibrium is maintained by rapid double bond isomerisation of 1-hexene to internal olefins. The latter proposal is supported by the observation that the dimer distribution remains relatively unchanged with time even though little 1-hexene remains after 30 minutes.

Selectivity

It has been proposed that the Lewis acid co-catalyst affects the activity but not the selectivity of the catalyst [67]. This has been shown to be untrue for the $[Ni(acac)_2]_3$ catalyst, as changing from a chloride-free to a chloride-containing co-catalyst resulted in a different distribution of dimer products. $[Ni(en)Cl_2]$ exhibits significant dimerisation activity in conjunction with both $Al_2Et_3Cl_3$ and $AlEtCl_2$ co-catalysts. It can be seen in Fig. 4.24 that altering the chloride containing co-catalyst does not dramatically alter the dimer distribution. This unchanged selectivity implies that the active species and dimerisation mechanism are similar in both systems.

4.4.2.2 Structural Effects

Three nickel(II) complexes of en, each representative of a different structure, have been tested for catalytic activity.

The $[Ni(en)Cl_2]$ catalyst discussed above has a polymeric octahedral structure. The $[Ni(en)_2Cl_2]$ complex (more correctly formulated as $[Ni_2(en)_4Cl_2]Cl_2$) is present as a six-coordinate dimer with *cis*-bridging chlorine atoms. $[Ni(en)_3]Cl_2$ is a six-coordinate monomer with the anions outside the coordination sphere.

The above complexes were tested catalytically in the presence of a ten molar excess of $AlEtCl_2$.

Dimerisation

Both the $[Ni(en)_2Cl_2]$ and $[Ni(en)_3]Cl_2$ systems dimerise 1-hexene (no higher oligomers are formed). In each case, however, the initial activity is lower than for the $[Ni(en)Cl_2]$ catalytic system (Fig. 4.25). This may be ascribed to an extended induction period necessary to bring about catalyst dissolution and formation of the active complex. While it appears that dimerisation activity is dependent on the structure of the nickel complex precursor, the fact that all the above complexes are indeed active, implies that a square planar configuration for the catalyst precursor is not a prerequisite for such activity. It is likely that interaction of the catalyst with the co-catalyst gives rise to a square planar catalytic species, irrespective of the initial coordination structure of the nickel complex.

Isomerisation

For each of the systems, the isomerisation reaction is virtually instantaneous. It is thus not possible to examine the effect of nickel complex structure on the isomerisation reaction. The equilibrium distribution of the hexene isomers is similar in each case.

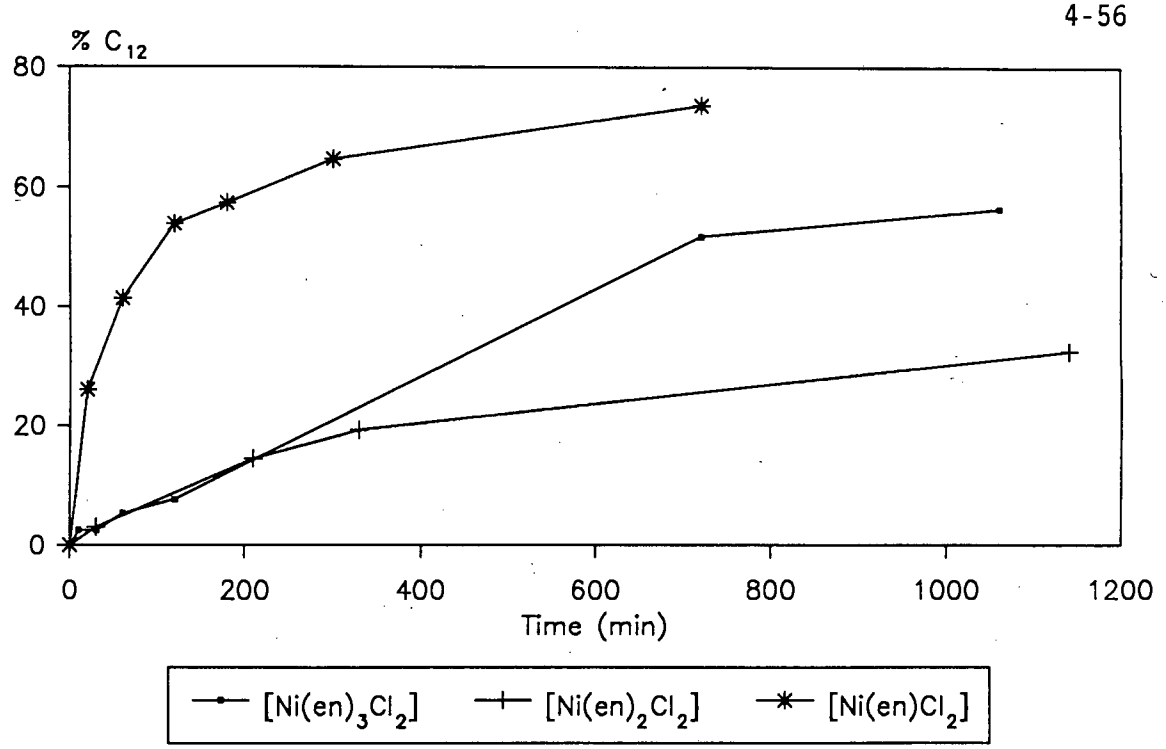

Cat : $AlEtCl_2$ = 1 : 10

T = 40°C

Figure 4.25 Graph of the effect of catalyst structure on dimerisation activity.

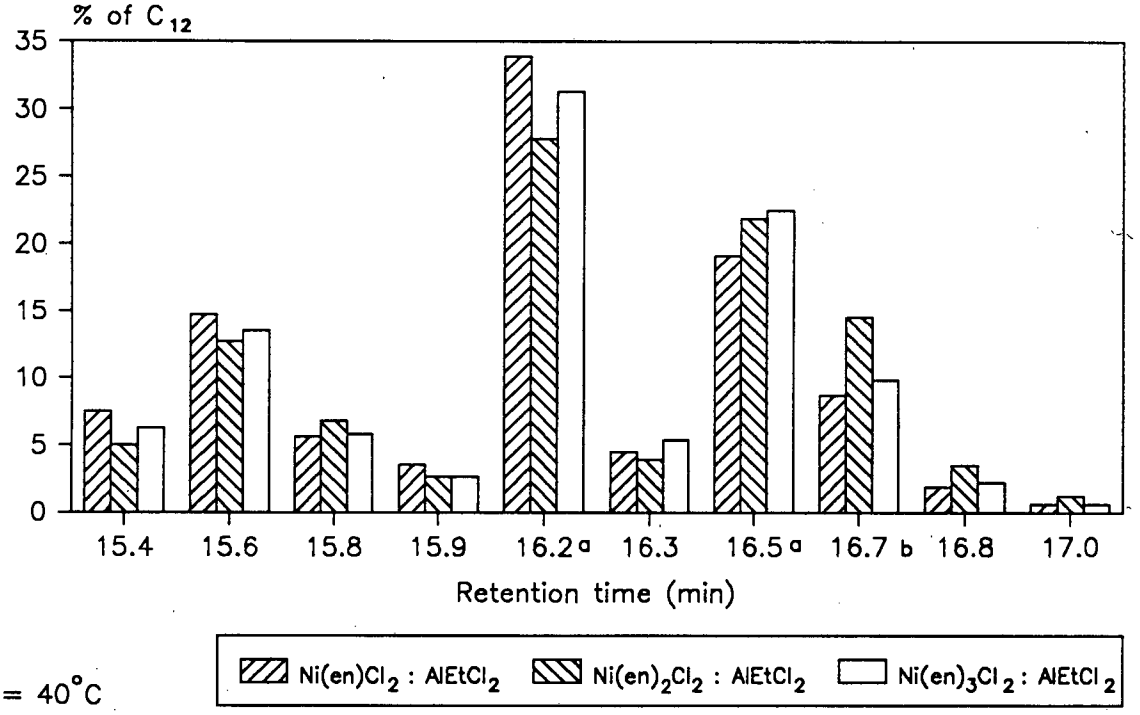

T = 40°C

Cat : Co–cat = 1 : 10

a = unresolved isomers , b = linear dodecene

Figure 4.26 Graph of the effect of catalyst structure on selectivity.

Selectivity

The similarity in the C_{12} isomer distribution (Fig. 4.26) is indicative of a similar active species and dimerisation mechanism for each catalytic system. This supports the proposal of an active complex in which the chelating ligands are dissociated from the nickel. The nickel may then interact with the Lewis acid *via* bridging chlorine atoms and take up a square planar configuration. This species has also been put forward by Bogdanovic [67].

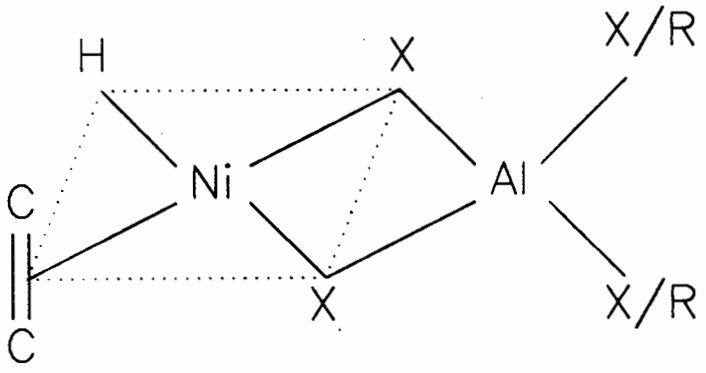

Figure 4.27 Active species for nickel complex catalysis [67].

Such a species is independent of the initial structure of the nickel complex.

REFERENCES

1. A. Werner, Z. anorg. Chem., **21** (1899) 199.

2. A. Sabatini and S. Califano, Spectrochim. Acta, **16** (1960) 677.

3. A. Diot and T. Theophanides, Can. J. Spectrosc., **17** (1972) 67.

4. K. Nakamoto, in "Infrared and Raman Spectra of Inorganic and Coordination Compounds", 4th Ed., (1986), Wiley-Interscience, New York.

5. I. Nakagawa and S. Mizushima, J. Chem. Phys., **21** (1953) 2195.

6. A. Nakahara, Y. Saito and H. Kwroya, Bull. Chem. Soc. Japan, **25** (1952) 331.

7. H. Scouland and C.H. Carlisle, Acta Cryst., **6** (1953) 651.

8. J.V. Quagliano and S. Mizushima, J. Amer. Chem. Soc., **75** (1953) 6084.

9. L.N. Swink and M. Atoji, Acta Cryst., **13** (1960) 639.

10. A. Yokozeki and K. Kuchitsu, Bull. Chem. Soc. Japan, **44** (1971) 2926.

11. A-L. Borring and K. Rasmussen, Spectrochim. Acta, **31A** (1975) 889.

12. D.M. Sweeny, S. Mizushima and J.V. Quagliano, J. Amer. Chem. Soc., **77** (1955) 6521.

13. J.L. Sudmeier, G.L. Blackmer, C.H. Bradley and F.A.L. Anet, J. Amer. Chem. Soc., **94** (1972) 757.

14. L.S. Magill, J.D. Korp and I. Bernal, Inorg. Chem., **20** (1981) 1187.

15. G.W. Watt and D.S. Klett, Inorg. Chem., **5** (1966) 1278.

16. D.B. Powell and N. Sheppard, J. Chem. Soc., (1961) 1112; Spectrochim. Acta, **17** (1961) 68.

17. M.N. Hughes and W.R. McWhinnie, J. Inorg. Nucl. Chem., **28** (1966) 1659.

18. J.R. Durig and D.W. Wertz, Appl. Spectrosc., **22** (1968) 627.

19. K. Krishnan and R.A. Plane, Inorg. Chem., **5** (1966) 852.

20. Z. Gabelica, Spectrochim. Acta, **32A** (1976) 327.

21. A. Earnshaw, L.F. Larkworthy and K.C. Patel, J. Chem. Soc. (A), (1969) 1339.

22. Y. Omura, I. Nakagawa and T. Shimanouchi, Spectrochim. Acta, **27A** (1971) 2227.

23. A.B.P. Lever and E. Mantovani, Inorg. Chim. Acta, **5** (1971) 429.

24. D.M. Adams, in "Metal Ligand and Related Vibrations", (1967), Edward Arnold, London.

25. K. Nakamoto and P.J. McCarthy , in "Spectroscopy and Structure of Metal Chelate Compounds", (1968), Wiley, New York,.

26. J. Gouteron-Vaissermann, C. R. Acad. Sci. Paris, **B275** (1972) 149.

27. J. Gouteron, J. Inorg. Nucl. Chem., **38** (1976) 63.

28. G. Borch, P.H. Nielsen and P. Klaboe, Acta Chem. Scand., **A31** (1977) 109.

29. G. Borch, P. Klaboe and P.H. Nielsen, Spectrochim. Acta, **34A** (1978) 87.

30. G. Borch, J. Gustavsen, P. Klaboe and P.H. Nielsen, Spectrochim. Acta, **34A** (1978) 93.

31. J.H. Clark and M.L. Greenfield, J. Chem. Soc. (A), (1967) 409.

32. D.W. James and M.J. Nolan, Inorg. Nucl. Chem. Lett., **9** (1973) 319.

33. K. Rasmussen, Spectrochim. Acta, **30A** (1974) 1763.

34. D.A. Thornton, Coord. Chem. Rev., **55** (1984) 113 and references cited therein.

35. I.M. Procter, B.J. Hathaway and P. Nicholls, J. Chem. Soc. (A), (1968) 1678.

36. A.B.P. Lever and E. Mantovani, Inorg. Chem., **10** (1971) 817.

37. G.W. Rayner Canham and A.B.P. Lever, Can. J. Chem., **50** (1972) 3866.

38. Z. Gabelica, Spectrochim. Acta, **32A** (1976) 337.

39. E. Uhlig, B. Machelett and R. Treffurt, Z. anorg. allg. Chem., **438** (1978) 242.

40. G. Diaz Fleming and R.E. Shepherd, Spectrochim. Acta, **43A** (1987) 1141.

41. G. Diaz, C. Bustos and R.E. Shepherd, Inorg. Chim. Acta, **133** (1987) 23.

42. J.R. Durig, R. Layton, D.W. Sink and B.R. Mitchell, Spectrochim. Acta, **21** (1965) 1367.

43. R.W. Berg and K. Rasmussen, Spectrochim. Acta, **28A** (1972) 2319.

44. R.W. Berg and K. Rasmussen, Spectrochim. Acta, **29A** (1973) 37.

45. R.W. Berg and K. Rasmussen, Spectrochim. Acta, **30A** (1974) 1881.

46. A.B.P. Lever and E. Mantovani, Can. J. Chem., **51** (1973) 1567.

47. J. Csàszàr, Acta Chim. Acad. Sci. Hung., **75** (1972) 23.

48. A.B.P. Lever, J. Lewis and R.S. Nyholm, J. Chem. Soc., (1963) 2552.

49. G. De, P.K. Biswas and N.R. Chaudhuri, Bull. Chem. Soc. Japan, **56** (1983) 3145.

50. T. Iwamoto and D.F. Shriver, Inorg. Chem., **10** (1971) 2428.

51. G. Newman and D.B. Powell, J. Chem. Soc., (1961) 477.

52. G. Devoto, M. Massacesi, G. Ponticelli, R. Medda and G. Floris, Polyhedron, **5** (1986) 1023.

53. G. Giuseppetti and F. Mazzi, Rend. Soc. Mineral. Ital., **11** (1955) 202.

54. D.F. Billing, R. Dudley, B.J. Hathaway, P. Nicholls and I.M. Procter, J. Chem. Soc. (A), (1969) 312.

55. A.D. Allen and C.V. Senoff, Can. J. Chem., **43** (1965) 888.

56. M.E. Baldwin, Spectrochim. Acta, **19** (1963) 315.

57. L. Sacconi, A. Sabatini and P. Gans, Inorg. Chem., **3** (1964) 1772.

58. I.S. Ahuja, D.H. Brown, R.H. Nuttall and D.W. Sharp, J. Inorg. Nucl. Chem., **27** (1965) 1105.

59. R.J.H. Clark and C.S. Williams, Inorg. Chem., **4** (1965) 350.

60. R.J.H. Clark and C.S. Williams, Spectrochim. Acta, **22** (1966) 1081.

61. J.F. Jackovitz, J.A. Durkin and J.L. Walter, Spectrochim. Acta, **23A** (1967) 67.

62. Y. Saito, M. Cordes and K. Nakamoto, Spectrochim. Acta, **28A** (1972) 1459.

63. L.G. Hulett, PhD Thesis, University of Cape Town, (1972).

64. M. Cola, G. Giuseppetti and F. Mazzi, Atti. Acad. Sci. Torino, **96** (1962) 381.

65. G.C. Percy and D.A. Thornton, Spectrosc. Lett., **3** (1970) 323 and references cited therein.

66. J.R. Ferraro, in "Low Frequency Vibrations of Inorganic and Coordination compounds", (1971), Plenum Press, New York, p. 175.

67. B. Bogdanovic, Adv. Organomet. Chem., **17** (1979) 105.

CHAPTER 5

POLYMER SUPPORTED COMPLEXES

5.1 INTRODUCTION

The problems encountered in separating products from the catalyst in homogeneous systems have led to heterogeneous systems being the favoured choice industrially. A relatively new field that has sparked extensive interest is that of supported metal catalysis, in which a homogeneous complex is heterogenised onto an insoluble support. This is a growing field and a large number of reviews give comprehensive coverage of the subject [1-4].

In order to appreciate the reasons for interest in supported metal catalysts, in our case those used for the oligomerisation of olefins, it is necessary to consider the advantages and disadvantages of homogeneous and heterogeneous catalysis. Homogeneously catalysed reactions are generally more efficient (all the catalyst molecules are involved), specific (usually only one active site is involved) and reproducible (the reaction has a fixed stoichiometry) than those catalysed heterogeneously. Heterogeneous catalysts are chemically and thermally more stable and also obviate the separation problems encountered in homogeneous catalysis.

By heterogenising promising soluble nickel-complex catalysts, it is hoped to benefit from the advantages of both homogeneous and heterogeneous systems. In addition to the advantages already mentioned, the metal complex-support interaction may lead to enhanced selectivity *via* electronic and steric effects [5].

The soluble complexes $[Ni(acac)_2]_3$ (Hacac = 2,4-pentanedione) and $[Ni(SacSac)(PPh_3)Cl]$ (HSacSac = 2,4-pentanedithione) have been selected as a basis for preparing polymeric analogues, the former for its selectivity in forming linear isomers when used with a weak trialkylaluminium co-catalyst [6], and the latter for its high activity [7]. In each polymer the nickel environment is similar to that of the homogeneous analogue. In this way it is hoped that the above mentioned advantages will be retained in the heterogeneous systems.

The preparation of polymer (I) (Fig. 5.1) was based on the work of Thornton [8] and Jones *et al*. [9] and proceeded *via* the formation of a nickel monomer and subsequent polymerisation of this complex.

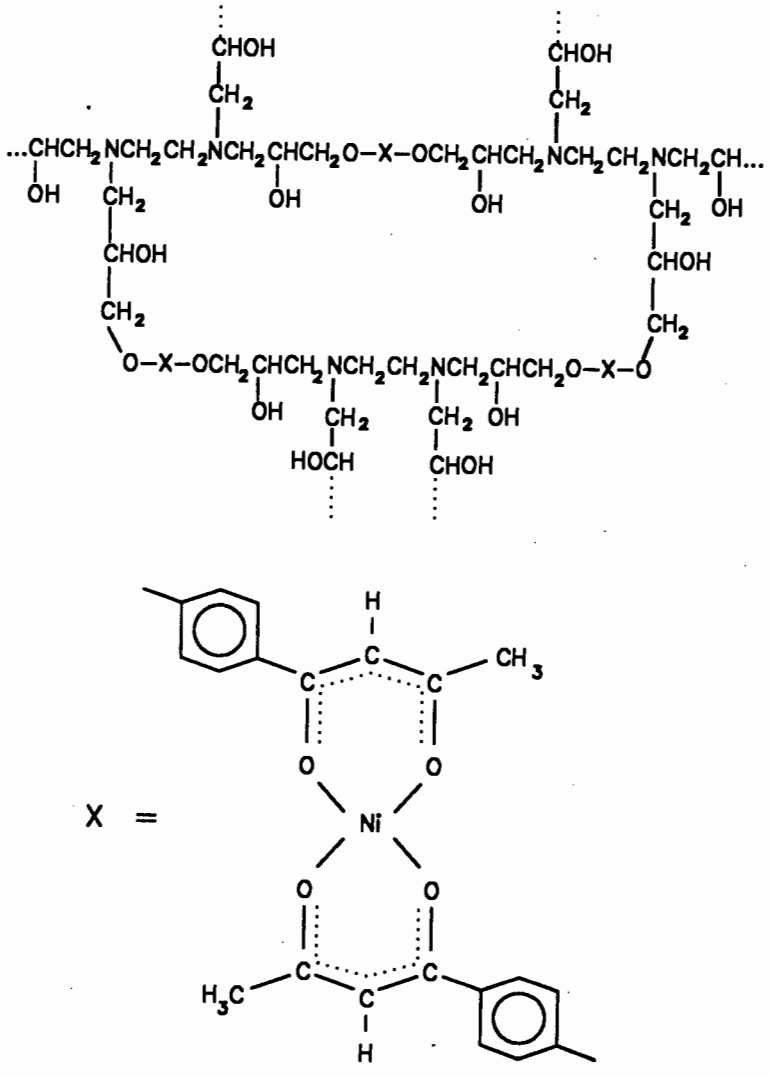

(I)

Figure 5.1 Structure of the nickel epoxy polymer, (I).

There are several key advantages to this method of catalyst preparation. Firstly, the concentration of the monomer can be controlled. Secondly, the nature of the polymer matrix is determined by the choice of

comonomer and polymerisation method. Thirdly, the degree of cross-linking may be varied. Finally, an even distribution of the complex throughout the polymer is ensured which, in turn, allows a higher concentration of active sites, and therefore greater activity, than surface bound complexes. However, it is also possible that monomers containing transition metal complexes may undergo undesirable side reactions which preclude optimal catalytic performance.

The second polymer, (II) (Fig. 5.2), was prepared following the method outlined by Cavell and Masters [7]. This involved the immobilisation of the [Ni(SacSac)PPh_3Cl] complex onto a polystyrene polymer. Bonding to the polymer occurred through the phosphine ligand *via* a ligand displacement reaction.

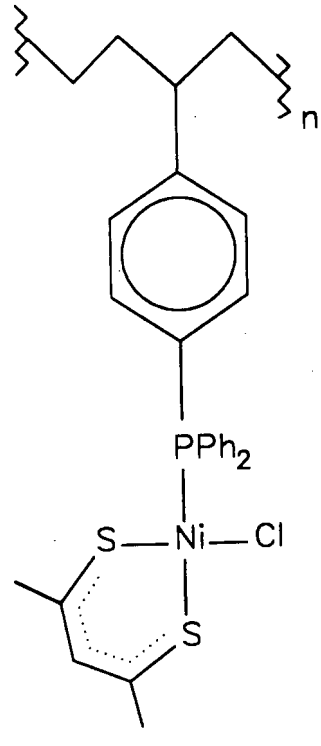

(II)

Figure 5.2 Structure of polystyrene supported nickel complex, (II).

The extensive use of phosphines for anchoring metals to supports may be attributed to the donor properties of ligands such as tertiary phosphines which usually offer sufficient ligand strength to prevent

complexes from dissociating. Furthermore, phosphines provide steric and electronic environments important to reaction dynamics.

Several spectroscopic techniques are necessary in order to fully characterise polymer supported catalysts. Infrared spectroscopy has been found to be the most powerful as characteristic bands may be identified and species present in low concentration may be detected [10]. Raman spectroscopy has yet to be successfully applied to these catalysts due to the low concentration of the metal species and the fluorescence associated with the support. ^{31}P NMR has been used to characterise various phosphine bound rhodium species [11]. However, this technique is not successful with typical polymer supports, since the environment around the phosphorus is not uniform and they have low phosphorus loadings. The EXAFS technique is potentially valuable for structural characterisation. For example, an EXAFS study of a polymer bound rhodium complex established the Rh-Cl and Rh-P interatomic distances which are in agreement with those determined by X-ray crystallography of the molecular complex [12]. Finally, polymers have been analysed using electron microprobe techniques to determine profiles of metal and functional groups [13]. This technique allows quantitative analysis of a 1 μm^3 volume of catalyst and may therefore indicate the uniformity of the incorporation of the complex into the support.

Several complex catalysts, active in the homogeneous oligomerisation of olefins, have been heterogenised onto supports and their activities recorded. Cavell and Masters [7] supported the highly active [Ni(SacSac)(PPh_3)Cl] catalyst through a phosphine linkage to both organic and inorganic matrices. In each case the supported complex exhibited reduced propene oligomerisation activity but extended lifetime. The product selectivity differed for each catalyst system. Peuckert and Keim [14] studied the oligomerisation of ethene over polymer bound nickel phosphine complexes. When silica and silica-alumina were used as supports, their acidity functions caused the oligomerisation activity to exceed that of the homogeneous system, but selectivity to linear products was lowered due to enhanced double bond isomerisation. The use of polystyrene supports enhanced activity and lead to >95% selectivity to linear products. Metal leaching occurred when the complex was bound to the resin through the phosphine ligand

[Fig. 5.3(b)] but not when it was bound through the chelating ligand [Fig. 5.3(a)].

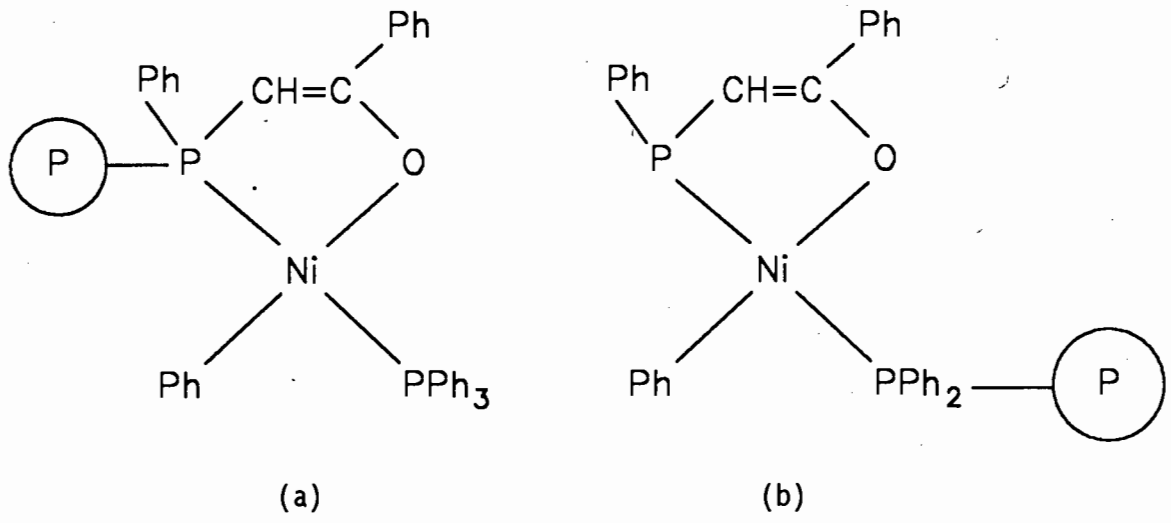

Figure 5.3 Alternative modes of binding to polystyrene [14].

The results of Zhou *et al.* [15] are also of interest. When a nickel β-ketoenolate complex was supported on SiO_2, they observed that, while activity was less than half that of the analogous homogeneous system, the specificity to linear products was retained. This specificity was absent when Al_2O_3 was used as a support due to the acidity of Al_2O_3.

In this work, the polymeric complexes prepared above, and their homogeneous precursors, have been investigated as catalysts for the oligomerisation of 1-hexene using both $AlEt_3$ and $AlEtCl_2$ co-catalysts. Finally, the active polymer (I) and its precursor complex (III) (shown in Fig. 5.4 [page 5-7]) have been tested with propene feed in order to ascertain detailed product selectivities.

5.2 EXPERIMENTAL

5.2.1 Preparation of Polymers

All solvents used were analytical grade. Once prepared, the compounds were filtered, washed and dried over silica gel at reduced pressure. After each step the isolated product was fully characterised.

5.2.1.1 Preparation of [*Bis*(*p*-Hydroxyphenyl-1,3-butanedionato)M(II)] (M = Ni, Cu, Zn) and the Polymeric Nickel Complex, (I)

A scheme for the preparations of the nickel chelate (III) and the nickel epoxy polymer (I) is shown in Fig. 5.4.

p-*Acetoxyacetophenone*

p-Hydroxyacetophenone (0.0367 mol) was dissolved in a solution of NaOH (0.0734 mol) in water (20 ml). Acetic anhydride (0.734 mol) and ice were added and the mixture shaken. A granular white solid precipitated which was filtered and washed with ice water.

p-*Hydroxyphenyl-1,3-butanedione*

BF_3(g) was passed into acetic acid (0.5 mol) at 0°C until solidification occurred. Dichloroethane (20 ml) was added to facilitate stirring. A mixture of *p*-acetoxyacetophenone (1 mol) and acetic anhydride (2 mol) was added over 4 minutes. The resulting yellow solution was stirred for 2.5 hours after which it was added to a solution of sodium acetate (4 mol) in water (500 ml). The dichloroethane and some water were removed under reduced pressure and the remaining solution boiled under reflux for 40 minutes. After cooling, the solid was collected by filtration. The filtrate was adjusted to pH 5 by addition of aqueous sodium bicarbonate and subsequently extracted 3 times with ether. The red extracts were combined with the solid and extracted 3 times with 5% w/v

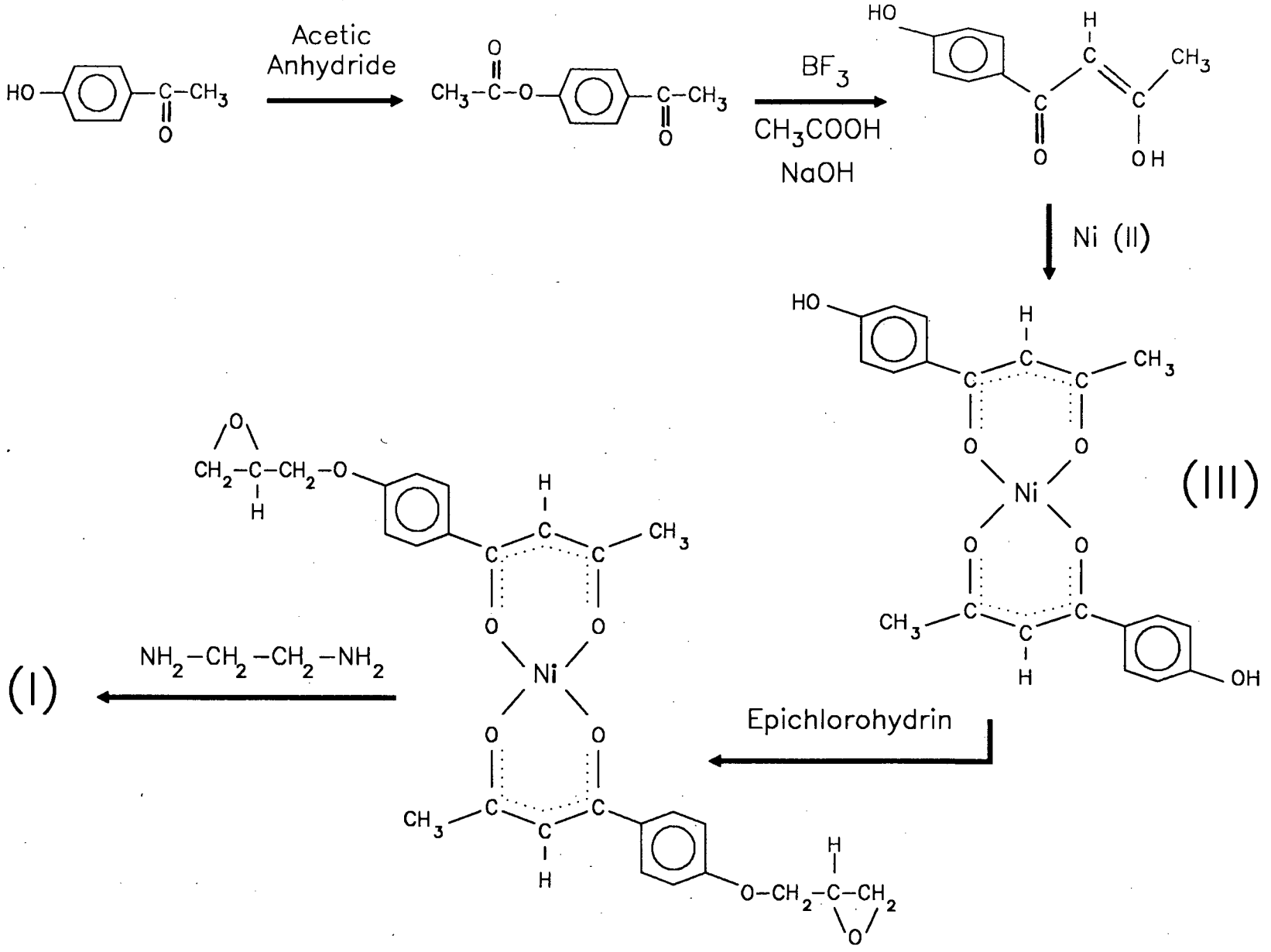

Figure 5.4 Scheme for the preparation of nickel chelate (III) and polymer (I).

NaOH. The resulting solution was acidified with dilute HCl to yield an orange precipitate. Recrystallisation from boiling benzene led to pure red needles.

*[(*p*-Hydroxyphenyl-1,3-butanedionato)M(II)]*

M = Ni [complex (III)]

p-Hydroxyphenyl-1,3-butanedione (0.02 mol) was dissolved in hot methanol (8 ml) and added to nickel acetate (0.01 mol) in hot water (45 ml). A precipitate formed immediately. The mixture was stirred and heated for 30 minutes and then filtered while hot and the product washed with water. The dried product was green and microanalysis revealed two water molecules associated with the compound. When dried under reduced pressure at 80°C the water molecules were removed and the complex turned brown.

M = Cu

p-Hydroxyphenyl-1,3-butanedione (2 mmol) was dissolved in warm methanol (2 ml) and added to a solution of copper(II) nitrate (1 mmol) in water (2.5 ml) and concentrated ammonia (0.36 ml). The resulting precipitate was filtered and washed with water. No further purification was necessary.

M = Zn

p-Hydroxyphenyl-1,3-butanedione (2 mmol) was dissolved in a minimum of hot methanol and added to a solution of zinc acetate (1 mmol) in water (5 ml). The resulting mixture was stirred and heated for 30 minutes after which the solid was filtered hot and washed with water.

Nickel Epoxy Resin

The nickel complex (III) was suspended in water (16 ml) and heated to 50°C. Aqueous 1M NaOH (9.4 ml) was added causing partial dissolution of the nickel chelate. Epichlorohydrin (9.7 mmol) was added and the solution stirred for 30 minutes after which time a pale green precipitate had formed. Further 1M NaOH (aq) (1 ml) was added and the solution stirred for 3 hours. The precipitate was filtered and washed with water until the washings were neutral.

Polymer (I)

The epoxy resin (3.4 mmol) was suspended in dioxane at 60°C. Gradual addition of ethylenediamine (6.8 mmol) in dioxane and subsequent stirring at 60°C for 4 hours, resulted in a yellow powder. To effect cross-linking, the powder was refluxed in dioxane for 4 hours. At the end of this time the polymer had formed as a brown oil. The supernatant was removed and the polymer dried and crushed to a powder.

5.2.1.2 Preparation of the Polystyrene Supported Polymer, (II)

A scheme for the preparation of polymer (II) is shown in Fig. 5.5.

Polystyrene polymer, 2% cross-linked with divinylbenzene and functionalised with PPh_3 at a concentration of 0,00306 mol PPh_3/g polymer, was purchased from Aldrich Chemie GmbH. [Ni(SacSac)(PPh_3)Cl] was prepared as outlined in Section 3.2.2.5.

[Ni(SacSac)(PPh_3)Cl] (4.5 mmol) was dissolved in deoxygenated benzene (50 ml). Sufficient PPh_3-functionalised polystyrene polymer (2.0 g) was added to the solution which was then refluxed for 48 hours. The dark brown, polymer supported nickel complex (II) was filtered and washed with benzene until the washings were colourless.

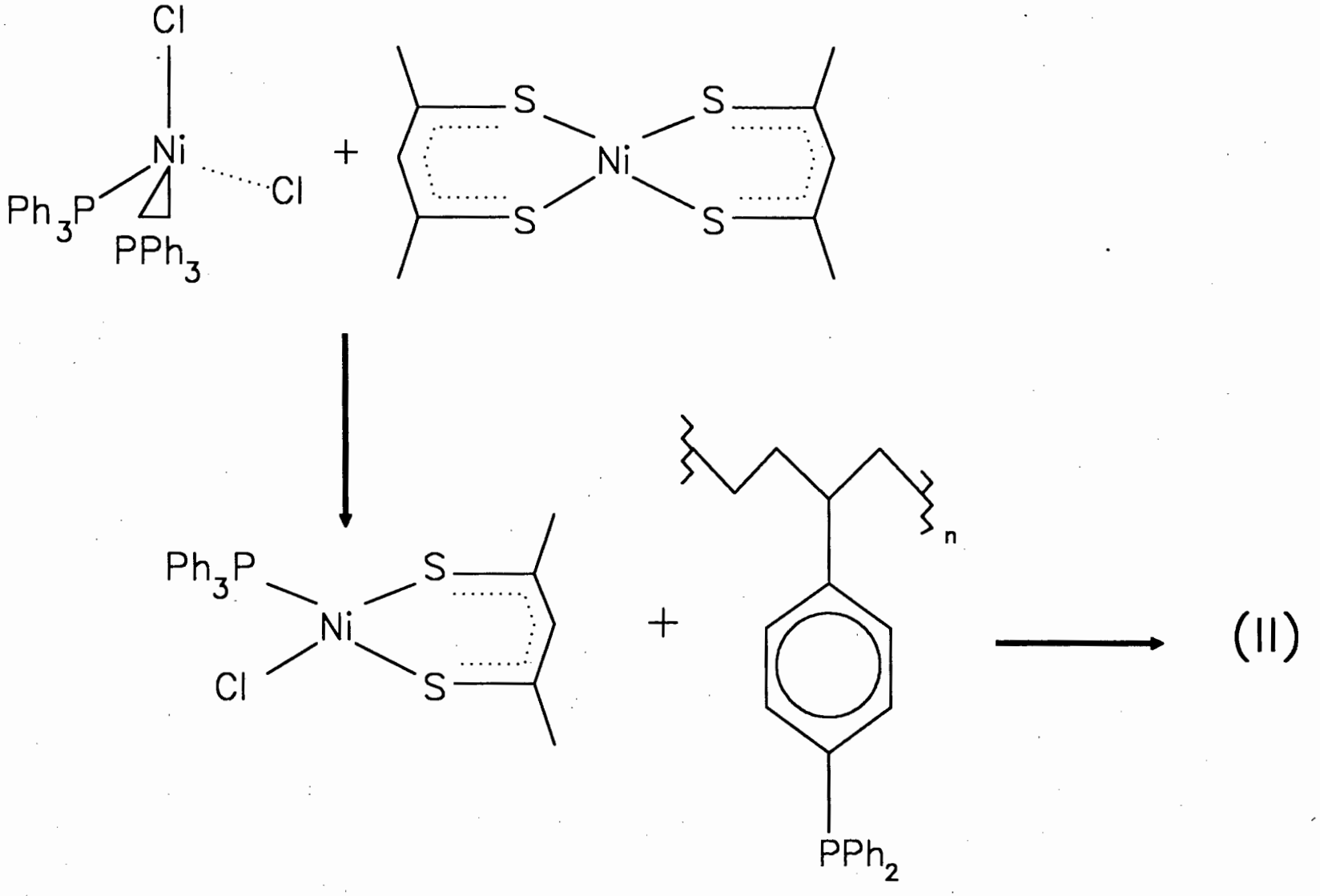

Figure 5.5 Scheme for the preparation of polymer (II).

5.2.2 Thermal Analyses

The polymer sample (10 mg) was placed in a furnace and the temperature raised from 40°C to 850°C at 10°C/minute in flowing air (30 ml/min). The mass losses are recorded as a percentage of the initial sample mass.

5.2.3 Energy Dispersive X-ray Analysis (EDX)

An aluminium electron microscopy stub was coated with a mixture of a thick graphite emulsion and waterbased glue. The sample was sprinkled onto this base and coated with a splattering of carbon. The analysis was performed at the following settings:

HD = 25 mm (Horizontal distance from sample to detector)
WD = 23.5 mm (Working distance between final lens and sample)
TILT = 20° (Tilt angle of stub)
THETA = 70° (Angle of incidence)
WT = 26 (A factor used in background removal)
E_o = 20 kV (Accelerating voltage)

Spectra were acquired for 125 s. The nickel kα peak (covered by a window from 7.26-7.66 keV) was ratioed against a background window (6.66-7.06 keV). Three spectra were acquired for each standard and six for each unknown sample and the values obtained averaged.

5.2.4 Catalysis

5.2.4.1 1-Hexene Oligomerisation

Experimental procedure and product analysis was carried out as described in Section 2.2.2. The insoluble polymers were slurried in the toluene solvent prior to the addition of the co-catalyst.

5.2.4.2 Propene Oligomerisation

The reactions were carried out as for 1-hexene oligomerisation but using a feed of Sasol off-gas consisting of 85% propene and 15% propane by mass. Unlike the 1-hexene oligomerisation reactions, this was done on a continuous basis. The reaction mixture was saturated with dry, deoxygenated feed prior to the introduction of the co-catalyst. After the addition of the co-catalyst the feed was constantly bubbled into the reaction mixture to ensure the continued presence of excess propene available for reaction.

Analysis of the effluent gas and feed streams was performed on a Gow-Mac 750p gas chromatograph using a 6.35 mm I.D., 3 m long, stainless steel column packed with *n*-Octane/Porasil C.

The following settings were used:

Detector	Flame Ionisation
Flowrates: N_2	41.2 ml/min
H_2	30.8 ml/min
Air	297.0 ml/min
Injector temperature	150°C
Detector temperature	250°C
Column temperature	Isothermal 50°C (28 min)
Sample volume	10 μl

Identification of C_6 isomers was carried out by Mr R. Forrester of the CSIR using a 50 m long capillary column coated with a 1 μm film of BP-1 (equivalent to OV-1). The following settings were used:

Detector	Flame Ionisation
Flowrate He(carrier)	23.2 cm/s
Injector temperature	200°C
Detector temperature	250°C
Column temperature	Isothermal 30°C until all C_6's had eluted
Sample volume	0.5 μl
Split ratio	45:1

5.2.4.3 Propene Oligomerisation at Variable Temperature

Runs at temperatures other than 40°C, were carried out in a stainless steel autoclave. Toluene solvent (150 ml) and the nickel catalyst were placed in the autoclave under argon and the required temperature established. The co-catalyst was then added and the autoclave pressurised with dry propene (8 atm). When the pressure dropped to below 4 atm further propene was admitted. Samples were taken at intervals by means of a stainless steel sampling tube attached to an exit valve.

5.2.4.4 Propene Oligomerisation at High Pressure and High Temperature

The reactor system used for propene oligomerisation is shown schematically in Fig. 5.6. Calcination of the catalyst (1 g) took place at 80°C under reduced pressure (1 mmHg) for 2 hours in a 2 x 20 cm tubular stainless steel reactor **(7)** housed in a heated brass block. The feed, 85% propene and 15% propane by mass was stored as a liquid in a Cadac No. 7 domestic gas cylinder **(1)**. This was inverted to ensure that only liquid was released. Water and entrained impurities were removed from the feed by passing it over 3Å molecular sieves **(2)** and through a 0.5 μm filter **(3)**. A high pressure diaphragm pump **(5)** was used to obtain a reaction pressure of 30 atm. Axial temperature profiles were measured within the reactor by a movable thermocouple **(TI)**. After reaction the pressure was reduced to 1 atm and liquid and gaseous reaction products were collected in a liquid catchpot (15°C) **(10)** and a gas sampling loop, respectively **(12)**.

After calcination, the reactor was cooled to 50°C and propene was admitted. The temperature was raised 50°C every 2 hours until a final temperature of 300°C was reached. Samples were taken at hourly intervals.

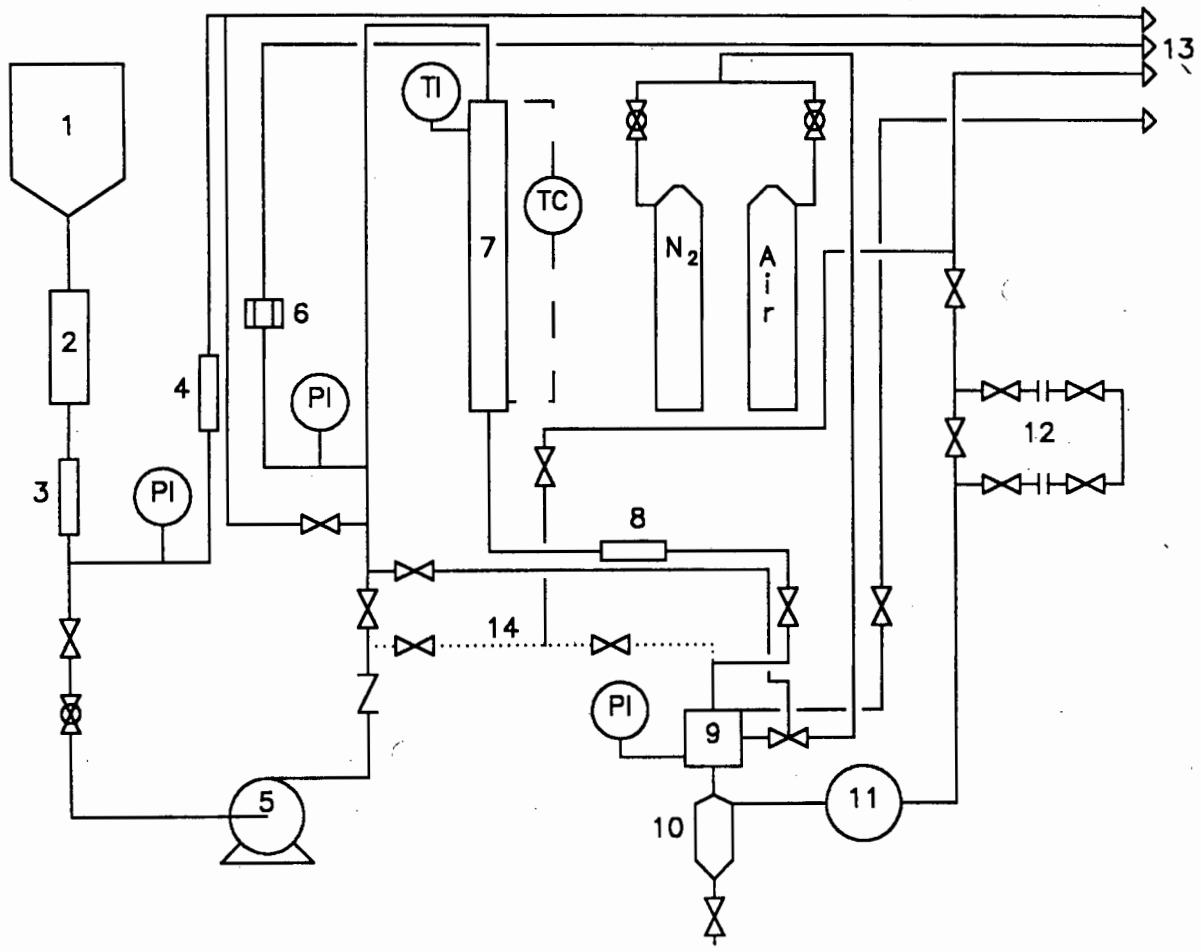

1. Feed cylinder
2. Molecular sieves (3Å)
3. 0.5 μm filter
4. Pressure relief valve
5. High pressure diaphragm pump
6. Bursting disc
7. Reactor
8. 0.5 μm filter
9. Back pressure regulator
10. Liquid catchpot
11. Wet gas flowmeter
12. Gas sampling loop
13. Flare lines
14. Bypass line

PI Pressure gauge
TI Temp. readout
TC Temp. controller

Figure 5.6 Diagram of a high pressure oligomerisation rig.

5.3 RESULTS

5.3.1 Microanalytical and EDX Data

Table 5.1 Microanalytical and EDX Data.

Compound	Calculated %C	%H	%N	%Ni[a]	Found %C	%H	%N	%Ni[a]
p-acetoxyacetophenone	67.4	5.7	-	-	67.4	5.5	-	-
p-OH-BA[b]	67.4	5.7	-	-	67.4	5.8	-	-
[Ni(*p*-OH-BA)$_2$]	58.2	4.4	-	13.6	57.7	4.1	-	13.8
[Cu(*p*-OH-BA)$_2$]	57.5	4.3	-	-	55.5	4.3	-	-
[Zn(*p*-OH-BA)$_2$]	57.2	4.3	-	-	56.7	4.9	-	-
Ni-epoxy resin	52.4	4.4	-	-	52.1	5.1	-	-
Polymer(I)	c	c	c	c	50.6	4.3	8.7	14.3
Polymer(II)					67.3	4.0	-	6.2
Polymer(I)[d]					20.8	4.8	2.0	3.5
Polymer(II)[d]					70.2	5.6	-	0.8

a - % Ni determined using EDX

b - *p*-OH-BA = *p*-hydroxyphenyl-1,3-butanedione

c - theoretical values are dependent on the degree of cross-linking which is not known

d - polymers isolated after catalytic runs

5.3.2. Infrared Data

Table 5.2 Infrared frequencies (cm^{-1}) and assignment of characteristic vibrations for the polymeric complex, (I), and its precursors.

p-A-AP	*p*-OH-BA	[M(*p*-OH-BA)$_2$]			Epoxy resin	Polymer (I)	Assignment
		M = Ni	Cu	Zn			
3488							
3335					3401br		
	3181	3318	3304	3294			νO-H
						3281	νN-H
						3164	
3101					3070		
3071	3000	3076br	3050br	3100br	2990	2928	νC-H
2999					2927	2881	
1775					1730w	1745w	
1753					1709w	1705w	
1713					1666	1659	
1674		1611	1609	1610	sh		
1638	1610	1600	1593	1600	1590	1590	νC=O
1596	1591	sh		1569	1562	1563	
1585	1550	1549	1534br	1546	sh		
		1526		1528	1521	1518	
1502	1512	1501	1505	1501	1497	1491	νC=C
1423		1446	1440	1448	sh	sh	
1412	1412				1419	1418	
1368	1367	1384	1386	1383	1393br	1396	
1356	1357	1311	1316	1311	1302	1300	
1297	1286	1276	1289	1274	1270	1270	
1266	1260	1238	1250	1239	1251	1247	
1216	1219	1215	1208	1213	1214	1208	
1196	sh	1176	1172	1175	1173	1168	
1167	1169	1119	1123	1118	1118	1114	
1105	1113	sh	sh	sh	sh	sh	
1074	1098	1060w	1075w		1072w	1079	
1041	1076				1031		glycidyl
1022	1007	1011	1018	1008	1009	1021	ρCH$_3$

Table 5.2 Contd...

p-A-AP	*p*-OH-BA	[M(*p*-OH-BA)$_2$]			Epoxy resin	Polymer (I)	Assignment
		M = Ni	Cu	Zn			
1012	1002						
958	965	957	959	954	955	960	
			939		912	886	
914	850	860	863	859	858	869	
853	826	843	841	843	841	841	
833	817	827sh	sh				
802	784	778	781	781	770	767	
	771	748w	752	747w			
738	750						
632	735	697	699	697	697	698	
		648	665	644	657	655	ring def
624	637	637		637	633	632	
		607	601	601	601	611	ring def
592	592	590		577	590	583	
560	548						
494	510						
472	501	501	502	499	501	501	
398	481	450	480	447	480		
		435	469	430	435	429	νM-O
		350	379	334	380		
309	424	316	319	309			
282	318	298	309		300w		
		271	293	246	270	276	νM-O
		223sh	253				
			242				
		207	205	202			
			165	166			
		151	135	147			
		89	91	91			
		68	64				

p-A-AP = *p*-acetoxyacetophenone

p-OH-BA = *p*-hydroxyphenyl-1,3-butanedione

br = broad, w = weak, sh = shoulder

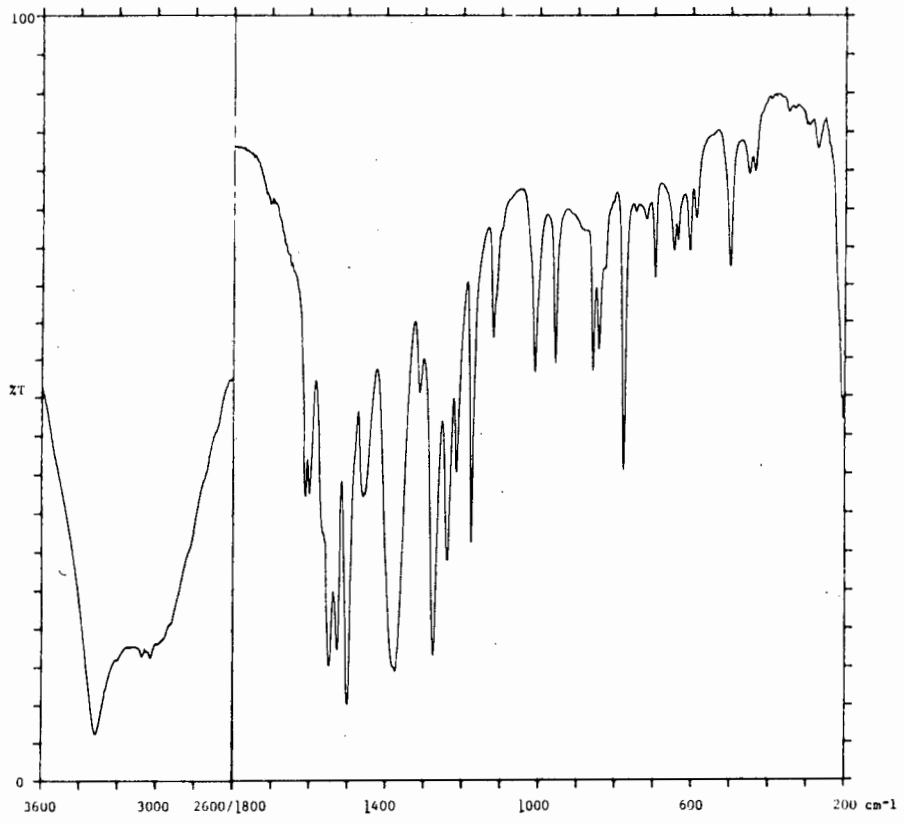

Figure 5.7(a) Mid-infrared spectrum of [Ni(*p*-OH-BA)$_2$(H$_2$O)$_2$]. HCBD: 3600-2600 cm^{-1}, Nujol 1800-200 cm^{-1}

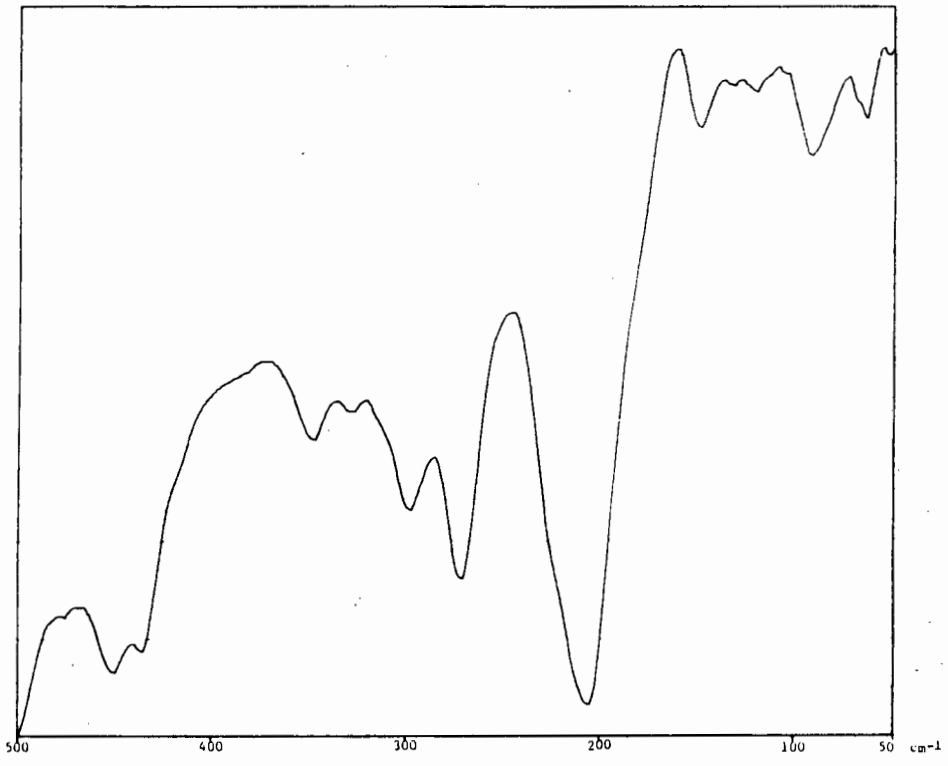

Figure 5.7(b) Far-infrared spectrum of [Ni(*p*-OH-BA)$_2$(H$_2$O)$_2$].

Table 5.3 Far-infrared frequencies (cm^{-1}) and assignments for the polystyrene supported complex (II), and its precursor, [Ni(SacSac)(PPh_3)Cl].

[Ni(SacSac)(PPh_3)Cl]	Polymer (II)	Assignment
497	489	phosphine ligand
477	469	
457	464	
431	456	
421	422	
402	414	
381	386	νNi-S
358	371	δCCS
	346	
	338	
332	320	νNi-Cl
290	288	νNi-S
275	273	phosphine ligand
249	262	νNi-P
(249)	252	νNi-P/polymer
226	235	δNi-S
202	220	
197	183	δCPC
175	169	δNi-Cl
	159	
146	143	πCCS
	135	
	124	
111	112	δNi-P
105	108	
	93	
84	80	lattice + δCH_3
79	71	
55	60	

5.3.3 ^{1}H and ^{13}C NMR Data

Table 5.4 ^{1}H and ^{13}C NMR chemical shift data for *p*-acetoxyacetophenone.

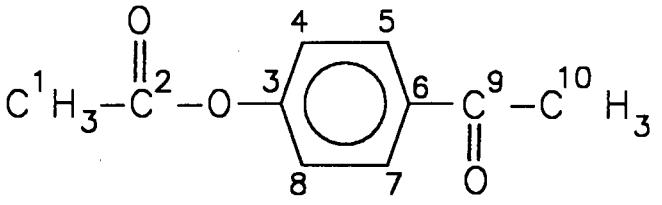

^{1}H NMR (ppm)*		^{13}C NMR (ppm)*	
$C^{1}H_3$	2.3	C^{1}	20.94
$C^{10}H_3$	2.5	C^{10}	26.61
$C^{5}H$, $C^{7}H$	8.1(doublet)	C^{5}, C^{7}	130.52
$C^{4}H$, $C^{8}H$	7.3(doublet)	C^{4}, C^{8}	122.75
		C^{3}	135.64
		C^{6}	155.43
		C^{2}	169.26
		C^{9}	196.80

* Spectra were run at ambient temperature using acetone-d_6 as reference and solvent

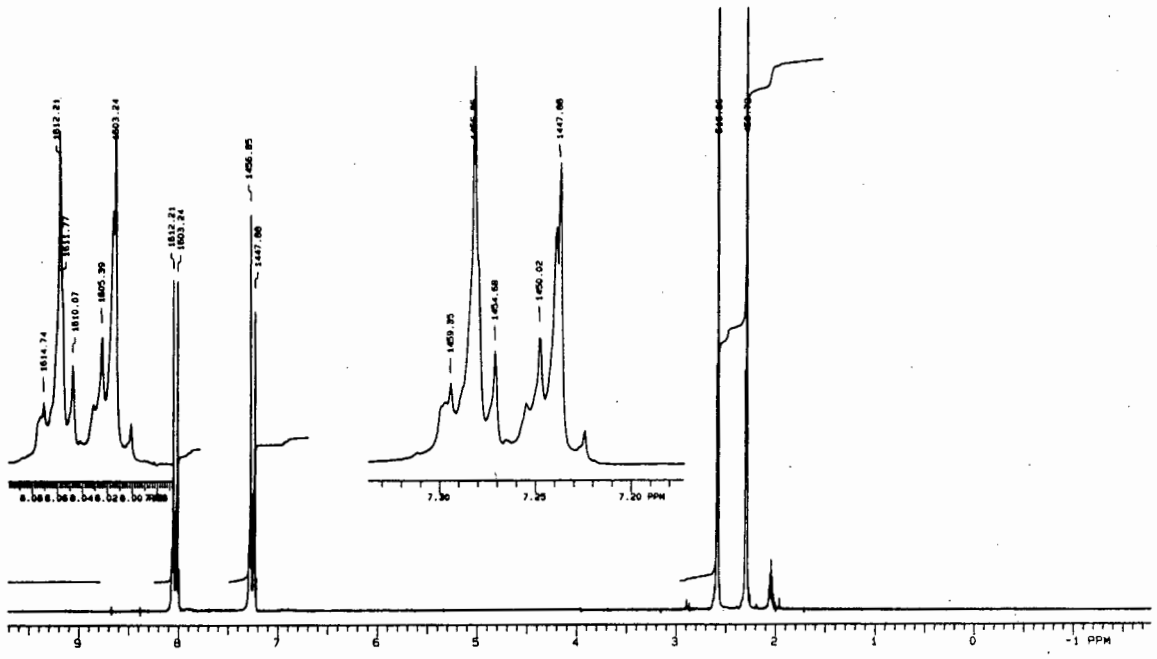

Figure 5.8(a) ^{1}H NMR spectrum of *p*-acetoxyacetophenone, (0-10ppm).

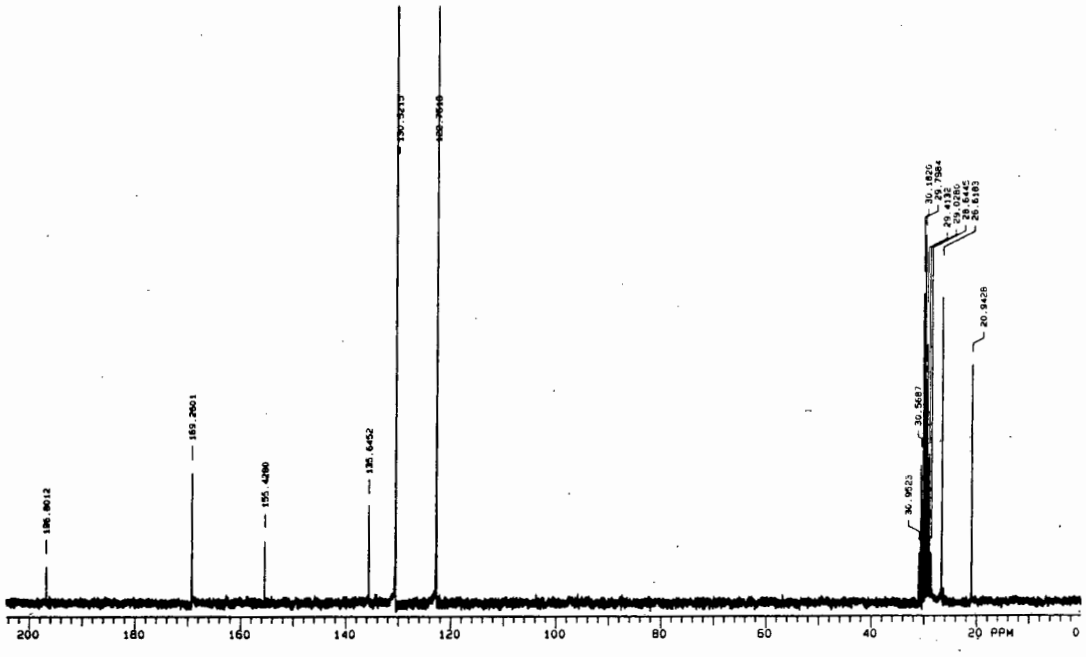

Figure 5.8(b) ^{13}C NMR spectrum of *p*-acetoxyacetophenone, (0-200ppm).

Table 5.5 ^{1}H and ^{13}C NMR chemical shift data for *p*-hydroxyphenyl-1,3-butanedione.

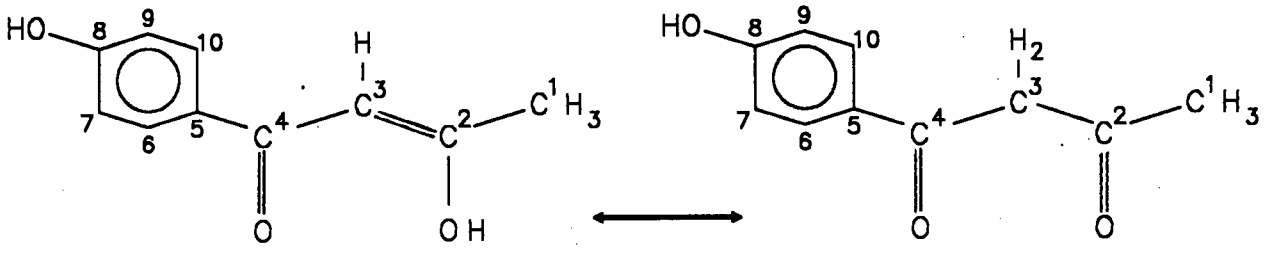

(a) (b)

^{1}H NMR (ppm)*		^{13}C NMR (ppm)*	
$C^{1}H_3$(a)	2.1	C^{1}	24.79
$C^{1}H_3$(b)	2.2		
$C^{3}H$(a)	6.3	C^{3}(a)	96.05
$C^{3}H_2$(b)	4.1	C^{3}(b)	54.30
$C^{7}H$, $C^{9}H$	7.9(doublet)	C^{7}, C^{9}	116.30
$C^{6}H$, $C^{10}H$	8.9(doublet)	C^{6}, C^{10}	130.25
OH	9.2	C^{5}	131.91
		C^{8}	162.48
		C^{4}	185,71
		C^{2}(a)	191.89

* Spectra were run at ambient temperature using acetone-d_6 as reference and solvent

5.3.4 Thermal Data

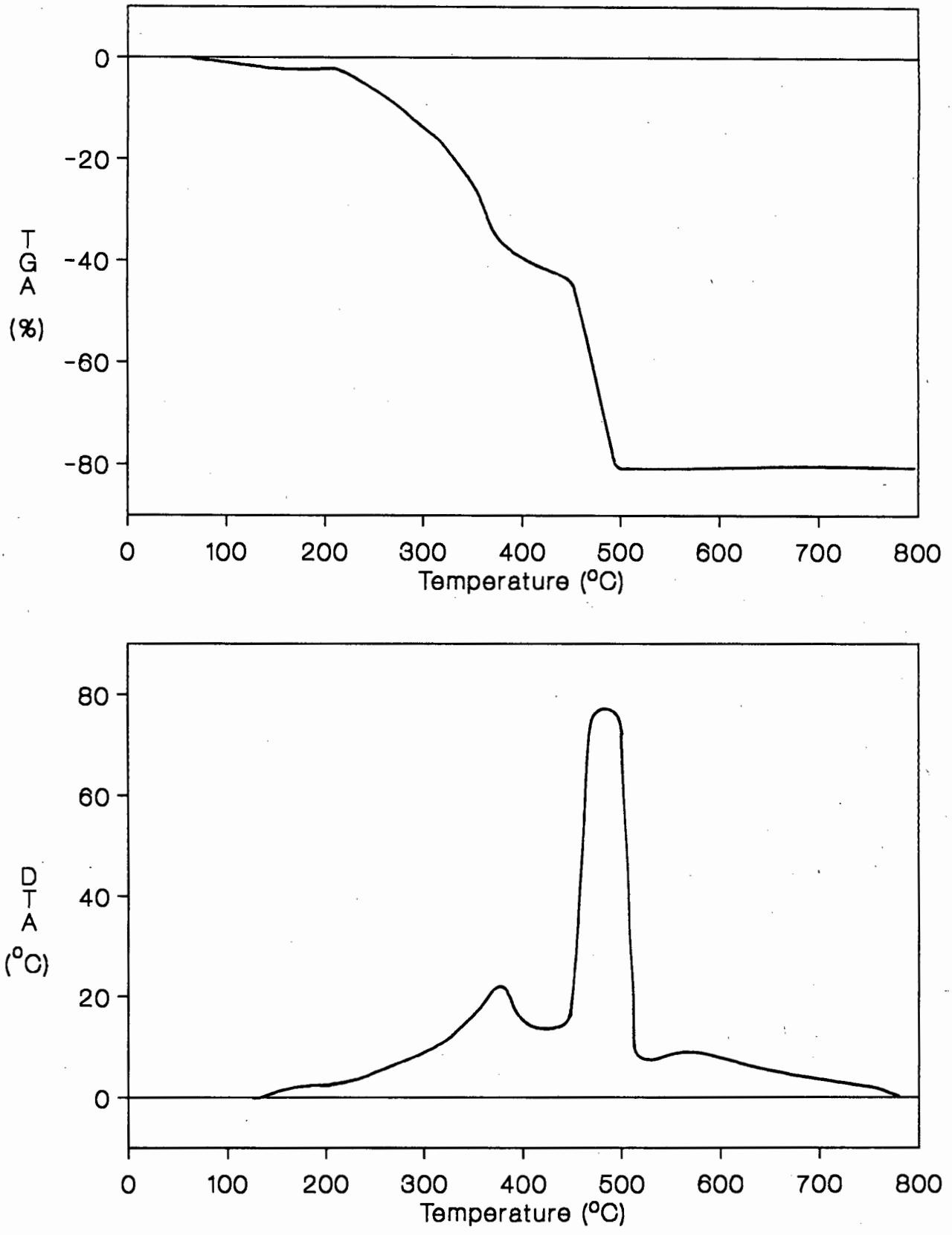

Figure 5.9 TGA and DTA curves for polymer (I).

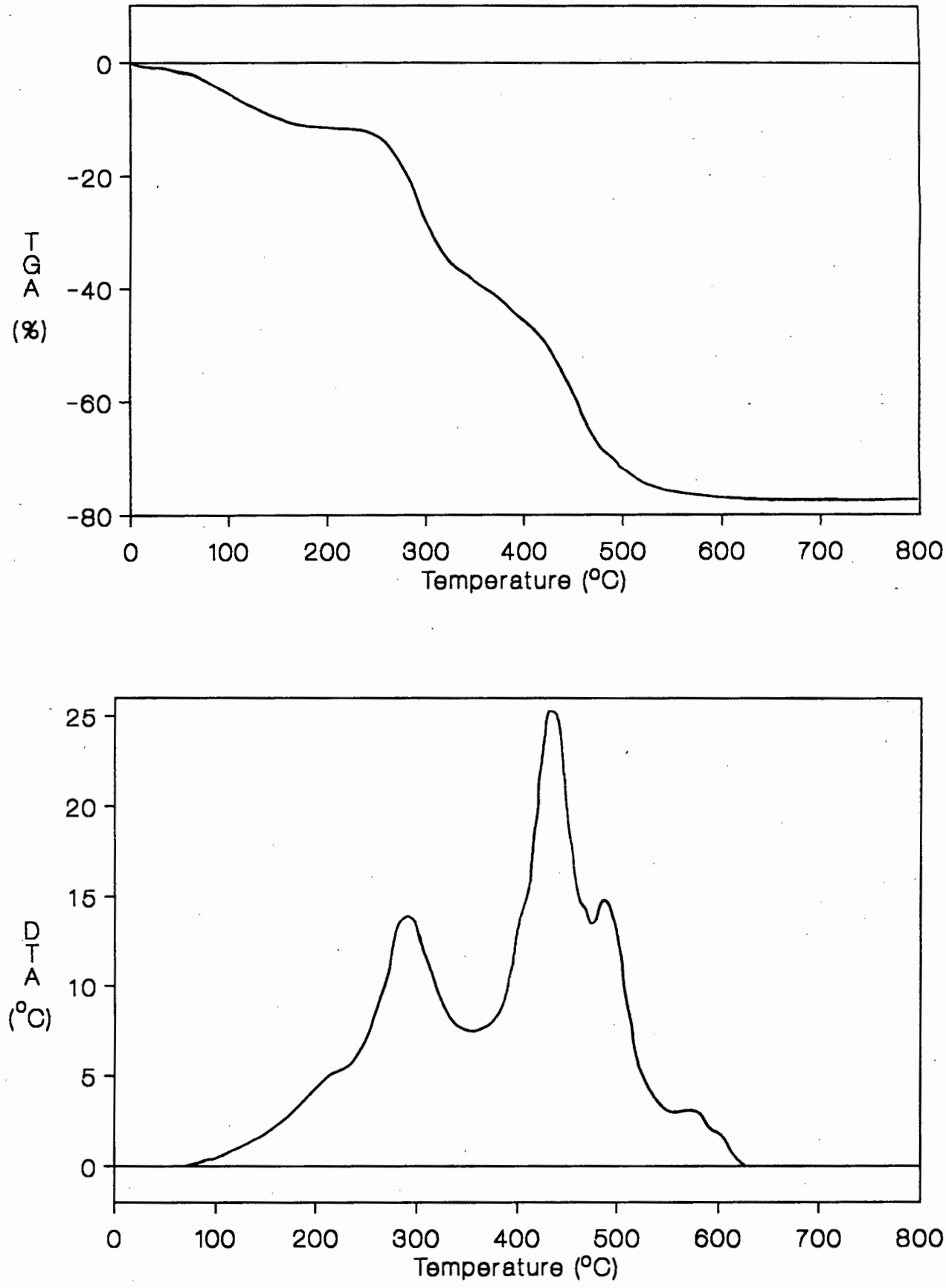

Figure 5.10 TGA and DTA curves for polymer (II).

5.3.5 Mass Spectra

Table 5.6 Fragmentation pattern of *p*-acetoxyacetophenone.

CH_3-C(O)-O-C_6H_5-O-CH_3

Mass	Fragment
178	M^+
136	$[CH_3\text{-}C(O)\text{-}O\text{-}C_6H_5]^+$
121	$[C(O)\text{-}O\text{-}C_6H_5]^+$
93	$[O\text{-}C_6H_5]^+$
77	$[C_6H_5]^+$

Table 5.7 Fragmentation pattern of *p*-hydroxyphenyl-1,3-butanedione.

HO-C_6H_5-C(O)-CH=C(OH)-CH_3

Mass	Fragment
178	M^+
163	$[O\text{-}C_6H_5\text{-}C(O)\text{-}CH\text{-}C(OH)]^+$
121	$[O\text{-}C_6H_5\text{-}C(O)]^+$
93	$[O\text{-}C_6H_5]^+$
77	$[C_6H_5]^+$

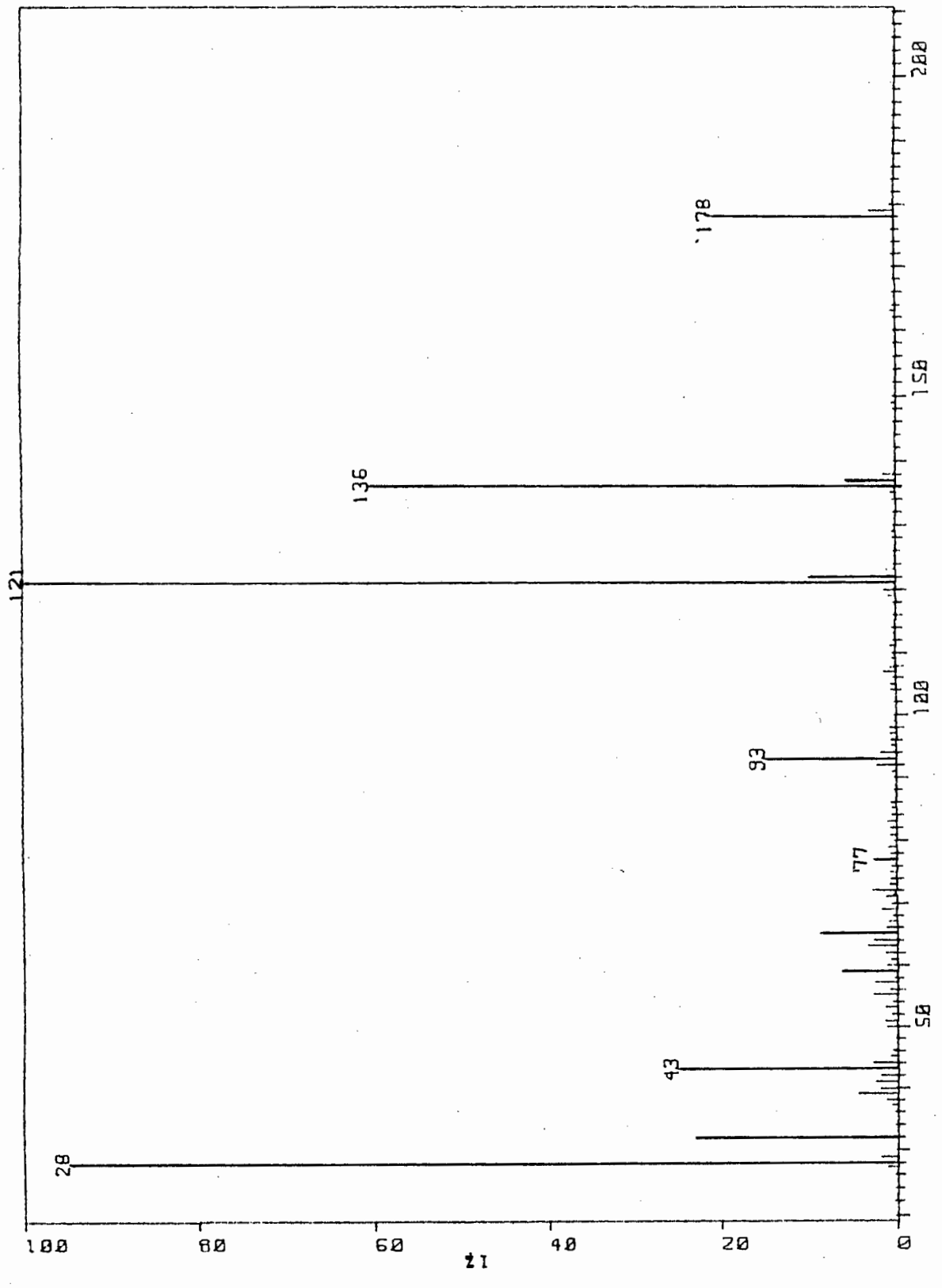

Figure 5.11 Fragmentation pattern of *p*-acetoxyacetophenone (molar mass = 178).

Table 5.8 Fragmentation pattern of the nickel chelate (III).

$[Ni(HO\text{-}C_6H_5\text{-}C(O)\text{-}CH{=}C(O)\text{-}CH_3)_2(H_2O)_2]$

Mass	Fragment
178	$[HO\text{-}C_6H_5\text{-}C(O)\text{-}CH\text{-}C(OH)\text{-}CH_3]^+$
163	$[HO\text{-}C_6H_5\text{-}C(O)\text{-}CH\text{-}C(OH)]^+$
121	$[HO\text{-}C_6H_5\text{-}C(O)]^+$
93	$[HO\text{-}C_6H_5]^+$
77	$[C_6H_5]^+$

5.3.6 Catalytic Run Data

Each of the Tables below represents the data accumulated by gas-liquid chromatographic analysis of the liquid samples taken at various time intervals during the catalytic run. The catalyst, co-catalyst and relative molar amounts of each are given above each Table. Except where otherwise specified, runs were carried out at 40°C and 1 atm.

5.3.6.1 1-Hexene Oligomerisation (Batch Runs)

Each % value in the Tables is the percentage of the total mass of olefins present in the sample.

Table 5.9 Nickel chelate (III) : $AlEtCl_2$ = 1 : 10

Time(min)	%1-hex[a]	%3-hex	%*tr*-2-hex	%*cis*-2-hex	$\%C_{12}$
0	100.0	-	-	-	-
10	2.3	6.0	21.8	5.8	64.1
30	0.5	5.3	19.0	2.9	70.0
60	0.4	4.5	17.6	4.5	73.0
120	0.4	3.6	17.4	4.2	74.4
240	0.3	4.1	15.5	4.0	76.1
480	0.3	4.0	14.0	3.6	78.2
1260	0.3	3.6	12.5	3.1	80.6

[a] hex = hexene
tr = *trans*

Table 5.10 Polymer (I) : $AlEtCl_2$ = 1 : 10

Time(min)	%1-hex	%3-hex	%*tr*-2-hex	%*cis*-2-hex	$\%C_{12}$
0	100.0	-	-	-	-
10	1.2	16.0	57.9	15.1	9.9
30	1.0	12.7	45.6	12.1	28.6
60	0.8	10.7	37.7	9.9	40.9
120	0.8	9.8	34.8	9.1	45.6
240	0.6	7.3	26.6	6.9	58.6
480	0.5	5.7	20.8	5.4	67.6
1020	0.4	5.0	18.5	7.7	71.7

Table 5.11 Polymer (II) : $AlEtCl_2$ = 1 : 10

Time(min)	%1-hex	%3-hex	%*tr*-2-hex	%*cis*-2-hex	$\%C_{12}$
0	100.0	-	-	-	-
10	65.4	3.2	18.3	1.2	1.6
30	3.2	7.7	36.4	22.6	9.8
60	1.2	11.6	57.4	14.0	15.9
120	1.0	12.4	44.6	11.5	30.5
240	0.7	8.6	30.2	7.8	53.1
480	0.5	6.1	21.9	5.7	65.8
1260	0.4	5.2	18.6	5.0	70.3

5.3.6.2 Propene Oligomerisation (Continuous Runs)

Due to the irregular structures of the polymers, the results are expressed as grams of product per gram of nickel (gC_x/gNi). Examples of original spectra are given in Appendix III.

Table 5.12 Nickel chelate (III) : $AlEtCl_2$ = 1 : 10

Time(min)	gC_6/gNi	gC_9/gNi	gC_{12+}/gNi
0	0.0	0.0	0.0
20	135.7	16.3	4.3
40	214.1	35.8	6.9
60	292.7	49.3	9.0
120	324.6	63.0	21.7
240	340.2	63.7	24.0
330	355.0	67.6	26.0
420	358.0	70.0	27.7

Table 5.13 Polymer (I) : $AlEtCl_2$ = 1 : 10

Time(min)	gC_6/gNi	gC_9/gNi	gC_{12+}/gNi
0	0.0	0.0	0.0
20	30.5	2.0	1.0
40	59.5	4.0	2.7
60	95.8	5.5	3.0
120	125.0	6.8	3.5
240	250.0	8.5	4.0
360	357.5	10.0	4.3
420	381.3	10.5	4.6
630	395.0	10.9	4.8
720	430.0	11.5	4.9

Table 5.14 Polymer (II) : $AlEtCl_2$ = 1 : 10

Time(min)	gC_6/gNi	gC_9/gNi	gC_{12+}/gNi
0	0.0	0.0	0.0
20	37.3	2.1	1.8
40	67.6	4.5	2.1
90	137.3	5.6	2.3
150	173.5	6.2	2.8
210	200.0	6.7	3.3
270	203.7	6.9	3.5
510	212.4	7.0	3.7

Table 5.15 Polymer (I) : $AlEtCl_2$ = 1 : 10
Temperature = 100°C, Pressure ~ 6 atm.

Time(min)	gC_6/gNi	gC_9/gNi	gC_{12+}/gNi
0	0.0	0.0	0.0
10	744.3	7.1	0.0
30	925.5	15.2	3.2
60	1310.3	24.4	8.7
120	1629.8	44.1	17.0
180	1713.3	44.2	20.0
900*	1629.1	167.0	28.7

* - system was sealed and left stirring overnight at 100°C

Table 5.16 Polymer (I) : $AlEtCl_2$ = 1 : 10
Temperature ~ -40°C, Pressure ~ 6 atm.

Time(min)	gC_6/gNi	gC_9/gNi	gC_{12+}/gNi
0	0.0	0.0	0.0
240	0.0	0.0	0.0

Neither polymer (I) nor polymer (II) was active when tested between 50 and 300°C at 30 atm without co-catalyst or solvent.

5.4 DISCUSSION

5.4.1 Infrared Spectra

5.4.1.1 Epoxy Polymer(I) and Precursor Complexes

The infrared spectra listed in Table 5.2 show characteristic peaks by which the ligands and complexes may be identified. On converting *p*-acetoxyacetophenone to *p*-hydroxyphenyl-1,3-butanedione, a large peak at 3181 cm^{-1} appears. This is the νO-H mode. νC=O occurs at 1610 cm^{-1} for *p*-hydroxyphenyl-1,3-butanedione and this band is shifted 10 cm^{-1} to lower wavenumber after complexation with a metal ion has occurred.

In the metal complex spectra, characteristic νC=O and νC=C vibrations are observed near 1600 and 1500 cm^{-1}, respectively. These vibrations are also observed in the epoxy resin and the final polymer product, indicating that the ligand is not decomposed and is still complexed to the metal. Of most interest are the M-O stretching vibrations which are easily assigned by comparison with the β-ketoenolate complexes discussed in Chapter 2. These assignments are further supported by the observed shifts on substituting copper and zinc for nickel. If all three complexes were square planar then the νM-O frequencies would be expected to appear in the order Ni > Cu > Zn. Two water molecules are associated with the nickel complex. The observed νM-O frequency order Ni < Cu > Zn, suggests that this water is coordinated to the nickel complex resulting in an octahedral conformation. νM-O in the spectrum of *trans*-$[Ni(acac)_2(H_2O)_2]$ is observed at 427 cm^{-1}. This mode is shifted to 454 cm^{-1} on substitution of copper for nickel. The analogous band in the spectrum of the nickel chelate complex (III) is observed at 435 cm^{-1} and is shifted to 469 and 430 cm^{-1} on substitution of nickel by copper and zinc, respectively. A second νM-O vibration observed at 271 cm^{-1}, is observed at 255 cm^{-1} for *trans*-$[Ni(acac)_2(H_2O)_2]$.

The far-infrared spectra of the epoxy resin and the polymer (I) are more complex and the absorption peaks less resolved. However, the νM-O bands at 435, 270 cm^{-1} and 429, 276 cm^{-1} in the spectra of the epoxy resin and

polymer (I), respectively, are similar to the νM-O frequencies recorded for the nickel chelate (III). This suggests that the nickel environment is relatively unchanged.

The bands at 3281 and 3165 cm^{-1} are assigned to the antisymmetric and symmetric N-H stretches in (I) which do not occur in the spectrum of the precursor (III). The presence of medium intensity νN-H modes indicates that a limited degree of cross-linking has been achieved and suggests that a low molecular weight polymer has formed. The absence of any bands which may reasonably be assigned to νNi-N eliminates the possibility of ethylenediamine being coordinated to the metal.

Of additional interest is the appearance of a strong vibration at 1031 cm^{-1} in the spectrum of the epoxy resin. This is characteristic of the glycidyl group and is absent from the spectrum of the final polymer.

5.4.1.2 Polymer (II) and the Precursor Complex, [Ni(SacSac)(PPh_3)Cl]

The far-infrared spectrum of the complex [Ni(SacSac)(PPh_3)Cl] has been assigned in Chapter 3. A similar band pattern is observed for the polystyrene supported complex (II), and assignments are made accordingly. The presence of added bands in the spectrum of the polymer may be attributed either to polystyrene modes or to distortion of the square planar symmetry of the supported complex.

5.4.2 NMR Spectra

Each spectrum clearly reflects the structure of the compound. (See Tables 5.3 and 5.4). Assignments are made with reference to the index compiled by Bremser *et al.* [16]. For *p*-acetoxyacetophenone, the methyl peak adjacent to the acetyl group, CH_3-CO-O-, is assigned upfield of the analogous peak for the group, CH_3-CO-, due to the inductive effect of the extra oxygen atom which shields adjacent atoms. Furthermore, the presence of a carbonyl group adjacent to the phenyl ring results in deshielding of C^5 and C^7 relative to C^4 and C^8.

Assignment of the spectrum of *p*-hydroxyphenyl-1,3-butanedione is complicated by the presence of both enol(a) and keto(b) tautomers. In the ^{1}H NMR, the fact that the $C^{3}H$ resonance (6.3 ppm) integrates for more protons than $C^{3}H_{2}$ (4.1 ppm), indicates that the enol tautomer predominates in acetone solution. In the ^{13}C NMR, replacement of the acetyl group of *p*-acetoxyacetophenone by a hydroxyl moiety results in an upfield shift of the C^{6}, C^{10} resonance. The C^{2}(b) resonance, which is expected to occur near 200 ppm [16], is absent. This is not unexpected as quaternary carbon resonances are usually weak and only a small amount of the compound is in the keto form.

The limited solubility of the nickel complex (III) and the polymers (I) and (II) precluded characterisation by solution NMR.

5.4.3 Thermal Analyses

Thermogravimetric analyses indicate the degree of thermal stability of the polymers. High stability allows the use of elevated reaction temperatures often desirable for less active heterogeneous systems.

The TGA/DTA curves for (I) and (II) are shown in Figs. 5.9 and 5.10, respectively. While the epoxy polymer (I), appears to be largely stable up to 200°C, the polystyrene supported complex (II), exhibits mass loss at much lower temperatures (50°C). A total mass loss of 80% is observed for polymer (I). If, as expected on combustion of the polymer, NiO is finally formed, 14.5% of the polymer mass would be nickel. This is consistent with the EDX analysis which predicts 14.3% by mass of nickel. A total mass loss of 76% is observed for polymer (II). The residue is green and insoluble in acid implying that NiO is not formed, but rather a more complex oxide including phosphorus or sulphur.

5.4.4 Catalysis

5.4.4.1 1-Hexene Oligomerisation

Neither polymer was active when tested with an equimolar amount of $AlEt_3$. It is possible that the stability of the complexes, coupled with their insolubility, may preclude the formation of the active species in the presence of the weak Lewis acid.

The polymeric nickel complex (I) and its monomeric precursor (III) are both active as oligomerisation catalysts when a ten-fold excess of $AlEtCl_2$ is used as co-catalyst. Oligomerisation is accompanied by rapid isomerisation to internal olefins.

Figure 5.12 shows the conversion of 1-hexene using complex (III) as catalyst. This complex, which is suspended in toluene, dissolves on the addition of $AlEtCl_2$ and the reaction thus proceeds in a homogeneous manner. As for other homogeneous catalysts of this type, (III) exhibits high initial activity and in fact is a more active dimerisation catalyst than $[Ni(acac)_2]_3$. Two effects may influence the activity of this nickel complex. Firstly, the inductive effect exerted by the hydroxyl group draws electron density out of the chelate ring system. Secondly, the resonance effect directs electron density towards the chelating atoms. Keim *et al.* [17] observed that catalyst activity increases with increasing ligand acidity. If this is the case, the high activity of complex (III) is as expected for a β-ketoenolate complex with electronegative ligand substituents. The C_{12} isomers produced by the systems employing (III) and $[Ni(acac)_2]_3$ as catalysts are shown in Fig. 5.13. The selectivity of each system is similar and it is likely that a similar reaction mechanism is involved.

The epoxy polymer (I), exhibits a different trend from that observed for its homogeneous precursor (III) (Fig. 5.14). Although conversion is still rapid, the isomerisation reaction predominates in the early stages producing *cis*- and *trans*-2-hexene and 3-hexene. The short half-life observed for the homogeneous oligomerisation reaction does not extend to the polymer system and, after 20 hours, the amount of C_{12} produced

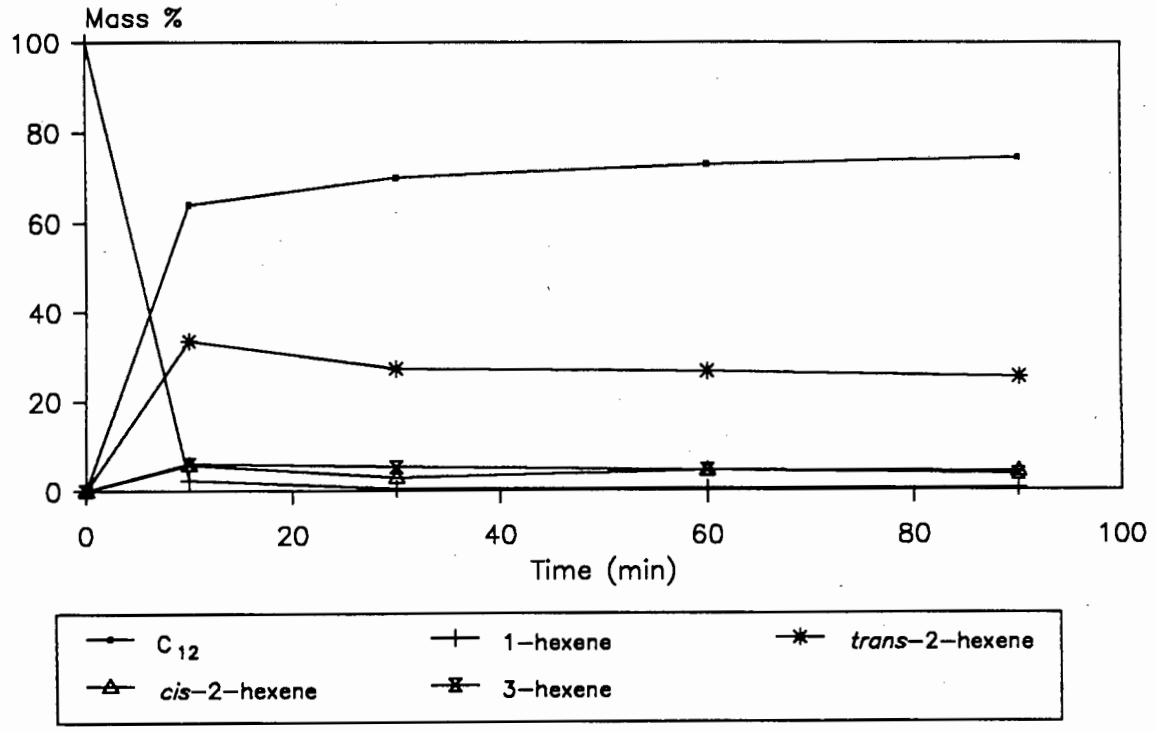

T = 40°C

Ni chelate : $AlEtCl_2$ = 1 : 10

Figure 5.12 Conversion of 1-hexene using nickel complex (III).

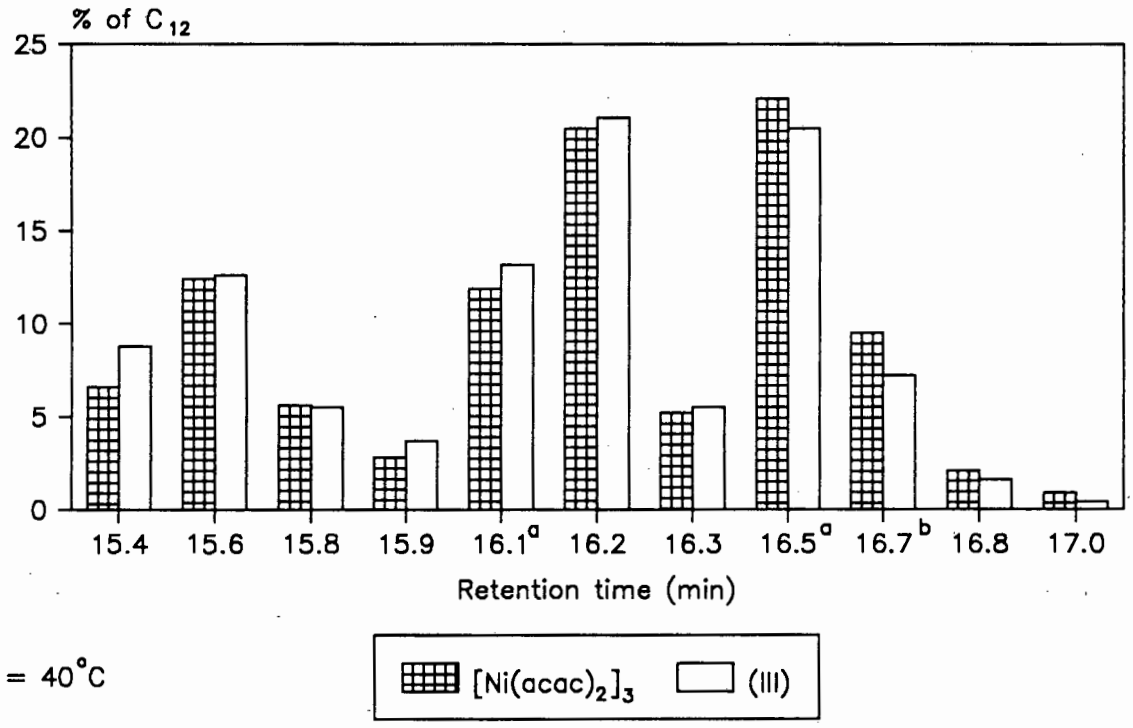

T = 40°C

Cat : $AlEtCl_2$ = 1 : 10

a = unresolved isomers, b = linear dodecene

Figure 5.13 Graph of the effect of catalyst on C_{12} isomer distribution.

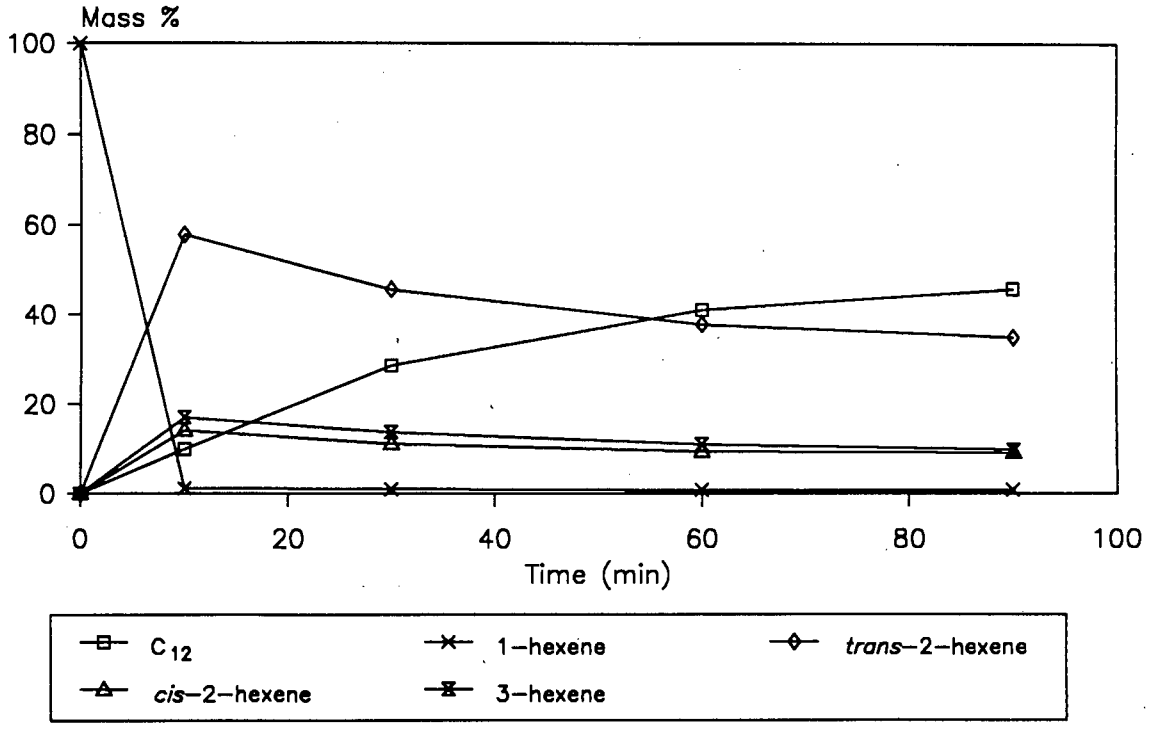

T =40°C

Polymer(I) : $AlEtCl_2$ = 1 : 10

Figure 5.14 Graph of conversion of 1-hexene using polymer (I).

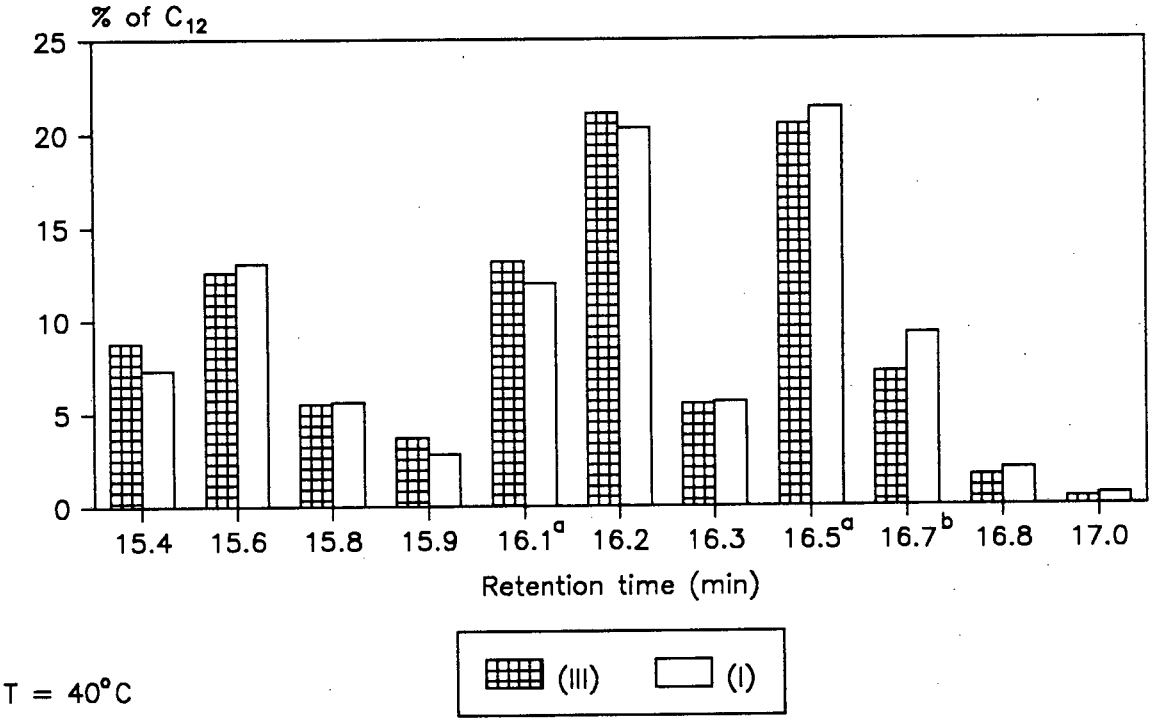

T = 40°C

Cat : $AlEtCl_2$ = 1 : 10

a = unresolved isomers, b = linear dodecene

Figure 5.15 Graph of the effect of catalyst on C_{12} isomer distribution.

approaches that of the homogeneous system. The products of both systems are predominantly dimers with little C_{18} product being formed. Extension of catalyst half-life when the catalyst is supported has also been observed by Cavell and Masters [7].

The slow oligomerisation reaction observed for (I) is probably due to the fact that, after the rapid isomerisation reaction, there is a limited amount of the reactive α-olefin remaining . In addition, it is likely that the active species takes some time to form due to the limited rate of diffusion within the polymer [2]. No active species have been presented in the literature to describe the activity of supported catalysts. However, the similarity in C_{12} isomer distribution for both the polymeric complex and its homogeneous precursor (Fig. 5.15) suggests that both systems comprise a similar active species. This may be explained in terms of a partial solubility phenomenon in which it is proposed that, while the complex is held by an insoluble polymer, the nickel and ligand components may effectively be in solution and are therefore able to form the active species.

Analysis of the polymer after the run revealed the presence of substantial amounts of aluminium and chlorine (15 and 30%, respectively). The presence of these elements leads to an increase in the polymer mass. Therefore, although the mass % of nickel decreased from 14.3 to 3.5%, only 25% of the nickel is lost from the polymer. The polymer is inactive in this form which suggests that the aluminium and chlorine are in some way complexed to the nickel.

For [Ni(SacSac)(PPh_3)Cl] and the polystyrene supported complex (II), the situation is similar to the systems described above in that the supported catalyst is initially less active than its homogeneous precursor. (Figs. 5.16 and 5.17) Similarly, C_6 isomerisation is dominant in the early stages of the polymer catalysed reaction [although not as rapid as for polymer (I)] and is followed by increasing oligomerisation (Fig. 5.17). The extended half-life observed for polymer (I) is also evident in this system. As observed by Cavell and Masters [7] who studied propene oligomerisation using [Ni(SacSac)PPh_3Cl] and a polymer supported analogue, the distribution of dimeric isomers is fairly similar when the homogeneous catalyst is heterogenised onto an

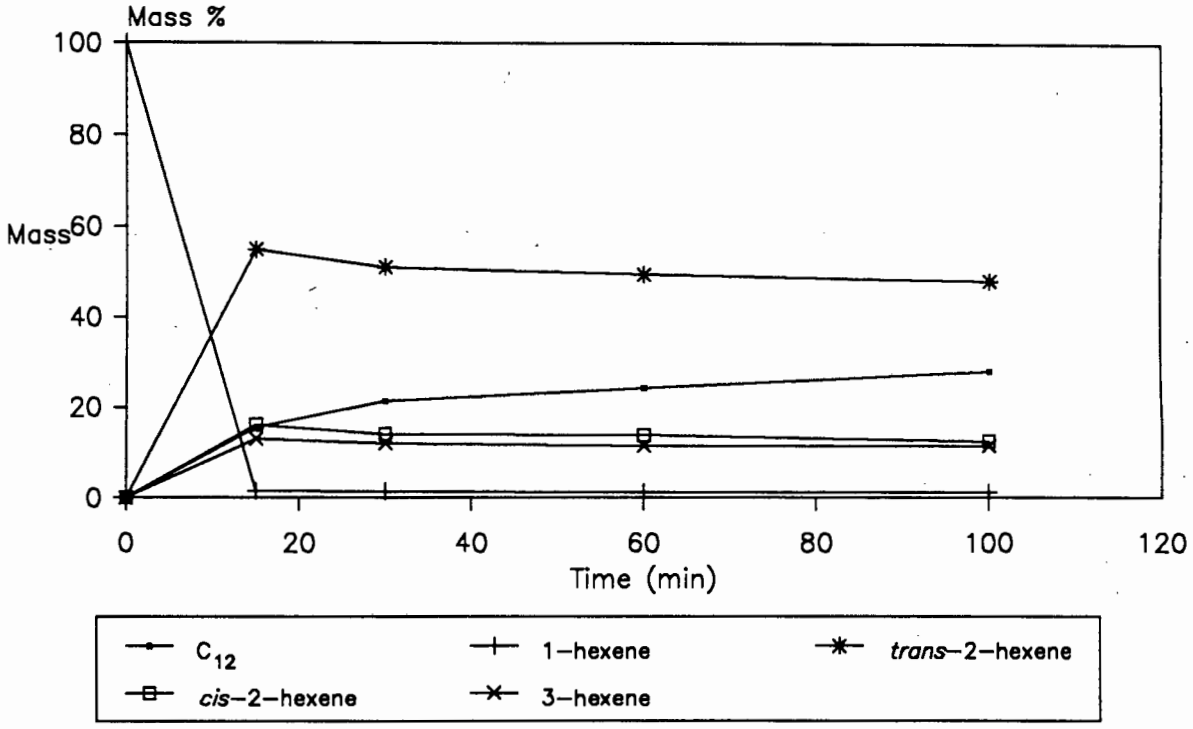

T = 40°C

[Ni(SacSac)(PPh_3)Cl] : $AlEtCl_2$ = 1 : 10

Figure 5.16 Graph of conversion of 1-hexene using [Ni(SacSac)(PPh_3)Cl].

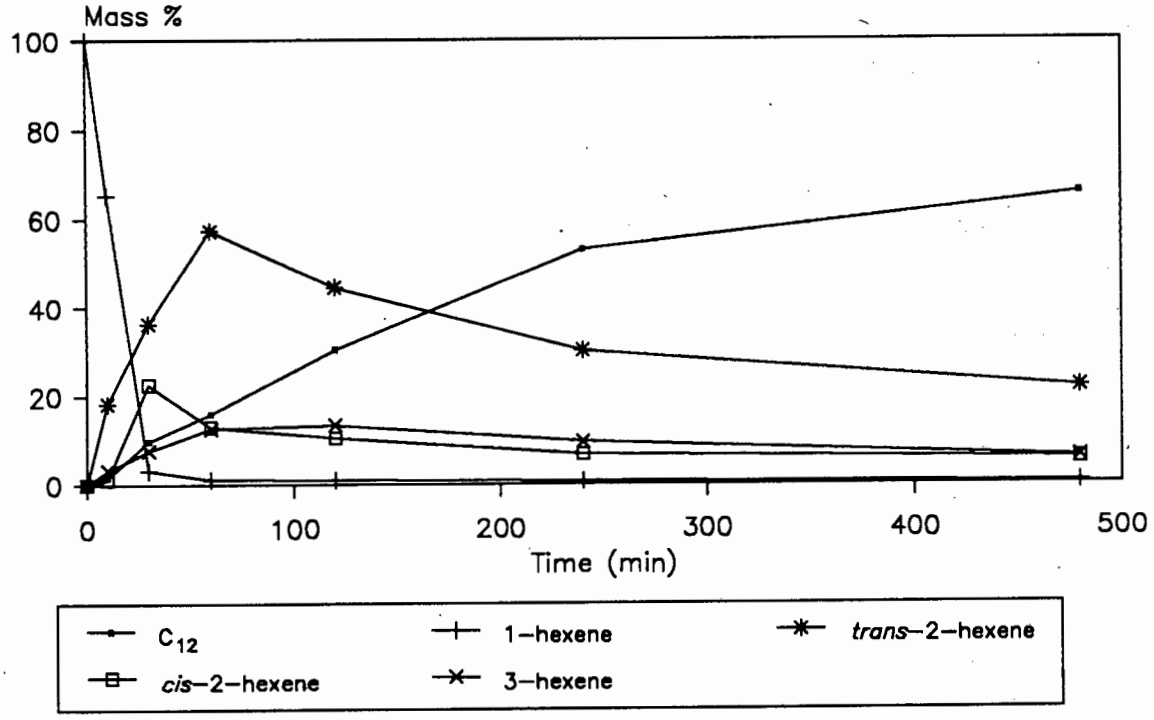

T = 40°C

Polymer(II) : $AlEtCl_2$ = 1 : 10

Figure 5.17 Graph of conversion of 1-hexene using polymer (II).

organic support (Fig 5.18). This is indicative of the operation of a similar active species in both systems. Comparison of the C_{12} isomer distribution formed by the respective polymeric complexes (I) and (II), reveals substantial differences between the two systems (Fig. 5.19). These differences may be ascribed to the "steering" influence of the phosphine ligand on the reaction [18].

Analysis of (II) after reaction revealed that the percentage nickel had decreased from 6.2% to less than 1%. This suggests excessive weeping and some doubt exists as to whether only polymer bound nickel was responsible for oligomerisation.

5.4.4.2 Propene Oligomerisation

The novel polymer (I) and the nickel chelate (III) have been tested as propene oligomerisation catalysts using a ten molar excess of $AlEtCl_2$ as co-catalyst.

As observed for 1-hexene dimerisation, the homogeneous system is initially more active than that employing the polymer catalyst (Fig. 5.20). However, after 5 hours of reaction the homogeneous system employing (III) as catalyst exhibits little activity, while the polymer system continues to dimerise propene. The homogeneous system has a more active oligomerisation reaction, *i.e.* produces more C_{9+} oligomers. This may be attributed to the presence of a large proportion of linear product from the dimerisation reaction (*vide infra*).

When the complex (III) is used as catalyst, the distribution of C_6 isomers changes with time (Fig. 5.21). After only 20 minutes of reaction approximately 52% of the dimer products are linear hexenes. This decreases to about 33% after 1 hour of reaction, probably due to the further reaction of this C_6 fraction to form higher oligomers. After 20 minutes the ratio of *cis*-2-hexene : *trans*-2-hexene : 3-hexene is ~ 1 : 4 : 1.4. While the ratio of *cis*- : *trans*-2-hexene remains constant, the proportion of 2-hexene drops after a further 20 minutes of reaction indicating that double bond isomerisation occurs. Double bond isomerisation of the methylpentenes is slower. The proportion of each

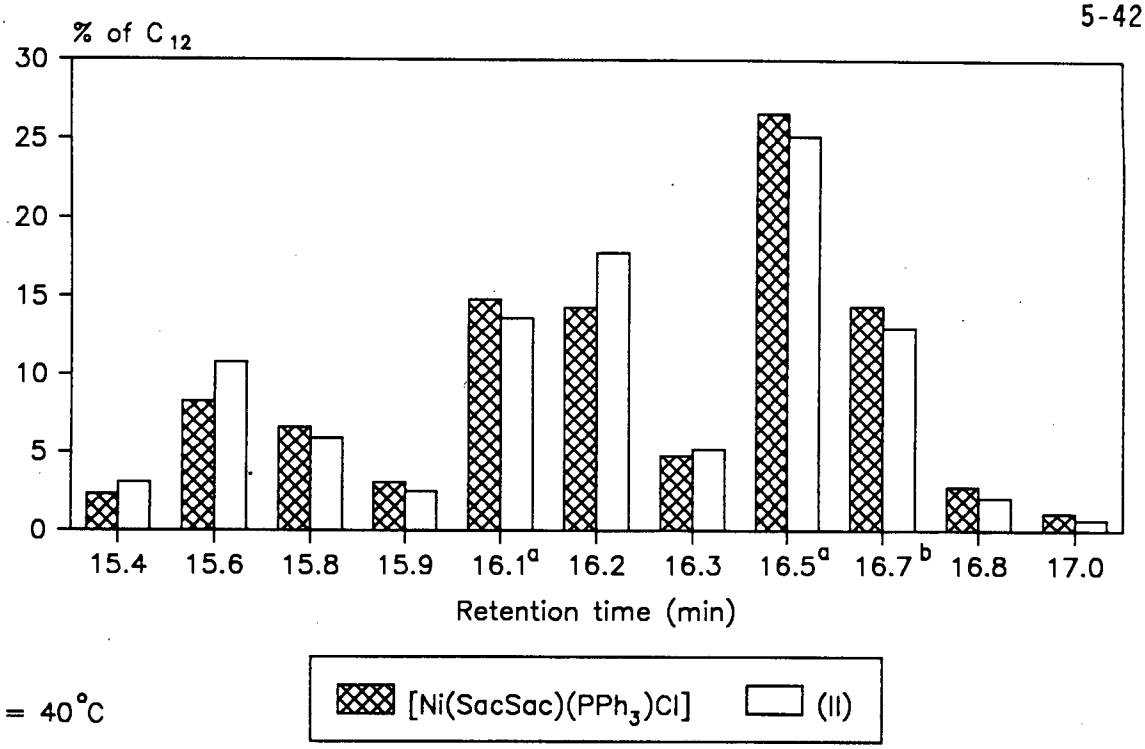

T = 40°C

Cat : $AlEtCl_2$ = 1 : 10

a = unresolved isomers, b = linear dodecene

Figure 5.18 Graph of the effect of supporting a catalyst on C_{12} isomer distribution.

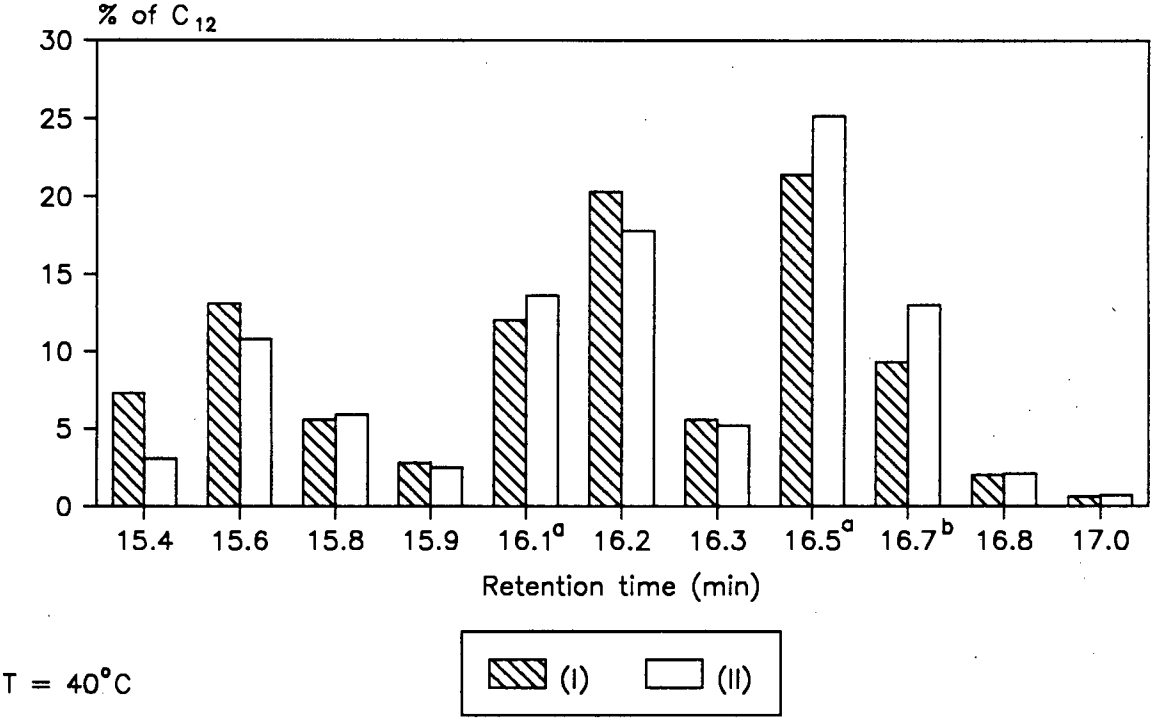

T = 40°C

Cat : $AlEtCl_2$ = 1 : 10

a = unresolved isomers, b = linear dodecene

Figure 5.19 Graph of the effect of catalyst on C_{12} isomer distribution.

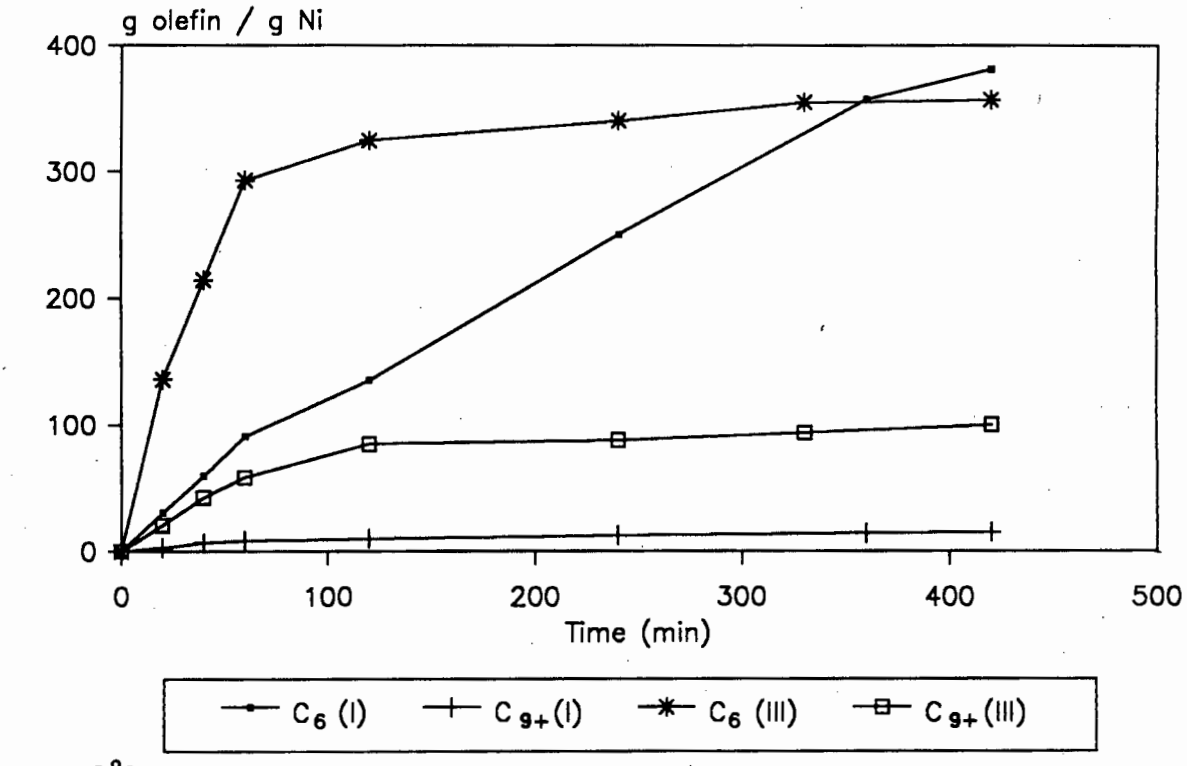

T = 40°C

Catalyst : $AlEtCl_2$ = 1 : 10

Figure 5.20 Graph of the effect of supporting a catalyst on the oligomerisation of propene.

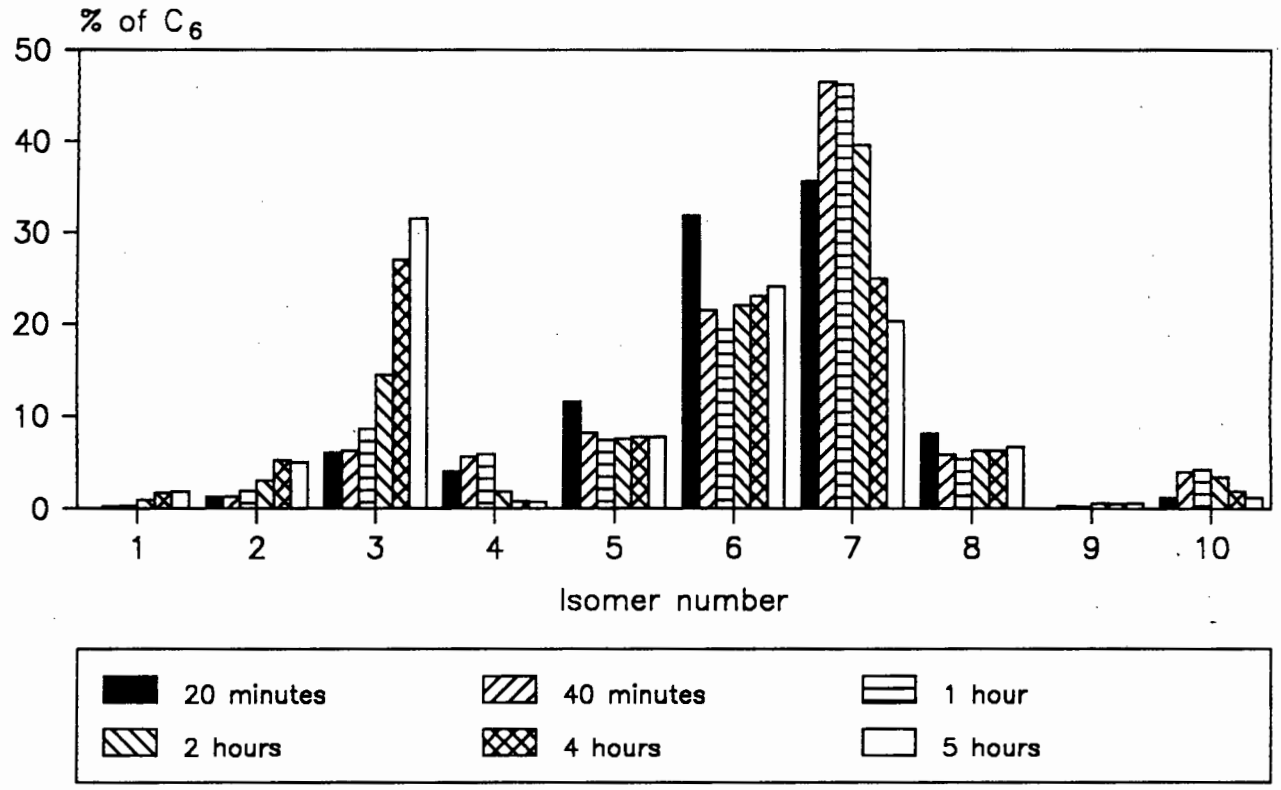

T = 40°C

Complex (III) : $AlEtCl_2$ = 1 : 10

Isomer no.	Identification
1	4-methyl-1-pentene + 3-methyl-1-pentene
2	2,3-dimethyl-1-butene + 4-methyl-*cis*-2-pentene
3	4-methyl-*trans*-2-pentene
4	1-hexene + 2-methyl-1-pentene
5	*cis*- + *trans*-3-hexene
6	*trans*-2-hexene
7	2-methyl-2-pentene
8	*cis*-2-hexene
9	3-methyl-*cis*-2-pentene
10	2,3-dimethyl-2-butene

Figure 5.21 Graph of C_6 isomer distribution using complex (III).

methylpentene isomer increases for the first hour of reaction, probably due to the decrease in the quantity of hexene. However, when the oligomerisation reaction has become more subdued, there is a marked decrease in the proportion of 2-methyl-2-pentene which is isomerised to the favoured 4-methyl-2-pentene isomer. Only a small quantity of 2,3-dimethylbutene is formed.

A slightly different trend is observed for the polymer system (Fig. 5.22). After 20 minutes of reaction approximately 30% of the dimeric products are linear hexenes and this percentage does not alter as the reaction progresses. Accordingly, few higher oligomers are formed. Furthermore, the ratio *cis*-2-hexene : *trans*-2-hexene : 3-hexene of 1 : 3.4 : 1.2 remains constant throughout the reaction indicating that double bond isomerisation is rapid. Isomerisation of 2-methyl-2-pentene to 4-methyl-2-pentene is reflected in the increase in the proportion of the latter at the expense of the former. The presence of 20% 4-methyl-2-pentene after only 20 minutes of reaction (relative to 6% for the homogeneous system) again indicates that isomerisation is rapid.

Variable Temperature Runs

When polymer (I) is tested as a catalyst, using a ten molar excess of $AlEtCl_2$ at 100°C and 6 atm, an active propene oligomerisation system results (Fig. 5.23). The turnover number is 1870 moles of propene per mole of nickel per hour (mol $C_3^=$/mol Ni/hr). The C_6 isomer distribution is similar to that of the analogous system at 40°C and 1 atm. However, the proportion of linear hexene decreases from 37.1% after 20 minutes of reaction to 27.6% after 2 hours (Fig. 5.24). Although trends vary with each catalytic system it appears generally that, while selectivity is relatively unaffected by reaction temperature, the dimethylbutene content of the product increases slightly with increasing temperature [19]. This is supported by the observation that the 2,3-dimethyl-2-butene content increases from approximately 1.9% to 3.0% when increasing the temperature from 40°C to 100°C.

Comparison of this, the most active system studied, with those previously published, is difficult due to the fact that experimental

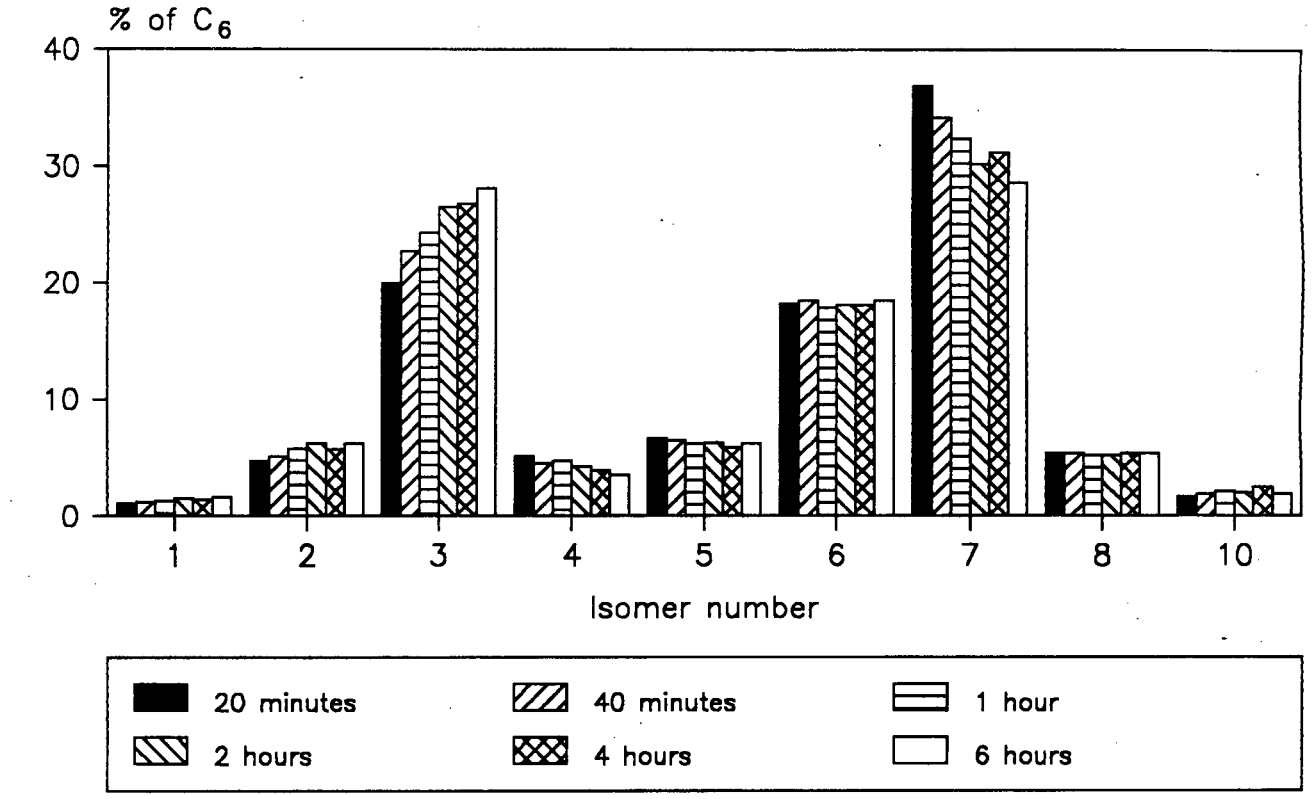

T = 40°C

Polymer (I) : $AlEtCl_2$ = 1 : 10

Isomer no.	Identification
1	4-methyl-1-pentene + 3-methyl-1-pentene
2	2,3-dimethyl-1-butene + 4-methyl-*cis*-2-pentene
3	4-methyl-*trans*-2-pentene
4	1-hexene + 2-methyl-1-pentene
5	*cis*- + *trans*-3-hexene
6	*trans*-2-hexene
7	2-methyl-2-pentene
8	*cis*-2-hexene
9	3-methyl-*cis*-2-pentene (not present)
10	2,3-dimethyl-2-butene

Figure 5.22 Graph of C_6 isomer distribution using polymer (I).

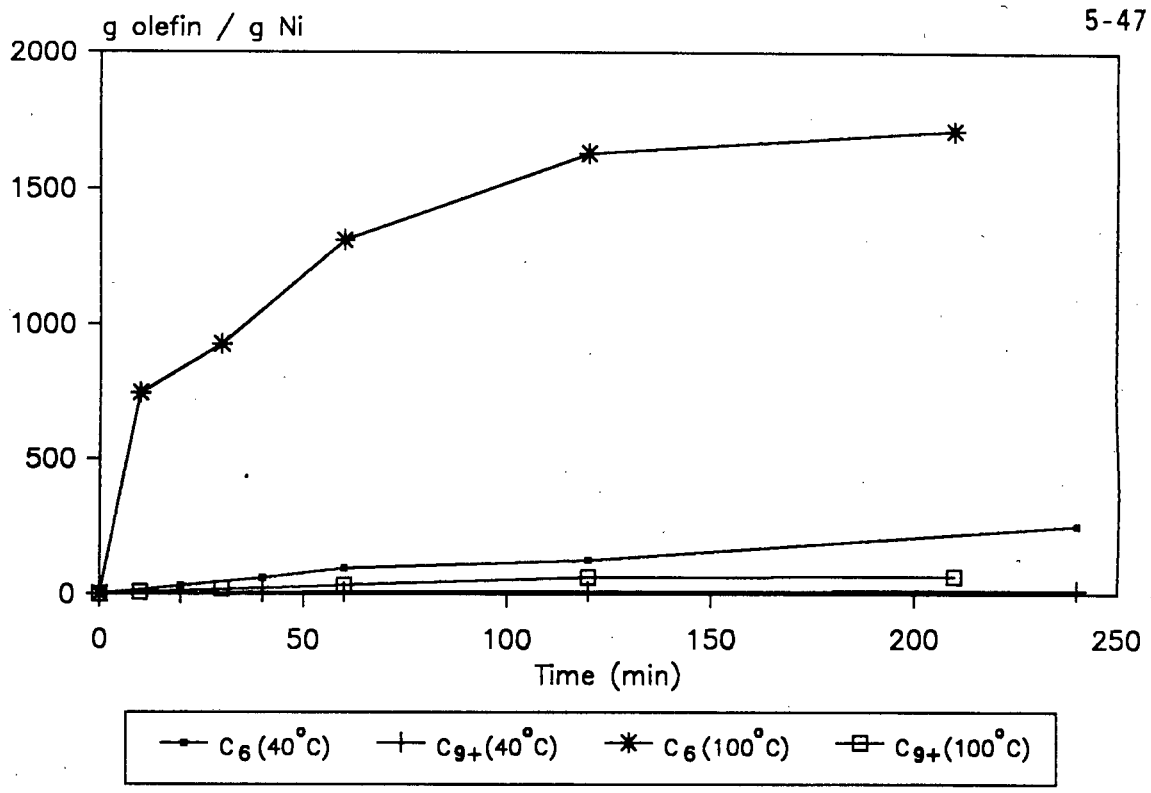

Polymer (I) : $AlEtCl_2$ = 1 : 10

Figure 5.23 Effect of temperature and pressure on the oligomerisation of propene.

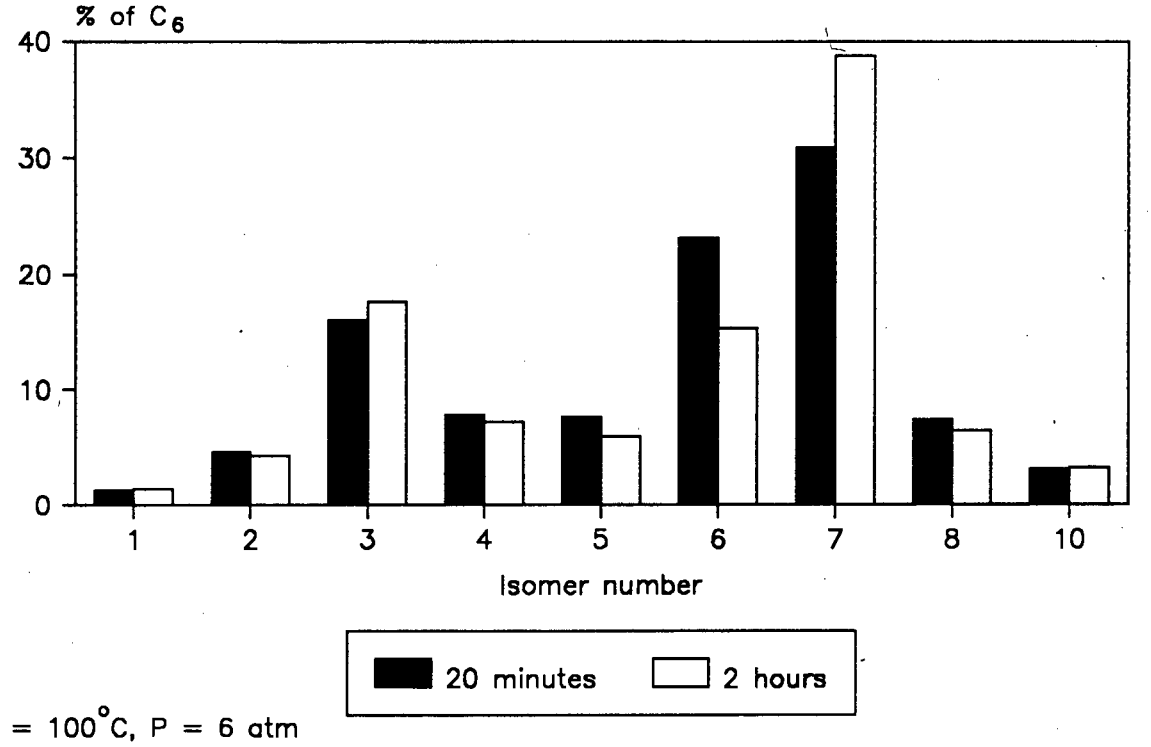

T = 100°C, P = 6 atm

Polymer (I) : $AlEtCl_2$ = 1 : 10

Figure 5.24 Graph of the C_6 isomer distribution obtained at 100°C. (For identification of isomers see Fig. 5.22)

parameters, such as temperature, pressure, solvent, co-catalyst, *etc.*, vary. Cavell and Masters [7] reported turnover numbers ranging from 25-2500 mol $C_3^=$/mol Ni/hr for supported nickel catalysts, while Peuckert and Keim [14] oligomerised ethene and recorded turnover numbers between 3600-216 000 mol $C_2^=$/mol Ni/hr. The high values reported by Peuckert and Keim are as expected for the reactive ethene monomer.

High Pressure and High Temperature Runs

No activity was observed for polymer (I) or (II) in the absence of co-catalyst, even at high pressures and temperatures. This highlights the essential role of the co-catalyst in forming the active complex.

REFERENCES

1. C. Dumas and C.C. Hsu, Rev. Macromol. Chem. Phys. C, **24** (1984) 355.

2. D.D. Whitehurst, Chem. Tech., Jan (1980) 44.

3. V.A. Kabanov and V.I. Smetanyuk, Sov. Sci, Rev., **13** (1980) 83.

4. F.R. Hartley, in "Supported Metal Complexes", (1985), D. Reidel, Holland.

5. F.R. Hartley and P.N. Vezey, Adv. Organomet. Chem., **15** (1977) 189.

6. J. R. Jones and T.J. Symes, J. Chem. Soc. C, (1971) 1124.

7. K.J. Cavell and A.F. Masters, J. Chem. Res., (1983) 72.

8. D.A. Thornton, S.A. Ind. Chemist, **12** (1964) 172.

9. M.E.B. Jones, M.F. Lynch, D.A. Thornton and R.F. Webb, Die Makromol. Chemie, **50** (1961) 232.

10. J. Lieto, D. Milstein, R.L. Albright, J.V. Minkiewicz and B.C. Gates, Chem. Tech., Jan (1983) 46.

11. A.A. Naakteboren, R.J.M. Nolte and W.J. Drenth, J. Amer. Chem. Soc., **102** (1980) 3350.

12. J. Reed, P. Eisenberger, B-K. Teo and B.M. Kincaid, J. Amer. Chem. Soc., **99** (1977) 5217.

13. D.L. Hanson, J.R. Katzer, B.C. Gates, G.C.A. Schuit and H.F. Harnsberger, J. Catal., **32** (1974) 204.

14. M. Peuckert and W. Keim, J. Mol. Catal., **22** (1984) 289.

15. K. Zhou, Z. Gao and W. Keim, Proc. VIIIth International Congress on Catalysis, Berlin, **V** (1984) 429.

16. W. Bremser, B. Franke and H. Wagner, in "Chemical Shift Ranges in Carbon-13 NMR", (1982), Verlag Chemie, Weinheim.

17. W. Keim, A. Behr and G. Kraus, J. Organomet. Chem., **251** (1983) 377.

18. B. Bogdanovic, Adv. Organomet. Chem., **17** (1979) 105.

19. G. Lefebvre and Y. Chauvin, in "Aspects of Homogeneous Catalysis", Carlo Manfredi, Milan, (1970), p. 107.

CHAPTER 6

PHYSICAL METHODS

6.1 INFRARED SPECTRA

The infrared spectra were recorded on a Perkin Elmer model 983 spectrophotometer using both Nujol mulls (2000-200 cm^{-1}) and hexachlorobutadiene mulls (4000-2000 cm^{-1} and 1500-1300 cm^{-1}), between caesium iodide plates. The far-infrared spectra were recorded as Nujol mulls (500-50 cm^{-1}) between polyethylene plates on a Digilab FTS 16 B/D interferometer.

The model 983 spectrophotometer is a double-beam, ratio-recording instrument with pre-sample chopping, and has integral data handling as well as digital display facilities. The optics are a purgeable F 4.2 monochromator with four gratings and nine filters. The quoted wavenumber accuracy is ~2 cm^{-1} over the range 4000-2000 cm^{-1} and ~1 cm^{-1} over the range 2000-180 cm^{-1}, with a reproducibility of better than 0.1 cm^{-1}. A resolution of 0.5 is obtainable using the highest scan mode.

The FTS 16 B/D is an automatic ratio recording, far-infrared vacuum interferometer with a resolution of 0.5 cm^{-1} throughout the spectral range of 500-10 cm^{-1}. The instrument consists of a model 296A Michelson interferometer, four interchangeable Mylar beam splitters, a high pressure mercury arc source, stored ratio optics and a remotely controlled sample carriage, a triglycine sulphate detector, an analog-to-digital converter, a data system with 8K of core memory, a 1.2 million word moving disc head, a digitally controlled plotter and related hard- and software.

6.2 NUCLEAR MAGNETIC RESONANCE (NMR) SPECTRA

Both the ^{1}H and ^{13}C NMR spectra were obtained at 200 and 50.3 MHz, respectively, on a Varian XL 200 continuous wave spectrometer. Depending on solubility, deuterated methanol (CH_3OD) or chloroform ($CDCl_3$) were used as solvent and lock, while tetramethylsilane (TMS) was used as the reference. Spectra were recorded at ambient temperature (25°C) using a sweep width of 0-10 ppm for ^{1}H NMR spectra and 0-200 ppm for ^{13}C NMR spectra.

6.3 MICROANALYSES

Complex purity was ascertained by microanalysis (C,H,N). These were performed by Mr W.R.T. Hemsted and Mr P. Benincasa, Department of Chemistry, University of Cape Town, on a Heraeus universal combustion analyser model CHN-MICRO.

6.4 GAS-LIQUID CHROMATOGRAPHIC SPECTRA

6.4.1 1-Hexene Oligomerisation

Liquid product analysis was performed using a Varian 3400 gas chromatograph with a Varian 8000 liquid autosampler linked to a Vista 401 data system for integration. The peaks detected were reported as mass percent. A 2.2 mm internal diameter (I.D.), 3 m long stainless steel column packed with 3% OV-101 on Chromosorb WHP-SP was used.

Analysis of isomer distribution was performed using a Varian 3600 gas chromatograph on a 0.531 mm I.D., 30 m long fused silica megabore column coated with a 1.5 μm film of DB-1 (100% methylpolysiloxane). The peaks detected were reported as mass percent.

6.4.2 Propene Oligomerisation

Liquid product analysis was performed using the Varian 3600 gas chromatograph as described above.

Identification of C_6 isomers was carried out using a 50 m long capillary column coated with a 1 μm film of BP-1 (equivalent to OV-1).

Effluent gas and feed stream analyses were performed on a Gow-Mac 750p gas chromatograph whose responses were monitored by a Varian 4270 integrator and reported as mass percent. A 6 mm I.D., 3 m long stainless steel column packed with *n*-Octane/Porasil C was used.

6.5 THERMAL ANALYSIS

Thermal stability of heterogeneous catalysts was investigated using thermal gravimetry and differential thermal analysis. This was performed using an STA-780 series furnace with a Stanton Redcroft Thermal Analyser. A Stanton Redcroft balance controller and Stanton Redcroft furnace controller controlled the balance and the furnace respectively. The signals were amplified by a Stanton Redcroft DC amplifier.

6.6 ENERGY DISPERSIVE X-RAY ANALYSIS (EDX)

A Cambridge S180 Scanning Electron Microscope (SEM) fitted with a Si(Li) detector coupled to a KEVEX model 7000 analyser was used. To prepare the sample, an aluminium electron microscopy stub was coated with a mixture of a thick graphite emulsion and a water based glue upon which the sample was sprinkled. The stub was then coated with a splattering of carbon.

6.7 MASS SPECTRA

Mass spectra were obtained on a V.G. Micromass 16F mass spectrometer operating in the electron impact mode, with an electron beam energy of 70 eV, an ion accelerating voltage of 4 kV and an ion source temperature in the range 180-210°C.

6.8 CRYSTAL STRUCTURE DETERMINATION

Crystal data was collected using an Enraf-Nonius CAD4 diffractometer. Cell parameters were obtained by least-squares analysis of the setting angles of 24 reflections in the range $16 \leq \theta \leq 17°$. Structure solution and refinement was carried out using SHELX-76, molecular parameters obtained from PARST, and drawings obtained with PLUTO-78. All computations were carried out on a VAX 8550 at the University of Cape Town.

APPENDICES

Appendix I. **GC spectra from analysis of 1-hexene oligomerisation runs**

Varian 3400 GC spectra (3m long stainless steel column).

a) $[Ni(acac)_2]_3$: $AlEt_3$ = 1 : 1

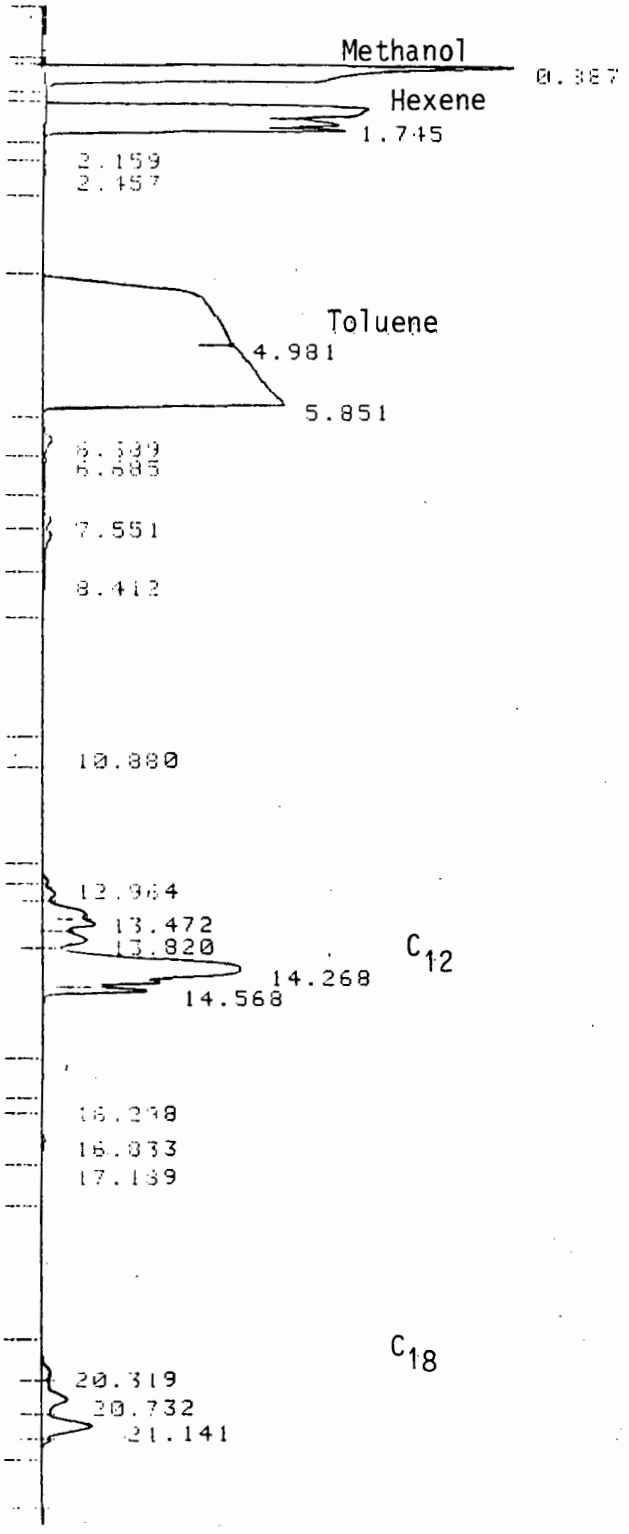

b) $AlEtCl_2$ only

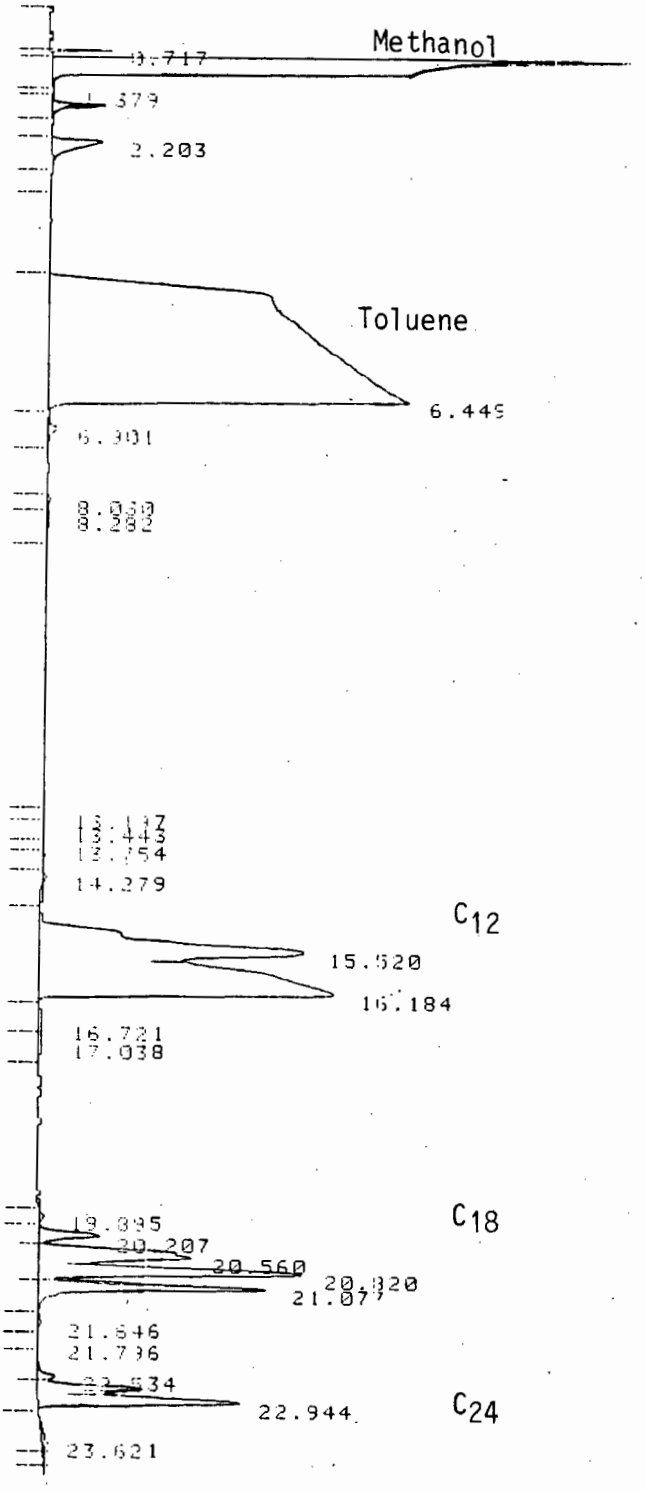

Varian 3600 GC spectra (30m long megabore column).

a) $[Ni(Sacac)_2]$: $AlEtCl_2$ = 1 : 10 →

b) Slow isomerisation of 1-hexene
↓

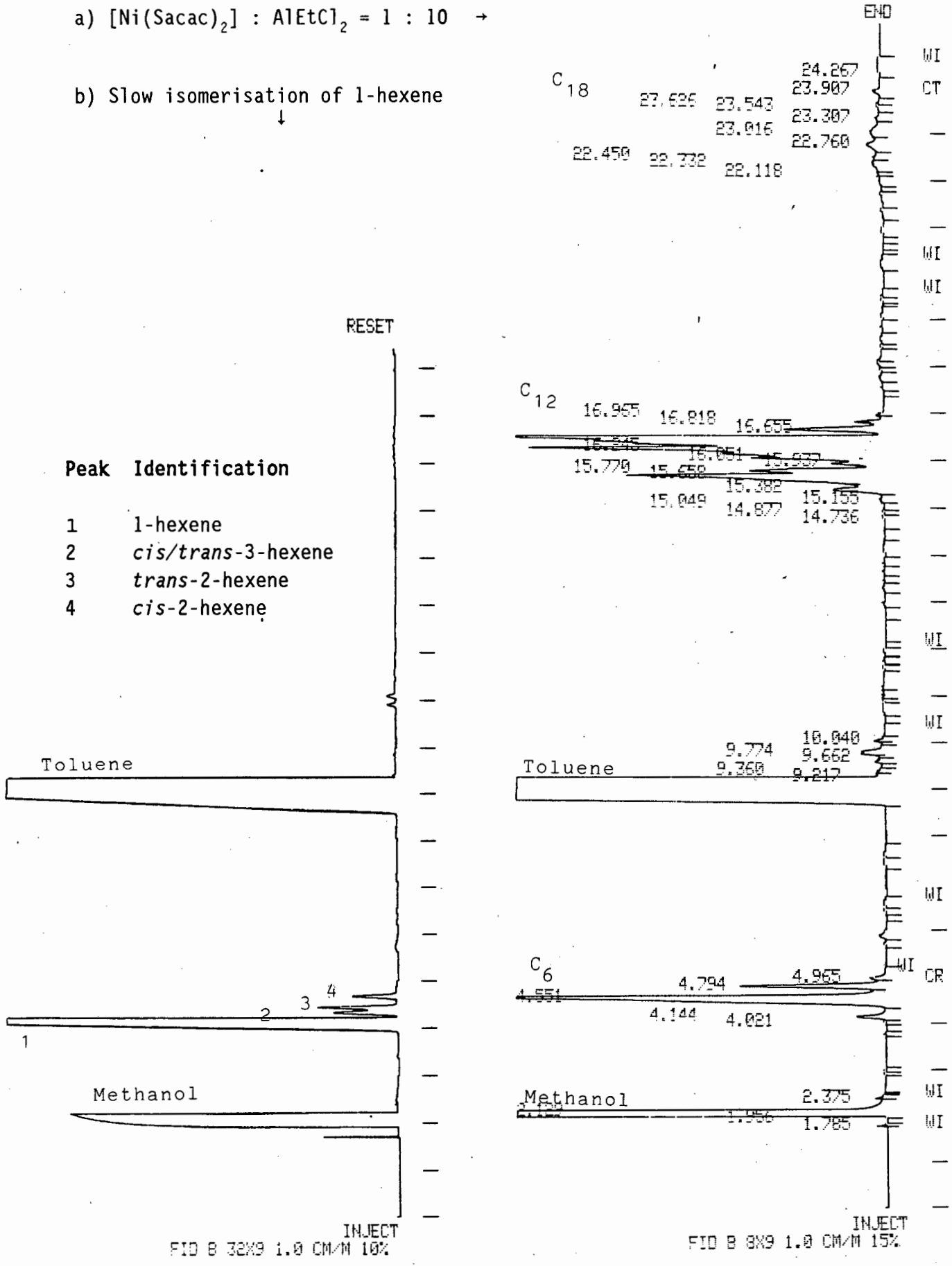

Peak	Identification
1	1-hexene
2	*cis/trans*-3-hexene
3	*trans*-2-hexene
4	*cis*-2-hexene

Appendix II. Crystal structure of [Ni(Sacac)(PEt_3)Cl]

Details of the crystal structure determination of [Ni(Sacac)(PEt_3)Cl] are given in the following Tables.

Table 1 Details of the data collection.

Scan mode	$\omega/2\theta$
Scan width (°)	$1.5(0.85 + 0.35\tan\theta)$
Aperture width (mm)	$1.5(1.20 + 1.05\tan\theta)$
θ Range scanned (°)	1-25
Range of hkl	$\pm$9; 0.21; 0.13
Absorption correction max/min/ave transmission (%)	100.0; 89.3; 95.1
No. of unique reflections collected	2492
No. of reflections with Irel > 2σIrel, N	2227
No. of parameters, NP	162

Table 2 Bond lengths (Å) for [Ni(Sacac)(PEt_3)Cl]*.

Ni(1)-P(1)	2.185(1)		
Ni(1)-Cl(1)	2.245(1)		
Ni(1)-S(1)	2.125(1)		
Ni(1)-O(1)	1.893(4)		
P(1)-C(111)	1.822(5)	C(111)-C(112)	1.487(9)
P(1)-C(211)	1.837(5)	C(211)-C(212)	1.521(8)
P(1)-C(311)	1.821(5)	C(311)-C(312)	1.528(9)
S(1)-C(1)	1.717(5)	C(2)-C(3)	1.419(8)
C(1)-C(11)	1.502(8)	C(3)-C(31)	1.494(8)
C(1)-C(2)	1.358(8)	C(3)-O(1)	1.254(6)

* estimated standard deviations are given in parentheses

Table 3 Bond angles (°) for [Ni(Sacac)(PEt_3)Cl]*.

Cl(1)-Ni(1)-P(1)	85.6(1)	S(1)-Ni(1)-Cl(1)	176.3(1)
S(1)-Ni(1)-P(1)	91.2(1)	O(1)-Ni(1)-P(1)	172.7(1)
O(1)-Ni(1)-Cl(1)	87.2(1)		
O(1)-Ni(1)-S(1)	96.0(1)		
Ni(1)-P(1)-C(111)	111.4(2)	C(111)-P(1)-C(211)	104.1(3)
Ni(1)-P(1)-C(211)	116.9(2)	C(111)-P(1)-C(311)	105.4(2)
Ni(1)-P(1)-C(311)	113.7(2)	C(211)-P(1)-C(311)	104.2(2)
P(1)-C(111)-C(112)	114.4(4)		
P(1)-C(211)-C(212)	116.6(4)		
P(1)-C(311)-C(312)	113.8(4)		
Ni(1)-S(1)-C(1)	111.0(2)	C(2)-C(1)-C(11)	119.9(5)
Ni(1)-S(1)-C(3)	134.3(4)	C(3)-C(2)-C(1)	126.7(5)
S(1)-C(1)-C(11)	113.7(4)	C(2)-C(3)-O(1)	125.4(5)
S(1)-C(1)-C(2)	126.3(4)	C(31)-C(3)-O(1)	115.2(5)
		C(31)-C(3)-C(2)	119.4(5)

* estimated standard deviations are given in parentheses

Table 4 Fractional atomic coordinates (x 10^4) for non-hydrogen atoms of $[Ni(Sacac)(PEt_3)Cl]^*$.

Atom	x/a	y/b	z/c
Ni(1)	355(1)	1191(1)	2954(1)
P(1)	-1447(2)	1402(1)	1314(1)
Cl(1)	343(2)	2427(1)	3219(1)
S(1)	339(2)	33(1)	2582(1)
O(1)	1866(5)	1136(2)	4430(3)
C(1)	1467(7)	-450(3)	3761(5)
C(11)	1396(9)	-1278(3)	3596(6)
C(2)	2342(7)	-153(3)	4786(5)
C(3)	2524(6)	612(3)	5076(5)
C(31)	3571(8)	840(4)	6240(6)
C(111)	-394(7)	1944(3)	201(5)
C(112)	1278(9)	1622(5)	-136(7)
C(211)	-2326(7)	587(3)	451(5)
C(212)	-3711(8)	734(3)	-619(6)
C(311)	-3395(7)	1929(3)	1600(5)
C(312)	-4507(8)	1555(4)	2496(7)

* estimated standard deviations are given in parentheses

Table for deposition H-atom coordinates (x 10^4) for [Ni(Sacac)(PEt_3)Cl]*.

Parent atom	H atom	x/a	y/b	z/c
C(11)	H(111)	832(9)	-1426(3)	2771(6)
	H(112)	846(9)	-1560(3)	4237(6)
	H(113)	2684(9)	-1391(3)	3659(6)
C(2)	H(2)	2748(7)	-633(3)	5177(5)
C(31)	H(311)	4064(8)	494(4)	6899(6)
	H(312)	3453(8)	1348(4)	6589(6)
	H(313)	4380(8)	860(4)	5585(6)
C(111)	H(11)	-152(7)	2453(3)	542(5)
	H(12)	-1229(7)	1979(3)	-560(5)
C(112)	H(13)	1614(9)	1893(5)	-868(7)
	H(14)	1665(9)	1092(5)	-169(7)
	H(15)	1860(9)	1860(5)	621(7)
(211)	H(21)	-2862(7)	251(3)	1033(5)
	H(22)	-1319(7)	328(3)	124(5)
C(212)	H(23)	-3924(8)	244(3)	-1036(6)
	H(24)	-3350(8)	1107(3)	-1216(6)
	H(25)	-4815(8)	904(3)	-293(6)
C(311)	H(31)	-4144(7)	1996(3)	806(5)
	H(32)	-3010(7)	2426(3)	1934(5)
C(312)	H(33)	-5564(8)	1874(4)	2563(7)
	H(34)	-3834(8)	1498(4)	3321(7)
	H(35)	-4892(8)	1056(4)	2173(7)

* estimated standard deviations are given in parentheses

Table for deposition Anisotrpic temperature factors ($Å^2 \times 10^3$) for non-hydrogen atoms of $[Ni(Sacac)(PEt_3)Cl]^*$.

Atom	U_{11}	U_{22}	U_{33}	U_{23}	U_{13}	U_{12}
Ni(1)	36(1)	34(1)	36(1)	0(1)	-2(1)	2(1)
P(1)	35(1)	33(1)	37(1)	1(1)	0(1)	1(1)
Cl(1)	57(1)	20(1)	45(1)	-8(1)	-22(1)	0(1)
S(1)	53(1)	34(1)	41(1)	-2(1)	-4(1)	5(1)
O(1)	47(2)	45(2)	38(2)	2(2)	-7(2)	4(2)
C(1)	42(3)	41(3)	44(3)	2(2)	8(2)	4(2)
C(11)	61(4)	37(3)	55(4)	6(2)	0(3)	12(2)
C(2)	52(3)	40(3)	47(3)	8(2)	0(3)	4(2)
C(3)	32(2)	52(3)	42(3)	3(2)	0(2)	4(2)
C(31)	51(3)	60(4)	51(3)	-2(3)	-14(3)	4(3)
C(111)	52(3)	39(4)	47(3)	8(2)	3(2)	-2(2)
C(112)	59(4)	90(5)	65(4)	10(4)	20(3)	-1(4)
C(211)	43(3)	44(3)	38(3)	0(2)	-5(2)	0(2)
C(212)	55(3)	52(3)	48(3)	0(3)	-11(3)	1(3)
C(311)	47(3)	43(3)	51(3)	3(2)	-1(2)	12(2)
C(312)	52(3)	78(4)	71(5)	6(3)	20(3)	18(3)

* estimated standard deviations are given in parentheses

Appendix III. GC spectra from analysis of propene oligomerisation runs

Capillary column (50m long)

Epoxy polymer (I) : $AlEtCl_2$ = 1 : 10

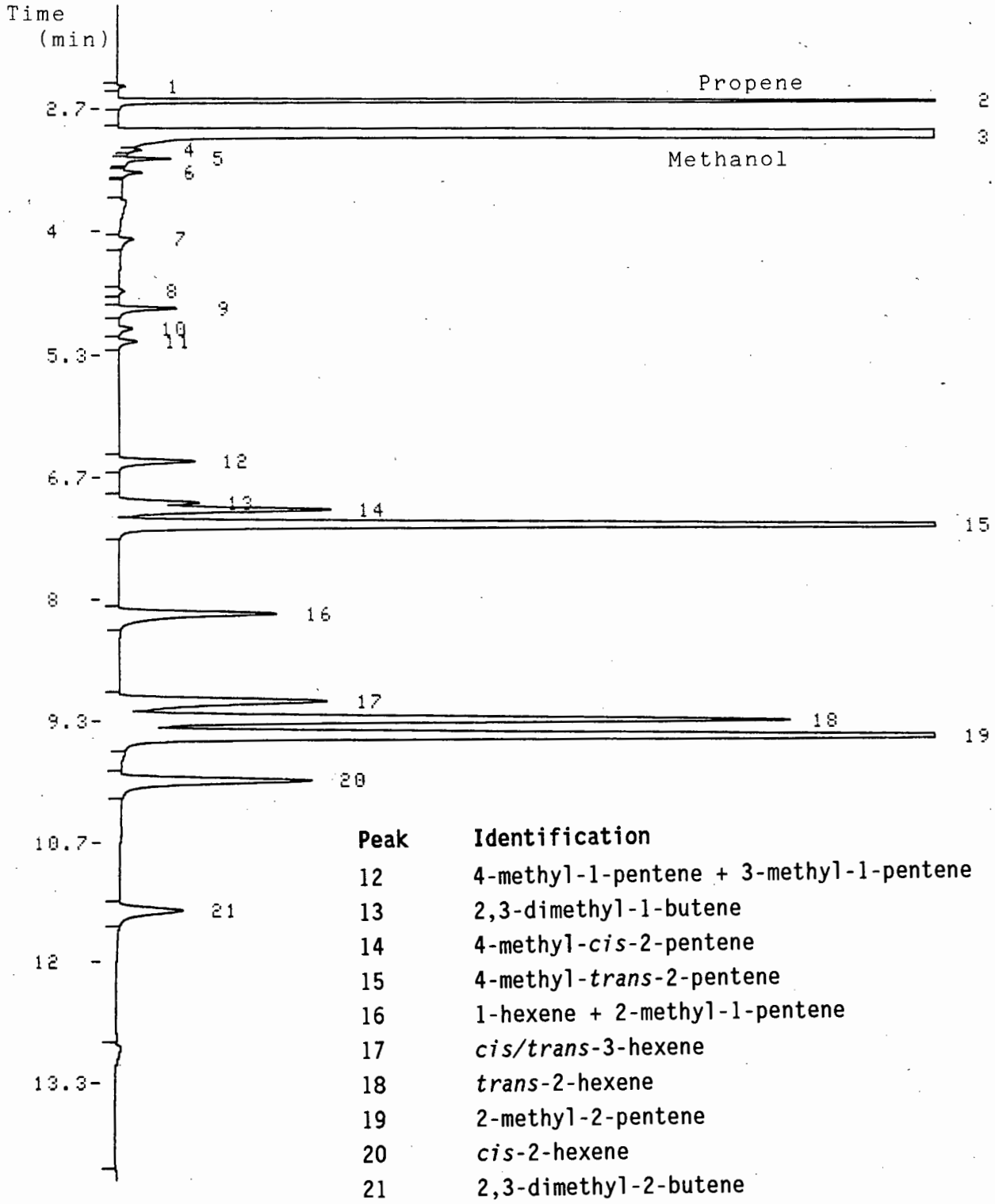

Peak	Identification
12	4-methyl-1-pentene + 3-methyl-1-pentene
13	2,3-dimethyl-1-butene
14	4-methyl-*cis*-2-pentene
15	4-methyl-*trans*-2-pentene
16	1-hexene + 2-methyl-1-pentene
17	*cis/trans*-3-hexene
18	*trans*-2-hexene
19	2-methyl-2-pentene
20	*cis*-2-hexene
21	2,3-dimethyl-2-butene

Gow-Mac 750p spectrum (3m long stainless steel column)

Propene feed as supplied by Sasol (85% propene/15% propane).

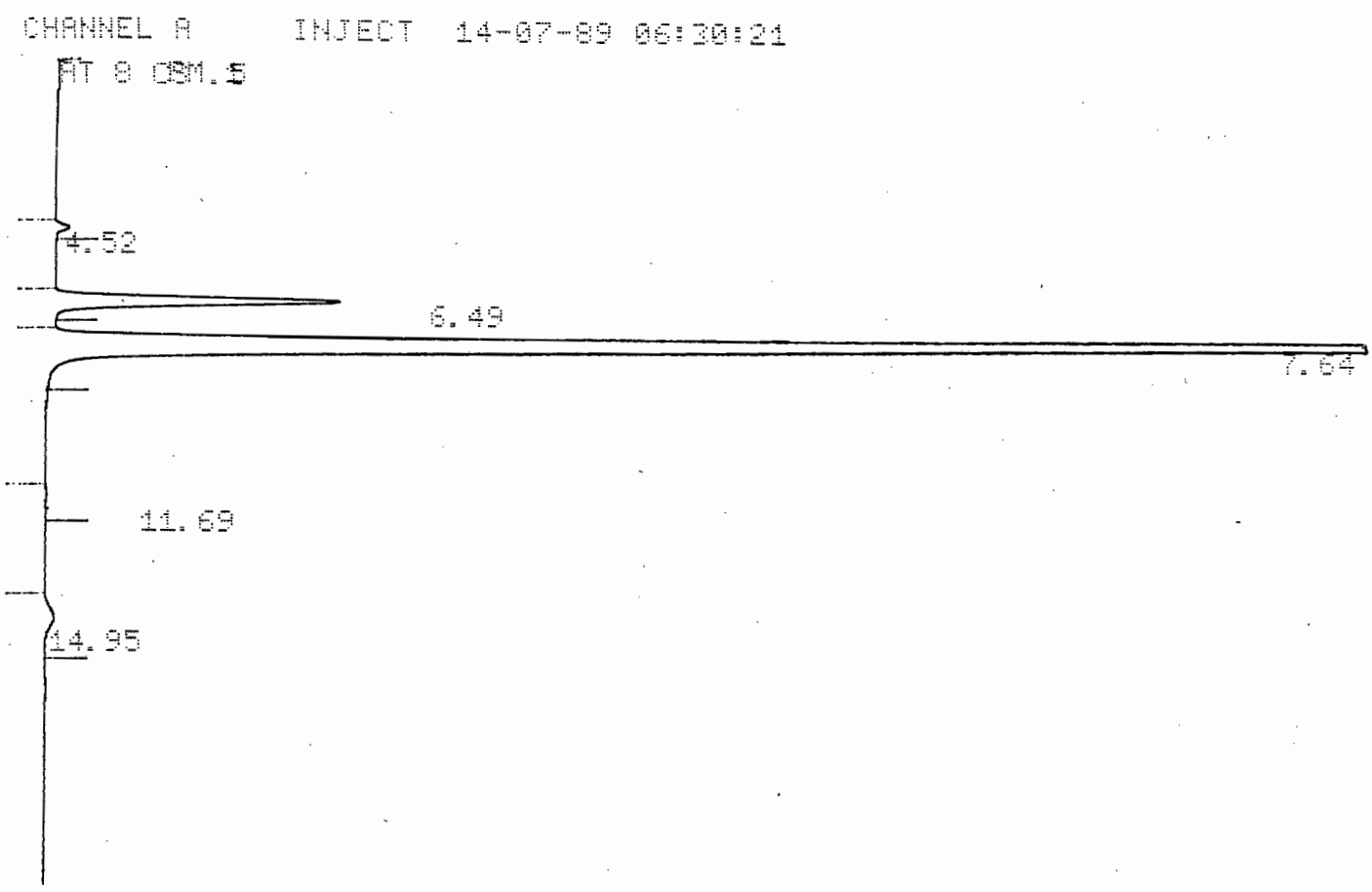

14-07-89 06:30:21 CH= "A" PS= 1.

FILE 1. METHOD 1. RUN 663 INDEX 663

NAME	MASS %	RT	AREA BC	RF
ETHAN	0.409	4.52	1705 01	1.024
PROPA	11.034	6.49	47135 01	1.
PROPE	87.442	7.64	384667 01	0.971
NBUTA	0.118	11.69	491 01	1.029
NBUTE	0.997	14.95	4032 01	1.056
TOTALS	100.		438030	